



NOVA

University of Newcastle Research Online

nova.newcastle.edu.au

**Gopalan, A.-I., Komathi, S. & Muthuchamy, N. et al. (2019) Functionalized conjugated polymers for sensing and molecular imprinting applications, Progress in Polymer Science, 88, p1-129**

**Available from:** <http://dx.doi.org/10.1016/j.cub.2019.06.077>

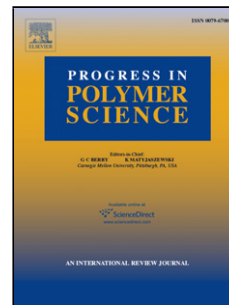
© 2019. This manuscript version is made available under the CC-BY-NC-ND 4.0 license  
<http://creativecommons.org/licenses/by-nc-nd/4.0/>

**Accessed from:**

## Accepted Manuscript

Title: Functionalized conjugated polymers for sensing and molecular imprinting applications

Authors: Anantha-Iyengar Gopalan, Shanmugasundaram Komathi, Nallal Muthuchamy, Kwang Pill Lee, Michael J. Whitcombe, Lakshmi Dhana, Gopalan Sai-Anand



PII: S0079-6700(17)30151-X  
DOI: <https://doi.org/10.1016/j.progpolymsci.2018.08.001>  
Reference: JPPS 1097

To appear in: *Progress in Polymer Science*

Received date: 27-6-2017  
Revised date: 2-8-2018  
Accepted date: 6-8-2018

Please cite this article as: Gopalan A-Iyengar, Komathi S, Muthuchamy N, Lee KP, Whitcombe MJ, Lakshmi D, Sai-Anand G, Functionalized conjugated polymers for sensing and molecular imprinting applications, *Progress in Polymer Science* (2018), <https://doi.org/10.1016/j.progpolymsci.2018.08.001>

This is a PDF file of an unedited manuscript that has been accepted for publication. As a service to our customers we are providing this early version of the manuscript. The manuscript will undergo copyediting, typesetting, and review of the resulting proof before it is published in its final form. Please note that during the production process errors may be discovered which could affect the content, and all legal disclaimers that apply to the journal pertain.

# Functionalized conjugated polymers for sensing and molecular imprinting applications

Anantha-Iyengar Gopalan<sup>1</sup>, Shanmugasundaram Komathi<sup>1</sup>, Nallal Muthuchamy<sup>1,#</sup>, Kwang Pill Lee<sup>1,\*</sup>, Michael J Whitcombe<sup>2</sup>, Lakshmi Dhana<sup>3</sup>, Gopalan Sai-Anand<sup>4</sup>

- 1 Research Institute of Advanced Energy Technology, Advanced Nanomaterials Laboratory, Kyungpook National University, Daegu 41566, South Korea
- 2 University of Leicester, University Road, Leicester, UK LE1 7RH, United Kingdom
- 3 King's College London, Strand Campus, London, UK WC2R2LS, United Kingdom
- 4 Environment, The University of Newcastle, Callaghan 2308, New South Wales, Australia

# Present address: Department of Chemistry, Pusan National University, Busan 46241, South Korea

## Abstract

The electronic conjugation between each repeat unit in conducting polymers (CPs) provides semiconducting molecular architectures and intriguing properties to suit for sensing applications. Therefore, considerable progress has been demonstrated on sensor designs with CPs. Unfortunately, the most essential requirements of sensors such as selectivity of an analyte and detection of a specific analyte in a complex environment are hard to achieve with pristine CPs. These constraints in pristine CPs along with processability limitations necessitate the development of functionalized CPs (FCPs) through intelligent structural modification of pristine CPs or inclusion of a functional property modifying components with CPs. On perusal of the literature in last 10-15 years on the use of FCPs for sensor application reveal that FCPs can out-perform basic function at the molecular levels, such as recognition and control of chemical processes, as well as inform that the unique physical, chemical and electrochemical properties of FCPs could be effectively exploited to improve the selectivity, sensitivity, and throughput of sensors beyond the limits of existing detection techniques. Herein, we provide the first review of FCP materials utilized for sensor fabrications highlighting, in particular, the advances in the synthesis of FCPs employing strategies for the inclusion of functional group/functional component(s) to suit for sensing the specific analyte(s), the improvements in sensor performances (detection limit and linear range) and the role of FCPs in the sensing process. The in-depth analysis of the literature on the use of FCPs for sensors suggests that these research activities are rapidly maturing at the convergence of nanotechnology and biotechnology. We arrange the great number of FCPs utilized for sensing element into four categories; substituted or derivatized FCPs (category I), biofunctionalized FCPs (category II), nanostructured FCPs (category III) and multicomponent FCPs (category IV). This review highlights

prominent examples of FCPs as applicable to main type of CPs such as polypyrrole, polyaniline, polythiophene, polyfluorene and other CPs. We also identify how certain functionalization improves sensor performances. In addition, this review presents a discussion of state of the art of FCPs used in the preparation of molecular imprinted polymers (MIPs) intended for molecular recognition/sensor applications. In the final stage, we summarize the characteristics of FCPs with relevance to MIP and sensor designs and propose several prospectives for using FCP as a new sensing platform for the development of next-generation sensors.

**Key words:** *Conducting polymer; Functionalization; Nanostructuring; Multicomponent; Sensor; Molecular imprinting*

**\*Corresponding Author:** [kplee@knu.ac.kr](mailto:kplee@knu.ac.kr); Tel: +82 53 9505901. Fax: +82 53 9505899;

## Contents

Abstract	1
Abbreviations	5
1. Introduction	8
1.1. Background	8
1.2. Scope of the review	10
2. Categories of functionalized conducting polymers (FCPs)	12
3. FCPs for sensors	15
3.1. Functionalized polypyrroles (F-PPys)	16
3.1.1. <i>Substituted or derivatized F-PPys</i>	16
3.1.2. <i>Functional compound included PPys</i>	20
3.1.3. <i>Grafted PPys</i>	24
3.1.4. <i>Biofunctionalized PPys</i>	24
3.1.5. <i>Nanostructured F-PPys</i>	28
3.1.6. <i>F-PPys with multicomponent</i>	32
3.2. Functionalized polyanilines (F-PANIs)	37
3.2.1. <i>Substituted or derivatized F-PANIs</i>	38
3.2.2. <i>Functional component inclusion into PANIs</i>	42
3.2.3. <i>Grafted PANIs</i>	48
3.2.4. <i>Biofunctionalized F-PANIs</i>	49
3.2.5. <i>Nanostructured F-PANIs</i>	51
3.2.6. <i>Multicomponent in F-PANIs</i>	57
3.3. Functionalized polythiophenes (F-PTs)	67
3.3.1. <i>Substituted or derivatized F-PTs</i>	68
3.3.2. <i>F-PTs containing a functional component</i>	76
3.3.3. <i>Biofunctionalized F-PTs</i>	77
3.3.4. <i>Nanostructures of F-PTs</i>	80
3.3.5. <i>Multicomponent included F-PTs</i>	82
3.4. Functionalized Polyfluorene (F-PFs)	88
3.4.1. <i>Substituted F-PFs</i>	89
3.4.2. <i>Nanostructured F-PFs</i>	95
3.5. Functionalized polyacetylene (F-PAs)	96
4. Molecular imprinted polymers (MIPs) based on FCPs	97
4.1. Molecular imprinting concept	97
4.1.1. <i>Molecular imprinting methods</i>	97
4.2. MIPs with pristine CPs	100
4.3. MIPs using FCPs	103
4.3.1. <i>MIP based on F-PPys</i>	104
4.3.2. <i>MIP based on F-PANIs</i>	110
4.3.3. <i>MIPs based on F-PTs</i>	115
4.3.4. <i>MIPs based on polycarbazole and polyindole</i>	116
5. Summary and perspectives	117
Acknowledgement	121
References	123

**Abbreviations**

AA	Ascorbic acid	LBL	Layer-by-layer
BBVs	Boronic acid functional viologens	LCST	Lower critical solution temperature
BPA	Bisphenol A	LPG	Liquefied petroleum gas
BSA	Bovine serum albumin	<i>m</i> -BBV	N,N'-4,4'-bis(benzyl-3"-boronic acid)-bipyridinium dibromide
CBT	2-cyano-6-methoxybenzothiazole	MEs	Modified electrodes
CDS	Cyclodextrin sulfonate	MPTS	(3-mercaptopropyl) trimethoxysilane
CEL	Celecoxib	MTPPP	Metallotetraphenylporphyrin
ChEt	Cholesterol esterase	NBDAE	4-(2-acryloyloxyethylamino)-7-nitro-2,1,3-benzoxadiazole
CNT	Carbon nanotubes	nbe-nose	Nanobioelectronic nose
CO	Carbon monoxide	nbe-tongue	Nanobioelectronic tongue
CP	Conducting polymers	ND	Nanodiamonds
CPEs	Conjugated polyelectrolytes	NDDEAEA	N-(N',N'-diethyldithiocarbamoyl ethylamidoethyl) aniline
CS	Chitosan	NEES	Nanopillar-enhanced electrodes
CSA	Camphor sulfonic acid	NFM	Nanofibrous membrane
CVD	Chemical vapour deposition	NHS	(N-hydroxysuccinimide)
Cys	Cysteine	NPG	Nanoporous gold
DA	Dopamine	<i>o</i> -BBV	N,N'-4,4'-bis(benzyl-2"-boronic acid)-bipyridinium dibromide
DFT	Density functional theory	ODN	Oligonucleotides
DHP	2,5-dihydroxyphenyl	OECT	Organic electrochemical transistor
DMA	N,N-dimethylaniline	OFL	Ofloxacin
DMcT	2,5-dimercapto-1,3,4-thiadiazole	P(DPA-co-2ABN)	Poly(diphenylamine-co-2-aminobenzonitrile)
DMMP	Dimethyl methylphosphonate	P3ACIT	Chloropoly(3, $\beta$ -chloroalkylo-4-chlorothiophenes)
DNA	Deoxy ribo nucleic acid	P3BSIT	Poly(3-butyne triisopropylsilyl thiophene)
DNT	Dinitrotoluene	P3CA	Pyrrole-3-carboxylic acid
E. coli	Escherichia coli	P3HT	Poly(3-hexylthiophene)
ECL	Electrochemiluminescence	P3TzdHT	Poly(3-triazole dihexyl thiophene)
EDC	(N-(3-dimethylaminopropyl)-N'-ethylcarbodiimide hydrochloride)	P3TzHT	Poly(3-triazole hexyl thiophene)
EpCAM	Epithelial cell adhesion molecule	PA 6	Polyamide 6
FAD	Flavin adenine	PA	Polyacetylene
FCPs	Functionalized CPs	PAA	Poly acrylic acid
FETs	Field effect transistors	PABS	Poly(4-aminobenzene sulfonic acid)
FRET	Fluorescence resonance energy transfer	PAMAM	Poly(amidoamine)
F-PAs	Functionalized polyacetylene	PANI	Polyaniline
F-PANIs	Functionalized polyanilines	PASA	PANI sulfonate
F-PFs	Functionalized Polyfluorene	PATP	Poly(4-amino thiophenol)
F-PPys	Functionalized polypyrroles	PATP	Poly(2-aminothiophenol)
F-PTs	Functionalized polythiophenes	PAzoTAc	Poly(2-[4-(4'-nitrophenylazo)-N-ethyl-N-phenylamino]ethyl-3-thienylacetate)
G	Graphene	<i>p</i> -BBV	N,N"-4,4"-bis(benzyl-4"-boronic acid)-bipyridinium dibromide
GC	Glassy carbon	PBP	Poly(9,9-bis(6'-benzimidazole)hexyl)fluorene- <i>alt</i> -1,4-phenylene
GNR	Gold nanorod	PCPBT-FC	Poly(4-(Ferrocenylmethylidene)-4 <i>H</i> -
GO	Graphene oxide		
GOx	Glucose oxidase		
GS	Graphene sheet		
Hb	Haemoglobin		
HDT	1,6-hexanedithiol		
HFIP	Hexafluoroisopropanol		
HQ	Hydroquinone		
HQS	N-Hydroquinone monosulfonate		
HRP	Horseradish peroxidase		
ITO	Indium tin oxide		

	cyclopenta[2,1-b:3,4-b']-dithiophene)	PTA	Phosphotungstic acid
PDA	Polydopamine	PTAA	Poly(3-thiopheneacetic acid)
PDPA	Poly(diphenyl amine)	PTCA-Cl	Poly[N,N,N-trimethyl-4-(thiophen-3-ylmethylene)-cyclohexanaminium chloride]
PDT	Poly(3-dodecylthiophene)	PTEBS	Poly[2-(3-thienyl)ethoxy-4-butylsulfonate]
PdTPP	Palladium tetraphenylporphyrin	PTMSPA	Poly[N-(3-trimethoxyl silyl)propyl aniline]
PEDOT	Poly(ethylene dioxy thiophene)	pTSA	P-toluene sulfonic acid
PEG	Polyethylene glycol	pTTBA	Poly(terthiophene benzoic acid)
PET	Poly(ethylene terephthalate)	PTTCA	Poly(5,2':5,2''-terthiophene-3'-carboxylic acid)
PF	Polyfluorenes	PURET	Poly [2-(3-thienyl)ethanol n-butoxycarbonylmethylurethane]
PFAB	Poly{(1,4-phenylene)-2,7-[9,9-bis(6'-N,N,N-trimethyl ammonium)-hexyl fluorene] dibromide}	PVA	Poly(vinyl alcohol)
PFO	Poly(9,9-dioctylfluorene)	PvdF	Poly(vinylidene fluoride)
PHET	Poly(3-(2-hydroxyethyl)thiophene)	PVP	Poly(vinyl pyrrolidone)
PHexOxT	Poly(3-hexyloxythiophene)	PVSA	Polyvinylsulfonic acid
PHexTAc	Poly(hexyl-3-thienylacetate)	QMB	Quartz crystal microbalance
PI	Polyindoles	RGO	Reduced Graphene oxide
PIL	Polymerized ionic liquid	RS	Rhodamine 6G derivative
PL	Photoluminescence	S. Aureus	Staphylococcus aureus
PMB	Poly(methylene blue)	SC	Sildenafil citrate
PMMA	Polymethylmethacrylate	SO	Sulfite oxidase
PMNT	Poly[3-(3'-N,N,N-triethylamino-1-propyloxy)-4-methyl-2,5-thiophene hydrochloride]	SPAN	Sulfonated polyaniline
PMTEMA	Poly(2-(2-(4-methylthiophen-3-yloxy)ethyl)malonate acid)	SPCE	Screen-printed carbon electrode
PMTPA	Poly(3-(4-methyl-30-thienyloxy)propyltrimethylammonium)	SPR	Surface plasmon resonance
PNCEPy	Poly(N-2(cyanoethyl)pyrrole)	SWNT	Single-walled carbon nanotubes
PNMA	Poly(N-methyl aniline)	TMA	Trimethylamine
POA	Poly(o-anisidine)	TMB	3,3',5,5'-tetramethylbenzidine
ppt	Parts per trillion	TNT	2,4,6-trinitrotoluene
Ppy	Polypyrrole	Tppp	Tetraphenylporphyrin
PSS	Polystyrene sulfonate	UA	Uric acid
PT	Polythiophenes	VOCs	Volatile organic compounds
		$\beta$ -CD	$\beta$ -cyclodextrin

## 1. Introduction

### 1.1. Background

Following the invention of conductive polyacetylene [1], conducting polymers (CPs) have received significant attention and rapid developments. The electronic conjugation between each repeat unit in CPs creates semiconducting molecular wire architectures to impart CPs with interesting optical and electronic properties. Many different CPs have been extensively investigated for practical applications; the most prominent types of CPs are polyaniline (PANI), polypyrrole (PPy), polythiophene (PT), polyfluorene (PF), polyacetylene (PA), and derivatives thereof. CPs are especially good prospects for use in chemical or electrochemical sensors [2, 3]. CPs can be employed for the fabrication of sensors in two ways: (i) as transduction or sensing materials and (ii) as an immobilization matrix. The basic strategy towards the design of CP based chemical sensors for neutral molecules, ions and biomolecules (in the gaseous or liquid state) is to generate a measurable signal. This is achieved by connecting a molecular recognition site that uses a CP as a receptor with a signal-receiving/transducing unit in such a way that a binding event between the CP and target analyte changes the properties of the CP. The redox or electronic state of the CP is modulated by interactions with the analyte and the signal generated can be quantified as the sensor response. In general, the use of CPs as the molecular recognition receptor allows various types of signals to be assessed, such as optical (fluorescence or absorption) or electrical (redox properties, capacitance, or resistance/conductivity) properties [4]. Thus, CP-based sensors can be formulated in different transduction modes that can be divided into a few main classes depending on the operating principle, including amperometric, potentiometric, conductometric, calorimetric, fluorometric, magnetic and gravimetric, etc. (for details, readers can refer to Supporting information: SI: 1). Such CP-based sensors can provide analyte recognition through covalent or physical interactions between the analyte and the CP depending on the intrinsic electrostatic/optical and chemical characteristics of the CP, with specific properties of CPs exploited for each sensing approach. CPs are also categorized as an important group of chemically modified electrodes (MEs). Control over the complex area, simultaneous deposition and post-deposition conditioning of several layers, and electropolymerization are important features of MEs that complement the trends towards miniaturization and multi-sensing. Furthermore, the ease of preparation, stable adhesion, and long electrode lifetime, as well as suitable spatial, electrostatic, and chemical microenvironments constructed on the ME surface, constitute desirable qualities of CPs for analyte sensing, and these advantages are associated with the structure, composition, and properties of CPs.

An ideal sensor should satisfy a few requisite parameters, such as high sensitivity, low detection

limit, good selectivity for the analyte of interest, broad dynamic range, minimal calibration, rapid response, reproducibility, reversibility, and stability [5]. Also, miniaturization of sensors is also considered important for practical application and for generating multi-sensing chips. In practice, the fabrication of a high performance sensor possessing all of the requisite performance characteristics is a challenging task for sensory scientists. Innovative detection systems involving novel materials are likewise being developed for miniaturized, high throughput, and highly sensitive systems. A great deal of effort has been directed towards achieving good sensor performance with pristine CPs. However, selectivity towards a specific analyte is still a challenge. Also, the widespread application of pristine CP-based sensors is limited because designing sensors with pristine CPs for detecting a specific target analyte in a complex environment is rather difficult. Functionalization of CPs is being effected to modify the properties of CPs in an attempt to improve the selectivity towards the target analyte.

It is now possible to progress beyond the conventional approach used in sensor design with pristine CPs and develop novel CP-based materials through intelligent structures that can perform basic functions at the molecular level, such as recognition and control of chemical or electrochemical or optical processes. Importantly, the unique physical, chemical, and electrical properties of the intelligently modified CPs can be effectively exploited to improve the sensitivity, selectivity, and other sensing characteristics in order to outperform the limits of existing detection techniques. To enhance sensor performance, two factors can be modified by molecular design or functionalization of CPs: (i) the affinity between the molecular recognition site and the target analyte and (ii) the transduction efficiency of converting the binding with the analyte into a measurable signal. The former factor leads to specific or stronger receptor–analyte complexes that influence the selectivity of the sensor. It must be noted that selectivity can be influenced by both the specificity and binding efficiency of the analyte with the modified CP. The second factor is the sensitivity of the sensor. The sensitivity is dependent on the type of signal generated through the receptor–analyte interaction. Considering these two factors, the development of new CP-based materials for improved high-performance sensors that fulfill many of the requisite parameters (e.g., sensitivity, selectivity, response time, and reproducibility) can be categorized based on the specific approach used. One of the approaches involves creating novel CPs for use as an active sensing component, where the specifically designed properties of a CP are actively involved in signal production or transduction. Increased sensitivity and selectivity of the intended measurement is often the goal of this approach. CPs constitute a 3D network of molecular wires comprise of monomeric units capable of functionalizing with various substituents. By varying the nature of these groups, specific interactions with external physical or chemical stimuli can be developed in these materials, leading to high-performance sensors, and a fascinating challenge has emerged in correlating the structure–property–sensing relations in modified CPs. In an another approach, multi-sensing and online monitoring

sensor systems have been developed using novel CP-based materials.

## 1.2. Scope of the review

There are a few reviews that analyze the synthesis and applications of simple (i.e., nonfunctionalized) CPs for sensing applications [6-10]. Moreover, reviews are available on the use of CPs that are based on sensory principles such as gas sensors [11], potentiometric ion sensors [12], and electrochemical biosensors [13]. The inclusion of functional moieties with CPs and the development of modified CPs in the form of functionalized CPs (FCPs) represents the next step towards intelligent materials for sensor applications. Functionalization of the CP skeleton or integration of functional components along with CPs is an effective approach that uses structural-level modification. The steric and electronic effects introduced into the FCPs through functionalization can fine-tune the electronic distribution along the effective conjugation length of the  $\pi$ -conjugated system. Also, the optical and electrical behavior of CPs are influenced by the intermolecular interactions in the solid state. The interchain and intermolecular interactions can also be controlled through chemical functionalization and by the selection of film deposition technique [14]. Significantly, the introduction of substituents onto the parent unit (aniline, thiophene, pyrrole, and so forth) of the main chain can confer selective recognition properties. Publications on the sensor applications of CPs reveal that FCPs have been designed in diverse ways and applied to improve the performance characteristics of the sensors. In such instances, the properties of the CPs are modified or tuned to augment the sensor performance and features. The selection of the functionalization strategy to modify the properties of the CPs or to improve the sensor performance depends on the analyte and the sensing/transduction signal mechanism. A few FCPs containing immobilized enzymes have been utilized for the recognition of an analyte or transduction of an electrochemical signal. Nevertheless, the literature available on the various types of FCPs used in sensing applications has not until now been reviewed. Such a review will certainly provide a platform for understanding the logic of CP functionalization and sensor performance improvements. Furthermore, to realize next generation high-performance sensors based on FCPs, there is a necessity to make an in-depth analysis of the literature on the use of FCPs for sensors and rationalize the conceptual projection of prospects, especially towards the development of new FCPs.

In this review, we focus on the rational design of FCPs and the optimization needed for the development of efficient sensors. Hence, the aim of this review is to describe studies that focused on the introduction of substituents into the core monomeric structure or integration of functional components into CPs resulting in additional or modified properties. The behavior of FCPs relative to the parent CP and how certain functional groups or functional components improve sensor properties are described in detail throughout this review. The references cited herein are meant to highlight specific aspects and methods

that are important in the synthesis of FCPs and their application as diverse types of sensor, such as gas, chemical, electrochemical, ionic, and bio-sensors. We address recent research endeavors on the utility of FCPs for sensors regarding (i) the fabrication of FCP-based sensors, (ii) the relationship between FCP characteristics and sensor operation, and (iii) the need for consolidation of additional components into FCP-based sensing systems. We simultaneously provide a view of the scientific and technological challenges for the growth of new FCPs for next generation sensors. Except for a few important references in the years before 2004, the references are mostly selected from the last 13 years to highlight specific aspects and applications that are related to the synthesis and application of FCPs. The citations in this review do not reflect the chronology of the improvements on the topic. We likewise do not present every reference on this issue, as our aim is to highlight the specific aspects relevant to the use of FCPs for sensor applications.

This review also presents a discussion of state-of-the-art FCPs used in the preparation of molecular imprinted polymers (MIPs) intended for molecular recognition applications. MIPs can be used to fabricate synthetic receptors with high selectivity and stability, as well as sensors that offer good sensitivity with the possibility of compact design and miniaturization. Pristine CPs, have been employed in molecular imprinting, and the retention of the electrical conductivity of pristine CPs in MIP fabrication is quite an interesting phenomenon. Moreover, the crosslinking conditions used in the fabrication of pristine CP-based MIP membranes introduce difficulties that preclude the utilization of these membranes for electrochemical sensing applications. Alteration of the basic building blocks of CPs can result in binding interactions with templates, adherence to a range of transducer surfaces, improved processability, and better integration of MIPs with electrode surfaces. In the case of combined MIP–sensor applications, the development of electron transduction or an electron transfer pathway in the matrix should be analyzed through a critical review.

**Scheme 1** compares the general operational principle with regards to conventional sensors and MIP based sensors upon using FCP as the sensor matrix. The pre-synthesized FCP can generally offer electrostatic or covalent or hydrogen bonding or metal center co-ordination link or ionic interactions with the analyte *via* the functional group present in FCPs (**Scheme 1(A)**). Concurrently, there can be changes the physical/chemical properties of the FCP. As a consequence, quantifiable sensor signal (electrochemical or optical or mass changes etc.) is being transduced for measurement. The type of interactions and the signal transduction depend on the functional group(s) in the FCP and the nature of analyte (neutral or ionic or biological). The performance characteristics such as concentration range, sensitivity and selectivity depend on the analyte-FCP interactions. The analyte molecule generally do not retain its molecular configuration within FCP matrix due to the absence of the complementary sites for the analyte within the sensor matrix. With regards to MIP-sensors, complementary sites for the analyte

molecule are generated during MIP formation (**Scheme 1 (B)**). The analyte molecules accommodate within the complementary sites generated in MIP. Hence, analyte molecules occupy within the complementary sites and interact with the functional groups of FCPs. As a consequence, MIP based sensors are highly selective towards an analyte. While the analyte molecules pervade into the three dimensionally generated complementary sites in MIP–sensor matrix, predominant surface interactions are possible in conventional sensing process. Interesting results and sensor performances were reported in both cases with the use of FCPs. Selectivity is conferred to the conventional sensors through immobilization of suitable enzymes, in the case of biosensors. Considering the network generated in MIP film with complementary sites for the analyte molecule, the coverage of analyte molecules within MIP matrix is expected to be wider as compared to the predominant initial surface coverage of analyte molecules on the conventional sensor matrix. Nevertheless, literature reveals that interesting results on sensor performances are continuously being reported on both cases of sensors. A greater emphasis is given in this review on papers published over the last 10 years with regards to the case of FCP based MIP-sensors on reviewing the use of FCP-based MIPs towards sensor applications.

### Scheme 1

## 2. Categories of functionalized conducting polymers (FCPs)

With the advancement of FCPs in the area of sensing elements, many FCPs have been prepared, and the corresponding sensor fabrication methods have been produced in the past few years. **Scheme 2** depicts the categories of FCPs based on the functionalization with representation for the each kind of FCP categories in terms of parent structure modifications. Precisely, FCPs are arranged in four categories (**Scheme 2**) based on structural modifications through functionalization or the inclusion of one or more functional components: substituted or derivatized FCPs (Category I), biofunctionalized FCPs (Category II), nanostructured FCPs (Category III), and multicomponent FCPs (Category IV).

Category I deals with the FCPs associated with functional groups (**Scheme 2**) through (a) substituents on the parent CP unit (aniline, thiophene, pyrrole, etc.), copolymerization of an unsubstituted monomer with another substituted monomer, (b) functional groups containing ions (dopant ions) to compensate the charge of the CP chains and (c) grafting of CP chains onto a polymer/other substrate that includes nanomaterial/nanocomponent and d) physical adsorption of material containing functional groups into the CPs. The simplest FCPs in **Category I** are CPs that themselves possess functional groups (i.e., substituted CPs) such as cyano (–CN), carboxyl (–COOH), hydroxyl (–OH), etc. in the parent structure (pyrrole, aniline, or thiophene) (**Category I(a), Scheme 2**). The introduction of various substituents along the CP backbone, either on the aromatic or heterocyclic ring or on the heteroatom in

the main chain, not only improves the processability of the CPs but also modifies the physical properties in ways that are not possible with the unsubstituted parent CPs. For example, the properties of some substituted CPs can be exploited to detect, transduce, and in a few cases amplify physical or chemical information into an electrochemical or optical signal. Conjugated polyelectrolytes (CPEs) belong to a type of CP that contains side chains with ionic functionalities [15]. The solubility of CPEs in polar solvents, such as water and methanol, is not only dependent on the ionic side groups but is likewise regarded by the hydrophobic aromatic backbones [16]. Doping of CPs provides another approach for including functional groups or ions in CPs. CPs with functional groups that contain ions (**Category 1(b), Scheme 2**) exhibit ion-dependent properties. The type and level of doping in the CP units determines the conductivity and forms the basis of deciding the operating principle of most electrical-based CP sensors. The dopant anion can serve as a specific binding site for the analyte. Unlike external doping, the counter ions or functional groups in self-doped CPs are covalently bound to the CP chains [17]. A series of self-doped CPs were developed that contained covalently linked ionic functional groups (i.e., counter ions). Furthermore, the high solubility in various solvents, processability, and electrochemical properties of this self-doped CPs rendered them useful for sensor applications. Water solubility inducted in self-doped CPs is necessary for biosensors because biological systems are stable in aqueous environments. Grafting chains of CPs onto electrode surfaces or preformed polymer or another substrate (**Category 1(c)**) can be utilized to establish electrical wiring between target molecules and electrodes. Graft and di-block copolymerization represent an interesting strategy to generate FCPs. Grafted CPs are obtained either by “grafting from” or “grafting to” methods. The “grafting from” technique involves polymerization of the monomer at the substrate by attached (usually covalently bound) initiating groups. The initiating sites are incorporated by copolymerization or in a pre-reaction of the substrate or are an inherent part of the first polymer. The “grafting to” technique involves the reaction of end-functionalized CP molecules with complementary functional groups on the surface or in another polymer, resulting in tethered chains. Brush-like layers are formed owing to the excluded volume effect when the substrate is covered with a relatively dense monolayer of grafted polymer chains. In addition, FCPs was developed by grafting PANI, PPy, and PT chains onto other nanomaterials, such as carbon nanotubes (CNTs)[18], graphene (G)[19], nanodiamonds (NDs) [20], metal/inorganic nanoparticles (NPs), semiconductor nanocrystals, and other polymer nanostructures [21], through chemical linkages. Grafting CPs with nanomaterials changes the electronic structure of the functionalized nanocomposites and can increase the interactions with analytes. Also, FCPs were generated through incorporation of functional groups containing nanocomponents (CNTs or G or ND) into pristine CP matrix. In these cases, the nanocomponents can have a functional group for potential interactions with the CP or the analyte or function as the dopant for CP. Importantly, the second component improves the properties of the sensing film, participates in electron or proton transfer [22], interacts with analytes [23], establishes the device configuration [24, 25], or improves the

stability of the sensor [26]. The nature and amount of functional components in this type of FCP influence the sensor performance [27, 28]. Physical adsorption and entrapment of functional group containing additive into pre-synthesized CP (PANI, PPy, PT etc.) also can result FCPs. The preparation of FCP via physical adsorption/entrapment can be done easily by contacting the pre-synthesized FCP with the functionalizing additive. Of course, this approach can be the simplest approach for the preparation of FCP. The **category 1** excludes especially the biomolecules related structural modifications of CP (Please note that biofunctionalized FCPs are grouped separately as **Category II**).

## Scheme 2

Among the various functional groups that can be attached to the CP main chain, special interest is focused on functionalization with biomolecules or enzymes or biopolymers, resulting in biofunctionalized CPs (**Category II, Scheme 1**) [29, 30]. Biofunctionalized FCPs can be obtained through two major ways; i) physical adsorption/entrapment of biomolecules within CP/substituted CP and ii) covalent binding of biomolecules with CP/substituted CP. Additionally, doping renders pre-synthesized CP/substituted CP can be utilized to bonding a wide range of biomolecules as long as they are charged. For biosensor applications, an electrical connection between the biomolecule or enzyme and electrode surface has to be established. In the majority of biosensors, this operation involves the immobilization of the biorecognition element on the active area of the transducer to capture the target molecule and transduce the signal. The optimization of performance factors, including selectivity, limit of detection, and sensitivity, mainly concerns the “bio-interface” (i.e., the location where the biomolecule interacts with the transducer and where biomolecular recognition occurs). FCPs in **Category II** can be generated through (a) functionalization with biomolecules (**Category II(a)**), (b) cross-linking CPs with enzymes through covalent bonds (**Category II(b)**), or (c) physical entrapment (**Category II(c)**) (**Scheme 2**).

Another set of reviews details the various interface-specific properties and phenomena pertaining to biologically important events supporting to understand molecular recognition in simple aqueous/non-aqueous media [31-39]. Apart from the aforementioned articles, the readers can refer the fabrication of enzyme degradable and size-control protein nanowires [40] possessing biological functionalities such as high level avidin–biotinyl interactions and peroxidase activity.

The advent of nanotechnology has prompted the integration of nanostructured (NS) materials, such as nanowires (NWs) and nanotubes (NTs), as transducers. Recently, nanostructured forms of several FCPs were prepared (**Category III, Scheme 2**) and used in sensors. Alternatively, pristine nanostructured CPs can be functionalized to afford NS-FCPs. Such integration (NS and FCP) greatly benefits sensors through the addition of an ultrahigh surface-area-to-volume ratio, subtle physical

properties, electrical transport properties within the NS materials, improved sensitivity and limit of detection (potentially single molecule detection), and improved response time by nonplanar radial diffusion. Importantly, the enhanced specificity and reproducibility of the sensors originates from the desired physical properties incorporated into NS-FCPs *via* rational molecular design or subsequent covalent functionalization. The impedance between electrodes and electrolytes is lowered as NS-FCPs offer good conductivity, large specific surface areas, short path lengths for ion transport, and mixed electronic and ionic conductivities. Compared with the parent CPs, NS-FCPs are expected to exhibit improved performance in technological applications because of their nanoscale dimensions.

To further broaden the understanding of this review, the readers are encouraged to refer some of the recent reviews, regular articles and perspectives on the fabrications/preparations of semiconducting or conjugate polymer nanoparticles highlighting the recent advances and developments [41-45]. Typically, semiconducting polymeric dots are a special class of conducting polymer nanoparticle, exhibiting exceptional photophysical properties such as small particle size (20 – 30 nm) and high brightness, besides having good biocompatibility and surface properties [46, 47]. An interesting article describes the preparation of copolymer nanowires comprising of photosensitive polymer, azo and fluorene through single nanoparticle nanofabrication technique (SPNT) [48]. It was possible to control the radius (6 – 8 nm) and morphology (straight or wavy) of the fluorene-azobenzene based copolymer nanowires through tuning the components of both. The development of this kind of copolymers with electro-mechanical attributes can be considered as an advancement in this field. Similarly, authors demonstrate the fabrication of the nanowires by utilizing the conjugating polymers such as PFO, regioregular poly-3-hexylthiophene and poly[2-methoxy-5-(2'-ethylhexyloxy)-1,4-phenylenevinylene] and polystyrene derivative *via* alkyne click function [49, 50].

Multicomponent systems are often used in sensors to meet multiple requirements that cannot be fulfilled by simple materials [51]. For example, electrode-modifying materials for electrochemical sensors are expected to possess characteristics such as good electron transduction, stable enzyme immobilization, bioactivity, easy accessibility to the analyte, and a large surface area. However, all these important characteristics are not inherent to a single material. Hence, there is a great demand for the development of multicomponent materials, composed of two or more components, to achieve adequate sensor performance [52-56]. Hybrid multicomponent organic–inorganic materials comprising CPs or FCPs as one component and functional group incorporated metal and carbon nanostructures (**Category IV, Scheme 2**) have shown interesting properties owing to the size, composition, and shape of the individual components [57]. In this review, we define multicomponent FCPs about sensor application as materials included with FCP or CP and two or more additional functional components or functional group incorporated components.

Synthetic strategies evolved for the preparation of the different categories of FCPs (**Scheme 3**) are either based on conventional methodologies described widely in the literature or case specific methodology. **Scheme 3** depicts the important strategies used to synthesize FCPs for sensor applications. The precursors for the preparation and the generally utilized methodology for the preparation of each category of FCP is briefly tabulated (**Scheme 3**). Category I and II FCPs can be prepared using conventional methodologies employed for the preparation of pristine CPs, whereas special methods or specific approaches are utilized for the synthesis of Category II, III and IV FCPs. The readers can refer to the details of the conventional synthetic methods used for the preparation of FCPs in (Supporting information: SI: 2). Notably, sensor fabrication with CPs or FCPs involves film formation on a suitable substrate. The electrochemical synthetic method for FCPs offers the advantage of in situ film formation, whereas chemically synthesized CPs or FCPs require an additional film deposition step, such as dip-coating, spin-coating, layer-by-layer self-assembly, or drop-casting. The conditions or methodologies adopted for the fabrication of sensors with specific FCP are detailed in the appropriate sections below (especially for Category II, III and IV).

### Scheme 3

### 3. FCPs for sensors

FCPs prepared through functionalization/derivatization of parent structure of PPy, PANI, PT, PF and other CPs, were utilized for the fabrication of various types of sensors (gas sensors, biosensors and ion sensors, etc.) with the motivation to improve the sensor performances as compared to sensors fabricated with pristine CPs. The pie chart in **Fig. 1(A)** gives a quick idea about the proportion of publications (%) in each category of FCPs (listed in Scheme 1) on sensor applications. FCPs deduced from structural modification/derivatization of parent CP structure predominates (Category I, Scheme 1) for sensor applications with a higher proportion of publications (41%). The advent of nanotechnology and utilization of multicomponent in material design significantly increases the proportion of publications for Category III (22%) and Category IV (28%). The bar chart in **Fig. 1(B)** allows us to compare the publications (%) of FCPs based on PPy, PANI, PT, PF and PA in the four categories (**Scheme 2**) toward sensor fabrications. The details of the expanding diversity of FCPs based on PPy (Section 3.1), PANI (Section 3.2), PT (Section 3.3), PF (Section 3.4) and PA (Section 3.5) and innovative sensing mechanisms, improvements in sensor performances for various kinds of sensors (gas sensors, biosensors and ion sensors etc.) in different signal transduction (electrochemical, optical etc.) modes are detailed in the forthcoming Sections (3.1 to 3.5 and 4).

Fig. 1

### 3.1. Functionalized polypyrroles (F-PPys)

The major problems with the use of pristine PPy in sensor application are its very fragile structure and poor adhesion to electrodes. Attempts to overcome these issues have focused on incorporating PPy into a support matrix or functionalizing the PPy. Functional moieties are introduced into the sensor matrix in the form of F-PPys either as covalently bound functional groups in PPy structure, dopant ions for PPy chains containing the functional groups, or grafted polymers or nanocomponents containing the functional groups along with pristine PPy or F-PPys. Among substituted PPys, 3- and N-substituted PPys are the most commonly utilized FCPs for sensor applications. 3-Substituted pyrroles are asymmetric, whereas N-substituted pyrroles are symmetric. Polymerization of N-substituted pyrroles yields backbones with increased order and planarity compared with those obtained using 3-substituted pyrroles. Hence, N-substituted pyrroles are more commonly utilized for sensor applications. The electrical, electrochemical, and optical properties of F-PPys have been exploited as signal transducers [58]. Predominately, gas sensors, ion sensors, and biosensors have been fabricated with F-PPys. Table 1 summarizes the most significant aspects of each F-PPy including the functional group/ functional component(s) involved in the functionalization, the characteristics of sensors fabricated and the role of F-PPys for improving the sensor performances. **Table 2** provides the summary of the cross-sectional information amongst the various categories of F-PPys with respect to the fabrication of electrochemical, optical and other sensors. The details in Table 2 are provided for the sake of understanding the signal transduction wise utilization of the various categories of F-PPy.

**Table 1**

#### 3.1.1. Substituted or derivatized F-PPys

##### 3.1.1.1. Modification(s) of the parent PPy structure

###### **Gas sensors**

Earlier, F-Ppys such as poly(N-ethyl pyrrole), poly(N-(2-carboxy ethyl)pyrrole), poly(N-(6-hydroxy hexyl pyrrole)) and poly(N-(6-tetrahydroxy hexyl)pyrrole), were prepared by electrodeposition and utilized towards the fabrication of sensors for volatile organic compounds (VOCs) and chemical vapours such as hexane, toluene, methanol and triethyl amine, etc. sensors were fabricated. Different kind of

interactions such as dispersion forces, polarizability, hydrogen bond, etc was attributed to the sensing of an individual vapor compound. However, specificity to individual vapor was not demonstrated [59]. Over the periods, various gas sensors were fabricated with different F-PPys and specificity to analyte was demonstrated in the individual case. Few 3-alkyl substituted PPy derivatives were examined for the selectivity towards VOCs [60]. The authors demonstrated that selectivity towards organic vapors could be controlled by changing the substituents on the pyrrole ring. The introduction of longer alkyl group in 3-position of pyrrole rings increased the selectivity towards non-polar solvent vapors. Gas sensors have been developed for different types of solvent vapors and gas molecules, e.g., ammonia (NH<sub>3</sub>) and nitrogen dioxide (NO<sub>2</sub>), using PPy derivatives [61-64]. PPy functionalized with 5,10,15,20-tetraphenyl-21*H*,23*H*-porphyrin iron(III) chloride was used as a carbon monoxide (CO) gas sensor [65]. The CO molecule interacted with the central iron atom of the porphyrin, not with the nitrogen of PPy, and contributed electrons to the vacant Fe *d*-orbital. The injection of electrons into the PPy chains significantly reduced the hole charge carriers, resulting in increased resistance. Copper phthalocyanine substituted PPy was used for the detection of chemical vapors (methanol, NH<sub>3</sub> and NO<sub>2</sub>) [66]. The possible formation of charge transfer complex between phthalocyanine and NO<sub>2</sub> was suggested as the reason for good sensitivity with NO<sub>2</sub> as compared to methanol and NH<sub>3</sub>. The abilities of two *N*-cyanoethyl-substituted PPy derivatives to detect vapors of few aqueous or nonaqueous solvents were investigated [67]. Quantum mechanical calculations were attempted to investigate the affinity of PPy and poly[*N*-(2-cyanoethyl)pyrrole] (PNCEPy) toward different solvents (i.e., water, methanol, acetonitrile, and chloroform) and their influence on the geometric parameters (dihedral angle, inter-ring bond length, and bond length alternation) and electronic properties (ionization potential and  $\pi$ - $\pi^*$  lowest transition energy). Neutral PNCEPy interacted more favorably with polar molecules, such as water and methanol than unsubstituted PPy. The affinity of PNCEPy towards chloroform was relatively poor because chloroform interacted more favorably with the N-H unit in PPy than with the -CN group in PNCEPy. The superior response of PCNEPy to the vapors was explained regarding a secondary oxidation process resulting in the formation of carbonyl groups that could actively participate in recognition of analytes. Compared with unsubstituted PPy, PCNEPy had an increased oxidation potential and improved electron transport along the polymer backbone.

### **Biosensors**

There are several reports on the use of boronic acid-substituted PPys for various saccharides detection. A 3-(1*H*-pyrrol-1-yl)phenyl boronic acid-substituted PPy-based sensor was investigated for saccharide detection [68]. The binding interaction between PPy-phenylboronic acid and the saccharides had affinities in the following order: D-fructose > D- glucose > D-galactose > D-lactose > D-sucrose.

Ultrathin electrodeposited films of PNCPy and poly(*N*-methyl)pyrrole (PNMPy) and their composites with Au NPs were used for the electrochemical detection of dopamine (DA) [69]. Au NPs interacted more favorably with PNCPy than PNMPy and enhanced the electronic transfer and charge migration processes of DA oxidation. Quantum mechanical calculations performed using Gaussian D3 to examine the geometry and strength of the binding between the CPs and oxidized DA, showed that although PNMPy has a reasonable interaction with DA, the molecular rigidity of this polymer limits the detection process. On the other hand, the flexibility of the cyanoethyl group in PNCEPy induces a rearrangement of DA. This indicates that the interaction of oxidized DA with PNCPy is stronger than that with PNMPy allowing the electrochemical detection of DA at sub-micromolar concentrations (from 100  $\mu$ M to 10 mM). Functionalized PPy/ $\beta$ -cyclodextrin (PPy/ $\beta$ -CD) film deposited by electropolymerization of the pyrrole monomer in the presence of CD was utilized for the simultaneous detection of polyhydroxyphenols and neurotransmitters (epinephrine, metanephrine, and L-dopa (L-3,4-dihydroxyphenylalanine)) derived from pyrogallol and catechol [70]. The individual CDs could slide along and rotate around the polymer axes, allowing the glucose (Glu) units of CD to orient in the most favorable configuration and maximize their binding interactions. No peaks were observed at the PPy electrode with the analytes, including L-DA, D-DA, benzimidazole, and epinephrine, whereas fast and reversible peak responses were obtained at the PPy/ $\beta$ -CD-ME.

### ***Ion sensors***

The electrochemical sensing of dihydrogen phosphate ion was achieved using pyrrole-containing (ferrocenyl methyl)trialkyl ammonium derivatives [71]. The ion-pairing interactions between (ferrocenyl methyl)tetraalkylammonium cations and dihydrogen phosphate or adenosine triphosphate (ATP) anions were attributed to the sensing action. A rhodamine derivative of PPy (Rh-PPy) was synthesized with rhodamine B hydrazide and pyrrole-2-carboxaldehyde and used as fluorescence “turn-on” probe for  $\text{Cu}^{2+}$  detection [72]. Rh-PPy showed binding selectivity for  $\text{Cu}^{2+}$  over another co-existent alkali, alkaline-earth, and transition metal ions. Poly(11-*N*-pyrrolylundecanoic) acid and poly(*N*-undecyl pyrrole) were used as pH or hydrogen ion sensors [73]. The pH sensing behavior was attributed to the sensitivity of the carboxylic acid ( $-\text{COOH}$ ) groups to changes in the proton concentration.

#### ***3.1.1.2. Functional ion-doped PPy***

Since the first report on the electrosynthesis of PPy using tetraethyl ammonium tetrafluoroborate as an electrolyte [74], various other electrolyte compositions have been tried. As a consequence, a great structural diversity of produced PPy films has been achieved. During electrosynthesis, PPy is oxidized in

the presence of the electrolyte; hence, counter ions from the electrolyte can be incorporated into the PPy film to maintain its electroneutrality. In addition, other methods, such as vapor deposition of PPy films in the presence of anion dopants, have been utilized to incorporate the required anionic species into the film.

### **Gas sensors**

The gas sensing mechanism of neutral and doped PPy was compared through structure simulations considering the intermolecular interactions and charge transfer process between the analyte and F-PPy [75]. Doped PPys are predicted to exhibit remarkable interaction with  $\text{NH}_3$  through ion-dipole electrostatic forces. Frontier molecular orbital energies of the neutral PPy-gas molecule and doped PPy-gas molecule interactions confirm that the internal energy of PPy is perturbed by the gas molecule and PPy is selective towards  $\text{NH}_3$  gas as compared to  $\text{CO}_2$  and  $\text{CO}$ . The sensors based on doped PPys demonstrated fast response time and sensitivity towards aromatic hydro carbons (benzene, ethyl benzene, toluene, 1,3,5-trimethylbenzene) through  $\pi$ - $\pi$  electron donor-acceptor interaction with CP backbone. Phthalocyanine-doped PPy was fabricated on interdigitated electrodes for the detection of  $\text{NO}_2$  gas [76]. PPy was combined with ionic macrocycles as the counter ions and used for  $\text{NH}_3$  sensing. They explained that compared with PPy, the interaction of  $\text{CO}$  with  $\text{NH}$  groups in the phthalocyanine doped PPy caused the generation of positive charges/polarons and resulted an increase in conductivity. The transition metal ion in conjunction with PPy provided an electron transfer pathway. The N-sulfonated cobalt phthalocyanine doped PPy was electrodeposited on micropatterned microelectrodes and used for the detection of  $\text{NH}_3$  [77]. This sensor discriminated between concentrations of  $\text{NH}_3$  in the range of 20–80% relative humidity (RH), in contrast to traditional gas sensors. A film of dodecyl sulfate (DS)-doped PPy was prepared by vapor deposition polymerization of pyrrole on the surface of a polymer fiber in the presence of DS as an anion dopant [78]. A sensor was developed by the electrochemical functionalization of PPy with ferrocenylmethyltrimethylammonium iodide as a co-dopant [79]. PPy-zirconium(IV)selenol iodate (PPy/ZSI) cation exchange composite membrane was utilized towards the detection of formaldehyde gas [80]. The sensing mechanism involves the decrease in charge carrier mobility due to the interaction between the lone pair of electrons on the oxygen atom of formaldehyde and carbocation of PPy chains.

### **Ion sensors**

A hydroquinone sulfonate (HQS)-doped PPy electrode showed a significantly improved potentiometric response towards pH changes [81]. The potentiometric response was due to the  $-\text{NH}-$

groups in the PPy chain and the hydroquinone functionality. The –NH– groups are protonated or deprotonated as a function of pH, and HQS has a dual function as a dopant of PPy and an electroactive species that responds to pH changes. Therefore, incorporation of HQS into the PPy backbone increased the electrode sensitivity towards pH changes. The Triton doped PPy film was developed for the fluorescence detection of Fe<sup>3+</sup> ions. The sensor was fabricated exploiting the emission peak at 350 nm corresponded to Triton [82]. The ability of the anionic complexing ligand (Alizarin Red S) to extract the Ag(I) ion into the PPy membrane was utilized for the fabrication of an electrode towards Ag<sup>+</sup> ion sensitivity [83].

### 3.1.2. Functional compound included PPyS

#### Gas sensors

Pristine PPy based gas sensors exhibited moderate efficiency and longer reactivity time. On perusal of literature, it is known that the use of PPy-metal oxide NCs exhibited fast, reversible, reproducible and higher responses to gases than pristine PPy [84-86]. The readers can refer the review that details the crucial factors for the development of ultrafast responsive and high sensitive gas sensors based on G and reduced graphene oxide (rGO) [87]. The review includes the sensing mechanisms of gases for few of the G/rGO-CP NCs. The study on the NH<sub>3</sub> sensor based on rGO-PPy NC film informs that the NH<sub>3</sub> sensing responses of the rGO-PPy hybrid are higher than that of pristine PPy and its selectivity extends to ppm levels of NH<sub>3</sub>. Typically, 5 wt% rGO-PPy hybrid exhibited 2.5 times higher sensor response than that of pure PPy for 10 ppm NH<sub>3</sub>. The NH<sub>3</sub> sensing mechanism involves deprotonation-protonation processes through adsorption/desorption on the surface of the rGO-PPy hybrids. The specific enhancement of NH<sub>3</sub> sensing properties by the rGO-PPy hybrid is attributed to the high electron mobility of G to result in fast carrier transport, large surface area of G (that facilitation of adsorption of NH<sub>3</sub>), the possible  $\pi$ - $\pi$  stacking and H-bonding formation between PPy and rGO (**Fig. 2**) [88]. Also, the combination of n-type inorganic semiconductors (such as ZnO, SnO<sub>2</sub> and TiO<sub>2</sub>) and p-type semiconducting polymers such as PPy, was utilized towards the development of gas sensors due to their advantages of improved selectivity, sensitivity, and room temperature sensing characteristics. The PPy/ZnO nanohybrid (NH) sensor exhibited much better sensing properties towards low concentrations of NH<sub>3</sub> than the sensors based on either ZnO or PPy alone. When the NHs of PPy/ZnO contact with NH<sub>3</sub> gas, the adsorbed NH<sub>3</sub> molecules donate electrons to PPy. As a result, PPy was deprotonated and exhibited increased resistance. The 3D structure of PPy/ZnO NH allows the diffusion of NH<sub>3</sub> molecules further into PPy layer and to the inter-face between PPy and ZnO [89]. PPy was oxidized over ZnO NRs during the in-situ oxidative polymerization, and the resulted ZnO-PPy NC showed good selectivity

towards  $\text{NH}_3$  gas with a high sensor response as compared to pristine PPy. The high response of ZnO-PPy NC is attributed to the large surface area of ZnO NRs and camphor sulfonic acid (CSA) doping. Doping leads to improved charge transfer with extended delocalization of  $\pi$  - electrons over Ppy chains [90]. A similar sensing behavior was notified for PPy coated  $\text{SnO}_2$  NCs towards  $\text{NH}_3$  gas [91] and by Kelvin-probe force microscopy investigations [92]. The effect of nanofillers on the  $\text{NH}_3$  sensing efficiency of the PPy/ZnO NC-based sensors has been studied. The better  $\text{NH}_3$  sensing performance of PPy/ZnO-based sensor is correlated to the adsorption/desorption process of  $\text{NH}_3$  gas due to hollow nanotubular morphology as compared to a non-hollow structure [93]. The  $\text{NH}_3$  sensor based on bis-phthalocyanine modified PPy was developed for the detection of  $\text{NH}_3$  and putrescine in beef extracts. A possible coordination interaction between the Fe and nitrogen of amine compounds is suggested [94]. The geometrical as well as the electronic structures of 3PPy, before and after interaction with  $\text{SO}_2$ ,  $\text{NH}_3$ ,  $\text{H}_2\text{O}$ ,  $\text{CO}$ ,  $\text{CH}_4$  and  $\text{CO}_2$  are considered to correlate the chemical structure and their related properties towards the selection of the support matrix for an appropriate sensor [95]. The energy level of highest occupied molecular orbital/lowest unoccupied molecular orbital (HOMO/LUMO) level, as well as the density of states, provide evidence for hybridization between the sensing species and 3PPy. Natural population analysis and Milliken charge analysis showed that the interaction of 3PPy with all individual spices, except for  $\text{CH}_4$  and  $\text{SO}_2$ , results in the transfer of electrons from the analyte to 3PPy, but the reverse action happens for  $\text{CH}_4$  and  $\text{SO}_2$ .

**Fig. 2**

### ***Biosensors***

The biosensor performances of pristine PPy have been reported to be improved when PPy is functionalized or combined with carbon nanostructures, metal NPs, metal oxides because of the additional component contributes to high electrical conductivity, large surface area, and fast electron transfer rates. The electro-catalytic sites of PPy are additionally generated because of entrapped or entrapment metal NPs/G or graphene quantum dots (GQD) and form the basis for the development of several PPy-functional nanocomponent based biosensors. Besides, the sensitivity and selectivity of the PPy-nanocomponent composite based biosensors are improved, their detection limits reduced. Meng Lin [96] reported the fabrication of the Au NPs/ over-oxidized PPy (o-PPy) nanotube (NT) arrays composites electrode for the electrochemical determination of DA. The effective area of Au NPs on the surface of o-PPy NT arrays as well the increase in the electrostatic interactions between Au NPs and DA molecules are the reasons for good electrocatalytic activity towards DA. A fluorescent sensor for DA was developed based on PPy/GQDs core-shell hybrids [97]. The addition of DA quenches the fluorescent of PPy/GQD.

A non-enzymatic Glu sensor was developed based on PPy–NiO coated glassy carbon electrode (PPy–NiO/GCE). Glu oxidation was electrocatalyzed by PPy–NiO redox couple through the transfer of NiO to NiOOH and Ni(OH)<sub>2</sub> [98]. Periasamy et al. [99] developed a Cu<sub>2</sub>O/PPy based enzymatic Glu sensor. Oxidation of Glu on the surface of Cu/Cu<sub>2</sub>O mediates through Cu(II)/Cu(III) transitions or Cu/Glu complexes to convert Glu into gluconic acid and subsequently generate the carbonate structure via C-C bond cleavage. When Cu<sub>2</sub>O is combined with PPy, the electrochemical stability of Cu<sub>2</sub>O is improved over a wider potential window. The catalytic activity towards Glu electro-oxidation is attributed to the stability of the Cu<sub>2</sub>O/PPy electrode that is provided by PPy and high index facets of Cu<sub>2</sub>O octahedra [99]. A non-enzymatic electrochemical hydrogen peroxide (H<sub>2</sub>O<sub>2</sub>) sensor was fabricated based on PPy/Pt NC, prepared via microwave-assisted polyol process. The PPy/Pt electrode exhibited better electroactivity as compared to bare Pt electrode [100]. Prussian blue (PB) nanocubes are densely distributed onto hollow PPy (H-PPy) to form PB/H-PPy NC on the electrode surface and used for the electrochemical detection of H<sub>2</sub>O<sub>2</sub>. The fabrication of PB/H-PPy electrode involves deposition of PB on the surface of PPy and addition of acidic K<sub>4</sub>Fe(CN)<sub>6</sub> for dissolving the Fe<sub>2</sub>O<sub>3</sub> to obtain the hollow structure of PPy along with PB [101]. Electrocatalytic reduction based H<sub>2</sub>O<sub>2</sub> sensor was developed using the micro trunk like shaped PPy-Cu NC [102]. The electrochemical synthesis involves the inclusion of small sized functional dopant ion into PPy film and subsequent de-doping of PPy by electroreduction. The electroreduction introduces a cationic “pseudo dopant” during de-doping process of PPy chains. The sensing mechanism comprised of electroreduction of PPy-Cu(II) to PPy-Cu(I) and a chemical reduction of PPy-Cu(I) by H<sub>2</sub>O<sub>2</sub> to result OH<sup>-</sup> ions with the regeneration of PPy-Cu(II) catalyst. The high available surface area of as-synthesized PPyMTs-CuNPs sensor contributed to the high sensitivity and selectivity, wider linear range and the lower detection limit for the amperometric sensing of H<sub>2</sub>O<sub>2</sub>.

### ***Ion sensors***

A potentiometric Hg<sup>2+</sup> ion sensor was fabricated by plasticizing PPy with bis(1-benzyl-benzimidazolium-4-methyl sulfonamide; a bidentate bis N-heterocyclic ligand ionophore (NHCL) [103]. The NHCL ionophore exhibited the best Nernstian response towards Hg<sup>2+</sup> due to the strong selective complexation reaction between the ligand and Hg<sup>2+</sup> leading to the formation of Hg-carbon complex. PPy coated Pt NC was used as the Hg<sup>2+</sup> sensors based on functional particles included PPy composite. The faster electron transfer properties and electrocatalytic activity towards Hg<sup>2+</sup> were due to the increased surface area of Pt, higher conductivity of the composite and the existence of pores in the Pt/PPy NC. PPy backbone is partially oxidized by Hg<sup>2+</sup> ions, reduced to Hg<sup>2+</sup>, and subsequently complexed with PPy [104]. An electrochemical Pb<sup>2+</sup> sensor was fabricated based on cysteine functionalized GO to generate (sGO)/PPy NC. The PPy film was grown on sGO via  $\pi$ - $\pi$  stretching interaction and hydrogen bonding.

The sGO/PPy NC film showed electron transporting properties, large surface area, good conductivity and high affinity to  $\text{Pb}^{2+}$  [105]. Surface plasmon resonance based optical sensor for  $\text{Mn}^{2+}$  ions was constructed using  $\text{ZnO}_{(1-x)}\text{-PPy}_x$  NC. The change in dielectric constant of  $\text{ZnO}_{(1-x)}\text{-PPy}_x$  by  $\text{Mn}^{2+}$  ions was exploited for designing the  $\text{Mn}^{2+}$  ions sensor. The performance of PPy-ZnO NC towards  $\text{Mn}^{2+}$  ions was reported to depend on the individual components. ZnO is responsible for shifting the resonance wavelength to the longer range, and PPy reinforces ZnO matrix to function as a  $\text{Mn}^{2+}$  ions sensing layer. The sensing process involves the population of outer most three electrons of every  $\text{Mn}^{2+}$  ions and the electrons of the  $\pi$ -orbital conjugation of PPy in ZnO matrix [106]. The phytic acid functionalized PPy/GO ME was developed for the simultaneous determination of  $\text{Cd}^{2+}$  and  $\text{Pb}^{2+}$ . The resolved peak signals for  $\text{Cd}^{2+}$  and  $\text{Pb}^{2+}$  were obtained during electrochemical stripping detection of phytic acid functionalized PPy/GO NC. The reason is ascribed to the synergistic influence of the components; the enhanced electron transfer process of PPy, the existence functional groups with negative charges on phytic acid and the high surface area of GO [107].

### 3.1.3. Grafted PPys

As compared with the noncovalent mixing of G and the PPy, the establishment of a covalent linkage between G and PPy, via grafting, generates promising electrode materials for biosensors. J. Li et al.[108] reported a strategy (**Fig. 3**) to synthesize PPy-grafted nitrogen-doped G (PPy-g-NGE) towards developing an electrochemical sensing platform for paraquat (PQ). The PPy-g-NGE exhibited excellent electrochemical performances and electrocatalytic activities towards the redox reactions of PQ. G sheets are connected to PPy via covalent bonding as compared to the  $\pi$ - $\pi$  interactions for the PPy-G mixture. The covalent bonding was involved for the immobilization of the Pt NPs into 3-carboxylated PPy NPs over the surface of an amine ( $-\text{NH}_2$ ) functionalized interdigitated array electrode. The Pt-3-carboxylated PPy NC was anchored onto the substrate through the condensation reaction between carboxyl ( $\text{COOH}$ ) group of the NPs and  $-\text{NH}_2$  groups of the substrate. The Pt-3-carboxylated PPy NC-based field effect transistor (FET) exhibited high sensitivity towards DA. The DA sensing mechanism involves adsorption of DA molecules at the Pt-3-carboxylated PPy NC surface via  $\pi$ - $\pi$  interaction between the five-membered Py ring of 3-carboxylated PPy and six-membered benzene ring of DA, electrooxidation of adsorbed DA to o-dopamine quinone at the surface of Pt particles (through catalytic effects) and electron transfer to PPy [109].

**Fig. 3**

### 3.1.4. Biofunctionalized PPys

Biofunctionalization of CPS has been demonstrated to be an essential step in the fabrication of biosensors. The “biorecognition element” is usually immobilized onto the active area of the transducer for the analyte to be captured to achieve efficient signal transduction to occur. A variety of methods, such as electrostatic interactions, covalent interactions, and passive adhesion, is used to include the biofunctional element in the sensor matrix to obtain longer lifetimes and better immobilization control. In the one step biofunctionalization process, the appropriate covalent grafting of a pyrrole monomer by a biological molecule allows its immobilization onto the surface via electropolymerization. Biofunctionalization of ssDNA to PPy was done based on the one-step process [110]. However, for other cases such as enzymes and antibodies or proteins, additional grafting chemistry for relevant biomolecule is required. For example, a two-step biofunctionalization (post-functionalization) involves functionalization of pyrrole monomer by activated ester to allow binding of biomolecules [111]. The third method of biofunctionalization of PPy involves biotin/avidin system where biomolecules could be anchored to a biotinylated pyrrole [112]. Few of the nanostructured PPy/PPy derivatives were also biofunctionalized and utilized for sensor applications, and such details are discussed in the subsequent sections.

### **Biosensors**

Cellulose (the biopolymer) is a biocompatible matrix for enzyme immobilization. The immobilization of enzyme into cellulose happens via electrostatic interactions between the negatively charged cellulose and cationic species. The electronic characteristics of PPy are retained when PPy combines with cellulose and in addition to the retainment of biocompatibility and structural advantage of cellulose for enzyme immobilization. The synergistic effects of PPy-cellulose nanocrystal based composite were demonstrated towards improved electrochemical Glu detection [113]. Electropolymerization was performed with 3-(1-pyrrole) propionic acid in the presence of the enzymes, followed by the treatment with 1-ethyl-3-(3-dimethyl ammonium propyl) carbodiimide (EDC) to result in covalent linkage between glucose oxidase (GOx) and PPy derivatives. A few N-substituted pyrroles, such as *N*-(*p*-benzoic acid)polypyrrole (NpbPPy), *N*-(*o*-aminophenyl)polypyrrole, and *N*-(*m*-nitrophenyl)polypyrrole, were utilized for the fabrication of Glu biosensors [114]. The surface functionalization of PPy with *N*-(2-carboxyl-ethyl)-*N'*-(4-vinylbenzyl)-4,4'-bipyridinium dichloride (CVV) led to subsequent covalent immobilization of GOx [115]. Viologen was synthesized and covalently linked to PPy and then served as an anchor via its –COOH groups for the covalent immobilization of GOx. CVV acted as a mediator to transfer electrons between the electrode and enzyme and regenerated the enzyme through an enzymatic reaction with Glu. An enzymatic biosensor for Glu biosensor was fabricated by immobilizing GOx into PPy NT array through crosslinking of glutaraldehyde in the presence of BSA [116].

The Glu sensing performance of the biosensor fabricated with GOx immobilization via crosslinking was almost six times increased as compared to the biosensor fabricated using immobilized GOx via physical entrapment. An impedimetric biosensor was also constructed by electrodepositing  $\alpha$ -carboxy pyrrole ( $\alpha$ -COOH-PPy) onto an underlying film of PPy and subsequently immobilizing cytochrome c (cyt-c) [117]. The modified cyt-C/ $\alpha$ -COOH-PPy electrode was used for the electrocatalytic reduction of  $H_2O_2$ . The superior interaction between cyt-C and the negatively charged polymer surface was augmented by the applied potential.

**Fig. 4**

**Fig. 5**

The ribonucleic acids and microRNAs (miRNAs) are considered as the non-invasive biomarkers for early cancer diagnosis due to their altered expression levels in cancers. A detection platform for the breast cancer biomarker miRNA, (mir-21) was developed via doped PPy prepared via electropolymerization [118]. The results showed that doping of antimir-21 during polymerization increases the chance of hybridization due to the increased number of molecules as compared to the simple physical entrapment in the PPy film. A biosensor for DNA hybridization was reported based on a copolymer containing ferrocenyl-substituted pyrrole as an electrochemical probe and *N*-hydroxy phthalimide as a leaving group for the covalent attachment of DNA [119]. The DNA probes containing the amino groups were covalently linked through NH groups (**Fig. 4**). Thus, receptors were covalently linked to PPy through the reactive group of the monomer units in the polymer backbone. A label-free DNA sensor film was obtained by covalently linking oligonucleotides (ODNs) onto an electropolymerized film of poly(pyrrole-co-4-(3-pyrrolyl)butanoic acid [120]. The binding interaction between a biotinylated pyrrole derivative and a biological probe was utilized to construct a DNA biosensor [121]. The label-free electrochemical detection of the hybridization of short target DNA (18- and 27-mers) was reported based on electrochemically driven chloride ion exchange in films of 2,5-bis(2-thienyl)-*N*-(3-phosphorylpropyl)pyrrole modified with phosphoric acid (pTPTC3- $PO_3H_2$ ) [122]. The binding of the DNA probe with the phosphoric acid groups was mediated by  $Mg^{2+}$  ions. The excessive negative charges in the PPy-pTPTC3- $PO_3H_2$ - $Mg^{2+}$  probe DNA-ME blocked negative ion exchange and caused a decrease in the current. Charge neutralization of the nucleic acid was achieved through interactions of the phosphate groups, sugar hydroxyls, and endocyclic nitrogen atoms of the nucleobases with the positively charged metal ions. The electrostatic binding of  $Mg^{2+}$  to the phosphate groups provided significant stabilization of the double-helical structure. The increase of negative charges at the barrier owing to the formation of the double helix during hybridization was key for the detection of DNA hybridization. The electroconductivity of the PPy derivatives was exploited to trigger the electrochemiluminescence of a DNA sequence labeled

with a luminol derivative. A redox acridone derivative (RAD) was chemically linked to the electrode surface via an electropolymerized PPy derivative film containing *N*-hydroxysuccinimide groups [123]. The hybridization between two oligonucleotides (dsDNA-ssDNA) derived from a fragment of the West Nile virus envelope protein-coding region (1145–1180) through “fishing” out the duplex was determined using these MEs. Illustrative structures of few functionalized pyrrole monomers that have been developed for DNA detection are shown in **Fig. 5** [124]. Superoxide dismutases (SODs) are metallo-enzymes and they protect the organism against the toxic effects of superoxide ions. SOD is a first line defense against the oxidative stresses. A label-free electrochemical immunosensor for the detection of superoxide dismutase (SOD1) was developed based on the modification of screen printed electrode (SPE), via biofunctionalization of electro synthesized PPy with monoclonal antibody (anti-SOD1) (**Fig. 6**) [125]. The SOD1 immunosensor anti-SOD1/SAM/GNP/PPy/SPCE exhibited an excellent detection of SOD1 within nanomolar concentration and micromolar concentrations that are normally found in cyto sol of neuronal calls, plasma, serum, and blood. An electrochemical immunosensor was developed for the detection of melanoma cells immunosensor based on the affinity between cell surface melanocortin in 1 receptor (MC1R) antigen [126]. The anti-MC1R antibody (MC1R-Ab) was immobilized in amino-functionalized silica nanoparticles (n-SiNPs)-PPy NC. The authors could achieve a detection limit of 20 cells/MC modified on SPE (MC1R-Ab/n-SiNPs/PPy/SPE). An electro chemiluminescence (ECL) immunosensor based on PPy intercalated NH<sub>2</sub>GO (PPy-NH<sub>2</sub>GO) was reported for the detection of a reliable tumor biomarker CA72-4. The ECL immunosensor showed lower detection limit due to the excellent conductivity and catalytic activity of PPy-NH<sub>2</sub>GO and the large specific surface area of PPy-NH<sub>2</sub>GO [127]. The ability of the sensor to detect specific DNA segments was evaluated. PPy functionalized with  $\omega$ -(*N*-pyrrolyl)-octyl thiol moieties was immobilized with bovine serum albumin (BSA) and in vitro evaluation of an amperometric biochip designed for monitoring analytes such as Glu and lactate was described. Because of the expected blocking properties of the BSA layer, the electroactivity of the composite electrodes was attenuated before and after BSA adsorption [128].

**Fig. 6**

A herbicide biosensor electrode was fabricated based on the immobilization of anti-atrazine antibodies through binding to an *N*-substituted nitrilotriacetic acid (NTA)–PPy film electrogenerated on a gold electrode [129]. The poly NTA–PPy film was modified by the coordination of Cu<sup>2+</sup> ions with the chelating NTA centers and used for the determination of atrazine. The immune reaction of atrazine on the attached anti-atrazine antibody directly triggered an increase in the charge transfer resistance that was proportional to the atrazine concentration.

### **Ion sensors**

An impedimetric biosensor for detecting trimethylamine was developed based on ferrocenyl-substituted PPy [130]. A flavin-containing monooxygenase enzyme was copolymerized through covalent bonding. The ferrocenyl-substituted PPy can form covalent bonds with enzymes and ethylamine ferrocene through reaction with the terminal amine groups of the protein and the ferrocenyl group. The ferrocenyl group in the PPy matrix serves as a redox probe for monitoring the response of trimethylamine. Demirel Özel et al. [131] reported the synthesis of a PPy-containing vitamin B<sub>12</sub> derivative through the electrochemical copolymerization of vitamin B<sub>12</sub> with pyrrole to obtain an anion selective PPy-B12 film (pyrrole substituted corrin). They proposed a mechanism for thiocyanate ion selectivity involving cobalt coordination with the anion of interest. The selectivity could be modified by changing the nature of the environment that surrounds the corrin ring. The trace level detection of Hg<sup>2+</sup>, Cu<sup>2+</sup>, Pb<sup>2+</sup> and Cd<sup>2+</sup> was achieved using PPy-GOx [131-133]. The decrease in GOx activity with increasing metal ion concentration is correlated to the interaction between thiol group of the GOx and Hg<sup>2+</sup>. A label-free electrochemical aptasensor was developed to detect K<sup>+</sup> ions by using a PPy-co-3-pyrrolylacrylic acid copolymer film combined with a K<sup>+</sup>-specific guanine-rich aptamer as sensing probe. The K<sup>+</sup> ion specific guanine-rich base imparts selectivity towards K<sup>+</sup> ions [134].

### **3.1.5. Nanostructured F-PPys**

PPy nanostructures have large surface-to-volume ratios as compared with those of their conventional bulk counterparts and have the ability to offer amplified sensitivity and real time responses owing to the enhanced interactions between the NS-PPy and analytes. Also, PPy nanostructures can be functionalized to improve the selectivity towards an analyte. Mostly, biosensors and gas sensors have been fabricated using NS-PPys. Specifically, nanotubes (NTs) and nanowires (NWs) of F-PPys were predominantly utilized for the fabrication of biosensors and gas sensors. The sensor applications of nanostructured F-PPys other than NTs and NWs or NFs are detailed in Supporting information: SI:3.

#### **3.1.5.1. F-PPy Nanotubes**

##### **Biosensors**

Mainly, few papers have been published on the utility of NTs of carboxylated PPy (PPy-COOH NTs) for biosensors [135-143] and ion sensors [144]. The -COOH groups were appended onto the PPy

NTs using pyrrole- $\alpha$ -carboxylic acid. A liquid-ion gated FET sensor for the recognition of thrombin was fabricated with PPy-COOH NTs [141, 144]. The -COOH groups of the PPy-COOH NTs were used to immobilize the NTs on a sensor substrate and also to bind heparin. The sensing mechanism involved the reduction of the charge carrier density in the PPy-COOH NTs by screening the negative charge of heparin. The surface of a microelectrode substrate was modified with 3-aminopropyl tri-methoxy silane and PPy-COOH NTs were immobilized through coupling reactions [138]. Amine-terminated thrombin aptamers were selectively bound to the PPy-COOH NTs as receptors after modifying the 3'-end of the thrombin aptamer with primary aliphatic amine groups (**Fig. 7**) [137]. The selective recognition ability of the thrombin aptamers combined with the charge transport ability of the PPy-COOH NTs enabled the direct and label-free electrical detection of thrombin proteins. Upon exposure to thrombin, the PPy-COOH NT sensors showed a decrease in current flow due to the dipole-dipole or dipole-charge interactions between thrombin and the aptamer-conjugated polymer chains. A strategy to detect heat shock protein 90 (Hsp90) inhibitors as anti-cancer agents were developed with a FET sensor based on PPy-COOH NTs. Hsp90 was attached to the surface of the PPy-COOH NTs through condensation reactions between the terminal amino groups of Hsp90 residues and the -COOH groups on the PPy-COOH NTs. The enzymatic reaction product, H<sub>2</sub>O<sub>2</sub>, played a pivotal role in modulating the charge transport properties of the PPy-COOH NTs. A high-performance FET sensor based on an anti-vascular endothelial growth factor (VEGF) RNA aptamer conjugated with PPy-COOH NTs (CPNTs) was demonstrated [135]. A biosensor based on poly(ionic liquids) functionalized PPy NTs (PILs/PPyNTs) was prepared, and its electrocatalytic application has been demonstrated towards the simultaneous determination of DA and AA [135, 139]. The presence of PILs on the surface of PILs/PPyNTs not only changed the surface charge property and dispersibility of PPyNTs, but also effectively improved the transmission mode of electrons and conferred the differences in the electrocatalytic performance between the oxidation of DA and AA. A high-performance FET type Glu sensor was developed based on rGO - carboxylated PPy(C-PPy) NT hybrids using GOx as the Glu probe high coupling interaction between C-PPy NTs and enzyme via covalent bonding. The conductivity of rGO/C-PPy NT hybrid was higher than that of GO C-PPy NTs. C-PPy NT acted as a conductive channel to connect the G layer and enabled a decrease in resistance for rGO/C-PPy hybrid [143]. The invitro electrochemical detection of the VEGF cancer biomarker was examined using a p-type FET biosensor. The VEGF target molecule acted as a gate dielectric for the p-type FET sensor and specifically interacted with the anti-VEGF aptamer attached to the CPNT surfaces. A liquid-ion gated FET sensor based on enzyme (GOx)-functionalized PPy NTs was employed as the conductive channel towards the fabrication of Glu sensor [140]. The PPy NTs were immobilized onto a microelectrode substrate via covalent linkages followed by covalent binding of GOx to the NTs. The fabricated FET sensor provided a real-time response to Glu. The human taste receptor protein, hTAS2R38, functionalized with PPy-COOH NT-FET was developed as a nanobioelectronics tongue (nbe-tongue) and

displayed human-like performance with high sensitivity and selectivity [142]. The conversion of PPy-COOH NT-FET into a nbe-tongue was achieved by immobilizing the taster/non-taster receptors onto PPy NTs via covalent anchoring. The signal generated by the specific binding of target tastants or taste receptors was measured regarding the drain-to-source current. A highly sensitive and selective human nose-like nbe-nose for gaseous odorants was reported [136]. The enhanced electrical contacts between the electrodes, NTs, and the human OR protein not only provided excellent reproducibility but also improved the signal-to-noise ratio of the sensor. Moreover, increasing the contact area between the target molecules and PPy-COOH NTs induced a higher density of polaron or bipolaron states in the backbone of the PPy-COOH NTs. The human olfaction mechanism was mimicked by using PPy-COOH NTs with the human OR protein.

**Fig. 7**

### ***Ion sensor***

An electrochemical biosensor based on PPy-COOH NTs coupled with a tripeptide (Gly-Gly-His) was fabricated for  $\text{Cu}^{2+}$  ion sensing. The modification of COOH group of the polymer was done to accommodate tripeptide for the  $\text{Cu}^{2+}$  capture. The modification of PPy-COOH NT array electrode has been done via EDC/N-hydroxy succinimide (NHS) chemistries [144].

### ***Gas sensors***

The fabrication of open polyamine-modified conducting PPy NTs (PPy-NH<sub>2</sub> NTs) and their application as chemiresistive vapor sensors for acetic acid detection was reported [145]. PPy-COOH NTs were prepared as the precursor to PPy-NH<sub>2</sub> NTs using vapor deposition polymerization mediated by anodic aluminum oxide (AAO) template. Various amino-functionalized NTs were synthesized by modifying the surface of the PPy-COOH NTs with polyamidene chains containing different numbers of amine spacers. Ethylenediamine (EDA), diethylenetriamine, triethylenetetramine, and tetraethylenepentamine were employed as the open polyamine chain models. The structurally modified NTs were used as volatile analyte detectors. Negatively charged counter ions ( $\text{CH}_3\text{COO}^-$ ) were incorporated into the polymer to compensate for the positive charges on the polymer backbone, and the emergence of polaron or bipolaron states enhanced the conductivity. The PPy-EDA NTs exhibited a faster response than the PPy-COOH NTs because of an enhanced polymer/gas partition coefficient. They reported the increase in conductance due to compensated positive charges on the polymer backbone by

negatively charged acetate anions. Ag NPs were uniformly decorated onto the surface of PPy NTs to form PPy/Ag composite NTs and used for the construction of NH<sub>3</sub> vapor sensor [146]. Compared with PPy NTs, the introduction of metal onto the PPy NTs effectively promoted a chemiresistor response to NH<sub>3</sub>. The NH<sub>3</sub> sensor was fabricated using high-oriented single crystal PPy NT (SCPNT). The SCPNT based sensor NH<sub>3</sub> detected down to 1 ppb. The ultra-high sensor performance is attributed not only to the hollow structure and high surface area of PPy NT but also from the high crystallinity of intrinsically anisotropic PPy. The increased crystallinity caused decreased interchain hopping resistance [147]. A gas sensor for sarin simulant dimethyl methyl phosphonate (DMMP) was fabricated using PPy-COOH NT transducers. Force field calculation revealed the intermolecular interactions between PPy-COOH and DMMP via the formation of hydrogen bond and non-covalent coupling with the oxygen atom in the phosphoryl group of DMMP and P-COOH [148]. The sensing behavior by PPy-COOH is attributed to the doping effect of -COOH groups in PPy, the hydrogen bonding between DMMP and PPy-COOH NT.

### 3.1.5.2. F-PPy NFs/NWs

#### *Biosensors*

F-PPy NFs/F-PPy NWs and their composites were used for fabrication of biosensors and gas sensors [149-151]. An enzymatic electrochemical Glu sensor was fabricated utilizing the porous PPy NF network [152]. The good sensitivity for Glu was related to the strong affinity between GOx and PPy NF. An amperometric non-enzymatic Glu sensor was fabricated utilizing the electrocatalytic activity of o-PPy NWs modified with nickel hydroxide nanoflakes (nf-Ni(OH)<sub>2</sub>@o-PPyNW) [153]. The three-dimensional structure of o-PPy NW provides higher specific surface area and a vast number of micropores. The Ni(OH)<sub>2</sub>/NiOOH redox couple contributes to the electrooxidation of Glu. The possibility of the loading of Ni(OH)<sub>2</sub> nanoflakes with a high specific surface area onto a large amount of the o-PPy NWs surface, enhances the Glu oxidation rate and sensitivity of the nf-Ni(OH)<sub>2</sub>@o-PPyNW probe. Vertically self-assembled diphenylalanine peptide nanowires (PNWs) functionalized with PPy were demonstrated as suitable materials for cellular biosensing. The modified PPy-PNW electrodes were used as amperometric DA sensors [154]. The avidin-streptavidin PPy-NW generated changes in resistance down to 1 nM. Biologically functionalized PPy was formed by electropolymerization of an aqueous solution of monomeric pyrrole and avidin- or streptavidin-conjugated ZnSe/CdSe quantum dots [155]. EDC chemistry has been used to establish covalent surface biofunctionalization of PPy NWs with a cancer antigen (CA 125) antibody towards the fabrication of a nano-immuno sensor for the detection and quantification of CA 125 [156]. There was no loss of performance upon exposure to CA 125 in spiked human blood plasma, demonstrating the clinical importance of these sensors for cancer marker detection.

### **Gas sensors**

A highly orientated PPy-coated polyacrylonitrile (PAN) (PPy-PAN) NF yarn was prepared by electrospinning and used for the fabrication of NH<sub>3</sub> gas sensor. The nanosized coaxial PPy-PAN NF provides high surface area to volume ratio to benefit the sensor with more adsorption sites for the analyte molecule and unidirectional electron transfer path. The sensing mechanism involves the reversible interactions between the holes from PPy and NH<sub>3</sub> molecules to result in electron transfer and changes in resistance of the materials [157].

#### **3.1.6. F-PPys with multicomponent**

We reviewed the utilities of F-PPys containing two or more components, comprising of one or more nanomaterials, towards improving sensor performances.

### **Biosensors**

A multi-component (MC) matrix composed of chitosan (CS), PPy nanotubes (PPy-NTs) and Au-NPs (CS/PPy-NTs/Au-NPs) was developed for the immobilization of (GOx/CS/PPy-NTs/ITO) and a Glu biosensor was fabricated [158]. The inclusion of Au NPs facilitates the redox process with the electrodes. The PPy NTs promotes the electron transfer between GOx and electrode surface and CS offers a biocompatible environment for the enzyme to retain its natural enzyme activity. The MC material comprising of a PPy, Nafion (Nf) and functionalized MWCNTs (f-MWCNT) was immobilized with GOx and used for Glu sensing [159]. The presence of Nf provides stability to the film, good dispersion of fMWCNTs and covalent immobilization of GOx. The MC included F-PPy provides a biocompatible environment, increases the electrocatalytic activity of the immobilized enzyme, good electron transfer rate, and minimum GOx leaching. All these features contributed to high Glu sensor performances. A non-enzymatic Glu sensor was fabricated using a one-step electrodeposition method of PPy-CS-Iron oxide (Fe<sub>3</sub>O<sub>4</sub>) NC films onto indium tin oxide (ITO) electrode [160]. A two-step strategy was used to anchor NiCo alloy NPs onto PPy/rGO NHs towards the construction of a Glu sensor [161]. The Glu sensing process involves the transformation of NiO and CoO to Ni(OH)<sub>2</sub> and Co(OH)<sub>2</sub> and further to NiOOH and CoOOH, respectively. The electrooxidation of Glu was catalyzed by CoOOH/CoO<sub>2</sub> and NiOOH/Ni(OH)<sub>2</sub> redox processes. The PPy/rGO enhances the electrical conductivity and improves the catalytic property of NiCo alloy NPs. The combination of PPy and rGO resulted in higher electrical conductivity than the individual counter parts and provided more catalytic active sites. Additionally, PPy/GO NC augments good dispersion of NiCo

alloy NPs on the surface of the hybrids. A highly sensitive MC based non-enzymatic Glu sensor was constructed based on loading Au dispersed NiO NPs into PPy matrix [162]. The NiO@PPy/Au NC exhibited excellent catalytic performance toward Glu sensor due to synergistic effects of the components. The MC included with PPy NFs, Cu<sub>x</sub>O (Cu and Cu<sub>2</sub>O composite) NPs and rGO (Cu<sub>x</sub>O/PPy/rGO/GCE) was used for the detection of Glu [163]. A wide linear Glu concentration range up to 10 mM has been demonstrated because of the beneficial characteristics such as, more available active sites, high catalytic properties and large surface area of Cu<sub>x</sub>O/PPy/rGO/GCE. Nanopillar-enhanced electrodes (NEEs) were functionalized with GOx/PPy and used for the detection of Glu [164]. NEEs were fabricated by electrodepositing gold through porous AAO templates. NEEs were functionalized with GOx/PPy by electropolymerization and deposition via a galvanostatic process. The obtained NEE/GOx/PPy film was highly sensitive towards Glu.

The MCNCs composed of hydrophilic polymers (HP) such as polyacrylamide (PAM), polyacrylic acid (PAA) and polyvinylpyrrolidone (PVP)), functionalized PPy/GO nanosheets (HP/PPy/GO) were prepared by covalent modification on the surface of vinyl groups containing PPy/GO nanosheets [165]. The HP/PPy/rGO based sensor electrodes distinguish the DA and AA effectively in a mixture due to the role of the HPs having different hydrophilic groups and chemical properties. The rGO was electrodeposited onto positively charged poly(dimethyl diallyl ammonium chloride) modified polycaprolactone (PCL)@PPy membrane (rGO/PDDA/PCL@PPy NCs) and utilized for the construction of a DA biosensor [166]. The introduction of well-dispersed rGO onto the PCL@PPy fiber networks improved of the electrical conductivity and selectivity towards DA detection. An ECL sensor was fabricated for DA based on GO/PPy/CdSe NC [167]. The ECL sensing mechanism involves the production of sulfate ion radicals SO<sub>4</sub><sup>•-</sup> by the interaction with PPy matrix, and reaction between CdSe and SO<sub>4</sub><sup>•-</sup>. The ECL emission of CdSe was enhanced by the participation of PPy and rGO. Poly(3-(1-vinylimidazolium-3-yl)propane-1-sulfonate), (kind of poly(zwitterionic liquid)) functionalized PPy/GO exhibited good electrochemical catalytic activity towards the electrochemical detection of DA [168]. The DA cations are enriched on the electrode surface by the electrostatic interactions utilizing the negatively charged -SO<sub>3</sub><sup>-</sup> groups of the pendant chain in the zwitterionic polymer. The amine groups of DA interacts with oxygen-containing groups in PPy/GQD NC to result in intramolecular charge transfer or photoinduced electron transfer with a concomitant decrease in emission intensity [169].

An electrochemical H<sub>2</sub>O<sub>2</sub> biosensor was developed based on the modification of boron-doped diamond with mesoporous platinum and poly(pyrrole-3-carboxylic acid) based copolymer [170]. The amount of polymer coating and the copolymer composition influence the H<sub>2</sub>O<sub>2</sub> sensing characteristics. Particularly, the PPy copolymer exhibits minimum electrode fouling for real sample analysis. A non-

enzymatic  $\text{H}_2\text{O}_2$  sensor was developed based on core/shell/shell structure of  $\text{Fe}_3\text{O}_4/\text{PPy}/\text{Ag}$  NCs [171]. The  $\text{Fe}_3\text{O}_4/\text{PPy}/\text{Ag}$  NCs, PPy ME exhibited enhanced sensing signal for  $\text{H}_2\text{O}_2$  because of the increased conductivity of PPy, large surface area for the immobilization of Ag NPs, catalytic nature of  $\text{Fe}_3\text{O}_4$  and Ag NPs towards  $\text{H}_2\text{O}_2$  electrochemical reaction. In an, another report, a core-shell based NC with a composition of  $\text{Ag}@PPy/\text{polycaprolactone}$  was developed for the construction of a  $\text{H}_2\text{O}_2$  biosensor [172]. A non-enzymatic  $\text{H}_2\text{O}_2$  sensor was developed using PPy NFs–Ag NPs NC [173]. PPy NFs provide high surface area and the over-oxidation with concomitant reduction of  $\text{H}_2\text{O}_2$ .

The MCNC containing the combination of PPy, MWCNTs, and a dendrimer PAMAM G4 and rGO has been utilized as the transducer for pathogenic DNA in a complex matrix such as PCR samples to discriminate the mismatch bases of DNA from drug-resistant Mycobacterium tuberculosis [174]. Wrapping of MWCNTs with PPy and functionalization with PAMAM G4 on the surface avoid nonspecific interaction between MWCNTs and DNA. A high sensitivity DNA hybridization assay was proposed using an integrated PPy–Au NP composite [175]. The probe strand labeled with HRP was hybridized to the target (**Fig. 8**). The large surface area of Au NP for immobilizing the capture strand led to a current with an excellent signal-to-noise ratio, even at a low DNA concentration (150 pM). The sensitivity of the PPy–Au NP nanocomposite ME was 628% greater than that of the PPy ME. Moreover, the absolute currents measured at each DNA concentration were significantly higher because of the increased concentration of DNA capture strands when the Au NPs were present. Ag NPs functionalized with PPy-PANI NTs were prepared by a chemical method [176]. DNA labeled at the 5'-end using 6-mercapto-1-hexane (HS-ssDNA) was immobilized on the PPy-PEDOT-Ag surface to form PPy-PEDOT-Ag-S-ssDNA, and the hybridization sensing was carried out (**Fig. 9**) [177]. Similarly, a good platform for anchoring the thiolated HS-ssDNA is established by dispersing Ag NPs into PPy-PEDOT NTs. The hybridization efficiency was enhanced 2.7 times because this platform accommodated the optimum probe DNA density and the micro dispersed Ag NPs in the PPy-PEDOT nanostructure were sufficiently separated from each other to provide high target coiling efficiency. The beneficial properties of DNA biosensor, such as high catalytic efficiency, surface area and electrical conductivity, were collectively achieved. An electrochemical immunosensor was established for the detection of ofloxacin (OFL) based on a dual signal amplification strategy.

The immobilization of cholesterol oxidase (ChOx) and cholesterol esterase (ChEt) on a film comprising PPy, MWNT-COOH, and pTSA was carried out to fabricate a cholesterol sensor. ChOx and ChEt were immobilized on a PPy-MWNT nanocomposite electrode using DCC and NHS chemistry [178]. During the biochemical reaction, the positive charge of the PPy-MWNT biosensor accepted electrons from the re-oxidation of ChEt and ChOx before the evolution of oxygen, resulting in an enhanced current response for the biosensor. A biocompatible PPy film–Au nanocluster matrix was employed as a sensor

platform, and multienzyme-antibody-functionalized gold nanorods (GNRs) were fabricated as electrochemical detection probes [179]. Because of the dual signal amplification strategy of the Au nanoclusters/PPy architecture and the multi-HRP-GNR-Ab<sub>2</sub>, the electrochemical response of the fabricated immunosensor was greatly enhanced. While Au cluster-PPy provided the special structure to load a large amount of OFL antigen, GNRS served as a carrier to load a large amount of HRP.

**Fig. 8**

**Fig. 9**

### ***Ion sensors***

Femto molar detection of Hg<sup>2+</sup> was achieved using a MCNC comprised of PPy, pectin, and G [180]. Hg<sup>2+</sup> sensing is influenced by the high surface area and electrical conductivity of G, increase in the binding sites of the MCNC for Hg<sup>2+</sup> and interaction between the lone pair of electrons present on the reduced PPy and Hg<sup>2+</sup>. The PPy-chitosan/CoFe<sub>2</sub>O<sub>4</sub>-NPs MCNC was developed to detect As(V) ions using SPR signals. As(V) ions were adsorbed by CS and the magnetic properties of CoFe<sub>2</sub>O<sub>4</sub>-NPs contributed to the SPR signals. Magnetic response sensing was derived as the amino groups in CS involved in complexation in with As(V) and the generated defect-induced ferromagnetism [181].

### ***Gas sensors***

The MCNC consisting of p-type conductors (PPy and G nanoplatelets (GNs)) and TiO<sub>2</sub> nanoparticles were synthesized by a sol-gel process and used for the fabrication of NH<sub>3</sub> sensor. PPy-GN interacts with TiO<sub>2</sub> and restricts the motion of PPy chains. Two factors mainly contributed to the enhanced sensitivity towards NH<sub>3</sub> detection. First, TiO<sub>2</sub>@PPy-GN NC had a large surface area to enhance the gas diffusion and penetration into the depth of sensing layer. The second factor is the possible formation of p-n junction between TiO<sub>2</sub> and PPy-GN. The under particle electron transport from TiO<sub>2</sub> to PPy-GN, and creation of positively charged depletion layer caused a decrease in activation energy and enthalpy for the physisorption of NH<sub>3</sub> [182]. Multisegmented NWs (Au-PPy-Ni-Au) were synthesized by electrodeposition, and the sensor response towards NH<sub>3</sub> was demonstrated [183]. The components in the multisegmented NWs were integrated using magnetic dipole interactions between the ferromagnetic segment of the NW and electrode. NH<sub>3</sub> acted as a Lewis base and was reduced, and the transfer of electrons to PPy in the multicomponent array caused a decrease in conductivity. The utility of SnO<sub>2</sub>-ZnO/PPy coaxial nanocables prepared via electrospinning PVA containing SnO<sub>2</sub> and ZnO, followed by vapor-phase deposition of PPy, has been demonstrated [184]. Various sulfonic acids, such

as  $\beta$ -naphthalene sulfonic acid (NSA), dodecyl benzene sulfonic acid (DBSA), CSA and p-toluenesulfonic acid (p-TSA) etc. doped PPy-metal oxide NCs have been investigated for sensing properties. The structural and chemical nature of polymer is changed for creating more active centers for gas adsorption [185-187]. The p-TSA doped Ag-PPy thin film was found to be most sensitive and selective towards  $\text{NO}_2$  gas [188]. The improved response kinematics was attributed to the porous structure and faster charge transfer through ohmic contacts between PPy and Ag NPs upon interaction with  $\text{NO}_2$  molecules. Upon introduction of the  $\text{NO}_2$  gas on CSA (10–50%)-doped PPy–NiO NC matrix, CSA increases the rate of interaction between the sensor matrix and  $\text{NO}_2$  by offering further active sites to the PPy–NiO NC to result in the generation of polarons and bipolarons. Polarons are produced upon extraction of negative charge from the neutral PPy chain, and further removal of negative charge from PPy chains caused bipolarons. Thus, the dopant CSA alters the selectivity of PPy–NiO NC towards  $\text{NO}_2$  and generates more active sites for  $\text{NO}_2$  gas upon introduction of  $\text{NO}_2$  gas. The polaron-bipolaron densities are increased due to the interaction between  $\text{NO}_2$  gas and CSA doped PPy–NiO NC [186]. A similar sensing behavior was notified for DBSA-doped PPy– $\text{WO}_3$  hybrid NC-based sensor upon adsorption of  $\text{NO}_2$  gas [185]. A Pd– $\text{TiO}_2$ @PPy MCNC based hydrogen molecule sensor was developed [189]. The Pd– $\text{TiO}_2$ @PPy MCNC sensor exhibited enhanced sensor responses for  $\text{H}_2$  as compared to  $\text{TiO}_2$ @PPy NC and Pd@ $\text{TiO}_2$  NC. Zinc oxide-incorporated PPy (PPy/ZnO) NCs have been synthesized using ultrasound-assisted in situ mini emulsion polymerization of pyrrole in the presence of ZnO NPs and were used as a sensor for the detection of liquefied petroleum gas (LPG) [190]. A wider space charge layer is created through adsorption of LPG on the PPy surface and electron donation to result in more acceptor ions on the p-sided. As the surface of ZnO NPs is generally covered with negatively charged  $\text{O}^-$  ions, an electron depletion layer was created on the n-side of the junction. As a result, the carrier concentration at the p–n hetero (PPy(p-type)/ZnO(n-type)) junction was believed to be decreased, and the potential barrier height of the heterojunction increased, resulting in an increase in the resistance of the PPy/ZnO NC. Thus, the PPy/ZnO NC was sensitive to LPG and exhibited the properties of a p-type semiconductor. On the other hand, pristine ZnO is an n-type semiconductor and sensors based on ZnO are usually operated at higher temperatures. Transition metal ion-substituted Dawson-type polyoxometalates (POM)-doped PPy films exhibited a good response to  $\text{H}_2\text{O}_2$  [191]. An inner sphere electron transfer mechanism involving Fe(II)/Fe(III) was suggested for the electro catalytic behavior toward  $\text{H}_2\text{O}_2$  reduction. The parent Dawson POMs did not show any electrocatalytic response to  $\text{H}_2\text{O}_2$ .

On perusal of **Table 2**, one can understand that electrochemical sensors are predominantly fabricated using biofunctionalized and multicomponent categories of F-PPys.

**Table 2**

### 3.2. Functionalized polyanilines (F-PANIs)

Functionalized PANIs (F-PANIs) occupy a major proportion among FCPs developed for sensor application (Scheme 3). F-PANIs were developed for sensors in all four categories (Scheme 1). **Table 3** provides the information on the various F-PANIs developed through functionalization strategies, type of sensor fabricated with the individual F-PANI, the superior sensor performances achieved through functionalization and the mechanism of sensing involving the PANI FCPs. In general, PANI exists in three interconvertible redox states, namely, fully reduced leucoemeraldine (LE), half oxidized emeraldine (E) and fully oxidized pernigraniline, depending on the proportion of arylamine and quinone imine form in its structure. LE and E structures can be either in salt or base form [192]. The three forms of PANI exhibit different colors, conductivities, and stability. The sensors are fabricated utilizing the property changes in the three forms of PANI upon interaction with the analyte. Particularly emeraldine base (EB) form of PANI can be transferred into emeraldine salt (ES) form during the interaction of EB form of PANI with acidic moieties via transfer of protons to the nitrogen site. As an outcome, the lone pair of electrons at nitrogen are unpaired with a concomitant delocalization of the electrons over the conjugation length of the PANI chain. These modifications in PANI structure result in changes of electronic conductivity or resistivity. In the case of F-PANIs or derivatized PANIs, the functional groups participate in the analyte interaction process and alter the electronic conductivity of PANI structures.

**Table 3**

### **3.2.1. Substituted or derivatized F-PANIs**

The physicochemical properties of PANI-based MEs towards interaction with analytes were enhanced by the introduction of specific prospective groups into PANI chains through polymerization of substituted PANI or copolymerization of aniline monomer with substituted anilines or through the blending of another functionalized material with PANI or grafting of PANI or substituted PANI chains onto another substrate. In the latter methods of generating F-PANIs, a few functional nanocomponents, such as MWNT-COOH, were also included along with the PANI.

#### **3.2.1.1. Structural modification(s) of the parent structure**

##### ***Ion sensors***

A series of substituted PANIs based on 2-bromoaniline, 2-chloroaniline, 3-chloroaniline, 4-

chloroaniline, *o*-toluidine, *m*-toluidine, *p*-toluidine, *N*-methyl aniline, and diphenyl amines (DPA) were utilized for pH sensing. The changes in the color of the films showed a strong dependence on variations in pH [193]. Compared with PANI, poly(diphenylamine) and *N*-substituted PANI derivatives showed distinct and different pH sensing capabilities [194]. The protonation and deprotonation of PDPA chains and pristine PANI occur in entirely different pH ranges. The variation in the redox characteristics of these materials contributed to the notable difference in optical sensor characteristics towards pH. PDPA showed pH dependent optical responses in the pH range from 2 to 13. A Humidity sensor was developed using poly(diphenylamine sulfonic acid) [195] by electrochemical impedance spectra (EIS) measurements. A sensing mechanism involving the ion transport via doped ions was suggested. In general, metal ion sensors have been developed utilizing the interaction between metal ions and functional groups in PANI FCPs. An imidazole functionalized PANI (IMPANI) has been developed as a  $\text{Pb}^{2+}$  ion sensor [196]. The selectivity for  $\text{Pb}^{2+}$  ions was due to the complexation of  $\text{Pb}^{2+}$  ions with IMPANI. A PANI–Rhodamine 6G derivative (RS) (PANI–RS) was subjected to photovoltaic measurements in the presence and the absence of  $\text{Hg}^{2+}$  [197].  $\text{Hg}^{2+}$  was detected by the photon excitation from the RS– $\text{Hg}^{2+}$  complex. The energy level diagram based on the spectrophotometric and electrochemical properties of the RS dye and PANI predicted a photocathodic response towards  $\text{Hg}^{2+}$  for the PANI–RS composite electrode. An impedimetric sensor for  $\text{Pb}^{2+}$  ions was developed based on a PANI–pseudo-poly rotaxane film formed by the inclusion of PANI in amino-functionalized  $\beta$ -cyclodextrin ( $\beta$ -CD). The spatial conformation changes in PANI chains were attributed for sensing action [198, 199]. The heptakis-(6-amino-deoxy)-cyclomalto heptase ( $\beta$ -CDpNH<sub>2</sub>) was used as a host for complexation with aniline monomers, and subsequent polymerization resulted in PANI– $\beta$ -CDpNH<sub>2</sub> film. The impedance changes of the PANI– $\beta$ -CDpNH<sub>2</sub> ME upon interaction with  $\text{Pb}^{2+}$  cations were investigated. The bulk resistance of the PANI– $\beta$ -CDpNH<sub>2</sub> film increased with  $\text{Pb}^{2+}$  concentration, indicating a high activity and mobility of the cations within the film because of the presence of  $\beta$ -CDpNH<sub>2</sub>. The CN<sup>−</sup> groups containing poly(diphenylamine-co-2-aminobenzonitrile) (P(DPA-co-2ABN)) film was obtained through electrodeposition and used for the simultaneous determination of  $\text{Cd}^{2+}$  and  $\text{Pb}^{2+}$  [200]. The CN<sup>−</sup> groups in the P(DPA-co-2ABN) film coordinated with the heavy metal ions  $\text{Cd}^{2+}$  and  $\text{Pb}^{2+}$ , and improved the preconcentration at the electrode surface. The electrochemical stripping of  $\text{Cd}^{2+}$  and  $\text{Pb}^{2+}$  ions with P(DPA-co-2ABN) was compared with that of pristine poly(diphenylamine) (PDPA) (does not contain CN<sup>−</sup> groups) to highlight the significance of the CN<sup>−</sup> containing polymer for trace level detections. Further, the covalent attachment of the –CN groups to the polymer backbone improved the sensor performance even at pH > 4, whilst pristine PANI or PDPA could not be improved. The electronic transitions in PDPA are significantly different from those in pristine PANI because PDPA can exhibit characteristics of both PANI and Poly(*p*-phenylene). PDPA showed electronic transitions that corresponded to the existence of diphenosemiquinone amidoamine and diphenoquinone diimine structures [201].

### **Biosensors**

Simultaneous determination of DA and AA was achieved due to preferential oxidation of AA ahead of DA with a potential difference of 325 mV between them. The readers can refer to books and reviews concerning boronic acid-based optical and electrochemical sugar sensors [202-205]. Recently, there have been a few reports on the use of poly(3-aminophenyl boronic acid (PAPBA) based sensors [206, 207]. A photonic crystal based Glu sensor was developed used to continuously monitor relatively high Glu concentrations by tethering boronic acid recognition molecules to a polymerized crystalline colloidal array [208]. The sensing mechanism indicated that Glu binding depended on the concentration of boronic acid. The aniline and dithiocarbamate ester groups containing monomer, *N*-(*N*',*N*'-diethyldithiocarbamoyl)ethylamidoethyl)aniline (NDDEAEA), was synthesized and used to prepare poly(NDDEAEA) [209]. Poly(NDDEAEA) has integrated functionalities (e.g., conductivity and molecular recognition, catalysis, and controlled transport properties) for sensor applications.

### **Gas sensors**

A variety of substituted PANIs, such as poly(*o*-toluidine), poly(*o*-anisidine), poly(*N*-dimethylaniline), poly(ethylaniline), poly(2,3-dimethylaniline), poly(2,5-dimethylaniline) and poly(diphenylamine), were used for sensing different alcohol vapors (methanol, ethanol, propanol, butanol, and heptanol) [201]. The changes in the resistance of the polymers on exposure to alcohol vapor were monitored. However, a quantitative conclusion relating structural modifications to sensor performance has not been derived.

#### **3.2.1.2. Functional ion-doped PANIs**

In general, doping and undoping of anions were found to occur in the redox reactions of PANI to compensate charges in the polymer chain. The doping level of PANI chains can be controlled via a non-redox acid-base doping-dedoping processes. The dopant in the PANI chains can be removed by a reversible reaction through interaction with any strong base or proton abstracting molecules. The dopant removal from the PANI chain is associated with conductivity changes. Thus, redox active chemicals or gasses can change the conductivity of PANI by changing its oxidation states. Functional groups containing ions, derived from electrolyte or surfactant, such as sodium dodecyl sulfate (SDS), are

incorporated into the PANI matrix via doping. Doped PANIs are thus suited for ion/gas sensor applications because they not only show high conductivity and electroactivity but can also be functionalized to improve selectivity towards certain ions.

### **Gas sensors**

PANI films doped with hexafluoroisopropanol showed good sensitivity to hydrazine [210]. PANI was doped due to the interaction between hexafluoroisopropanol in the PANI matrix and hydrazine generated hydrofluoric acid and increased the conductance. The  $\text{NH}_3$  gas sensing properties showed variations between SDS doped PANI prepared through two oxidizing agents, ammonium peroxodisulfate (APS) and potassium dichromate (PDS) [211]. Typically, the APS oxidized PANI-DBSA film has shown better  $\text{NH}_3$  sensing properties a compared to chromate oxidized PANI film. This has been explained based on the multiple oxidation states for chromium while oxidizing aniline by PDC. Doped (PANI-HCl)/PET films showed linear optical responses to  $\text{NH}_3$  gas [212]. A dioctyl sodium sulfosuccinate-doped PANI optical microfiber sensor was fabricated for the detection of alcohols [213]. The sensor response was associated with the changes in refractive index of the solution depending on the chain length of the alcohols. Aliphatic alcohol vapor sensing characteristics were evaluated using doped polyvinyl alcohol (PVA)-PANI membrane [214]. PVA-PANI membranes were doped with various dopants, namely, CSA, p-TSA and L-ascorbic acid. The PVA-PANI membrane based sensors exhibited a spontaneous decrease in electrical resistance upon exposure to the aliphatic alcohol. A faster recovery back to the original oxidation state of PANI is regulated by air. The functional groups (i.e.,)  $-\text{SO}_3\text{H}$ ,  $-\text{COOH}$ ,  $-\text{OH}$  in the respective dopants favorably interact with the PANI chains and generate H-bonding/dipole interactions with alcohol molecules causing delocalization of electrons in the polymer back bone and turn decrease the resistance. The more polar group-containing alcohol responds to the membrane effectively making the sensing response towards alcohols in the order: methanol>ethanol>isopropanol>propanol. Molecular modeling on the effect of different functional groups was carried out on deciding the ability of SPAN for  $\text{CO}_2$  sensing and was compared to pristine emeraldine-PANI [215].

### **Biosensors**

Cupric ion doped PANI hybrid matrix ( $\text{Cu}^{+2}$ /PANI) was developed as an optical non-enzymatic Glu sensor based on the generation of selective Glu catalytic sites due to the combined presence of  $\text{Cu}^{+2}$  ions and PANI. The oxidized products were to monitored using a dyes based indicator system monitor Glu sensing in aqueous solution as well as in biological fluids [216]. Polyoxometalate (POM), an anionic

metal-oxygen cluster, doped PANI was developed as a nanopillar electrode and used for the detection of  $\text{H}_2\text{O}_2$  [217]. The improved  $\text{H}_2\text{O}_2$  sensing performance of POM-PANI-nanopillar electrodes is explained. The large surface area of 1D nanostructure POM-PANI-nanopillar electrodes and the multiple redox reactions of POMs contribute to the rapid and efficient ion and electron transfer during the electrochemical process. An immunosensor was fabricated based on Ag NPs doped PANI through immobilization of polyclonal anti-poly chlorinated (PCB) antibody via glutaraldehyde as the covalent linker [218]. The transducer fabrication involves enamine formation from PANI upon interaction with glutaraldehyde and transformation into the imine upon adding the antibody. The presence of Ag NPs and chloride ions contribute to the simultaneous PANI doping. The immuno- biosensor exhibited good analytical parameters (limit of detection (LOD) and limit of quantification (LOQ)) against PCB 28.

### ***Ion sensors***

A hand held sensing system had been developed by exploiting ion sensitive FET to couple with electrochemical signal wirelessly to a smart phone [219]. The sensor fabrication involves the use of dinonylnaptalene sulfuric acid doped PANI (PANI-DNNSA) layers as the transducing layer between the electrically conductive and ionically conductive, ion selective membranes. The PANI-DNNSA layer significantly reduces the drift of the electrodes as compared to a configuration without the transducing layer. The other advantage is the easiness to use with a transistor based detection that can be modified for a vast variety of existing potentiometric tests. PANI was electro-synthesized on the surface of SCE in the presence of SDS as the dopant and used as a transducer in a solid-state ISE for  $\text{Hg}^{2+}$  ions [220]. The  $\text{Hg}^{2+}$  ions sensing mechanism consists of the steps; i)  $\text{Hg}^{2+}$  ions adsorption and ii) deposition of  $\text{Hg}^0$  and iii) stripping of  $\text{Hg}^0$ .

### ***3.2.2. Functional component inclusion into PANIs***

#### ***Gas sensors***

Carbon nanomaterials (MWNT, SWNT, and G) have been tested for sensing various gas molecules, and much efforts have been put into the development of  $\text{NH}_3$  gas sensors in conjunction with F-PANIs. The gas sensing mechanism is based on the changes in conductivity as the consequence of charge transfer between electron donating/electron withdrawing molecules and the semiconductors carbon nanomaterials. A facile electrochemical method to functionalize SWNTs with PANI derivative was demonstrated. SWNTs were covalently attached to poly (m-aminobenzene sulfonic acid) (PMABS), and the  $\text{NH}_3$  sensor was fabricated [221]. When  $\text{NH}_3$  molecules interact with PABS chains, it caused changes

in the electronic structure of PMABS. The formation of zwitter ionic state with SWNT caused good sensor performances (**Fig. 10**). PANI-SWNT network exhibited a good response to  $\text{NH}_3$  gas [222]; this gas sensor was sensitive, had a very low detection limit, and had good reproducibility compared with pure SWNT-based sensors. The  $\text{NH}_3$ ,  $\text{NO}_2$ , and  $\text{H}_2\text{S}$  gas sensing properties of PANI-SWNTs were investigated and the gas-sensing mechanisms involving the deprotonation of PANI by  $\text{NH}_3$  were proposed [223]. In the case of unfunctionalized SWNTs, the sensing mechanism for  $\text{NH}_3$  involved electron transfer between electron donating molecules and the SWNTs. In the case of the PANI-SWNT-based sensor, gaseous  $\text{NH}_3$  molecules adsorbed on the SWNT-PANI deprotonated the  $\text{N}^+\text{-H}$  sites of the emeraldine-PANI salt to form  $\text{NH}_4^+$ . Sensing experiments performed with different gas analytes, such as  $\text{NH}_3$ ,  $\text{NO}_2$ , and  $\text{H}_2\text{S}$ , revealed that PANI-SWNTs responded to conductivity changes by transferring  $\pi$  electrons from PANI to  $\text{NO}_2$  and by the partial dissociation of  $\text{H}^+$  and  $\text{HS}^-$  with  $\text{H}_2\text{S}$ . Dimethyl-methyl-phosphonate (DMMP) is a typical simulator of sarin. A DMMP gas detection method has been developed using a semiconducting SWCNT and conducting PANI composite [224]. DMMP molecules donate electrons to SWCNT during the interaction between DMMP and SWNT, and the interactions could be enhanced by functionalization of SWNT with COOH groups. The donated electrons to SWNT decrease the electron density and increase the resistance of the SWNT-PANI composite. PANI matrix preferably adsorbs DMMP molecules and decrease the density of polarons and PANI resistance. These features cause good response time for SWNT-PANI composite. The effects of radio frequency oxygen plasma treatment on the  $\text{NH}_3$  gas-sensing characteristics of multi-walled carbon nanotube (MWNT)/PANI composite films were investigated using sensor devices fabricated on a microelectromechanical system-hotplate [225]. The oxygen-containing defects on the surface of plasma-functionalized MWNTs (pf-MWNTs) provided binding sites for PANI, facilitated the CNT-PANI bond, and promoted conduction between the MWNTs and PANI. The pf-MWNT/PANI films exhibited a superior linear response for detection of  $\text{NH}_3$  with a 3-times higher sensitivity than the corresponding pristine MWNTs. This dramatic improvement was attributed to a resistance change of PANI owing to deprotonation and a resistance increase of the MWNTs because of electron transfer from PANI to the MWNTs. Similarly, the sensing capability of a PANI/MWNT-COOH NC to different chlorinated methane vapors was examined and compared with that of pure PANI [226]. The MWNT-COOH favorably interacted with the PANI chains, created a pathway for strong dipole interactions with chloroform molecules, facilitated electron delocalization and charge transport through the PANI chain. Consequently, the resistance exposed NC decreased. A new biaxially stretchable  $\text{NO}_2$  gas sensor, derived from integrated micro super capacitor was developed. The integrated gas sensor comprises of PANI wrapped MWNT and an ion gel. The  $\text{NO}_2$  sensing mechanism includes the withdrawal of electrons from the G and enhancement of hole concentration upon adsorption of  $\text{NO}_2$  onto G [227].

**Fig. 10**

G is a promising candidate for gas sensor because of the large surface area, good interaction between adsorbates and G sheets via weak van der Waals forces to strong loading, high carrier mobility (low resistivity) and low noise for charged electron fluctuations. Substitutional doping of G with hetero atoms (e.g., B or S) causes disruption of  $sp^2$  hybridization and creates the possibility of making p or n doping for G. Due to the inclusion of heteroatoms; band gap opening has also been notified to alter the electronic band structure. G or GO in combination with polymers exhibited an improved sensitivity for gas sensors. The NC of GO-doped PANI was utilized as a methanol vapor sensor and compared with pure PANI [228]. The resistivity of PANI increased exposure to methanol vapor because of strong hydrogen bonding interactions between methanol and the PANI chain. Compared with pure PANI, the presence of GO in the PANI/GO composite increased the sensitivity towards methanol. The gas sensing features of G are detailed in a review [229]. The enhancement of sensing properties for the S, N: GQDs/PANI hybrid is due to the increased hole like carriers generated by S, N:QDS, the reversible acid-base doping-dedoping process of PANI and interaction of  $NH_3$  molecules through  $\pi$  electron networks [230]. Zhang et al. [231] compared the effectiveness of sensing with B and N doped G towards gas sensing through theoretical conclusions. In a report on flexible  $NH_3$  sensor based on PET film loaded with rGO–PANI NH, the sensor performance improvements are ascribed due to the large surface area of the NC, enhanced  $NH_3$  adsorption/desorption processes, high carrier mobility from rGO, and electron transfer between conjugated PANI chains and GO through  $\pi$ - $\pi$  interactions [232].

Sulabha Kulkarni et. al., demonstrated that the inclusion of gold nanostar in PANI film enhanced the sensing activities towards  $NH_3$  [233]. Au nanostar makes intimate contact with PANI and favors the formation of semi-covalent dative bond between in PANI and Au atoms. This feature is possible because of the presence of the kink and sharp tips in the Au stars making the N atoms in PANI as electron deficient. ZnO NRs were loaded with a layer of PANI through spray coating and utilized for  $NH_3$  sensing. The porous structure, the high aspect ratio of NR and the cracks developed during the synthesis contributed for high sensitivity for  $NH_3$  detection as compared to pristine PANI [234]. The gas sensing properties of Cu NPs incorporated PANI NC thin films toward  $NH_3$ , CO,  $CO_2$ , NO and  $CH_4$  were evaluated at room temperature [235]. Sensing of  $NH_3$  is based on the deprotonation and reprotonation processes. The intercalated Cu NP within PANI matrix contributed towards improved charge transport and the interaction with the gas analyte. The aliphatic aldehyde gas sensing ability of poly(*o*-anisidine) [(PoANIS) $_x$ MoO $_3$ ] organic–inorganic layered composite was studied along with a (PANI) $_x$ MoO $_3$  composite [236]. The (PANI) $_x$ MoO $_3$  hybrid film showed a strong response in the form of resistance change to formaldehyde, a medium response to acetaldehyde, and a less significant response to *n*-hexaldehyde, indicating that the sensor behavior depended on the molecular size of the aldehyde. However, the (PoANIS) $_x$ MoO $_3$  hybrid film

showed an almost equal response to formaldehyde and acetaldehyde. The extraction of dopant ion from the sensing matrix and withdrawal of protons from PANI chains were assigned as the reasons for the sensing action. Similarly, the layered organic/inorganic hybrid thin film composed of  $\text{MoO}_3$  and poly(*N*-methylaniline) (PNMA) was prepared and used as a VOC sensor [237]. The  $(\text{PNMA})_x\text{MoO}_3$  hybrid thin film was formed by intercalation and ion-exchange of sodium ions for PNMA into  $\text{MoO}_3$  interlayers. The sensing ability of the  $(\text{PNMA})_x\text{MoO}_3$  hybrid thin film toward acetaldehyde was as high as to formaldehyde, whereas typical organic/ $\text{MoO}_3$  hybrids and PANI/ $\text{MoO}_3$  showed a higher sensitivity to formaldehyde than to acetaldehyde.

**Fig. 11**

An  $\text{NO}_2$  gas sensor was fabricated based on PANI-ZnO NC [238]. The enhancement in sensing performance is supposed because of the maximum adsorption sites and trapping of electron transfer from the valence band to the conduction band (**Fig. 11**). A cigarette smoke sensor was developed using a PANI/silicon carbide (PANI/SiC) NC, prepared by an in situ chemical oxidative polymerization technique in an acidic medium [239]. A comparatively low response for  $\text{CO}_2$  and methanol and a good response for  $\text{NH}_3$  were observed. The conductivity changes are attributed to the neutralization of PANI chains through the interaction of a lone pair of an electron on the nitrogen atoms or interaction with the lone pair of an electron on the oxygen atom of  $\text{CO}_2$  or interaction of the lone pair of an electron in the oxygen atom of  $\text{CH}_3\text{OH}$ . The greater sensitivity and excellent reversibility of the PANI/SiC-NC are ascribed to the increase in the high surface area of PANI coated SiC NPs. This leads to the exposure of more active sites and adsorption - desorption possibilities.

### **Biosensors**

The channel of the field-effect device was modified with MWNT-COOH/PANI NC, and GOx and a Glu biosensor were fabricated [240]. The number of available holes and consequently the hole conductivity decreased significantly due to the electrostatic interaction between the negative surface charges of GOx and the accumulated positive charges in PANI chains. The changes in resistance due to electrostatic interacting provide the basis for Glu detection. The fabrication and performance of an impedimetric Glu biosensor based on PANI-PEO NC are reported [241]. An electrochemical compact disc platform was developed based on G-PANI NC, and cobalt phthalocyanine (CoPc) electrocatalyst and the Glu sensor was fabricated [242]. The sensor showed good selectivity towards Glu due to the shift in oxidation potential because of the presence of CoPc electrocatalyst. Carbon quantum dots (CQDs) are quasispherical NPs consisting of amorphous to nanocrystalline cores, predominantly derived from G and

GO sheets fused by diamond-like  $sp^3$  hybridized carbon moieties. Utilizing the FET between CQDs and PANI, an enzymatic Glu sensor was fabricated [243]. The Glu concentrations were correlated to the changes in the fluorescence quenching of CQDs caused by the presence of PANI layer. The synergistic effects such as large surface area and biocompatibility and a decrease in steric hindrance for the enzyme (GOx) towards the transfer of an electron to the electrode surface from the individual components contributed to the good Glu sensor performances. A non-enzymatic impedimetric Glu sensor was fabricated by including Au NPs into PANI film [244]. The sensor was designed based on the charge transfer reaction at the PANI-Au NC/Glu interface and associated impedance changes. A PAPBA/Au NC was synthesized by a one-pot chemical oxidative method and utilized as a sensing probe in a non-enzymatic Glu sensor [245]. The PAPBA/Au NC exhibited good electrocatalytic activity with high selectivity for the oxidation of Glu owing to the synergistic properties of the boronic groups, conducting PANI matrix, and Au NPs built into the NC. A core-shell type  $NiCo_2O_4@PANI$  NC was used to fabricate a non-enzymatic Glu sensor [246]. The core-shell  $NiCo_2O_4@PANI$  NC combined the advantages of the good contact with the analyte and efficient electron transport to the electrode. Typically, the core-shell  $NiCo_2O_4@PANI$  NC network provides effective electron conductive channel with a simultaneous shortening of electron transport distance to the electrode. These features contribute to high sensitivity towards Glu detection. D-glucosamine is an amino mono saccharide that can be found in connective tissues and mucosal membranes. D-glucosamine is used to alleviate the symptoms of osteo arthritis. A chip based electrochemical D-glucosamine sensor was developed using carbon paste electrodes modified with AuNPs and PANI [247]. The optimized conditions for achieving good sensor performances was derived based on a central composite design and a responsive surface diagram.

Layer by layer films comprising of alternate layers of poly(2,5-dimethoxyaniline) and phosphotungstic acid was fabricated through electrodeposition, and chemical dipping, respectively and an AA sensor was fabricated [248]. PANI has been uniformly coated on the surface of chemical vapor deposited CNTs to fabricate a three-dimensional network structure based AA sensor [249]. The PANI deposited on CNT caused improvement in electrochemical stability. Simultaneous determination of adenine and guanine was achieved through a  $MoS_2$ -SPAN/CPE based sensor [250]. The strong electrostatic repulsion between the negatively charged SPAN and  $MoS_2$  as well the  $\pi$ - $\pi^*$  stacking effect, between the SPANs and  $MoS_2$  were utilized towards the construction of the AA sensor. The alternate negative charges at the  $MoS_2$ -SPAN/CPE hybrid caused good adsorption of positively charged molecules. The fabricated  $MoS_2$ -SPAN/CPE owns a large surface area and excellent electrocatalytic ability to detect the positive and rich-conjugated molecules, such as the free base of DNA. Compared to the electrochemical performance of sole  $MoS_2$ /CPE and SPAN/CPE, extremely enhanced electrochemical responses such as widest detection range of guanine and adenine at the surface of the

MoS<sub>2</sub>-SPAN/CPE were ascribed due to the synergistic effects from MoS<sub>2</sub> and SPAN. Poly (4-amino thiophenol) (PAT) was incorporated with Au NPs, and an electrochemical sensor for the simultaneous detection of DA and AA was fabricated [251]. A selective electrochemical biosensor based on PANI/GO hybrid nanosheets was developed for the detection of prostate cancer cells [252]. The oxygen-containing -COOH groups in GO and PANI provide a suitable environment for the hybridization of DNA structures. The formation of complex DNA hybridization with GO/PANI NC and the associated changes in the conductivity provides the basis for designing an assay for different concentrations of DNA. Modification of the GCE with a composite of GO and PANI, immobilization of ssDNA and hybridization of complementary strands at the electrode surface were studied using CV and EIS techniques. In another report, based on G/PANI NC, the response of the DNA sensor was found to depend on the mass proportion of PANI to G [253]. Besides the sensor could discriminate single nucleotide polymer phases, the double-structured DNA could also be monitored by changing the mass proportion of PANI to G. The electrostatic interaction between DNA/single structured (ss) or double structured (ds) DNA probe and PANI or/and BSA keep the DNA on the surface. Also, both ssDNA and dsDNA could interact with G through  $\pi$ - $\pi$  stacking attractions. The mechanistic pathway for DNA sensing involves the competition between electrostatic attractions,  $\pi$ - $\pi$  stacking interactions and Brownian motion [253]. An electrochemical ssDNA sensor was fabricated based on Au NP@PANI hybrid [254]. The ssDNA detection was routed through Ag<sup>+</sup> ions utilizing the cytosine- Ag<sup>+</sup> - cytosine complex. Initially, DNA molecules are immobilized on the surface of PANI due to the electrostatic adsorption between the negative charges of phosphate groups in DNA strands and the positive charges of amino groups in PANI.

### ***Ion sensors***

Electrode modification was done on plastic films or the filter paper via drop casting the electrospun of G/PANI NC on the electrode. The resultant ME was utilized for the detection of Zn(II), Cd(II), and Pb(II) [255]. The co-operation of PANI and G improves the conductive pathways and electron transfer kinetics. Trace level detection of Cd<sup>2+</sup>, Pb<sup>2+</sup>, and Cu<sup>2+</sup> was reported based on Langmuir-Blodgett (LB) films involving PANI-ES and organophilic montmorillonite clay [256]. The enhanced performance is attributed to the stabilizing and ordering effects in PANI-ES LB film. The mechanism of trace level metal ion detection involves adsorption of the metal ions, reduction of metallic ions to the metal state and reoxidation to ionic states (**Fig.12**). The PANI/vanadyl phosphate composite, prepared through intercalation/exfoliation method was used for the electrochemical detection of Pb<sup>2+</sup> ions [257]. A water-soluble NC of PANI-wrapped MWNTs was prepared by in situ chemical polymerization in the presence of a sulfonic acid containing dopant and was used for optical pH sensing for the pH range from 1 to 12 [258].

Fig. 12

### 3.2.3. Grafted PANIs

Grafting PANI or substituted PANI chains onto another component, especially onto nanostructured carbonaceous materials, was carried out to synergistically augment the electrochemical properties of PANI or substituted PANI and carbon nanomaterials. Electrochemical grafting of the polymer chains was utilized for the fabrication of sensors.

#### *Biosensors*

Chains of PDPA (an N-substituted PANI derivative) were grafted onto the amine-functionalized sites of MWNTs (MWNT-*g*-PDPA) and utilized for the fabrication of CO [259] and H<sub>2</sub>O<sub>2</sub> [260] sensors. Few studies demonstrated that the electrochemical sensing performance of the analytes could be significantly improved by grafting PANI or PADPA chains onto CNTs [259-262]. Specifically, PANI grafted onto MWNTs (MWNT-*g*-PANI) was utilized for the amperometric detection of H<sub>2</sub>O<sub>2</sub> [262] and adsorptive reduction of celecoxib (CEL) [263]. The high surface area of MWNT and functional groups in PANI were synergistically utilized to preconcentrate CEL at the electrode through prior adsorption, and electron transfer was mediated through the covalently linked PANI units. Thus, the PANI-*g*-MWNT ME demonstrated the combined properties of PANI and MWNTs and exhibited excellent performance for the electrochemical detection of CEL at extremely low concentrations ( $1 \times 10^{-11}$  M). The sensitivity and selectivity of the PANI-*g*-MWNT ME towards CEL were superior to those of the MWNT/PANI (bilayer) electrode. Poly(4-aminobenzene sulfonic acid) (PABS) chains were grafted onto MWNTs (MWNT-*g*-PABS) were fabricated and utilized for the electrochemical detection of sildenafil citrate (SC; Viagra) [264]. The fabrication of this electrode involved the following steps: (i) preparation of MWNT-NH<sub>2</sub> and (ii) electrografting of PABS onto MWNT-NH<sub>2</sub> ME to obtain MWNT-*g*-PABS. At pH 2.0, the sulfonic acid groups in MWNT-*g*-PABS are negatively charged and the nitrogens in the piperazine units of SC are positively charged. Hence, the sulfonic acid groups in MWNT-*g*-PABS interacted with protonated SC (**Fig. 13**). As a result of the electrostatic interaction, the proportion of hydrazo benzene and azobenzene sulfonic acid in MWNT-*g*-PABS decreased. However, the pristine MWNT-NH<sub>2</sub> electrodes exhibited a negligible effect on the preconcentration of SC. In general, the performance (sensitivity and detection limits) of sensors fabricated from PANI or substituted PANI grafted onto MWNTs was superior to that of pristine PANI or substituted PANI, as well their bilayer PANI/MWNT or substituted PANI/MWNT counterparts.

Fig. 13

### 3.2.4. Biofunctionalized F-PANIs

Towards fabrication of biosensors, PANI structure was either modified with biomolecules or the functionalized PANI was covalently linked to enzyme or enzyme was entrapped into PANI/F-PANI matrix.

#### **Biosensors**

An impedimetric biosensor for carbohydrates was developed using mannosylated PANI (manno-PANI). Aniline monomers bearing a  $\alpha$ -mannoside residue in the *ortho*-position were electropolymerized to obtain a sensor film [265]. The conductivity changes are owing to the carbohydrate–protein interaction were exploited. The interconversion of amine to imine upon the binding of concanavalin A (ConA) was quantified by impedance measurements. Manno-PANI maintained the bioactivity of the natural sugar and directly transduced the carbohydrate–protein lectin binding to an electrical signal because of the extreme sensitivity of PANI to its protonation/deprotonation states. PANI/dinonyl naphthalene sulphonic acid (DNSA) film was used as a signal transducer layer and a potentiometric immunosensor was developed for the detection of troponin I–T–C (TnI–T–C), a complex of the three distinct single-chain troponin subunits [266]. An additional layer of poly(*o*-phenylene diamine) was formed over PANI/DNSA film to amplify the signal from the enzyme horseradish peroxide catalyzed reactions. A Glu sensor was designed based on the deflavination of the FAD co-factor to the GOx enzyme and subsequent reconstitution of apo-GOx by an FAD-boronic acid-complexed PAPBA layer. The higher sensitivity and selectivity arise from the reconstitution of GOx and the good electron transfer to the electrode surface as compared to the conventional GOx-based electrochemical biosensors. SPAN was adopted as the platform for a label-free, electrochemical self-signal amplifying DNA hybridization assay [267]. Negatively charged SPAN was mixed with Al(III) to form a SPAN–Al(III) mixture. Using  $\pi$ – $\pi$  interactions, electrostatic forces, and adsorption effects, ssDNA formed a hybrid with the SPAN–Al(III) mixture (SPAN–ssDNA). A recognition surface capable of detecting specific sequences of DNA was achieved by tethering the SPAN–ssDNA hybrid to an Au electrode via an anchoring self-assembled monolayer of *p*-aminothiophenol (PATP) through the phosphoramidite bond between the 5' phosphate groups of the DNA sequence and the –NH<sub>2</sub> of PATP. After the recognition surface was hybridized with the complementary DNA sequence, an amplified self-signal of SPAN was observed corresponding to the formation of the SPAN–dsDNA hybrid. Because of the differences between ssDNA and dsDNA, such as rigidity, stacking, charge distribution, and long-range electron transfer, the interaction of SPAN dsDNA or ssDNA caused conformational changes. An impedimetric sensor based on an electrodeposited ConA-lectin-functionalized PANI film was

fabricated through step wise sequential processes for the specific detection of bacterial toxins, such as lipopolysaccharide from *Escherichia coli* and lipoteichoic acid from *Staphylococcus aureus* [268]. EIS measurements revealed that the resistance charge transfer across the electrode/electrolyte interface increased when ConA lectin interacted with specific carbohydrate moieties present in bacterial toxins. An impedimetric immunosensor was fabricated by immobilizing polyclonal antibody fragments cleaved by 2-mercaptoethylamine onto a functionalized PANI matrix containing 2-aminobenzylamine (2ABA) units [269]. The  $-NH_2$  groups in 2ABA were utilized to covalently attach a sulfosuccinimidyl-4-(*N*-maleimidomethyl)cyclohexane-1-carboxylate linker (**Fig. 14**). The immunosensors specifically detected and differentiated between closely related human Ad serotypes with a limit of detection of  $10^3$  virus particles/mL. An electrochemical sensor for tetrodotoxin (TTX) was developed on a GCE that was modified with poly(4-styrenesulfonic acid)-doped PANI (PANI/PSSA) film. An amine-end functionalized TTX-binding aptamer, 5'  $-NH_2$  AAAAATTTACACGGGTGCCTCGGCTGTCC-3' ( $NH_2$ -Apt), was grafted via covalent glutaraldehyde cross-linking. The resulting aptasensor (C//PANI+/PSSA-glutaraldehyde- $NH_2$ -Apt) was investigated by CV and EIS measurements [270]. A bio-inspired sensor for the insect pheromone 2-heptanone based on a PANI-functionalized AFM cantilever was fabricated [271].

**Fig. 14**

### **3.2.5. Nanostructured F-PANIs**

Studies have demonstrated that PANI nanostructures (PANI-NS) are promising support matrices towards sensor fabrications [272]. Moreover, substituted PANI nanostructures or derivatized PANI NSs exhibit much-improved selectivity towards analyte gases than pristine PANI NS. Also, selectivity towards a particular analyte has been demonstrated to be improved with nanostructures of F-PANIs or derivatized PANI nanostructures. In the sub sections 3.2.3.1 and 3.2.3.2, we review the sensing characteristics of F-PANI NFs/NWs and F-PANI-NRs. Few other nanostructured forms of F-PANIs also find applications in sensor fabrications and those details are presented in Supporting information: SI:4.

#### **3.2.5.1. F-PANI-NFs**

##### **Gas sensors**

One of the notable advantages of PANI nanostructures for gas sensing application is the increased sensitivity due to their high surface area-to-volume ratio and short diffusion lengths. F-PANI NFs based gas sensors are easy to fabricate and can be used to detect a vast range of chemical vapor

analytes with ultra-low detection limits. F-PANI NFs, either in the form of composites or as hybrids, possess high surface area to volume ratio and high porous morphologies or exhibited superior  $\text{NH}_3$  (ppb level) sensing properties. PANI NFs were deposited on an alumina substrate using ZnO NP template and utilized as an  $\text{NH}_3$  gas sensor [273].  $\text{NH}_3$  sensitive PANI NF films were developed using a liquid-gas interfacial self-assembly method [274]. The mechanism for  $\text{NH}_3$  sensing with HCl doped PANI NF involves the formation of partial polar bonds between the N and H atoms to destroy the conjugation along the PANI chains and to resulting changes in the interchain electron transport distances. As a consequence, the resistance of PANI film decreased upon interaction with  $\text{NH}_3$ . A unique approach was developed for the preparation soluble PANI NF using terra-butoxy carbonyl (t-BOC) pre-treated PANI NF as the precursor [275]. The soluble t-BOC PANI NF was transformed into the conducting PANI NFs by subsequent treatment with HCl. The resultant porous, 3D, nonwoven, and conductive PANI NFs exhibited a faster response to  $\text{NH}_3$  (70 ppm).

Functionalization of PANI with external additives or internal structural modifications, are used to detect a specific analyte. The PANI-analyte interaction can dope or dedope the PANI chains. These kind of interactions are possible with nanostructured PANIs. To quote an example, a  $\text{H}_2\text{S}$  gas sensor can be fabricated with the inclusion of  $\text{CuCl}_2$  as an external additive to PANI NSs and the PANI- $\text{CuCl}_2$  interaction produces  $\text{CuS}$  and the byproduct HCl. L-lysine included PANI/PAN NFs were obtained by electrospinning, and the gas sensing properties towards  $\text{NH}_3$  (also ethanol, acetone, chloroform and DMF) were evaluated [276]. The enhanced response is attributed to the large surface area, the core-shell structure of the NFs and improved charge transfer processes. The sensing model includes stages such as; i) transformation of PANI chains through interactions with  $-\text{NH}_3^+$  and  $=\text{N}^+$  because of the doping with L-lysine and ii) interaction of  $\text{NH}_3$  gas to transform  $=\text{N}^+$  state to  $=\text{N}^-$  state (**Fig. 15**). Indium tin oxide ( $\text{In}_2\text{O}_3$ ) is an n-type semiconductor find and exclusive application in the fabrication of gas sensor. PANI was included into electrospun prepared  $\text{In}_2\text{O}_3$  NF and the resultant composite NFs (CNFs) was utilized for  $\text{NH}_3$  sensing [277]. The superior performance of  $\text{In}_2\text{O}_3$ /PANI CNF over the individual components and other  $\text{NH}_3$  gas sensor is attributed to the generation of p-n heterojunction, both the inside and outside of  $\text{In}_2\text{O}_3$ /PANI composite NF. As a result, the change in resistance was significant. A hierarchically nanostructured G-PANI composite film was used for the fabrication of a flexible  $\text{NH}_3$  sensor towards integrating into wearable and foldable electronic devices [278]. An artificial ions neural network like PANI NPs/rGO/PANI NF film was formed through aniline polymerization in rGO solution and simultaneously depositing onto flexible PET substrates. The sensor exhibited flexibility and high performance for  $\text{NH}_3$  sensing as the sensing channels generated by the artificial neural network-like structured film provide beneficial features such as improved charge transport, high surface-to-volume ratios of hierarchical NC, and the effective exposure active surface area of NF for the of the sensing materials. The high surface area ( $47.896 \text{ m}^2$

$\text{g}^{-1}$ ) for the NC as compared to  $41.016 \text{ m}^2 \text{ g}^{-1}$  for pristine PANI provides efficient adsorption/desorption of  $\text{NH}_3$ . The  $\text{NH}_3$  molecules are easily adsorbed onto PANI to supply electrons to the PANI chains and increase the resistance of PANI.

**Fig. 15**

The CSA doped PANI PEO CNF based  $\text{H}_2\text{S}$  gas was sensor developed for low concentration level (<20 ppm) detection [279]. The concentration of major charge carriers (holes), increased when PANI chains interact with  $\text{H}_2\text{S}$ . Due to the acidic nature of  $\text{H}_2\text{S}$ , further doping of PANI chains resulted through extraction of an electron from the N atom of amine groups in PANI. PANI was in situ polymerized on an electrospun PANI NF and subsequently modified with a dopant (5-sulfosalicylic acid dehydrate) to have specific binding with CO for achieving high performances in a CO sensor [280]. A spinous nanocore feature was introduced into PANI electrospun NFs. The densely assembled NCs on the PANI NFs enhanced the contact area at the interface between the PANI fibers and the analyte gas. The sensing mechanism involves the attraction between the lone pair of an electron at the nitrogen atom of PANI and the stable resonance ( $+\text{C}\equiv\text{O}^-$ ) form of CO with a positive charge at the carbon atoms. The enhanced sensitivity of the sensor was due to the high surface area of PANI NFs. The detection of trace amounts of HCl gas through the resonance frequency signal from a quartz crystal microbalance (QCM) sensor coated with PANI-functionalized polyamide 6 (PA 6) (PANI-PA 6) nanofiber-net-binary structured membranes has been described [281].

### **Biosensors**

An electrochemical enzyme immunoassay was developed for sensitive detection of a disease-related protein (alpha-fetoprotein, AFP) using a biofunctionalized dendritic nanostructured PANI NF (DPANF) as the signal-transduction tag [282]. The signal was amplified by glucoamylase-labeled, multi-armed DPANF conjugated with anti-AFP detection antibody. The presence of DPANF caused a signal increase in the PGM-based immunoassay. The reason was attributed to the conjugation of glucoamylase. When one pAb2 antibody reacts with target AFP, all labeled glucoamylase molecules on DPANF take part in the hydrolytic reaction and cause amplification of the digital signal. The nanostructured-PANI derivative bearing mono- and bis hydroxy functional groups were used to sense vitamin C through molecular interactions at the nanosurface [283]. The influence of nanosurface functionalization on the sensing ability was evaluated by comparing the sensor performance with pristine PANI NPs. The sensing capability of three types of PANI nanostructures (i) NFs with NH groups over the surface, (ii) nanospheres with N-H groups and monohybrid groups at the surface and (iii) nanospheres with N-H groups and

bishydroxyl groups at the surface were compared. The bis hydroxy-functionalized PANI nanospheres showed efficient molecular interactions with vitamin C, whereas nanospheres with a mono hydroxy group or unsubstituted nanofibers failed as sensing materials for vitamin C. Electrospinning was used for the preparation of a nanofibrous membrane (NFM)-based composite comprising poly(vinylidene fluoride) and poly(aminophenyl boronic acid) (PVdF/PAPBA-NFM) [284]. PVdF/PAPBA-NFM exhibited sensitive Glu detection because the boronic acid groups in PVdF/PAPBA-NFM bound the vicinal diol groups in Glu or any carbohydrate. PABA nanofibers with different morphologies (U-shaped and ring-shaped) and sizes were prepared by chemical polymerization of APBA in the presence of cetyl trimethyl ammonium bromide (CTAB) and NaF [285] and exhibited highly sensitive detection of D-Glu. The effective surface area of the PABA nanofibers and the high density of the boronic acid moieties enhanced the sensitivity of D-Glu detection based on the binding of D-Glu to the boronic acid moiety of PABA. A non-enzymatic H<sub>2</sub>O<sub>2</sub> sensor fabrication has been reported using PANI-MnO<sub>2</sub> CNF [286]. The electrocatalytic activity of MnO<sub>2</sub>, the good electrical conductivity of PANI, and the high surface area of the NF synergistically provide good sensitivity for the H<sub>2</sub>O<sub>2</sub> detection. An amperometric phenol biosensor was fabricated by immobilizing laccase (Lac) into porous PANI NF and subsequent crosslinking [287]. The Lac enzyme adsorption-crosslinking based biosensor showed high sensitivity for catalytic detection due to a combination of steps; enzyme adsorption and cross-linking, involved in the fabrication stages. The sea weed (SW) incorporated PANI NF were employed towards the construction of a uric acid biosensor [288]. The inter agglomeration of SW with PANI NF resulted into a porous structure and provided the basis for electrochemical detection of UA in neutral medium. An imbidometric electronic tongue was developed based on the distribution of polyamide/PANI CNF on an interdigitated micro electrode array [289]. The authors could demonstrate the principle compound analysis for the milk samples (skimmed and fat) using the fabricated e-tongue. An electrochemical sensor for the individual as well the simultaneous determination of adenine and guanine was fabricated using 1, 3, 5 trithiane (TAN)- Ag NP-decorated PANI NF [290]. The presence of TAN causes good peak current for adenine and guanine due to the hydrogen bonds between the sulfur atom of TAN and hydrogen atom in N-H groups of purine bases. The peaks are resolved because of the presence of Ag NPs. An immuno sensor for alpha-fetoproteins (a well-known hepta cellular carcinoma biomarkers) was fabricated using PANI NF functionalized with Au NPs [291]. While the enhanced current signal originates from PANI NF, Au NPs provide antifouling properties and biocompatibility, to the immunosensor.

### ***Gas and Ion sensors***

PANI NF reinforced NC-based quartz crystal microbalance sensor was fabricated for the selective detection on HCl [292]. Because of the large specific surface area, high porosity, the strong

adhesive force between PANI and the QCM electrode and doping induced mass changes, the sensors exhibited a rapid response, good reproducibility, and stability, and a low detection limit (7 ppb) for HCl at room temperature. The sensor detection system is designed based on the measurement of mass changes corresponding to a frequency shift of the modified quartz crystal as a result on the high dissociation capability of HCl in aqueous media. A fast and efficient protonation (doping) of PANI and rapid insertion of  $\text{Cl}^-$  counterions occur to maintain charge neutrality. A colorimetric  $\text{Hg}^{2+}$  ion sensor based on the leucoemeraldine form of PANI NF was fabricated by a blended electrospinning nanofabrication method [293]. The leucoemeraldine form of PANI NF has a specific interaction with  $\text{Hg}^{2+}$ , resulting in both “off–on” and “color-change” signals. The sensing process was explained through series of redox and doping reactions (**Fig.16**). The ‘turn on’ signal was generated due to charge transfer from benzoid to quinoid rings in PANI. A special doping mechanism involving  $\text{Hg}^{2+}$  was proposed. The two-step doping process involving  $\text{Hg}^{2+}$  resulted in the generation of imine nitrogen sites through oxidation by  $\text{Hg}^{2+}$  and further oxidation of imine nitrogen generates radical cations. The “color change” was ascribed due to the formation of azobenzene moieties.

**Fig.16**

### 3.2.5.2. F-PANI NWs

#### *Gas sensors*

Kaner and Weiler demonstrated that hydrogen gas interacts with PANI NWs and causes changes in conductivity [294]. The proposed hydrogen sensing mechanism involved the interaction of hydrogen with the imine sites of doped PANI, resulting in the dissociation of hydrogen and formation of N–H bonds at the amine sites of PANI chains. The original doped state of PANI was regenerated through charge transfer between adjacent amine sites. A chemiresistive sensor for  $\text{H}_2\text{S}$  detection based on a PANI nanowire (NW)–Au NP hybrid network was reported [295]. PANI NWs were synthesized using templateless electrochemical polymerization and then electrochemically functionalized with Au NPs by electrodeposition using cyclic voltammetry. The unfunctionalized PANI NW sensor did not show any change in resistance up to 500 ppm because of the poor doping ability of  $\text{H}_2\text{S}$ . On the other hand, the Au NP-functionalized PANI NW sensor showed an excellent response even at low concentrations of  $\text{H}_2\text{S}$  (~0.1 ppb). The change in the resistance of the PANI–Au NP network was explained by the formation of AuS and the enhanced doping level of PANI. PANI and Au NPs were also reported to act as a donor and acceptor, respectively, to transfer electrons from the p-type PANI network with a concomitant increase in conductance.

## Biosensors

A nanosensor for the label-free detection of proteins based on an aptamer-functionalized single PANI NW was developed [296]. Single PANI NW fabrication and IgE sensing were reported. To obtain direct growth of a single PANI NW, polymethylmethacrylate (PMMA) nanochannel was created using electron-beam (E-beam) lithography between pre-deposited Au electrodes on a Si/SiO<sub>2</sub> substrate. When aniline was dropped onto the nanochannel, the electrolyte solution spread, covered the entire channel and connected the two Au electrodes. The phosphate group on the 5'-ends of aptamers reacted with the amine groups on the surface of the PANI NWs with the assistance of EDC and NHS to form covalent bonds. The biosensing performance of the aptamer-functionalized PANI NW was tested with IgE and other nonspecific proteins. The sensing mechanism of this PANI NW biosensor was explained by the charge accumulation or depletion in the NW through the interactions of charge of the target analyte. An integrated 3D nanostructured PANI/CNT composite NW based nitrite sensor was developed by modifying PANI NW arrays with CNT-COOH through a self-assembly approach [297]. The enhanced electrocatalytic activity for nitrite reduction originates through interactions between PANI NW and functionalized CNT. The CNTs function as the conducting skeleton for the growth of PANI NWs. A non-enzymatic Glu sensor was developed by utilizing the nanocages-augmented PANI NWs (NCa-PANI NWs) on a Si substrate [298]. The fabricated NCa-PANI NWs electrode facilitates the generation of an ion-dipole between HN<sup>+</sup>(ES<sup>+</sup>) of PANI and neutral molecule like Glu and induces the conversion of PANI ES form to PANI LE form to result in redox current. Upon introduction of Glu, the LE state (insulating state) of PANI accepts an electron to change into PANI-ES state (conducting state) and behaves as an electron transporting system. As a consequence, the electrons are transported from Glu to the electrode. Chiral-PANI-cyclodextrin sulfonate nano bundle (C-PANI-CDS-NB) were prepared to discriminate between chiral compounds with different sizes by transforming PANI NW into NB [299]. The combined presence of a template, chiral inductor (CSA), and CDS in the aqueous media used for the interfacial polymerization led to the formation of C-PANI-CDS-NB. The presence of CDS in the NB imparted size-exclusion enantioselectivity. The preferred one-screw helical structure of PANI was maintained because of electrostatic bonding of CSA<sup>-</sup> anions to PANI HN<sup>+</sup> centers and hydrogen bonding of the carbonyl groups of CSA to NH sites. The sulfate groups in CDS acted as secondary dopants and forced PANI into an expanded helical structure over the interconnected CDS cones (**Fig. 17**). The chiral forms of arginine (i), cysteine (ii), phenylalanine (iii), histidine (iv), proline (v), tryptophan (vi), tyrosine (vii), and mandelic acid (viii) could be chirally discriminated owing to the end carboxylic groups that could dope PANI sites. C-PANI-CDS-NB could not discriminate compounds (iii-viii) containing bulky groups as steric hindrance prevents the approach of the analyte towards the enantiomeric sites of CSA in C-PANI-CDS-NB.

Fig. 17

### 3.2.6. Multicomponent in F-PANIs

The literature on the use of three or more functional components in F-PANI based sensors are discussed in this section. While few studies have focused on chemical sensors with multicomponent F-PANIs, a large number of reports are available in the fabrication of biosensors.

#### **Biosensors**

MWNT-COOH was immobilized with GOx by coupling through EDC-NHS chemistry and deposited with PANI by an electrochemical method (GOx-MWNT-PANI) [300]. This approach ensured the attachment of the enzyme to the NTs through amide bond formation, with the help of zero-length crosslinkers followed by the in situ electrochemical formations of the GOx-MWNT-PANI biosensing composite. An LBL film-based Glu biosensor comprising MWNTs, Au NPs, PANI, and GOx in alternating layers was fabricated. The synergistic advantages of MWNTs, Au NPs, PANI, and LBL assembly for effective electron shuttling between the electrode and GOx were effectively utilized to achieve greater sensor performance (**Fig. 18**) [301]. The fabrication of the biosensor involved the alternating construction of two layers. In one of the layers, MWNTs, PANI, and Au NP were integrated to form a single unit, and the subsequent layer consisted of GOx. The high sensitivity of the  $\{GOx/Au-(SH)PANI-g-MWNT\}_n$  biosensor originated from the combined influence of increased GOx loading and the Au-(SH)PANI-g-MWNT matrix. The favorable orientation of GOx in the  $\{Au-(SH)PANI-g-MWNT\}_n$  matrix established conducting channels between the prosthetic groups of GOx and the electrode surface. The GOx-MWCNT-PANI biocomposite was utilized for the Glu sensing. The surface modification of MWNTs using SPAN-based on an interconnected network (SPAN-ICNW) was reported [302]. In situ polymerization of diphenylamine-4-sulfonic acid, 4-vinylaniline, and 2-acrylamido-2-methyl-1-propane sulfonic acid were performed to generate MWNT-g-SPAN-NW. GOx was immobilized onto MWNT-g-SPAN-NW to fabricate MWNT-g-SPAN-NW/GOx. The MWNT-g-SPAN-NW/GOx biosensor displayed direct electron transfer from GOx to the electrode and a good performance in the electrochemical determination of Glu. An electrochemical biosensor for Glu based on an MCNC comprising MWNTs, silica, Nf, and PANI was developed [303]. The four components were integrated into the biosensor by employing the following steps (**Fig. 19**): (i) preparation of amine-functionalized MWNTs, (ii) preparation of a Nf-silica composite, (iii) loading MWCNT-g-PANI within the Nf-silica composite, and (iv) immobilization of GOx onto the Nf-silica/MWNT-g-PANI. The high sensitivity of the Nf-silica/MWNT-g-PANI/GOx biosensor electrode

towards Glu highlighted the importance of loading MWNT-*g*-PANI within the Nf-silica network. Also, Nf-silica/MWNT-*g*-PANI/GOx had a rapid response time (~6 s) to reach a steady state current because of the larger active surface area provided by the MWNTs and the augmented electron transduction. The Nf-silica/MWNT-*g*-PANI/GOx biosensor exhibited a combination of high sensitivity and fast response because of the combined presence of silica-Nf and MWNT-*g*-PANI. In another report, PB-PANI)/MWNT composite matrix was employed to immobilize GOx and a fabricated biosensor for in vivo monitoring of Glu in the rat brain [304]. MWNTs provide good electron transport for the PB combined PANI particles and stabilized them through 3D network formation. An electrochemical non-enzymatic Glu sensor was fabricated using Ni metal-PANI-rGO composite [305]. A mechanism consisting of Glu binding to Ni/PANI/rGO composite, oxidation of Glu through inner-sphere electron transfer and regeneration of electrocatalytic sites is suggested.

**Fig. 18**

**Fig. 19**

A three component based non-enzymatic Glu sensor comprising of copper oxide (CuO), nickel oxide (NiO) and PANI NF was developed [306]. The components were sequentially electrodeposited to fabricate the sensor electrode. The enhanced electroactivity towards Glu is attributed to the good electrical conductivity of PANI/NiO/CuO. The inclusion of CuO induces Ni<sup>3+</sup> ions in the PANI/NiO/CuO composite matrix through the transformation of NiO into NiO(OH). Glu is catalytically oxidized to gluconolactone by Ni<sup>3+</sup> species. In another non-enzymatic Glu sensor, the sensing electrode was fabricated based on three-dimensional NiO nanoparticles (NiONPs), PANi nanowire (PANiNW) and GO [307]. The involvement of NiOOH formed through the transformation of NiO was suggested as the reason for the electrocatalytic detection of Glu. A non-enzymatic Glu sensor based on CuNPs/PANI/G NC was fabricated via in-situ reduction of Cu precursor into PANI NFs followed by the mechanical mixing of G suspension [308]. The Cu NPs interact with PANI via the N atoms and enable fast electron transfer to Cu NPs via G and PANI. A multicomponent nanobead (MCNB, comprising of G, ferrocene, Cu NP, polyethylene imine (PEI) and PANI-co-anthranilic acid (PANI-COOH) was prepared through grafting of PANI-COOH onto G, covalent linking of Fc to G-PANI-COOH via PEI and electrodeposition of Cu NPs. The G-PANI(COOH)-PEI-Fc/Cu MCNB was utilized for electrochemical non-enzymatic sensing of Glu (**Fig. 20**) [309]. The G-PANI(COOH)-PEI-Fc/Cu MCNB, was designed to have conductive PANI (COOH), electron mediating Fc and electrocatalytic Cu NP for achieving high Glu sensor performances. A disposable G/PANI/AuNP/GOx biocomposite based ME coupled with a paper disk impregnated with the sample was fabricated [310]. The assay was based on the current decrease of flavin adenine dinucleotide in GOx caused by the enzyme-substrate reaction. Direct electrochemistry for GOx was witnessed. The

PANI/active carbon in the presence of nanometer-sized  $\text{TiO}_2$  ( $n\text{-TiO}_2$ ) was used for the fabrication of enzymatic Glu sensor [311]. Direct electron transfer for the immobilized GOx was witnessed. The Au NPs–polyvinylpyrrolidone–PANI (AuNP–PVP–PANI) ternary NC was used as a matrix for immobilization of GOx and a Glu biosensor was fabricated. Direct electron transfer was witnessed for GOx. Similarly, direct electrochemistry for GOx witnessed at the AuNP–PVP–PANI ternary electrode [312]. The Au NP-decorated PANI NW ME was fabricated, and an enzymatic Glu sensor was developed [313]. Other than GOx, different other biomolecules (such as ssDNA and Lamin A antibody were immobilized by covalent attachment. Due to that, detection of complementary and non-complementary strands could be discriminated. The electrocatalytic activity of NiO/CuO/PANI electrodes toward Glu was studied in alkaline electrolyte [314]. The properties of the sensors are based on these electrodes, such as selectivity, sensitivity, and the detection limit of Glu detection was investigated. The addition of  $\text{Cu}^+$  increases the concentration of  $\text{Ni}^{3+}$  ions and the  $\text{Ni}^{3+}$  ions in turn catalyze the electrooxidation of Glu. The fabrication of an enzymatic Glu sensor was demonstrated using poly[N-(3-trimethoxysilyl)propyl]aniline (PTMSPA) as the immobilization matrix. Electrochemical polymerization of TMSPA was performed in the presence of enzymes (HRP and GOx) to yield a PTMSPA/HRP–GOx composite [315]. The advantage of the polymer, poly[3-trimethoxysilylanyl-propyl-N-aniline] (TMSPA) lies in its usefulness as an enzyme entrapment matrix, coupled with its ability to act as a physicochemical transducer and convert a biochemical signal into an electrical signal, resulting in signal amplification and the elimination of electrode fouling. Moreover, because of the ability of TMSPA to bind biomolecules, both HRP and GOx became electrostatically or hydrophobically adsorbed on the electrode surface, and the silica network kept the two enzymes on its surface. A PTMSPA/HRP–GOx ME was demonstrated as a Glu biosensor. The enhanced response of the PTMSPA/HRP–GOx ME as compared with a silica–graphite/HRP–GOx ME was due to the fact that simultaneous immobilization could be possible because of the covalently linked PANI chains in the silica framework and the proximity between the enzymes and the PANI chains. Direct electron transfer was observed for HRP/PTMSPA@GNR as the PANI units in PTMSPA facilitated electron-wiring between HRP and the electrode. HRP/PTMSPA@GNR showed high sensitivity and selectivity towards  $\text{H}_2\text{O}_2$ . The efficient polymerization of aniline by the enzymatic reaction improved the sensitivity and detection limit for  $\text{H}_2\text{O}_2$  determination. A novel amperometric biosensor based on Pt NPs decorated on PANI-wrapped boron nitride nanotubes (BNNTs), (BNNT-PANI-Pt hybrids), was developed [316]. The  $\pi$  interactions between the N atoms of the BNNTs and the C atoms of PANI resulted in the water solubility of the PANI-wrapped BNNTs hybrids. The BNNT-PANI-Pt hybrid was used for the development of GOx-based Glu biosensors. The BNNT-PANI-Pt hybrid biosensor maintained a high GOx enzymatic activity even at  $60^\circ\text{C}$ . This might be attributed to the electrostatic field and hydrophobicity of the BNNTs. An amperometric Glu biosensor consisting of electrodeposited PANI in the presence of polyacrylic acid and GOx was fabricated [317]. The enzyme GOx was chemically linked to the carboxyl groups of PAA by esterification

with NHs and subsequent treatment with GOx. The sensing of Glu involves biocatalysis of GOx and electrocatalysis of PANI/PAA composite. Sulfonate (pyrene sulfonate/polystyrene sulfonate)-functionalized SWNT in PANI NCs were prepared in two configurations: planar PANI/SWNT films and micro rods (PANI/polystyrene sulfonate (PSS)), and the enhanced bioelectrocatalytic oxidation of Glu was reported [318]. The PANI/SWNT composite led to improved electrocatalytic oxidation of Glu due to the enhanced electrical contact of GOx and charge transport. The superior electron conducting properties of PANI/SWNT play a significant role in the improvement of sensor performance.

### Fig. 20

A sensor based on PANI/O,O'-bis (2-aminoethyl)polyethylene glycol-functionalized MWNT (PEG-MWNT) NCs was constructed for H<sub>2</sub>O<sub>2</sub> detection [319]. HRP immobilization was performed by combining the adsorption between the negatively charged PANI/PEG-MWNT film and the positively charged HRP with crosslinking between HRP and PANI via glutaraldehyde, resulting in an HRP/PANI/PEG-MWNT NC. The presence of PEG-MWNT in the PANI film suppressed the anionic transportation and improved the immobilization of HRP. In this sense, the doping capability of the composite was improved by fixing a high amount of HRP enzyme, yielding an efficient H<sub>2</sub>O<sub>2</sub> sensor. An amperometric H<sub>2</sub>O<sub>2</sub> biosensor was constructed using an MWNT-g-PANI(oxidized PANI (O))/cyt-C electrode [320]. Initially, PANI chains were grafted onto the amine-functionalized sites of MWNTs through electropolymerization, and subsequent oxidation resulted in oxidized PANI (PANI(O)). The positive charges in PANI(O) were utilized to immobilize cyt-C in the MWNT-g-PANI(O) matrix through electrostatic interactions. The direct electron transfer of cyt-C at the ITO/MWNT-g-PANI(O)/cyt-C film electrode was achieved via the synergistic influence of MWNT and PANI. The fabrication of a biosensor for H<sub>2</sub>O<sub>2</sub> based on the HRP-induced deposition of PANI on G-CNT-Nf/AuPt alloy NP-modified GCE was described [321]. The electronic conductivity between the enzyme and the electrode was enhanced because of the synergistic effect of the G-CNT hybrid materials, AuPt alloy NPs, and PANI. A one-step immobilization of HRP onto PTMSPA-covered GNRs was established for the fabrication of an amperometric H<sub>2</sub>O<sub>2</sub> sensor [322]. A layer of PTMSPA was coated onto the surface of the GNRs through the enzymatic polymerization of TMSPA using a mixture of H<sub>2</sub>O<sub>2</sub> and HRP. During the surface modification of the GNRs with PTMSPA, HRP was simultaneously entrapped in the PTMSPA matrix to generate an HRP/PTMSPA@GNR biosensor. PB/PANI/GO NCs were synthesized through spontaneous polymerization of aniline and formation of PB NPs onto PANI/GO surface [323]. Aniline was employed both as the precursor for PANI formation and the reductant for FeCl<sub>3</sub>-K<sub>3</sub>[Fe(CN)<sub>6</sub>]. An enhanced electron transfer rate, improved catalytic activity and the more catalytic surface for H<sub>2</sub>O<sub>2</sub> reaction were attributed to the large numbers of PB NPs and their well distributed narrow size distribution on the surface of PANI/GO in the case of non-

enzymatic  $H_2O_2$  sensor based on PB/PANI/GO. A PANI/MWNT-COOH NC was prepared by blending the emeraldine base form of PANI and MWNT-COOH [324]. HRP was immobilized within PANI/MWNT-COOH to fabricate an HRP/PANI/MWNT-COOH biosensor for  $H_2O_2$  sensing. The interaction between the negatively charged PANI/MWNT-COOH NC and the positively charged HRP resulted in very good sensitivity to  $H_2O_2$ . A modular approach was utilized towards the preparation of an ND-based nanosponge (NSP) comprising NDs enveloped in a biocompatible polymer network and entrapped with HRP (ND-NSP(HRP)) [325]. The preparation involved the formation of a ND-NS(HRP) interpenetrating polymer network comprising PANI and poly(2-acrylamidopropane sulfonic acid) (PAMPSA) interlinked through the cross-linkers *o*-phenylenediamine (OPD) and 2-vinylaniline (2VA) to the surface of amine-functionalized NDs (ND-NH<sub>2</sub>) in the presence of HRP. Importantly, HRP was entrapped in situ within the PANI–PAMPSA networks during formation of the ND-NSP. The beneficial characteristics of ND-NS(HRP) were exploited as an electrochemical probe for the detection of  $H_2O_2$ . The NDs and PAMPSA in ND-NSP(HRP) provided a biocompatible environment for HRP. The sulfonic acid groups in PAMPSA imparted hydrophilicity to the PANI–PAMPSA network, thereby improving the wettability of ND-NSP(HRP). The PANI chains in the PANI–PAMPSA network electrically wired the entrapped HRP and augmented the electrical connectivity to the electrode. The nanopores in the sponge structure provided 3D channels for the passage of analyte ( $H_2O_2$ ) into the matrix. A facile procedure was developed to support Pt NPs on PANI spatially confined in the channels of mesoporous silica film (MSF) [326]. Pt NPs were loaded into PANI spatially confined in the MSF to obtain Pt NPs@PANI-MSF, and an electrochemical  $H_2O_2$  sensor was fabricated. The loading of Pt NP into PANI in MSF resulted in stronger  $H_2O_2$  oxidation signal at a lower potential (0.80 V). PANI combined in the pores of MSF possesses good mechanical strength and lowers the surface-to-volume ratio. The Ag NPs/PANI/halloysite nanotubes (HNTs) NCs were synthesized through the direct loading of preformed Ag NPs over the surface of PANI/HNTs and used for fabricating a nonenzymatic  $H_2O_2$  sensor [327]. The good electrocatalytic current for the  $H_2O_2$  reaction is attributed to the high surface area from PANI/HNTs surface, and anchoring of Ag NP onto PANI/HNTs without agglomerations. An electrochemical DA sensor was fabricated using PANI-rGO-Nf NC to achieve high performances utilizing the synergistic effects from the components of the MCNC [328].

A functional NC, comprised of MWNTs grafted to a silica–PANI network (silica NW) and Au NPs (MWNT-*g*-silica NW/Au NPs), was prepared by chemical oxidative grafting of PTMSPA onto the surface of MWNT followed by electrodeposition of Au NPs, and used for the selective electrochemical detection of nanomolar concentrations of DA in the presence of AA [329]. The silica NW provides different environments for DA and AA as the porous silica NW contains hydrophilic –NH<sub>2</sub> groups and hydrophobic MWNT surfaces (**Fig. 21**). An electrochemical DA was fabricated based on flower-like ZnO/PANI/rGO NC [330]. The G decorated with ZnO/PANI/rGO NC provides the combinational features such as large active

surface area, strong adsorption capability of the G and ZnO and specific interaction ability to DA. An electrochemical sensor was fabricated for simultaneous determination of DA and UA. Utilizing the attraction between positively charged activated charcoals and CTAB as the soft template [331]. The CTAB/PANI/ activated carbon (AC) NC showed improved selectivity towards DA because of the negatively charged AC. The unique features of PANI, AuNPs, SiO<sub>2</sub>, and CS were used to fabricate a three layered SiO<sub>2</sub>@AuNP@PANI NC-based electrochemical sensor for simultaneous determination of AA and UA [332]. The MCNC sensor exhibited electroactivity at neutral medium because of the coordination bonds formed between N atoms of PANI and Au NP, as well the negatively charged Au NP function as a dopant for PANI. Further, Au NPs contribute to good electron transfer across PANI matrix during electrochemical processes. The electrostatic attraction between positively charged ES form of PANI and AA along with the hydrophilic nature of the NC to repel UA contribute to the simultaneous determination of UA and AA with a wider potential separation for the oxidation processes. A multifunctional nanoweb was fabricated using a (cyclodextrin-amino thiophenol) CD-AT inclusion complex, MWNTs, PVDF, and Au NPs [333].

### Fig. 21

Au/MWNT(CD-IC)/PVdF-NFM was electroactive and showed excellent electrocatalytic detection of AA. An MCNC based cholesterol biosensor comprising PANI–Au NPs, CS matrix and ChOx was fabricated [334]. A label-free electrochemical aptasensor was developed for the highly sensitive detection of thrombin using the direct electron transfer of GOx and an Au–PANI–GR hybrid for signal amplification [335]. **Fig. 22** illustrates the stepwise procedure for fabrication of this aptasensor. The large surface area of the Au–PANI–GR hybrid provided a biocompatible sensing platform for the immobilization of GOx. GOx was encapsulated into the 3D netlike (3-mercaptopropyl)tri-methoxy silane (MPTS) to form an MPTS–GOx biocomposite. The special features in MPTS–GOx biocomposite not only retained the native functions and properties of its components, but also exhibited tunable porosity, high thermal stability, and chemical inertness. Because of the thiol groups in MPTS, MPTS–GOx was able to chemisorb onto the surface of the Au–PANI–GR ME through an Au–S bond. This method avoided the unnecessary labeling of redox probes and increased the amount of electroactive GOx. The concentration of thrombin was monitored based on the decrease of the current response through cyclic voltammetry. With the excellent direct electron transfer of the double layer of the GOx membranes, the resulting aptasensor exhibited a high sensitivity towards thrombin. Multi-armed dendritic PANI nanofibers (MPANFs) were functionalized with HRP and carcinoembryonic antibody (anti-CEA) for the electrochemical determination of carcinoembryonic antigen (CEA) [336]. Anti-CEA-conjugated core-shell Au-Fe<sub>3</sub>O<sub>4</sub> NCs (GoldMag) were used as immunosensing probes. The MPANFs and core–shell GoldMag NCs were synthesized using an

initiator-induced wet chemical method and a seed-growth method, respectively. MPANFs were utilized as molecular tags for the conjugation of HRP and anti-CEA antibody and were prepared by the adsorption, precipitation, and crosslinking of HRP and anti-CEA (BGMBs). Using the conjugated HRP as a trace and  $\text{H}_2\text{O}_2$  as the enzyme substrate, a flow-through sandwich-type assay protocol was designed on the anti-CEA-functionalized GoldMag NCs. The MPANFs acted as a self-contained electron transfer mediator and the fabricated sensor did not include any additional diffusional mediators. The amplification strategy was based on the catalytic reduction of  $\text{H}_2\text{O}_2$  by the HRP-assembled MPANFs.

### Fig. 22

An electrochemical DNA biosensor was fabricated using the components such as PANI, Au NPs, and  $\beta$ -mercaptoethylamine (MEA) [337]. Au NPs incorporating PANI NWs were synthesized by interfacial polymerization. The ssdA ME was utilized as the sensing probe for the detection of complementary ssdT through dA–dT bond formation. A sandwich-type electrochemiluminescence biosensor was developed for the detection of DNA on the basis of a PANI–Au NP ME with a tris(2,2-bipyridyl)dichloro ruthenium(II) hexahydrate ( $[\text{Ru}(\text{bpy})_3]^{2+}$ )–nanoporous gold (Ru–NPG) composite as a label [338]. DNA capture was achieved through the interaction between the –SH groups in DNA and the Au NP. Ru–PANI-labeled reporter DNA was captured by the target DNA through a sandwich-type hybridization reaction. The electrochemiluminescence DNA biosensor enabled the determination of target DNA with a detection limit of 0.01 fM. An electrochemical label-free biosensor for ODNs was fabricated from a PANI NW decorated with Au NPs. The sensing ODNs (ssdA) bind covalently to the electrode via a thiol crosslinker [339]. An electrochemically active PANI NW was fabricated and utilized for the construction of a highly sensitive and selective electrochemical sensor for the hepatitis B virus gene [340]. The uniform PANI NW was prepared by enzymatic polymerization of aniline monomers on an amyloid-like NF (AP NW) through self-assembly of an aniline-attached nonapeptide and aniline-GGAAKLFFF (AP). The nucleic acid biosensor was constructed by modifying GCE with AP NWs functionalized with a designed DNA hairpin loop. PANI-NF were modified with Au NPs to afford an NC material (PANI-NF–Au NPs). Single-stranded capture DNA was then bound to the Au NPs and hybridized with a complementary target strand that was uniquely associated with the pathogen *Staphylococcus aureus* that causes mastitis [341]. Finally, a second HRP-labeled DNA strand was hybridized with the target, allowing the concentration of the target DNA to be detected by monitoring the reduction of a hydroquinone mediator in solution. An increased concentration of DNA capture was witnessed due to the presence of Au NPs. The PANI–AuNP ME was functionalized with –NH<sub>2</sub> groups for the attachment of the biomolecules. A functional multilayer was designed using two proteins, cyt-C and sulfite oxidase, and the PANI sulfonate polyelectrolyte [342]. The two proteins were co-immobilized in alternating layers by electrostatic interactions using the LBL technique. Aptamer

properties and single PANI NW attributes yielded an aptasensor with excellent specificity and ultra-sensitivity. Because of the excellent stability and reversible conformational changes of the aptamers, these aptasensors could be repeatedly regenerated and reused. An electrochemical DNA sensor for the detection of the BCR/ABL fusion gene of chronic myelogenous leukemia was developed using Au NPs, PANI, G-CS, and a functional hairpin structure probe [343]. The detection strategy exploited the advantages of the Au NP/PANI/CS-G composite, biotin–avidin signal amplification, and alkaline phosphates. Sequential stages were involved in the fabrication of this DNA sensor. The DNA probes exhibited amplified signal as the effective electrode area of PANI was increased by the deposition of Au NPs on the surface. Au NPs also strengthened the current response and served as the immobilizing material for DNA probes via Au–S bonds.

### ***Ion sensors***

A nitrite biosensor was fabricated by combining components (NDs, PANI, and Au NPs) that confer bioactivity (NDs), direct electrochemical electron transfer matrix (PANI), and catalytic properties (Au NPs) [344]. The individual components and cyt-C were integrated into a PANI-g-ND/Au/cyt-C biosensor with improved characteristics towards nitrite. First, the NDs and PANI were integrated by a facile electrochemical grafting approach to obtain PANI chains grafted onto NDs (PANI-g-ND). Au particles were subsequently electrodeposited onto the surface of PANI-g-ND, and cyt-C was immobilized on the surface of PANI-g-ND/Au. The surfaces of the NDs were covalently linked with PANI chains (PANI-g-ND) and utilized for enzyme immobilization, direct electrochemistry of the immobilized enzyme, and bioelectrocatalytic detection of nitrites. Au NPs were incorporated into PANI-g-ND to improve direct electron transfer of the redox protein to the electrode and the electrocatalysis of nitrite ions. The high performance of the nitrite biosensor was attributed to the “electron wiring” between the redox centers of the immobilized cyt-C and those of the “electron shuttling sites” in the PANI-g-ND/Au matrix. A multifunctional electroactive nano-bio web was prepared through gamma radiation-induced formation of silica-PANI and Au NPs within electrospun PVDF nanofibrous membranes [345]. Cyt-C was immobilized onto PVdF@silica/Au nanofibrous membranes and utilized for the determination of nitrite ions. Nanoflower architecture of a PANI derivative (PANI doped with polyvinyl sulfonate; PV-SO<sub>3</sub><sup>-</sup>) was prepared and used as a nitrite ion biosensor. NS-polystyrene (PS<sub>NP</sub>) latex beads functionalized with –NH<sub>2</sub> (PS<sub>NP</sub>-NH<sub>2</sub>) and sulfonate groups (PS<sub>NP</sub>-SO<sub>3</sub><sup>-</sup>) were alternately assembled through LBL onto the PANI–PVSO<sub>3</sub><sup>-</sup> ME [346]. The nano cauliflower-architected electrodes were applied as amperometric nanosensors for the detection of nitrite ions based on the electrocatalytic reduction of nitrite on the polymeric NC films. The sensor containing positively charged PS<sub>NP</sub>-NH<sub>2</sub> exhibited a higher sensitivity and lower detection limit than that with negatively charged PS<sub>NP</sub>-SO<sub>3</sub><sup>-</sup> or GCE/PANI without functionalized

polystyrene NPs. A sulfite oxidase (SO)-cyt-C-PANI sulfonate (PASA) multilayer film was formed by self-assembly [342]. An artificial electron transfer chain composed of cyt-C and SO was formed in the LBL-assembled film. The multilayer film was exploited as a biosensor for the detection of sulfite. Utilizing the beneficial characteristics of Nf, PANI, b-mercaptoethanol (b-ME), 1,6-hexanedithiol (HDT), 2,5-dimercapto-1,3,4-thiadiazole (DMcT), and MWNTs for the sensitive and specific adsorption of  $\text{Cd}^{2+}$  and  $\text{Pb}^{2+}$ , an MCNC based ME was designed [347]. The preparation of thiol-incorporated PANI/MWCNTs was carried out by the addition of either b-ME, DMcT, or HDT to an aqueous suspension of pre-formed PANI/MWCNTs. The high sensitivity of the thiol-incorporated PANI/MWCNT compared with those of pristine PANI and MWNT MEs was due to the thiol groups in b-ME, HDT, or DMcT, and the  $-\text{COOH}$  groups of the MWNTs. A sensitive and label-free optical sensor for  $\text{Hg}^{2+}$  ions was developed by utilizing cyano group-containing PANI (P2ABN), GNRs and a porous silica network (GNR@Silica-CN) [348]. The basic design of the optical  $\text{Hg}^{2+}$  ion sensor involved the modification of the GNRs with P2ABN embedded in a porous silica network.  $\text{Hg}^{2+}$  detection occurred through  $-\text{CN}$  chelation and amalgamation. The presence of the silica pores on the GNR surface (GNR@silica-CN) along with the silica-embedded P2ABN played an important role in the selectivity towards  $\text{Hg}^{2+}$  ions. To demonstrate the importance of these features, another material without the silica network (GNR@P2ABN) was utilized (**Fig. 23(A)**). The detection of  $\text{Hg}^{2+}$  ions by GNR@silica occurred through (i) binding of  $\text{Hg}^{2+}$  ions to  $-\text{CN}$  groups, (ii) preconcentration of  $\text{Hg}^{2+}$  on the surface of GNR@silica-CN, (iii) reduction of  $\text{Hg}^{2+}$  to  $\text{Hg}^0$  through nucleation catalysis using a reducing agent, (iv) amalgamation of the GNR surface, and (v) monitoring of the GNR surface plasmon resonance by optical measurements. The  $\text{Hg}^{2+}$  sensing mechanisms of GNR@silica-CN and GNR@P2ABN were different (**Fig. 23(B)**). In the case of GNR@silica-CN, the porous silica network allowed migration of  $\text{Hg}^0$  to the Au surface, causing amalgamation of the GNR surface. However, the absence of the silica pores in GNR@P2ABN did not allow migration of  $\text{Hg}^0$  to the GNR surface. As a result, GNR@silica-CN exhibited excellent sensitivity and selectivity for  $\text{Hg}^{2+}$  over a wide concentration range (50 nM to 5  $\mu\text{M}$ ). An electrochemical biosensor for the detection of  $\text{Pb}^{2+}$  biosensor was fabricated involving PANI, functionalized rGO and Au NPs [349]. A hollow spherical manganese dioxide was used as a nanocarrier to immobilized GOx, HRP to result in S3/H-Mn<sub>2</sub>O<sub>3</sub>/HRP/GOx bioconjugation. An electrochemical immunosensor based on a dual amplification strategy with a biocompatible Fe<sub>3</sub>O<sub>4</sub>/PANI/Nf layer as the sensor platform and multienzyme-antibody-functionalized highly carbonized spheres (multi-HRP-HCS-Ab<sub>2</sub>) as the label was constructed for the sensitive detection of benzo[a]pyrene (BaP) [350]. An enhanced electrochemical signal was achieved when Fe<sub>3</sub>O<sub>4</sub>/PANI was used for the multiplex binding of BaP–Ag and the multi-HRP-HCS-Ab<sub>2</sub> label was used as the electrochemical probe. Furthermore, Fe<sub>3</sub>O<sub>4</sub> NPs in the Fe<sub>3</sub>O<sub>4</sub>/PANI NC served as a biomimetic peroxidase for the reduction of H<sub>2</sub>O<sub>2</sub>. A graphenated PANI/tungsten oxide (PANI/WO<sub>3</sub>/GF) NC-based sensor for phenanthrene was fabricated by electrodeposition of WO<sub>3</sub>-incorporated PANI onto

the surface of a graphene-modified GCE and utilized for the determination of phenanthrene [351]. Ethylene glycol bis (succinic acid-N-hydroxy succinimide ester) (EG) modified cyt c P450 (CYP2E1) based biosensor was fabricated for rifampicin (RIF) using PVP-Ag NPs/poly (8-anilino-1-naphthalene sulfonic acid) NC. The mechanism of sensing was proposed based on RIF induced spin transition of the CYP2E1 ferri-heme.

**Fig. 23**

### **Gas sensors**

The p-TSA doped PANI along with  $V_2O_5$  exhibited synergistic enhancement for  $NH_3$  gas sensing. The inclusion of  $V_2O_5$  caused an increase in conductivity and mobility of charge carriers. The p-TSA doped PANI generated higher charge carriers than the HCl doped PANI [352]. Similarly, a tannin sulfonic acid doped PANI- $TiO_2$  (TANIPANI- $TiO_2$ ) composite was used for  $NH_3$  gas sensing [353]. The TANIPANI- $TiO_2$  composite was synthesized by a simple polymerization of aniline in the presence of tannin sulfonic acid and  $TiO_2$  nanoparticles. The inclusion of  $TiO_2$  showed prominent effect on  $NH_3$  sensing property. The localized polaron are generated because of coordination effects of  $TiO_2$  with the amine nitrogen of PANI. This coordination effect results in an electron withdrawing effect and causes the protons around PANI chains as more acidic. These sequence of reactions are the reasons for the efficient dedoping in the presence of  $NH_3$ . A strong interaction of metal oxide with PANI and formation of localized polaron band augmented the doping and de-doping processes of TANIPANI chains. Based on these features, a faster response time and better  $NH_3$  gas sensing characteristics were observed for the TANIPANI- $TiO_2$  composite. Electrospinning was utilized to produce CSA-doped poly(*o*-anisidine) (POA)–polystyrene (PS) composite fibers in a nonwoven mat form [354]. CSA-doped POA–PS–PANI composite fibers were fabricated onto interdigitated gold substrates for use as chemical vapor sensors. The sensitivity of the multicomponent POA composite fiber sensor was higher when exposed to water than when exposed to ethanol because water has a higher polarity and lower vapor pressure than ethanol. A layer of CSA-doped PANI was electrodeposited onto SWNTs, and a sensor for  $NH_3$  gas was fabricated [355]. The opposite electrical resistance responses of the CSA-doped PANI and SWNTs to humidity effectively canceled each other out and eliminated interference from humidity during the sensing measurements.

**Table 4** presents the summary of cross-sectional information on the detection method (electrochemical, optical etc.) based sensors amongst the four categories of F-PANIs. In recent years, electrochemical sensors are predominantly being developed for exploiting the functional properties of nanocomponents (such as nanocarbons, metal nanoparticles or metal oxide nanoparticles) utilizing functional nanocomponent included PANIs (Category I) and multicomponents (Category IV) included F-

PANIs.

**Table 4**

### **3.3. Functionalized polythiophenes (F-PTs)**

Various PT based FCPs (F-PTs) were developed in different categories; substituted/derivatized PT (category I), biofunctionalized PT (category II), nanostructured PT (category III) and multicomponent PT (category IV) (categories described in **Scheme 1**) through structural/functional modifications towards sensor applications. Table 3 summarizes the details on the structures of PT based FCPs, characteristics of the fabricated sensors, the major sensor performances achieved in the individual case using the specific FCP and mechanism of sensing using F-PTs. One important PT-based FCP, poly(3,4-ethylenedioxythiophene) (PEDOT), is particularly attractive owing to its excellent electrocatalytic activity, good stability [356], relatively low oxidation potentials [357, 358], and enhanced redox characteristics [359]. Interestingly, PEDOT has been utilized for sensor applications in all the four categories mentioned in **Scheme 2**. PEDOT can be doped with different types of functional anions, including smaller molecules (e.g., heparin), as well as macromolecular polyanions, such as PSS [360]. PEDOT has been used as doped PEDOT (Category I), biofunctionalized PEDOT (Category II), NS-PEDOT or PEDOT: PSS (Category III), and PEDOT in a multicomponent nanocomposite (Category IV).

#### **3.3.1. Substituted or derivatized F-PTs**

F-PTs of category 1 (Scheme 1) were synthesized either by parent PT structure modification with included substituents and by introducing functional group containing dopant ion along with pristine PT.

##### **3.3.1.1. Structural modification(s) of the parent PT structure**

The properties of PT are modified by functionalization of thiophenes at one or both of the  $\beta$ -positions. Thiophenes can be functionalized by a large variety of substituents with varying electron withdrawing/donating effects, sizes, and shapes, towards producing substituted PTs with varied electric, optical and physical properties that are different from those of unsubstituted PT. Neutral, cationic, and anionic-functionalized PTs have been used for sensor applications (**Table 5**). Several water-soluble PT derivatives have received attention as biosensor materials because of their advantageous properties including signal amplification and ease of fabrication.

Table 5

### 3.3.1.1.1. F-PTs with neutral side groups

#### Gas sensors

The PT derivatives such as poly(3-dodecylthiophene) (PDT), poly(2-[4-(4'-nitrophenylazo)-*N*-ethyl-*N*-phenylamino]ethyl-3-thienylacetate) (PAzoTAc), poly(hexyl-3-thienylacetate) (PHexTAc), poly(3-hexyloxythiophene) (PHexOxT), poly(3-thiopheneacetic acid) (PTAA), and poly(3-(2-hydroxyethyl)thiophene) (PHET) with different functional groups at the 3-position of the thiophene ring, such as –COOH, ester, ether, alcohol, alkyl, and azobenzene, were developed as optical sensors for the detection of VOCs (*n*-hexane, toluene, tetrahydrofuran (THF), chloroform, dichloromethane, and methanol) and water vapor [361]. Only poly(3-hexylthiophene) (P3HT), PDT, PHexOxT, and PHET films responded to VOCs in these optical sensor tests. P3HT and PDT showed a response to *n*-hexane, toluene, THF, chloroform, and dichloromethane but did not show any optical changes after exposure to methanol and water. PHexOxT responded only to THF, chloroform, and dichloromethane, whereas PHET only detected methanol and water. PAzoTAc, PHexTAc, and PTAA did not show a response to any of the analytes. The lack of water detection by these polymers (except PHET) was correlated to bulk effects in the diffusion process. The bulk effects include the presence of more closely packed polymer chains that decreased the free volume and segmental mobility of the polymer chains inside the films, permeation of analytes, solubility of the polymer, and swelling of these films by the analyte. P3HT was utilized for the detection of VOCs [362]. The sensor was tested in the presence of volatile gases, such as *n*-hexane, toluene, chloroform, dichloromethane, methanol, and THF. Methanol vapor showed the minimum response, whereas THF vapor afforded the maximum response. Non-polar, weak solvents, such as *n*-hexane and toluene, afforded intermediary responses. The response of the sensor to VOCs was due to weak physical interactions between the analyte and the swelling of the polymer film. Swelling of the polymer matrix increased the distance between polymer chains, thereby decreasing hopping conduction. Poly(3-triazole dihexyl thiophene) (P3TzdHT), poly(3-triazole hexyl thiophene) (P3TzHT), and poly(3-butyne triisopropylsilyl thiophene) (P3BSiT) were tested for their sensing abilities towards trinitrotoluene (TNT) and dinitrotoluene (DNT) [363]. The fluorescence of the three polymers was quenched by DNT in the following order: P3TzdHT > P3TzHT > P3BSiT. The differences in the sensing abilities of the polymers were correlated to the different dipole–dipole, dipole–induced dipole, and hydrogen bonding interactions of the analyte and the polymer chains. 1,2,3-Triazole has a large dipole moment (5 D) and therefore can interact with nitroaromatics via dipole–dipole interactions, hydrogen bonding, or a combination of the two.

The weak interaction between the nitro group and triazole enhanced the interaction between the analyte and the polymer chain, thus leading to the enhanced sensing ability of P3TzHT. The pendant 1,2,3-triazole with the bulky dihexyl side chain enhanced the sensing ability compared with polythiophenes with linear alkyl side chains. Poly(4-(ferrocenylmethylidene)-4*H*-cyclopenta[2,1-*b*:3,4-*b'*]-dithiophene) (PCPBT-FC) was electropolymerized and utilized as a humidity sensor [364]. PCPBT-FC incorporates two redox centers, the  $\pi$ -system of PT and the ferrocene moiety. The conjugation pathway in PCPBT-FC contributes both to electronic and redox conductivities. The ionic conductance of PCPBT-FC depended on the relative humidity. Water-assisted ion generation was proposed to explain the linear dependence of the conductance on the relative humidity.  $\text{Fe}^{3+}$  in the polymer acted as Lewis acid that transformed  $\text{H}_2\text{O}$  to  $\text{H}_3\text{O}^+$  and stabilized ferrocenium with  $\text{OH}^-$ . The affinity of three different [15]crown-5 ether-functionalized PTs towards alkali ions was explored [365]. Ab initio and DFT quantum mechanical calculations showed that the binding energy between neutral functionalized PTs and metal ions decreased as the size of the metal ion increased.

### ***Ion sensors***

The  $\text{Pd}^{2+}$  ion-sensing properties of 2,6-substituted pyridine derivatives of PT were examined. Specifically, the effects of 2,6-dithienyl-4-phenylpyridine (TPP) and 2,6-diphenyl-4-phenylpyridine (PPP) were compared [366]. The TPP polymer unit has thiophene groups, whereas the PPP unit has benzene groups in the polymer backbone. The TPP-based polymer showed a fluorescent response to  $\text{Pd}^{2+}$ , whereas the PPP-based polymer did not, indicating that the thiophene moieties played a very important role in the binding of  $\text{Pd}^{2+}$  ions. The fluorescence quenching was ascribed to intrachain TPP- $\text{Pd}^{2+}$  binding induced by the aggregation. The good sensing performance of the TPP-based polymer arises from the spatial matching for the selective binding of  $\text{Pd}^{2+}$  ions and the *meta*-substituted pyridine resulting in excellent electrocatalytic activity toward the nitrite electrochemical sensor [367, 368], iodate [369], and  $\text{H}_2\text{O}_2$  [370]. The chelating ability of the PT derivative, poly{3-[2-(2-dimethylamino-ethylamino)ethoxy]-4-methyl-thiophene} (PTMA) towards heavy metal ions ( $\text{Cu}^{2+}$ ,  $\text{Co}^{2+}$  and  $\text{Cd}^{2+}$ ) was explored [371]. PTMA has multi donor ligand groups and shows different correlation effects with metal ions. The fluorescent response of metal ions towards PTMSA has followed the strong fluorescent quenching effects with  $\text{Co}^{2+}$  and are due to the synergistic function of strong co-ordination with tridentate N/O ligand of PTMSA and paramagnetic properties of the metal ions. The fluorescent sensors were fabricated for the detection of trace metal ( $\text{Cu}^{2+}$ ,  $\text{Co}^{2+}$  and  $\text{Cd}^{2+}$ ) ions. The significant reduction of the fluorescence signal in the presence of  $\text{Cu}^{2+}$  is due to its special coordination with the ligands on the side chain of the polymer and shielding effect for other metal ions.

## Biosensors

The utilities of few water soluble PT derivatives (**Fig. 24**) towards the development of optical sensors for small molecules were reviewed [372]. The calorimetric or fluorescence responses to the analytes were attributed to the conformational changes or aggregation of the  $\pi$ -conjugated polymer backbone, induced by the interaction with the analytes. For example, poly(3-alkoxy-4-methylthiophenes) were utilized as optical sensors for nucleotides, folic acid, glutathione, inorganic anions, metal ions, and surfactants [373]. An enzyme-free potentiometric Glu sensor was developed using an electrodeposited poly(3-aminophenyl boronic acid-co-3-alkylthiophene) electrode [374]. The Glu sensing capability of the copolymer was explained in terms of octylthiophene group functioning as partition layer and phenyl boronic group acting as a complexing layer. The development of a disposable amperometric glycosylated hemoglobin HbA1C sensor for the finger prick blood test was reported using poly(terthiophene benzoic acid) (pTTBA) as the sensing layer [375]. The sensor probe was fabricated by electrodeposition of pTTBA onto an Au NP-coated screen-printed electrode, followed by the covalent attachment of APBA to pTTBA as a host to capture HbA1C. A quinine-linked PT-based ratiometric colorimetric sensor was designed for the detection of carbenicillin [376]. The quaternized quinine was linked to thiophene through the benzyl group, and favoured interactions of carbenicillin *via* electrostatic interactions, yielding a pharmaceutical and geometric matching effect. The sensor exhibited a colorimetric signal change upon addition of carbenicillin because of the formation of nonplanar structures. However, the addition of other  $\beta$ -lactam antibiotics or dicarboxylic acids caused no obvious change in the absorbance intensity ratio. The quinine-linked PT derivative contributes to the formation of a cavity by the semi-rigid framework and the binding with carbenicillin.

**Fig. 24**

The electrochemical behavior of bisphenol A (BPA) was studied by cyclic voltammetry using a PEDOT ME. The redox activity of PEDOT film was utilized for sensing BPA [377]. PEDOT-COOH was electrodeposited from 4-((2,3-dihydrothieno[3,4-*b*] [1,4]dioxin-2-yl)methoxy)-4-oxobutanoic acid in a microemulsion system. PEDOT-COOH MEs have developed either alone or along with inorganic nanoparticles for the determination of catechol, AA, acetaminophen, quercetin, epinephrine, and tryptophan [378]. An electrochemical sensor for the simultaneous determination of several neurotransmitters (DA, AA, and uric acid (UA)) was fabricated by spin-coating the ionic liquid 1-butyl-3-methylimidazolium chloride ([BMIM][Cl]) onto a pre-electrodeposited PEDOT-coated SPCE [379]. The differential pulse voltammetric measurements with the PEDOT/IL ME showed good electrocatalytic

activity and stability compared with those with the pristine SPCE/IL ME due to the synergistic effect of PEDOT and IL. The selective determination of DA was carried out using PEDOT-containing polydopamine (PDA). The hydrophobic interaction of PEDOT-PDA film with DA and electrostatic interaction with the interfering molecules like UA or AA were assigned as reasons for good selectivity [380]. The negatively charged surface of PEDOT/PDA electrostatically repelled AA and UA, allowing for the specific detection of DA over a wide linear range.

### 3.3.1.1.2. F-PTs with cationic side groups

#### **Biosensors**

Poly(3-(4-methyl-3-thienyloxy)propyl trimethyl ammonium) (PMTPA) was used for the detection of cysteine (Cys) and homocysteine (Hcys) through colorimetric and fluorescent sensing [381]. PMTPA forms weak interactions with bioanalytes, such as amino acids and peptides, through noncovalent interactions [382]. To enhance its interaction with Cys, an in situ reaction of Cys with 2-cyano-6-methoxybenzothiazole (CBT) was performed. Pristine PMTPA was optically inactive, and the addition of CBT-Cys into the PMTPA solution induced an intense circular dichroism optical signal in the  $\pi-\pi^*$  transition region of PMTPA. A sensor that could differentiate 15 nucleotide phosphates (XNPs, where X = A, U, T, G, C, and N = mono, di, and tri) was also developed using PMTPA [383]. The unique response from PMTPA towards different XNPs was a result of conformational changes and the aggregation mode of the PT backbones; specifically, the formation of an ordered phase of PTs was driven by ionic self-assembly between the quaternary ammonium moieties on the CP and the phosphate groups of the XNPs. Furthermore, multiple negative charges (triphosphate compared with monophosphate) and hydrophobic nucleotide base moieties (purine compared with pyrimidine) facilitated the formation of PMTPA aggregates. A specific signal transduction for nucleotide binding occurs by the interplay of hydrophilic and hydrophobic interactions, planarization of the PMTPA backbone and the formation of PMTPA aggregates with different molecular ordering. The interchain interactions between the ordered phases of substituted PTs result in the formation of small aggregates, contribute to scattering light at longer wavelengths and form the basis for an alternate transduction mechanism. A calorimetric sensor for folic acid was developed using PMTPA or PMTEA (contains one less alkyl group than PMTPA) [384]. Upon binding with folic acid, PMTPA takes a more planar conformation with stronger intermolecular  $\pi-\pi$  stacking interactions. Poly(1-ethyl-3-(2-((4-methylthiophen-3-yl)oxy)ethyl-1H-imidazol-3-ium bromide) (PEMTEI) was specifically localized within lysosomes and has been used as a fluorescent probe to detect ATP in cells through  $\text{Ca}^{2+}$ -regulated exocytosis in response to stimulation by typical lysosomal drugs [385]. Poly[3-(1,10-dimethyl-4-piperidinemethylene)thiophene-2,5-diyl chloride] (PTh-D) was used as the

luminescent material with the co-reactant of potassium persulphate ( $K_2S_2O_8$ ) for sensitive detection of DA [386]. When the potential was negative,  $S_2O_8^{2-}$  was reduced to  $SO_4^{\cdot-}$  and  $SO_4^{2-}$ . The strong oxidant  $SO_4^{\cdot-}$  further reacted with PTh-D $^{\cdot-}$  to generate the excited state PTh-D\* through electron transfer in the aqueous solution. The excited PTh-D\* state further relaxes to the ground state with a concomitant emission. The conformational changes of negatively charged ssDNA were detected using cationic poly(1*H*-imidazolium-1-methyl-3-{2-[(4-methyl-3-thienyl)-oxy]ethyl} chloride) and transduced complex formation through an optical (colorimetric or fluorometric) signal without any labeling of the probe or target [387].

### **Ion sensors**

Poly 3-[[1-(2-hydrazino-2-oxoethyl)piperidin-4-ylidene]methyl]thiophene hydrochloride (PM1·HCl) and poly 3-[[1-(3-hydrazino-3-oxopropyl)piperidin-4-ylidene]methyl]thiophene hydrochloride (PM2·HCl) were used as fluorescent metal ion sensing probes [388]. PM2·HCl responded selectively to  $Cu^{2+}$  due to strong Cu-N binding and coordination diversification but showed no significant changes in its fluorescence upon addition of  $Hg^{2+}$ . Poly[*N,N,N*-trimethyl-4-(thiophen-3-ylmethylene)-cyclohexanaminium chloride] (PTCA-Cl) was applied as a fluorometric probe for the detection of anionic surfactants [389]. The electrostatic attraction between the negatively charged sulfonate groups of the surfactants and positively charged PTCA-Cl was the driving force for the interaction. Furthermore, the hydrophobic interaction between the alkyl chains in the surfactants played an important role in the dissociation of PTCA-Cl aggregates. The PTCA-Cl aggregates dissociated into non-aggregated PTCA-Cl chains with a random-coil conformation, thus shifting the  $\pi$ - $\pi^*$  transition to a shorter wavelength and leading to a color change from red to light yellow. The absorption of PTCA-Cl showed drastic changes for anionic surfactants only and remained unchanged with cationic and nonionic surfactants.

#### **3.3.1.1.3. F-PTs with anionic side groups**

### **Biosensors**

Poly(2-(2-(4-methylthiophen-3-yloxy)ethyl)malonate acid) (PMTEMA) was developed for the detection of protamines [390]. The carboxyl groups on the side chains were utilized for binding the guanidine residues of protamines. The positively charged protamines formed a complex with PMTEMA through multiple electrostatic interactions, leading to conformational changes of the PT backbone from a random coil to a more planar and ordered phase. These changes led to fluorescence quenching and a

change in the color of the solution. The calorimetric detection of  $H_2O_2$  was investigated with an anionic PT derivative, poly[2-(3-thienyl)ethoxy-4-butylsulfonate] (PTEBS). PTEBS possesses intrinsic peroxidase-like activity capable of catalyzing the reaction of the peroxidase substrate 3,3',5,5'-tetramethylbenzidine (TMB) [391]. PTEBS adsorbed TMB by electrostatic interactions. The peroxidase-like activity of PTEBS originates from an increase in the electron density and mobility of PTEBS arising from the electron transfer from lone-pair electrons in the amino groups of TMB to the electronically delocalized backbone of PTEBS. Thus, the electron transfer from PTEBS to  $H_2O_2$  was accelerated. The APBA-functionalized poly-5,2':5,2''-terthiophene-3'-carboxylic acid (PTTCA) was developed as a non-oxidative voltammetric Glu sensor [392]. The probe was prepared by the electropolymerization and subsequent interaction between the  $-COOH$  group of PTTCA and the amine group of APBA. The formation of the tetrahedral boronate ester on PTTCA was witnessed.

### **Gas sensors**

PMTEMA, was utilized for  $CO_2$  sensing [393]. The conformation of PMTEMA alternates between the random coil and rod-like phases depending on the pH of the solution and this conformational change is associated with a distinct color change of the solution. This result was associated with an increase in the effective conjugation length of the PT backbone and formation of an ordered phase of PMTEMA.

#### **3.3.1.2. F-PTs having functional ion-dopants**

PT FCPs with functional groups included in the form of a dopant was used for sensor applications. Importantly, PEDOT formed the main polymer and was used in conjunction with a variety of dopant ions towards the fabrication of sensors. In this category of PT-doped FCPs, PEDOTs have been mostly utilized for the fabrication of ion, gas, and biomolecule sensors in combination with a variety of dopants [394]. Although PEDOT itself is not soluble in water, it is possible to make an aqueous suspension of PEDOT by forming a complex with PSS and PEDOT: PSS has been especially used in biosensors.

### **Biosensors**

An electrochemical sensor for isoniazid was developed using a PEDOT electrode, and the voltammetric behavior was studied in the presence of SDS and CTAB surfactants [395]. The surfactants

play a key role in the electrostatic attraction and repulsion of isoniazid towards the surface of PEDOT. Various anions included PT films or PEDOT films included with an independent inclusion of anions such as perchlorate, dodecyl sulfate (DDS), polystyrene sulfonate and surfactants such as poly(2-acrylamido-2-methyl-1-propanesulfonate), and polyoxyethylene-10-laurylether, were utilized for the electrochemical detection of acetaminophen [396]. The electrooxidation product of an acetaminophen, namely N-acetyl-p-benzoquinone-imine or the deprotonated species, is adsorbed on the electrode surface having the immobilized anionic dopants and subsequently involves in a reversible redox reaction. The electrocatalytic activity of acetaminophen showed dependence on the type of dopant ion included in PEDOT film. An SDS-doped PEDOT ME was fabricated for the electrochemical sensing of catecholamine and serotonin [397]. SDS played a key role in the electrostatic attraction of catecholamine and serotonin towards the PEDOT surface and caused the repulsion of interfering compounds such as AA, Glu, and UA. PEDOT/GO was electrodeposited on the surface of a GCE by a potentiostatic method and the PEDOT/GO film ME was used for the detection of acetaminophen [398]. An iodine-doped PEDOT film was fabricated and used for the electrochemical determination of arsenite(III). Nickel(II) hexacyanoferrate-doped PEDOT (NiHCF–PEDOT) films were electrodeposited onto a GCE and utilized for the selective determination of AA [399]. The results were compared with electrodeposited CuHCF–PEDOT and MnHCF–PEDOT films. Interestingly, the NiHCF–PEDOT, and CuHCF–PEDOT MEs exhibited a wide linear response range. However, MnHCF–PEDOT did not respond to AA. The network structure of PEDOT accommodates metal particles and accelerates electron transfer process. Dopant ion-included PEDOT films were prepared by the incorporation of two electroactive species, ferrocene carboxylic acid ( $\text{Fc}^-$ ) and ferricyanide ( $\text{Fe}(\text{CN})_6^{4-}$ ) [400]. The electroactivity of the  $\text{Fc}^-$ -doped PEDOT and  $\text{Fe}(\text{CN})_6^{4-}$ -doped PEDOT was tested for the simultaneous determination of vitamin B<sub>2</sub>, vitamin B<sub>6</sub>, and vitamin C. An oxidation mechanism of vitamin C involving two electrons, two protons for vitamin c and vitamin B<sub>6</sub> was suggested at the electroactive species  $\text{Fc}^-$  or  $\text{Fe}(\text{CN})_6^{4-}$  included PEDOT surface. An electrochemical sensor for the selective detection of hydroquinone (HQ) in cosmetics was developed based on CNT-doped PEDOT exploiting the catalytic properties of CNTs. Electrochemical polymerization of PEDOT in the presence of CNTs resulted in the fabrication of PEDOT-CNT for the detection of DA [401]. A GO-doped PEDOT composite was electrodeposited on a GCE [402] and utilized as an electrochemical sensor for the simultaneous detection of HQ and catechol.

### **Gas and ion sensors**

Gas sensors were developed using dopant-included PEDOT films. A resistive CO<sub>2</sub> gas sensor was fabricated by coating a layer of branched polyethylene imine (BPEI) and PEDOT on an interdigitated electrode [403]. The BPEI–PEDOT composite showed resistance changes upon exposure to CO<sub>2</sub> at 95%

RH. The BPEI layer on the surface of PEDOT dedoped PEDOT. On the interaction of PEDOT-BPEI with  $\text{CO}_2$  redoped PEDOT by the formation of hydrogen carbonate ion  $\text{HCO}_3^-$ . An efficient CO sensor was fabricated based on a bis(2-hydroxyphenyl)dihydropyrido[2,3-*d*:6,5-*d'*]dipyrimidine-tetraone (B2HDDT)-doped PEDOT:PSS ME [404]. B2HDDT selectively captured CO in the presence of other atmospheric gases. The composite film comprised of  $\text{ZnSnO}_3$  nanostructures, PEDOT and PSS, was used for impedance based relative humidity (RH) sensor. The inclusion of zing stannate ( $\text{ZnSnO}_3$ ) into PEDOT:PSS matrix improved the RH sensing range as well as the response and recovery because of the crystalline structure of  $\text{ZnSnO}_3$  and porosity induced in the NC [405]. HFIP-substituted PT (HFIP-PT) or poly(3-hexylthiophene) (P3HT)/SWCNT-based chemical sensors for dimethyl methyl phosphonate (DMMP) were reported [406]. The HFIP group was attached to PT through hydrogen bonding with phosphate ethers. GR-encapsulated PEDOT was synthesized by electrochemical polymerization of GO functionalized EDOT monomer and was utilized for the electrochemical determination of nitrite ions [407]. The catalytic response of PEDOT/GR towards nitrite ions was faster than that of pristine GR-based electrodes.

### 3.3.2. F-PTs containing a functional component

#### *Biosensors*

A sensor for AA was developed based on carboxylated MWCNTs (CA-MWCNTs) included PEDOT (CAMWCNTs-PEDOT) film [408]. The electro-catalytic performance of CAMWCNTs-PEDOT towards AA sense is attributed to the large electroactive surface area and the enhanced conductivity of the CAMWCNTs-PEDOT NC. Upon electrodeposition, PEDOT film became cationic and facilitated the electrostatic interaction with the negatively charged AA. PEDOT film modified GCE was prepared by using deep eutectic solvents and used for sensing of AA, DA and UA [409]. The high sensitivity towards AA was based on a doping/dedoping mechanism, and different mechanistic pathways operate in ethaline, glycerine and reline based eutectics (**Fig. 25**). An impedimetric DA biosensor has been reported based on the thin layer of the copolymer of 3-thienyl boronic acid (TBA) and thiophene (Th) [410]. The selectivity towards DA was due to the interaction between DA and boronic acid groups in the copolymer. The copolymer with a molar ratio of 50:50 between TBA:Th showed a wider range and lower detection limit for DA. The sensor for bisphenol A (BPA) was constructed based on PEDOT-ionic liquid (IL) (1-butyl-3-Methylimidazolium bromide (BMIMBr)) composites. Utilizing the adsorption capacity and defouling features of PEDOT-IL composites [411]. The surface hydrophilic anions ( $\text{Br}^-$ ) from the IL improved the electrochemical sensing towards bisphenol A.

**Fig. 25**

### **Gas sensors**

A smart NO<sub>2</sub> gas sensor was fabricated by loading the PTh-rGO hybrid on a flexible PET film [412]. The NO<sub>2</sub> sensing arises from three major contributions: i) good adsorption/desorption on the hybrid surface due to the large surface area provided by rGO, ii) good electron transfer rate for NO<sub>2</sub> sensing process because of the  $\pi$ - $\pi$  interactions between PTh and rGO and iii) the decrease in energy for delocalization of electrons upon interaction of NO<sub>2</sub> with PTh-rGO. In another report, the NO<sub>2</sub> gas sensing platform was designed using PTh-rGO hybrid electrodeposited onto the IDE and heated with a heater system [413]. The effects of the operating and annealing temperatures on the sensing performance towards NO<sub>2</sub> gas were investigated. The influence of humidity on NO<sub>2</sub> gas sensing could be overcome by operating at a higher temperature (80 °C).

### **3.3.3. Biofunctionalized F-PTs**

To tune the properties and explore the potential of PT based FCPs for biosensor applications, biofunctionalization of PT/F-PT or modification of PT structures with biomolecules/proteins has been effectively performed. Physical entrapment of enzymes within the polymer matrix of PT/F-PT or covalent attachment of biomolecule/protein to PT structure was tried in appropriate cases to enhance sensor performances.

### **Biosensors**

The copolymer of Th, thiophene-3-acetic acid (Th-COOH), and dicyclopentadienyl iron-1,4-dienylmethyl-2-(thiophen-3-yl)acetate (Th-Fc) was prepared by electrochemical copolymerization and fabricated as a Glu biosensor through immobilization of GOx into the polymer matrix [414]. GOx was covalently immobilized on the surface of the copolymer film through amide linkages, formed by the condensation reaction with COOH groups on the surface. Increasing the concentration of the Fc units resulted in an increase in the O<sub>2</sub> concentration near GOx and reduced the hydrophilicity of the copolymer. The reduced hydrophilicity of the copolymer diminished the penetration of Glu into the enzyme electrode and caused a decrease in the catalytic current. The number of Fc units in the copolymer film determined the catalytic current response in this system. The copolymer showed redox activity as electrons were transferred between the active site of GOx and the electrode. The 2,5-dihydroxyphenyl (DHP) group as

an electron mediator was introduced onto a GOx-immobilized electrode based on the copolymer of (P3HT)/thiophene-3-acetic acid (T3A)) by two approaches: (i) using alkylendiamines (C2–C12) or (ii) poly-L-lysine as linker molecules [415]. The sensitivity of the amperometric Glu sensing increased remarkably upon introduction of the DHP groups. With the alkylendiamine-containing electrode, the response current increased with the length of the alkylene chain, reflecting enhanced electron transfer owing to the high mobility of the bound DHP groups. On the other hand, the enzyme electrode with poly-L-lysine afforded an enhanced response current, suggesting that poly-L-lysine was an effective linker for GOx and DHP binding.

Poly(3-(3-bromopropoxy)-4-methylthiophene) functionalized with MB (PMT–MB) was used for the detection of ODN hybridization [416]. The increased current signal of PMT–MB was due to the electrostatic interactions between PMT–MB and dsODNs. An aptamer was fabricated for the determination of endocrine disrupting compound (EnDC) 17 $\beta$ -estradiol using a SELEX-synthesized 76-mer biotinylated aptamer incorporated into a dendritic generation 1 poly(propylene imine)-polythiophene (G1PPT-co-PEDOT) star copolymer via biotin–avidin interactions [417]. The response to 17 $\beta$ -estradiol was based on the decrease in the square wave voltammetry current on the binding of EnDC to the ssDNA aptamer on the biosensor. A label-free electrochemical sensor for the recognition of ODN was fabricated using poly(4-hydroxyphenyl thiophene-3-carboxylate) (PHPT) immobilized with ODN probes [418]. Electrochemical DNA sensors were fabricated with PT derivatives based on the protection of –COOH groups in pentafluorophenylthiophene-3-acetate, 4-chlorobenzylthiophene-3-acetate, and *N*-hydroxyphthalimidothiophene-3-acetate with substituted benzyl groups and coimmobilization with ODN for target recognition [419]. Biological recognition was monitored by comparison of the current signals for the hybridization of single and double strands of ODNs. The protecting groups (–COOH) were able to interact directly with –NH<sub>2</sub> groups in the probe ODN. A label-free DNA sensor was developed based on the PEDOT-organic electrochemical transistor with ssDNA probes immobilized on the surface of the Au gate electrode [420]. The sensing mechanism was attributed to the modulation of the surface potential of the gate electrode induced by the immobilization and hybridization of DNA molecules on the gate surface. The organic electrochemical transistor could detect complementary DNA targets at concentrations as low as 1 nM and the detection limit was extended to 10 pM by pulse-enhanced hybridization of the DNA. Ascorbate oxidase (AO) was immobilized onto lauroyl sarcosinate-doped PEDOT (AO/PEDOT–SL) and was utilized for the electrochemical determination of vitamin C [421]. AO immobilized in the polymer film involved in the bioelectrochemical oxidation of vitamin c and PEDOT-SL supports the electron transfer process. Sodium *N*-lauroylsarcosinate provided a good biocompatible environment for ascorbate oxidase. The composite film comprising PEDOT and the filamentous virus M13-K07 was prepared by electrooxidation of EDOT in an aqueous solution containing the virus [422]. The functionalization to PT

with carbonate moieties units was done by taking advantage of glycosurface chemistry of the PT having quinone moieties and used for the label-free detection of two bacterial cells (bacterial pili and lectin-LPS on Gram negative bacterias) biomarkers (**Fig. 26**) [423]. The specification and sensitivity of detection were enhanced because of polyvalent linking to carbohydrates via quinone moieties and electrochemical transduction of PT units. A microfluidic electrochemical biosensor was fabricated from Topas polymer using a bilayer composite, tosylate-doped PEDOT (PEDOT: TsO) and TsO doped hydroxyl derivative of PEDOT (PEDOT-OH). PEDOT: TsO was covalently functionalized with two aptamer probes with an affinity for ampicillin or kanamycin A [424]. A breathable membrane electrode was fabricated by immobilization of alcohol dehydrogenase onto vapor-phase-polymerized PEDOT [425]. The coenzyme  $\beta$ -Nicotinamide adenine dinucleotide was employed as the redox-mediator. The detection range of the sensor was suitable for detecting ethanol concentrations relevant for drunken driving. Tyrosinase (Tyr)-immobilized, PEDOT: PSS-modified SPCE (Tyr/PEDOT: PSS/SPCE) was fabricated and utilized for the detection of phenolic compounds in surface waters [426]. The amperometric response of Tyr/PEDOT: PSS/SPCE for the oxidation of BPA was  $\sim 6$  times more sensitive than that of a pristine Tyr-immobilized SPCE. This result implied that PEDOT: PSS had a catalytic effect on the transportation of electrons from the immobilized Tyr to the electrode surface.

**Fig. 26**

### **3.3.4. Nanostructures of F-PTs**

#### ***Biosensors***

The NWs of a copolymer of PEDOT and PEDOT-COOH NWs were electrodeposited between gold electrodes and two-terminal sensors for ODN was fabricated through covalently attached to an amino-modified probe ODN [427]. The target ODNs specific to human breast and ovarian cancer cells were detected at femtomolar concentrations, and negative controls (noncomplementary ODNs) were clearly discriminated by the sensor. The EIS of the virus-PEDOT nanodots films increased upon exposure to an antibody ( $p$ -Ab) that selectively binds to the M13 coat peptide. The PEDOT-COOH dots were fabricated as probes to capture enhanced cancer cells [428]. The -COOH groups of PEDOT were functionalized with EDC/NHS and streptavidin chemistries. The streptavidin-linked PEDOT-COOH dot probes were then incubated with the biotinylated capturing agent, antihuman EpCAM (anti-EpCAM), to direct the antibodies onto the surface. The cell capturing the effect of PEDOT-COOH/anti-EpCAM dot probes with MCF7 and HeLa cells was investigated. The specific capture of MCF7 cells over HeLa cells was utilized as a sensor (**Fig. 27**). A flexible nerve agent sensor was fabricated using PEDOT-OH NTs

[429]. The PEDOT-OH NTs interacted with the nerve agents through hydrogenation. The sensing response was attributed in terms of hydrogen bonding interaction between DMMP and PEDOT-OH NTs. PEDOT NPs were used as a sensing probe for the fluorescent determination of nucleic acids [430]. A nonenzymatic biosensor based on Pd NPs incorporated into PEDOT (Pd/PEDOT) was fabricated. PEDOT anchors Pd NPs and improves electrocatalysis of  $H_2O_2$  [370]. A non-enzymatic Glu sensor was developed using a nanometric film of poly(hydroxymethyl-3,4-ethylendioxythiophene). Utilizing the intermolecular polymer-polymer hydrogen bonding interactions [431]. The electrostatic interactions arising from the  $\pi$  conjugation of planar anti-conjugation are induced by the dioxane rings and in turn facilitate the accessibility of hydroxyl side groups towards PT chains. Thus, the activation of hydroxyl catalytic effects plays impart role in the Glu sensing process. The PEDOT-NR- rGO hybrid was used for the trace level detection of rutin, a kind of flavonoid (**Fig. 28**) [432]. The high electronic activity towards rutin was due to the synergistic effect of rGO and PEDOT NR. The over-oxidized PEDOT NFs modified pencil graphite electrode (Ox-PEDOT-nf/PGE) was developed for the determination of UA in body fluids. The over-oxidation of PEDOT NFs and other factors were optimized towards an increase in UA selectivity and sensitivity of Ox-PEDOT-of/PGE. The hydroxyl and carboxyl groups increased the interaction of DA with Ox-PEDOT-of/PGE and favored the voltammetric response towards DA [433]. The nanoporous-PEDOT exhibited good electron shuttling between the electrode surface and the electrolyte and utilized for the low potential electrocatalytic oxidation of NADH [434]. The porous network structure facilitates the electron transfer process to the electrodes. Biotinylated nano branched nanoparticle PT derivatives (PTBL) was developed to enhance the photoelectric conversion in the detection of streptavidin [435]. The orientation of the Au-nano branches provided pathways for the flow of the photogenerated charge carriers from the PTBL film to the electrode surface resulting separation of photogenerated hole and electrons. The PTBL/Au electrode was used for the label-free photoelectrochemical detection of streptavidin. The PEDOT/ $\beta$ -cyclodextrins ( $\beta$ -CDs) (PEDOT/ $\beta$ -CD) clusters were prepared via a one-pot chemical synthesis [436]. The  $\beta$ -CD played the roles of both stabilizer and substrate material. The sensing ability of PEDOT/ $\beta$ -CD was evaluated towards simultaneous detection of shikonin and hyperoside, the natural flavonoids used in traditional Chinese medicines.

**Fig. 27**

**Fig. 28**

### ***Gas and ion sensors***

The NC fibers containing ZnO NPs and PT NFs were used for the fabrication of  $NH_3$  sensor [437]. The p-n heterojunctions formed between the p-type PT and n-type ZnO generated an electron donor-

acceptor system. The  $\text{NH}_3$  molecules partially withdraw the holes from protonated PT backbone and labile form complexes with PT. Ag NP-decorated PEDOT NTs were prepared using metal ion reduction mediated vapor deposition polymerization [438] and used as an  $\text{NH}_3$  sensor. The  $\text{NH}_3$  sensing efficiency increased with increasing concentration of  $\text{Ag}^{2+}$  owing to the increased surface area and improved conductivity originating from the oxidation of PEDOT by Ag NPs. Poly[2-(3-thienyl)ethanol *n*-butoxycarbonylmethylurethane] (PURET) NPs were fabricated for the photoluminescence (PL)-based sensing of DNT and TNT [439]. PURET NPs were synthesized using a mini-emulsion technique with SDS. The high sensitivity of PURET NPs towards DNT was attributed to an improved polymer–DNT interaction. Efficient quenching of the two-photon induced fluorescence of PURET NPs was observed in the presence of the analytes. Patterned PEDOT: PSS NWs were formed by dip pen lithography onto comb microelectrodes, and the current changes caused by different concentrations of NO gas were measured [423]. PEDOT NTs were used for  $\text{NO}_2$  gas sensing. Upon  $\text{NO}_2$  adsorption onto the PEDOT NTs, the strong electron-withdrawing property of the  $\text{NO}_2$  molecules causes charge transfer to the PEDOT surface, enhances the hole-carrier density in PEDOT and results in enhanced conductance [440]. An aqueous dispersion of PEDOT and NRs stabilized by GO was prepared via interfacial polymerization of EDOT in the presence of GO [367]. PEDOT–GO exhibited catalytic activities for oxidation of nitrite ions. PEDOT hollow micro flowers electrodeposited using a film of ZnO micro flowers as the template was used as a nitrite sensor [441]. PEDOT NR/rGO NC was prepared via liquid/liquid interfacial polymerization and used for the electrochemical determination of  $\text{Hg}^{2+}$  ions [442]. The electrochemical determination of  $\text{Hg}^{2+}$  involved three steps: i) accumulation of  $\text{Hg}^{2+}$  at the sensor surface, ii) electrochemical reduction of  $\text{Hg}^{2+}$  to  $\text{Hg}^0$  and iii) electro-oxidation of  $\text{Hg}^0$  to  $\text{Hg}^{2+}$ . The deposition of rGO on a rod like PEDOT resulted in an enhanced pre-concentration of  $\text{Hg}^{2+}$  in step i) due to the large active sites available for the accumulation of  $\text{Hg}^{2+}$ .

### 3.3.5. Multicomponent included F-PTs

#### **Biosensors**

Conductive PEDOT: PSS redox polymer nanobeads formed from branched polyethyleneimine bound to ferrocene (BPEI–Fc) and GOx were drop-coated on an SPCE for Glu sensing (BPEI–Fc/PEDOT: PSS/GOx/SPCE) (**Fig. 29**) [443]. At neutral pH, GOx is negatively charged, and BPEI–Fc bears positive charges. Thus, GOx and BPEI–Fc can be blended owing to electrostatic affinity. The sensitivity of the BPEI–Fc/PEDOT: PSS/GOx/SPCE ( $66 \mu\text{A mM}^{-1} \text{cm}^{-2}$ ) towards Glu was 2.5 times higher than that of the BPEI–Fc/GOx/SPCE nanocomposite electrode fabricated in the absence of PEDOT: PSS. The PEDOT: PSS in BPEI–Fc/PEDOT: PSS/GOx/SPCE provides a facile kinetic pathway and enhances

the electron transfer rate in the polymer film. A graphene-doped PEDOT: PSS nanocomposite, synthesized by a one-step electrolytic exfoliation, was drop-coated onto an SPCE to generate a Glu sensor (GR-PEDOT: PSS/SPCE) [444]. GOx was immobilized onto GS-PEDOT: PSS/SPCE by GA crosslinking. The GOx/GR-PEDOT: PSS electrode exhibited an amperometric sensitivity ~13 times higher than that of the pristine GOx/PEDOT: PSS electrode than in the absence of GR. Poly(vinyl alcohol) (PVA)-incorporated PEDOT: PSS was prepared by the addition of PVA to a PEDOT:PSS solution (**Fig. 30**) [445]. A “micellar-assisted soft template” approach combined with electrodeposition was utilized for the fabrication of a PEDOT–Pd/GOx ME [446]. The initial PEDOT NWs were formed using a mixture of a surfactant (SDS) and an ionic liquid ([bmim][BF<sub>4</sub>]). In addition to its role as a co-surfactant with SDS to form micelles, [bmim]<sup>+</sup> [BF<sub>4</sub>]<sup>-</sup> also functioned as the dopant for PEDOT. The PEDOT–Pd/GOx ME showed good electrochemical activity towards Glu. The excellent performance for Glu sense was due to the synergistic effects of nanofibrous PEDOT and Pd NPs. A hybrid film of GOx-incorporated PEDOT was electrodeposited onto a nanoporous gold electrode (NPG/PEDOT/GOx) for an amperometric Glu biosensor [447]. The NC containing GO doped PEDOT and Cu NP (CuNP/PEDOT/GO) combines the salient properties of Cu NPs, PEDOT and GO towards nonenzymatic Glu detection [448]. In this NC-based Glu sensor, Cu NPs provide active sites for the catalytic oxidation of Glu, while the PEDOT/GO offers a large surface area for NPs loading and a conductive substrate for enhancing the electron transfer rate. The strategy for improving the immobilization of GOx was developed through modification of PEDOT film by the inclusion of polyacrylic acid (PAA) and poly(4-lithium styrene sulfonic acid) in towards the fabrication of Glu sensor [449]. The carboxyl groups in PAA was covalently linked to GOx via carbo dimide chemistry. The fabricated sensor exhibited longer stability (~30 days) because of the covalent linkage established between the sensor probe and GOx. Poly(2-(2,5-di(thiophen-2-yl)-1*H*-pyrrol-1-yl) acetic acid) (PSNS-acetic acid) was electrochemically deposited via cyclic voltammetry [450] and subsequently functionalized with lysine and poly(amidoamine) PAMAM derivatives (PAMAM G2 and PAMAM G4). The functionalized PSNS-acetic acid surface contained attachment sites for GOx, and a matrix for efficient Glu sensing was formed. An ME based on PEDOT and poly(methylene blue) (PMB) (PEDOT/PMB) was developed [451] and applied as an electrochemical sensor for ascorbate anions. Electron mediation by PMB was witnessed.

**Fig. 29**

**Fig. 30**

A DA sensor was fabricated by drop-coating an aqueous dispersion of PEDOT: PSS and Nf on the surface of a GCE [452]. Owing to the high conductivity of PEDOT: PSS and strong adsorptive ability of the binding agent Nf, the PEDOT: PSS–Nf GCE showed good electrochemical activity, reproducibility, water-stability, fast electrode transfer, and low swelling and disintegration. An electrochemical sensor for

DA was fabricated with Au NP coated PEDOT in the presence of SDS [453]. The hydrophobic interaction of dopamine cation ( $DA^+$ ) with hydrophobic part of PEDOT and Au NP along with the ability of Au NPs to promote electron transfer reaction was assigned as reasons for sensing DA. Eunchoe et al. [454] reported an electrochemical DA biosensor based on Pd/PEDOT/rGO NC. The inclusion of PdNPs onto PEDOT/rGO improved the electrocatalytic activity towards selective detection of DA in the presence of AA. Thiophene-3-boronic acid (TBA) was oxidized by sodium platinate in the presence of uricase and chitosan to result in CS/uricase-PTBA-Pt<sub>nano</sub> composite and used for uric acid sensing [455]. The biocomposite exhibited good biosensing performances for uric acid. A meldola blue-incorporated PEDOT:PSS hybrid film was utilized for sensing  $H_2O_2$  [456]. The electrocatalytic activity of the PEDOT:PSS-MDB electrode was superior to pristine PEDOT:PSS electrodes owing to the electron mediating effect of meldola blue through the PEDOT:PSS matrix. An electrochemical  $H_2O_2$  biosensor based on Au NP-loaded hemoglobin (Hb) incorporated into PEDOT nanowhiskers was fabricated [457]. The PEDOT nanowhiskers were prepared in [bmim]<sup>-</sup> [BF<sub>4</sub>]<sup>-</sup> ionic liquid. PEDOT nanowhiskers tethered to the GCE and Hb active center was generated by constant potential polymerization. The PEDOT single-molecular chain effectively transfers electrons from the active center of Hb to the underlying electrode without any electron mediator. Ethyl sulfate-included PEDOT was electrodeposited from EDOT monomers in the presence of 1-ethyl-3-methylimidazolium ethyl sulfate ([Emim][EtSO<sub>4</sub>]) [458]. The PEDOT-EtSO<sub>4</sub> electrode was modified with the inclusion of ascorbate oxidase and used to determine vitamin C at a low potential of 0.2 V. An electrochemical DNA biosensor was fabricated utilizing an Ag NP-incorporated PEDOT:PSS matrix [459]. *Ganoderma boninense* DNA was immobilized on the ME and hybridization was monitored via intercalation of a ruthenium complex into the hybridized DNA. Vapor oxidized PEDOT was deposited onto a Fe(III) tosylate-coated Au electrode. Au NPs were then electrodeposited onto a PEDOT ME to afford a PEDOT/AuNP nanocomposite electrode [460]. Thiolated capture strand ODN was immobilized, and the target oligo was then hybridized. A label-free DNA sensing probe was fabricated using Au NP-functionalized PEDOT (PEDOT/Au NPs) [461].

The incorporation of Au NPs into the PEDOT matrix increased the conductivity and also eliminated the direct functionalization of the native polymer for DNA attachment. A label-free assay for optical detection of miRNA and RNase H activity was established based on conformational and colorimetric changes of poly[3-(3'-N, N,N-triethylamino-1-propyloxy)-4-methyl-2,5-thiophene hydrochloride] (PMNT) of the DNA/PMNT duplex and DNA/miRNA/PMNT triplex [462]. Upon addition of complementary ssDNA, the absorption of the ssDNA/PMNT solution exhibited a marked red shift. The red-shifted absorption was derived from conformational changes of PMNT in the ssDNA/PMNT duplex form (highly conjugated, planar conformation). The results demonstrated that the conformational and colorimetric changes of PMNT in the DNA/PMNT duplex and DNA/miRNA/PMNT triplex could be

conveniently used to detect sequence-specific miRNA and RNase H activity. A dual-functional,  $\text{MnO}_2$ -decorated PEDOT (PEDOT/ $\text{MnO}_2$ ) nano ellipsoid was fabricated for the enhancement of neurite outgrowth during differentiation and real-time monitoring of PC12 cells [463]. The PEDOT nano ellipsoids were prepared by chemical oxidation polymerization in reverse microemulsions, and the  $\text{MnO}_2$  domains on the surface of the PEDOT were formed by redox deposition. The PEDOT/ $\text{MnO}_2$  nano ellipsoids had a low toxicity towards the cells owing to the biocompatibility of the PEDOT matrix. An electrochemical immunosensor for the detection of carcinoembryonic antigen based on AuNPs/PEDOT/GR NC was reported [464]. A GS-dispersed PEDOT: PSS ink solution was prepared by one-step electrolytic exfoliation and was used to modify the surface of an SPCE through a commercial inkjet printer [465]. The electrochemical behavior of analytes, including  $\text{H}_2\text{O}_2$ ,  $\text{NAD}^+/\text{NADH}$ , and  $\text{Fe}(\text{CN})_6^{3-/4-}$ , was studied with the G/PEDOT: PSS/SPCE. The catalytic redox peak current was  $\sim 13$  times higher for G/PEDOT: PSS/SPCE than for pristine SPCE. The G/PEDOT: PSS-ME exhibited a combination of good sensing performance along with high reproducibility. A disposable amperometric triglyceride biosensor was fabricated based on a Au/PEDOT: PSS nanocomposite and the co-immobilization of lipase, glycerol kinase, and glycerol 3-phosphate oxidase [466]. The electrochemical signal was significantly enhanced by the presence of Au NPs. A photodetector with a blend of poly[*N*-9'-heptadecanyl-2,7-carbazole-alt-5,5-(4',7'-di-2-thienyl-2',1',3'-benzothiadiazole)] (PCDTBT) and [6,6]-phenyl C71-butyric acid methyl ester (PC70BM) with PEDOT:PSS as the hole transport layer was fabricated for the detection of human thyroid-stimulating hormone [467]. A chemiluminescent immunoassay was employed to detect thyroid-stimulating hormone (TSH) with the generated light. A conductometric sensor for the detection of hydrazine and NADH was fabricated using a Pd NP-decorated PEDOT: PSS matrix [468]. The Pd NPs included in the PEDOT: PSS matrix served as reaction sites for the oxidation of hydrazine or NADH. Moreover, the released electrons reduced PEDOT, leading to an increased conductance. The pristine PEDOT: PSS electrode showed only weak changes upon exposure to hydrazine compared with Pd NP-decorated PEDOT: PSS. An anionic/cationic surfactant-doped PEDOT/MWNT nanocomposite electrode was fabricated through the electrochemical deposition of EDOT in the presence of SDS/CTAB on the surface of a pre-coated MWNT GCE [469]. The SDS/CTAB-doped PEDOT/MWNT electrodes were utilized for the voltammetric determination of pyrethroids and an organochlorine pesticide, dicofol. A sensor for acetylcholinesterase (AChE) was fabricated based on  $\text{Fe}_2\text{O}_3$ /PEDOT-rGO NC by immobilizing enzymes AChE and choline oxidase [470]. The synergetic effect of  $\text{Fe}_2\text{O}_3$ , PEDOT, and rGO provides a wide linear range, fair analytical recovery, reusability, significant selectivity and faster response towards ACh detection. An electrochemical hydrazine sensor was reported based on the three-dimensional PEDOT (3D-PEDOT) supported onto the  $\text{Cu}_x\text{O}$ . 3D-PEDOT- $\text{Cu}_x\text{O}$ , through a combination electrodeposition and cyclic voltammetry approaches [471].  $\text{Cu}_x\text{O}$  was included into the pores of 3D-PEDOT- $\text{Cu}_x\text{O}$  and the combined architecture was beneficial for electron transfer and mass transfer processes. The catalytic

properties for hydrazine arise due to the interactions between 3D-PEDOT–Cu<sub>x</sub>O.

### ***Gas and ion sensors***

A miniaturized chemiresistor sensor based on O<sub>2</sub> plasma-treated SWNTs and a PEDOT: PSS composite film was developed for sensing TMA gas [472]. Also, a composite film comprising PEDOT: PSS and O<sub>2</sub> plasma-treated SWNTs was prepared through dielectrophoretic assembly and utilized as an NH<sub>3</sub>/TMA sensor [473]. PVA incorporation was used subsequently for silanization via covalent linkages of biological moieties onto PEDOT: PSS films. A PVA/PEDOT: PSS film was used as the matrix for GOx and polypeptide functionalization to generate an OECT sensor. A conductometric interdigitated sensor was fabricated with electrospun nanofibrous titania as a transducer and PEDOT: PSS as a sensing matrix for the detection of nitric oxide (NO) [474]. The NC film of WO<sub>3</sub> and PEDOT: PSS was printed onto a flexible polyamide substrate to develop an NO<sub>2</sub> gas sensor [475]. The factors such as conducting channels provided by PEDOT: PSS and formation of hetero-junctions between n-type WO<sub>3</sub> and p-type PEDOT: PSS at the WO<sub>3</sub>-PEDOT: PSS interface determine the sensing characteristics. The p–n junction at the interface of p-type PEDOT: PSS with n-type WO<sub>3</sub> grains creates a space charge region. The adsorption of NO<sub>2</sub> causes a change in the depletion layer at both the WO<sub>3</sub> grain surface and p/n-junction of WO<sub>3</sub>-PEDOT: PSS. The adsorbed NO<sub>2</sub> removes electrons from the CB of WO<sub>3</sub>, forms NO<sub>2</sub><sup>−</sup> species and extends the depletion width. The inclusion of N-doped GQDs (N-GQDs) into PEDOT: PSS significantly improved the sensitivity and selectivity [476]. Besides the doping/dedoping processes, the swelling after diffusion of VOCs into the PEDOT–PSS contributed to the VOC detection. Typically, when methanol molecules diffuse into the PEDOT–PSS matrix, the electron hopping process becomes more difficult as the PEDOT interchain distance increases due to the swelling process. The effect of changing humidity was studied using The PEDOT: PSS/PVA-MC composite [477]. The PEDOT: PSS/PVA based humidity sensor operates due to the change in capacitive response as a result of inclusion into PEDOT: PSS. The capacitive response causes the decrease in the dielectric constant of the film. PVA–PEDOT: PSS composite thin films deposited on a piezoelectric substrate. The PEDOT: PSS/TiO<sub>2</sub>-IDE could detect NO concentrations down to 1 ppb and suited for asthma monitoring. Ultrathin free-standing iron oxide-embedded PEDOT: PSS nanocomposite films were fabricated by a single-step spin-coat deposition method, and the nanocomposite films were utilized as resistive humidity sensors [478]. The sensitivity of the PEDOT: PSS/iron oxide nanocomposite film to humidity increased with increasing iron oxide NP concentration. A wireless humidity sensor was fabricated with a magnetic ribbon-coated PEDOT: PSS matrix [479]. The sensor employed a mechanical resonance frequency change upon exposure to water and the PEDOT: PSS matrix expanded or contracted by several percents when water was absorbed or desorbed. A reduced graphene oxide (rGO)-included PEDOT film was fabricated by vapor phase

polymerization and was explored as a chemical sensor for VOC vapors. Polymerized ionic liquid (PIL) and  $\text{Fe}^{3+}$  ions were used as linkers (rGO: PIL/PEDOT) for the hybridization of PEDOT with rGO sheets [480]. The chemical sensor based on this hybrid film could detect different VOC vapors at ppm concentration levels in the following order: methanol > chloroform > THF > benzene. An SWCNT/*p*-tert-butyl calixarene-substituted PT composite was used as a resistance sensor for xylene isomers [481]. The calixarene was linked to PT to differentiate the isomers of xylene because of its shape-persistent hydrophilic binding pockets with a cone conformation. The PT units in the polymer were essential dispersing elements that prevented the aggregation of large SWCNT bundles and formed evenly distributed percolative networks. A calixarene-substituted P3HT sensor showed high sensitivity to *p*-xylene, *m*-xylene, and *o*-xylene. However, SWCNT/P3HT showed similar responses for all three isomers of xylene. An alcohol dehydrogenase biosensor was fabricated for ethanol by co-immobilizing the enzyme and  $\text{Ru}(\text{bpy})_3^{2+}$  on an ITO electrode functionalized with PEDOT-PSS-GF [482].

An MCNC based ME was fabricated using GS, PEDOT, and Co NPs as the modifying materials [483]. PEDOT and Co NPs were sequentially electrodeposited onto a GS-modified GCE and used for the electrochemical determination of nitrite ions. The individual components in the PEDOT GCE/PEI/ $\text{PMo}_9\text{V}_3$ /PEDOT-AuNPs NC provide beneficial characteristic to the nitrite sensor individually [484]. The S atom in the heterocyclic part of PEDOT binds the Au atom through chemical interactions, the  $\pi$  electron system in PEDOT provides good electron transport.  $\text{PMo}_9\text{V}_3$  acts as proton and electron reservoir and Au NPs facilitate the electron transfer process. PON is an amine generated in the reaction between nitric oxide and superoxide. PON can damage subcellular organelles, membranous and enzymes and its quantification is complicated by a number of obstacles. A PON sensor was fabricated exploiting the properties of BDD, hemin and PEDOT. The loading of PEDOT increases the response sensitivity of the sensor and the hemin–PEDOT polymer layer functions to catalyze the oxidation of PON [485]. PEDOT was used to stabilize Au NPs synthesized through the chemical reduction of chloroauric acid with EDOT monomers ( $\text{Au@PEDOT}$ ) [486]. An  $\text{Au@PEDOT-PSS}$  ME was investigated for the determination of  $\text{Hg}(\text{II})$  by linear sweep voltammetry. The metallic  $\text{Hg}^0$  formed at the ME amalgamates Au. A cotton fiber was functionalized with PEDOT: PSS by a simple soaking process [487]. The PEDOT: PSS-coated cotton fiber functioned as an OECT. The PEDOT: PSS is conducting channels directly interfaced with a liquid electrolyte and showed stable and reproducible current modulation for the electrochemical sensing of NaCl in water. The sensor for persulphate ( $\text{S}_2\text{O}_8^{2-}$ ) ion was fabricated by grafting silica molybdate (SiMO) and PEDOT onto MWCNT (SiMO–PEDOT/MWCNT hybrid NC) [488]. During the persulfate sensing process, the reduction of  $\text{S}_2\text{O}_8^{2-}$  was catalyzed both by SiMO and PEDOT.

### **Miscellaneous sensors**

A microfibrinous array of PVP-incorporated PEDOT: PSS (PVP–PEDOT: PSS) with a curled architecture was fabricated by combining electrospinning with simple harmonic motion [489]. The curled architecture of the PVP–PEDOT: PSS fibrous polymer arrays caused three times higher sensor performances (a reversible linear elastic response to the strain of up to 4%) than that of the electrospun non-woven mats. A room temperature VOC sensor based on the ternary NC composed of N-doped graphene quantum dots (N-GQDs) and PEDOT: PSS was fabricated. Non-lithographic, and planar, UV sensors were fabricated based on a ZnO NR array/PEDOT: PSS NH. The photoinduced holes are driven by depletion field to the surface, combine with surface oxygen ions and eliminate the barrier near the NR surface [490]. Electroactive interpenetrated PEDOT polymer network actuators were fabricated within a flexible solid polymer electrolyte that combined poly(ethylene oxide), and nitrile butadiene rubber [491], and the PEDOT-IPN was used as a mechanical sensor.

**Table 6** details the signal transduction (electrochemical, optical etc.) mode based sensors utilizing the four categories of F-PTs. Both electrochemical and optical sensors are fabricated utilizing all the four categories of F-PTs.

**Table 6**

### 3.4. Functionalized Polyfluorene (F-PFs)

PFs are the simplest regular step ladder-type polyphenylene vinylene and exhibit wide band gaps between 2.8 and 3.5 eV, excellent thermal stability, high photoluminescence quantum efficiency, and good charge transport properties, making them promising blue light emitting polymers for applications in chemosensors [492-494]. PFs have the ability to generate amplified response to analytes, with high sensitivity and selectivity [495]. PFs were used for sensor applications either as substituted PFs (Category I) or as a component in multicomponent based sensor material (Category IV, Scheme 1). The details of functional group incorporated/attached to PF backbone, sensing mode, the specific analyte for sensing and mechanism of sensing are detailed in **Table 7**. F-PFs show promising sensing capabilities for metal ions and analytes via “turn on” or “turn off” mechanisms (**SI: S1**). To the best of our knowledge, the majority of F-PFs for sensors have been utilized with the substituted type (Category 1, Scheme 1) and F-PFs of other categories have not explored until recently (**Table 7**). The challenge remains open for the development of F-PFs in biofunctionalized, nanostructured and multicomponent forms especially for the sensor fabrications.

Table 7

### 3.4.1. Substituted F-PFs

F-PFs containing neutral or ionic groups were developed through substitution of the parent structure of PF.

#### 3.4.1.1. F-PFs with neutral side groups

##### *Ion sensors*

Poly(9,9-bis(6'-benzimidazole)hexyl)fluorene-*alt*-1,4-phenylene (PBP) was developed as a fluorescence probe for the detection of inorganic phosphate (Pi) in human saliva through super quenching and dequenching processes [496]. Zn<sup>2+</sup> and Fe<sup>3+</sup> ions quenched the fluorescence of PBP at very high concentrations, whereas other metal ions had virtually no or negligible effect on the fluorescence. The remarkable fluorescence quenching by Fe<sup>3+</sup> was due to simultaneous electron transfer, efficient energy migration, and exciton delocalization along PBP. PBP thus exhibited exemplary activity as a noninvasive fluorescence sensor and proved viable for the in situ monitoring of important biological targets like Fe<sup>3+</sup> and Pi in saliva. 4-Poly[9,9'-(*N*-carbazole-hexyl)fluorene] (PNCHF), a tetramer with eight peripheral carbazole side chains, was synthesized. The Fe<sup>3+</sup> metal ion sensing ability of PNCHF was compared those of with poly[2,7-(9,9-dihexylfluorene)] and poly[2,7-(9-(2-ethyloctyl)-carbazole)] [497]. The PNCHF exhibited excellent fluorescence quenching sensitivity towards Fe<sup>3+</sup>. The introduction of carbazole groups in PNCHF was beneficial for specific detection of Fe<sup>3+</sup> through metal-ligand complex formation over other metal ions. Also, the location on the peripheral side chains improved the sensitivity of fluorescence detection compared with that of pristine poly[2,7-(9,9-dihexylfluorene)] and poly[2,7-(9-(2-ethyloctyl)-carbazole)]. A series of fluorene-based copolymers, poly[(9,9-bis(propenyl)-9*H*-fluorene)-*co*-(9,9-dihexyl-9*H*-fluorene)] (P1), poly[(9,9-bis(carboxymethylsulfonyl-propyl)-fluorenyl-2,7-diyl)-*co*-(9,9-dihexyl-9*H*-fluorene)] (P2), and poly[(9,9-dihexylfluorene)-*co-alt*-(9,9-bis-(6-azidohexyl)fluorene)] (P3), were synthesized by Suzuki coupling [498], and their Fe<sup>3+</sup> ion sensing capabilities were investigated. The prepared polymers possessed a fluorene backbone functionalized with different groups in the ninth position of fluorene. The alkyl side chain-substituted PFs exhibited high fluorescence quenching efficiency towards Fe<sup>3+</sup> ions, suggesting the probable formation of ferrocene-like complexes with PF. Poly[(4,4'-azobenzene)-2,7-[9,9-bis(6'-*N,N,N*,-trimethyl ammonium)hexyl fluorene]dibromide} (PFAB) was synthesized via Suzuki cross-coupling [499]. The azo group of nonfluorescent PFAB was converted to hydrazine via photoreduction to obtain fluorescent PFAB-L (**Fig. 31**). The pH sensing involved the

control of fluorescence of PFAB-L through protonation of –N-H-N-H-group and the resultant noticed through ‘turn on’ fluorescence. Also, the association between  $\text{Fe}^{3+}$  and the –N-H-N-H-group of PFAB-L disturb face to face  $\pi$ - $\pi$  interaction and quenching of fluorescence in the presence of  $\text{Fe}^{3+}$  ions. Optical measurements illustrated that the flexible hydrazine group induced a face-to-face arrangement of the phenyl–fluorene–phenyl moieties, resulting in excimer formation in PFAB-L. A multifunctional fluorene-based material containing triple azacrown ether (FTC) was developed [500] and utilized as a chemosensor for  $\text{Fe}^{3+}$  detection. The sensory function of FTC was explained through interaction between  $\text{Fe}^{3+}$  ions and the lone pair of electrons on the nitrogen atom of azo crown group and quenching of fluorescence by electron transfer from the fluorophore to the metal ion.

**Fig. 31**

A donor– $\pi$ -acceptor-type conjugated polymer based on the benzo[*c*][1,2,5]selenadiazole (BSe) moiety and fluorene was prepared by the Sonogashira–Hagihara reaction and was sensitive for the detection of  $\text{Hg}^{2+}$  ions through fluorescence quenching [501]. The polymer, PBSe, was selective to  $\text{Hg}^{2+}$  due to the structural rigidity of BSe unit, larger radical of  $\text{Hg}^{2+}$  ions and strong Hg-BSe binding. The visible color of the polymer (PBSe) disappeared upon addition of  $\text{Hg}^{2+}$  ions  $\text{Hg}^{2+}$ -BSe acted as a native naked eye indicator. Several *meta*- and *para*-linked poly(arylene ethynylene) derivatives containing L-aspartic acid-functionalized fluorene units were utilized for  $\text{Hg}^{2+}$  sensing in aqueous solution [502]. Both *meta*- and *para*-linked polymers were selective for  $\text{Hg}^{2+}$  in aqueous solution, but the different linkages had a remarkable effect on the detection of  $\text{Hg}^{2+}$ . The higher fluorescence response of the *meta*-linked polymer was ascribed to its higher conformational stability arising from the more efficient coordination between the aspartic acid groups in the polymer and the  $\text{Hg}^{2+}$  ions through a conformational transformation or reorganization. The synthesis of a PF copolymer with imidazole ligands in the side chain (poly[(9,9-dihexylfluorene-2,7-diyl)-alt-co-(9,9-bis[6'-(1-imidazolyl)hexyl]fluorene-2,7-iy)]) and its ability to sense  $\text{Cu}^{2+}$  ion was investigated by absorption and emission spectroscopy [503]. The sensor system was designed by taking advantage of the conjugated  $\pi$ -stacking luminescence properties of PF and the metal ion coordinating ability of imidazole. The fluorescence of PF was effectively quenched upon addition of  $\text{Cu}^{2+}$  ion. Imidazole-functionalized PF derivatives were synthesized and post-functionalized with a terminal group and utilized as fluorescent “turn-on” and “turn-off” sensors for  $\text{CN}^-$  and  $\text{Cu}^{2+}$ , respectively [504]. The fluorescent “turn off” sensor for  $\text{Cu}^{2+}$  was based on the selective quenching of PF fluorescence by coordination of the imidazole group in the PF-imidazole derivative with  $\text{Cu}^{2+}$  ions. The “turn-on” optosensor for  $\text{CN}^-$  was based on the emission recovery of the polymer that had been deactivated by a quencher species. A PF derivative prepared through the formation of a self-assembled monolayer on a glass plate via linking the  $-\text{NH}_2$  groups in PF with 3-glycidoxylpropyl silane on the glass surface (**Fig. 32**)

was tested for its fluorescence response towards  $\text{Cu}^{2+}$  [505].  $\text{Cu}^{2+}$  ions strongly quench the fluorescence of fluorophores via electron transfer. Furthermore,  $\text{Cu}^{2+}$  ions can chelate ligands with N or O atoms. The synthesis of copolyfluorene (PFBI) from poly[(9,9-dihexylfluorene)-*alt*-(9,9-dibromopentylfluorene)] (PFBBr) was demonstrated, and its chemosensory and electroluminescent characteristics were investigated [506]. The fluorescence of PFBI was dramatically quenched by  $\text{Cu}^{2+}$  ions, but only partially quenched by  $\text{Zn}^{2+}$  or  $\text{Cd}^{2+}$  ions. Bis-(bromohexyl)-PF has been synthesized by Suzuki cross-coupling polymerization and further converted to organoboron-appended PF (PFBP). PFBP was used as a fluorescent probe for the sensitive and selective detection of  $\text{CN}^-$  ions by a fluorescence “turn off” mechanism [507].

**Fig. 32**

The organoboron moiety was attached to bis-(bromohexyl)-PF by a postpolymerization reaction. The efficient quenching (“turn off”) and a decrease in average fluorescence lifetime of PFBP in the presence of  $\text{CN}^-$  was explained by a mechanism involving the complex formation of PFBP with  $\text{CN}^-$  and due to “soft–soft interactions” between the boron center and  $\text{CN}^-$  ions (**Fig. 33**). The coil–rod–coil ABA tri-block copolymer P(MMA-*co*-NBDAE)-*b*-PF-*b*-P(MMA-*co*-NBDAE) (where MMA and NBDAE are methyl methacrylate, and 4-(2-acryloyloxyethylamino)-7-nitro-2,1,3-benzoxadiazole, respectively) self-assembled into micellar NPs containing P(MMA-*co*-NBDAE) Coronas, a blue light-emitting PT core, and a green-emitting entity (**Fig. 34**) [508]. Sensitive and selective ratiometric  $\text{F}^-$  probes with enhanced sensing performance and visual detection were developed. The blue-emitting conjugated PF block and the green-emitting NBDAE moieties exhibit  $\text{F}^-$  “turn-off” characteristics and served as FRET donors and switchable acceptors, respectively. In the tri-block copolymer, the core-shell conformation brought the blue-emitting conjugated core and the NBDAE moieties into proximity within the micellar coronas, resulting in FRET.

**Fig. 33**

**Fig. 34**

### **Biosensors**

Neutral PF derivatives were used for the fabrication of various biosensors. A reusable fluorescent sensor for heme proteins (hemoglobin, myoglobin and cyt c) based on PF derivatized onto polystyrene electrospun nanofibrous membrane (P-PS) was reported [509]. The sensor fabrication involved the formation of a hydrophobic coating with trimethylchlorosilane and the deposition of the polymer PS

electrospun nanofibers. The quenching process was mainly based on FRET between the fluorescent PF and the heme prosthetic groups. The strong emission maximum ( $\sim 427$  nm) of the doped PF derivative and the maximum adsorption of prosthetic group of heme ( $\sim 405$  nm) formed the basis for FRET. The amino-functionalized PF derivative (poly[(9,9-bis(30-((*N,N*-dimethylamino)-*N*-ethyl ammonium)propyl)-2,7-fluorene)-*alt*-2,7-(9,9-*p*-divinylbenzene)-*alt*-fluorene)-*alt*-2,5-dimethyl-*p*-phenylenediamine] (PF-NH<sub>2</sub>) was synthesized and immunosensors were fabricated for the detection of the cancer biomarker ovarian protein antigen (CA125) [510]. PFO was transformed into fluorescent PF dots with surface carboxyl groups. PF dots can coordinate Tb<sup>3+</sup> ions and sensitized by calcium dipicolinate (CaDPA) [511]. Fluorescent semiconducting PFO and poly(styrene-co-maleic anhydride) (PSMA) were employed to prepare functionalized PFO dots. The hydrolysis of each maleic anhydride unit in PSMA resulted in two closely spaced carboxyl groups, and contributed to the high binding affinity with lanthanide ions such as Tb<sup>3+</sup> (**Fig. 35**). Thus, ratiometric luminescence with Tb<sup>3+</sup>-chelated PFO was obtained, and the sharp fluorescence peaks of the  $\beta$ -phase PFO dots and the narrow-band emissions of the Tb<sup>3+</sup> ions enabled ratiometric CaDPA detection.

**Fig. 35**

#### **Gas and other sensors**

A fluorescence “turn on” sensor was fabricated for the detection of methamphetamine (MAPA), a volatile amine using poly(1,9-dioctyl fluorine) (PFO) as the sensing material. The fluorescence of PFO was efficiently quenched by tetraphenyl porphyrin (TPPp) or metallotetraphenylporphyrin (MTPPp) via electron or energy-transfer in the solid state, and the reverse electron or energy-transfer restored the fluorescence when electron-donating amines were bound to TPPp or MTPPp. Different amines such as aniline, *N,N'* dimethyl aniline, benzyl aniline and *N,N*-dimethyl benzene amine and MAPA had different electron-donating abilities as well as diverse binding affinities with MTPPp for conferring the selectivity to the sensors. The electron density of TPPp or MTPPp was reduced by the hydrogen bonding with the amine [512].

#### **3.4.1.2. F-PFs with cationic side groups**

##### **Biosensors**

A method of DNA methylation for the detection of cancer using an optically amplifying poly{(1,4-phenylene)-2,7-[9,9-bis(6'-*N,N,N*-trimethyl ammonium)-hexyl fluorene] dibromide)} cationic PF derivative

(PF-C) was developed [513]. The methylated DNA was amplified by PCR, and the methylation level was detected through Fourier resonance energy transfer (FRET) between PF-C and fluorescein. Through an associated analysis, a threshold for cancer detection with a sensitivity of 85.7% was obtained. PF-C and a  $\alpha$ -mannose-containing PF derivative (PF-S) were prepared from a pristine PF polymer that contained 20% benzothiadiazole (BT) units in the backbone [514]. Owing to the sugar-bearing groups attached to the polymer side chains, the polymers showed good water solubility. The titration of Con A into PF-C did not result in an obvious change in fluorescence, whereas the fluorescence of BT in PF-S increased when concanavalin (Con A) was added. The BT emission intensity increased due to the specific interaction between Con A and  $\alpha$ -mannose and FRET occurs from the fluorene–phenylene segments to the BT units. A series of hyperbranched cationic PF derivatives (HP-PF) was developed for sensing heparin using fluorescence [515]. The quaternized side chains of HP-PF were positively charged in aqueous solutions and induced electrostatic interactions with sulfonic acid groups present in heparin. A biosensor was developed using a PF derivative containing 20 mol% 2,1,3-BT and a donor-acceptor architecture [516]. Few CPEs containing long-lived phosphorescent Ir(III) complexes were designed, synthesized and used for ratiometric and lifetime-based sensing of heparin utilizing the electrostatic interactions between the cationic polymers and anionic heparin. The electrostatic interaction between cationic PCPEs and heparin influences the FRET efficiency and changes the intensity ratio of luminescence from Ir(III) complex to PF. When heparin was added into the solution of PCPE, the aggregation of NPs with core–shell structure happened due to the electrostatic interaction between the cationic polymer NPs and anionic heparin, eventually producing efficient FRET from polyfluorene to Ir(III) complex [517].

### ***Ion sensors***

A PF derivative bearing two amino and four carboxylic acid groups in each repeat unit (PF-aa) was developed as a reversible pH sensor over a wide pH range (3–12) [518]. The protonation and deprotonation of the amine and carboxylic groups occurred at various pH values within this range. At a low pH ( $\text{pH} < 3$ ), both the carboxylate and amine groups were protonated, so that PFP-aa had two types of positive charge per repeat unit. However, at a higher pH ( $\text{pH} > 5$ ), the carboxylic acid groups were deprotonated, affording PFP-aa with four negative charges. At a relatively higher pH ( $\text{pH} > 10$ ), both the carboxylic acid and amine groups were deprotonated, affording PFP-aa six negative charges. The overall negative or positive charge of PFP-aa varied depending on the pH, and the charges caused electrostatic repulsion between the polymer chains, resulting in different aggregation states and energy transfer abilities. Thus, PFP-aa showed a pH-dependent fluorescence response. It was demonstrated that PFP-aa could be used as a pH sensor to detect D-fructose by fabricating a sensor with PFP-aa and boronic acid.

### Gas sensors

PFO films doped with palladium tetraphenyl porphyrin (PdTPP) were developed as a sensing medium for the detection of amines [519]. PdTPP effectively quenched the fluorescence of PFO via electron energy transfer. When an electron donating amine was bound to PdTPP, a “turn on” mechanism was established, and fluorescence was recovered through reversal of electron energy transfer. Based on the differences in the binding affinities of various amines, the fluorescence recovery was distinct for each amine.

#### 3.4.1.3. F-PFs with anionic side groups

### Ion sensors

Poly(9,9-bis(6'-sulfate)hexyl)fluorene-*alt*-1,4-phenylene sodium salt (P1), was synthesized and used for selective detection of Fe<sup>3+</sup> and Pi in blood serum. A phosphonate-functionalized fluorescent PF film was covalently immobilized onto a glass surface. The film exhibited good selectivity towards Fe<sup>3+</sup> ions over other common metal ions in both organic and aqueous solutions [520]. Dendronized PF derivatives with pendant –COOH groups were synthesized via Suzuki polycondensation of dendritic macromolecules and phenyl boronic acid. These PF derivatives were used as sensors for Hg<sup>2+</sup> and Cu<sup>2+</sup> [521, 522], as –COOH associated with the cations through electrostatic interactions. The behavior of the PF derivatives towards metal ions depended on the nature of their side chains. An anionic PF derivative with two L-aspartic acids in the side chain of every fluorene unit was used as a fluorescent sensor for Hg<sup>2+</sup> ions [523].

### Biosensors

A two-component sensor for D-fructose sensors were designed by combining anionic PF-CPEs (PBPSO<sub>3</sub>Na) and boronic acid functional viologens (BBVs): [N,N'-4,4'-bis(benzyl-2"-boronic acid)-bipyridinium dibromide (*o*-BBV), N,N'-4,4'-bis(benzyl-3"-boronic acid)-bipyridinium dibromide (*m*-BBV), and N,N'-4,4"-bis(benzyl-4"-boronic acid)-bipyridinium dibromide (*p*-BBV)] [524]. The PBPSO<sub>3</sub>Na/*o*-BBV, PBPSO<sub>3</sub>Na/*m*-BBV, and PBPSO<sub>3</sub>Na/*p*-BBV ensembles acted as sensors owing to the high affinity of D-fructose for the boronic acid groups. The different positions of the boronic acid groups in the BBVs and the electrostatic interactions of the BBVs with PBPSO<sub>3</sub>Na affected the sensing order towards D-fructose;

*m*-BBV/PBPSO<sub>3</sub>Na > *o*-BBV/PBPSO<sub>3</sub>Na > *p*-BBV/PBPSO<sub>3</sub>Na.

### 3.4.2. Nanostructured F-PFs

PF polymers allow flexible designing to develop NSs as well as functionalized NSs with multiple fluorophores as acceptors or functional groups. An anionic DNA-functionalized PF NPs (PF-DNA<sub>P</sub> CPNs) was used for label-free detection of oligonucleotides [525]. The hybridization of PF-DNA<sub>P</sub> CPNs with fully complementary ssDNA<sub>C</sub> resulted in efficient energy transfer. The emission spectrum of the complexes with one base pair mismatch was significantly different from that of the fully complementary case. Besides, the energy transfer efficiency decreased with an increasing number of mismatched base pairs in DNA strands. Fluorescent and clickable NWs were developed by cross-linking the polymers poly[(9,9-dihex-5-yn-1-ylfluorenyl-2,7-diyl)-co-(9,9'-di-noctylfluorenyl-2,7-diyl)] (F6E8) and poly[(9,9-dihex-5-yn-1-ylfluorenyl-2,7-diyl)-co-(2,2'-bithiophene)] (F6E2T) via irradiation to form 1D NSs (**Fig. 36**) [526]. The alkyne groups on the surface of NWs were functionalized with a fluorescent azide (5-TAMERA-PEG-3-azide) by click reaction. The FRET processes between 5-TAMERA and NWs could form the basis for biological sensing platforms. Hyper branched PF NPs were synthesized by coupling the repeat units, 9,9-dihexylfluorene, and triphenylamine. The hyper branched PFNPs exhibited selective and sensitive fluorescent detection of Fe<sup>3+</sup> [527]. The stronger electron withdrawing ability of Fe<sup>3+</sup> contributes to the generation of high charge density by partially filling the d-orbital through  $\pi$ -electron transfer complex with the PF NPs formation. Electrospun nanofibers of the rod-coil-coil tri-block copolymer polyfluorene-block-poly(*N*-isopropyl acrylamide)-block-poly(*N*-methyl acrylamide) (PF-*b*-PNIPAAm-*b*-PNMA) were prepared. The PF, PNIPAAm, and PNMA blocks were used for fluorescent probing, hydrophilic thermoresponsive, and chemical crosslinking, respectively (**Fig. 37**) [528]. At temperatures below the lower critical solution temperature (LCST) of PNIPAAm, the swelling of PNIPAAm blocks and absorption of incident light by the PF blocks resulted in stronger PL. At temperatures above the LCST of PNIPAAm, shrinkage of the NIPAAm chains suppressed light absorption by the PF blocks, resulting in PL quenching. The high surface-to-volume ratio of the nanofibers enhanced the sensitivity and temperature-response speed to compare with normal drop-cast films.

**Fig. 36**

**Fig. 37**

**Table 8** informs that F-PFs are well suited for the fabrication of optical sensors. Though F-PFs are electroconductive, the optical characteristics of the F-PFs are effectively manipulated for the designing of sensors.

Table 8

### 3.5. Functionalized polyacetylene (F-PAs)

PA-based FCPs were generally used for the fabrication of optical (fluorescence) sensors. A fluorescence “turn-on” probe for  $F^-$  sensing was developed using urea-functionalized poly(phenylenebutadiynylene) (poly-1) [529]. The binding of  $F^-$  to the urea groups on poly-1 via hydrogen bonding triggered structural changes in poly-1. This anion-induced fluorescence change was dependent on the type and basicity of the anion. Imidazole-functionalized PA hybridized with Au NPs was developed as a “turn on” fluorescent probe for the detection of  $CN^-$  [530]. Au NPs quench the imidazole fluorescence, but upon addition of  $CN^-$  ions, the Au NPs were transformed into Au-  $CN^-$  complex to cause suppression of fluorescence quenching. As a result, the quenched fluorescence was recovered, and the  $CN^-$  ions could be detected. Side-chain functionalization of poly(*p*-phenylene ethynylene) (PPE) with triazole linkers, amino donors/receptors, and solubilizing groups yielded remarkable fluorescence turn-on sensors for  $Zn^{2+}$  and  $Cd^{2+}$  ions in THF, and  $Cd^{2+}$  ions in water (**Fig. 38**) [531]. Click chemistry was used to generate a functionalized PPE (PPE-1). The 1,2,3-triazole in PPE-1 not only acted as a linker, but also quenched the PPE fluorescence. The fluorescence of PPE-1 was enhanced 51-fold upon addition of  $Zn^{2+}$  ions, and PPE-1 also had very high sensitivity towards  $Cd^{2+}$  ions (ca. 34-fold enhancement).

Fig. 38

## 4. Molecular imprinted polymers (MIPs) based on FCPs

### 4.1. Molecular imprinting concept

In nature, molecular recognition is driven largely by various non-covalent forces, including ionic interactions, hydrogen bonding, van der Waals forces, and hydrophobic effects. Molecular recognition relies on the formation of an energetically favorable complex between a receptor and a substrate on the basis of electrostatic and stereochemical complementarity. “Lock and key”—the analogy for molecular recognition—was first described by Emil Fischer over a century ago. In the case of MIPs, the “lock” is usually prepared by copolymerizing functional monomers and a crosslinker in a suitable porogenic solvent in the presence of the target analyte, the “key.” The template is then removed from the resulting polymeric matrix using a suitable physical or chemical method, leaving behind specific binding cavities that are complementary to the template/analyte in size, shape, and functional groups (**Fig. 39**). The resultant materials consist of rigid three-dimensional polymeric structures containing voids corresponding

to the imprint of the template molecule. These materials can, therefore, act similarly to, and hence serve as replacements for, natural antibodies in affinity separations, sensors, and medical devices. The varied applications of MIPs have been discussed in some review papers [532-537].

**Fig. 39**

#### **4.1.1. Molecular imprinting methods**

Generally, it is often useful to categorize MIPs according to the types of interactions between the template and polymer-forming material during the formation of the imprinted matrix. The commonly used classifications are covalent, non-covalent, semi-covalent, and metal-ion-based methods. In practice, MIPs may be prepared using a combination of the methods above, and some examples may defy unambiguous classification into one of these convenient descriptions.

##### **4.1.1.1. Non-covalent imprinting**

While the early methods adopted by Polyakov and Dickey can be described as non-covalent imprinting, it is Klaus Mosbach and coworkers who are credited with the introduction of non-covalent imprinting for organic polymers. The principal advancement in their work was the introduction of the concept of a “functional monomer,” such as methacrylic acid (MAA), used in conjunction with a matrix-forming crosslinker, such as ethylene glycol dimethacrylate (EGDMA). These types of polymers are called *non-covalently imprinted polymers* as the interactions between the template, and functional monomer can be due to relatively weak but directional interactions, such as hydrogen-bonding. Today, the non-covalent approach is the most widely used owing to its relative simplicity, ease of template removal, and the availability of a wide variety of potential functional monomers. However, this last reason can prove to be a drawback, as searching for optimum monomer compositions can be a daunting prospect. This problem has been solved by the use of combinatorial, computational [538], and chemometric [539] methods to aid in the design of non-covalently imprinted polymers. An intriguing alternative is the use of functional crosslinkers, such as *N,O-bis*-methacryloyl ethanolamine (NOBE), without any functional monomers [540]. These polymers are called one monomer molecular imprinted polymers (OMNiMIPs) and perform better than MAA-EGDMA-based polymers. In the case of NOBE, the use of additional functional monomers, such as MAA, actually deteriorates the performance of the obtained MIPs.

A major drawback of the non-covalent approach is the requirement for the template and target to form a sufficient number of non-covalent intermolecular interactions to allow the formation of a binding cavity during polymerization. Non-covalent imprinting is therefore not particularly successful for templates

that do not possess appropriate functional groups. Another disadvantage of the non-covalent approach is that, in most cases, an excess of the functional monomer must be used to ensure MIPs with a useable capacity is obtained. As a consequence, much of functional monomer is not associated with the template giving rise to the high non-specific binding and lowers the selectivity and specificity of recognition. Despite these drawbacks, non-covalent imprinting has become the most popular and generic synthesis strategy for the preparation of MIPs because of its ease, simplicity, and versatility [536]. After polymerization and removal of the template, the functionalized polymeric matrix can then rebind the target (template) via the same non-covalent interactions present in the polymerization mixture. These interactions can act cooperatively, giving rise to high affinity for the analyte.

#### **4.1.1.2. Covalent imprinting**

Covalent imprinting is another approach for the preparation of MIPs. Usually, in covalent imprinting, templates are bound to appropriate monomers, such as 4-vinylphenylboronic acid or 4-vinylbenzylamine, via condensation reactions, resulting in the formation of labile covalent linkages, such as a boronate ester or Schiff's base linkage [541]. After polymerization, the template can be released by hydrolysis of the covalent linkages (split-off) and removed from the polymer in a similar way to that used in non-covalent imprinting. Covalent bonds are reformed during the rebinding step. Owing to the greater stability of covalent bonds, covalent imprinting protocols yield a more homogeneous distribution of binding sites within MIPs. However, covalent imprinting is considered to be a less flexible approach than non-covalent imprinting and requires the presence of specific functional groups within the template. Therefore, templates suitable for covalent imprinting are limited.

#### **4.1.1.3. Hybrid approach**

A third protocol for the synthesis of MIPs involves a hybrid approach that combines both covalent and non-covalent techniques. For example, after a covalently bound template is split from a polymer by hydrolysis, non-covalent rebinding can then be achieved. This method is often referred to as the semi-covalent approach and was first proposed by Whitcombe et al [542, 543]. This method is characterized by the efficient incorporation of the template through covalent binding and mild conditions for non-covalent rebinding. Labile esters of a polymerizable acid in combination with an alcohol template was developed as a suitable system for this approach; however, hydrolysis in such cases is often not straightforward, and the steric requirements of an acid and alcohol in hydrogen-bonding contact are rather different from those of the corresponding ester making lesser ideal conditions for imprinting. Some of the limitations of the semi-covalent imprinting approach can be overcome by the use of a linker group

between the template and functional monomer that is lost on template removal (the sacrificial spacer method).

#### **4.1.1.4. Metal-mediation and surface imprinting**

This fourth method for the synthesis of MIPs uses metal atoms or ions to link the template and polymerizable monomers, with both units acting as ligands in the coordination sphere of the metal center [544]. Synthetic strategies for the generation of MIPs have been extensively reviewed by Mayes and Whitcombe [545]. Surface imprinting [546] is another interesting approach for the preparation of MIPs with cavities at the surface or close to the surface for facilitating the mass transport.

#### **4.2. MIPs with pristine CPs**

The physicochemical characteristics of acrylic polymers limit their ability to serve as natural electrical insulators; this restricts their application as electrochemical sensors and puts severe limitations on the efficiency of the signal transduction process. Therefore, a direct path is required for the conduction of electrons from the binding sites to the electrode, a feature that is lacking in conventional MIP-based systems. One of the best approaches to achieve transduction of the signal is the use of CPs. Integration between a MIP and a CP is a strategy that could take advantage of the properties of both materials. As a result of extensive crosslinking, it is extremely difficult to fabricate MIPs as films with adequate mechanical features. Furthermore, the time to attain equilibrium in MIPs is long. These aspects also limit the applications of conventional acrylic polymer-based MIPs in the field of sensor technology, where a fast response is mandatory. The attractive aspects of CPs for MIPs as compared with vinyl polymers is that in addition to chemical polymerization, CPs can be prepared by electrochemically incorporating a substrate into the polymer matrix. The electrochemically prepared CPs confer a defined specificity to an electrode and offer advantages for electrochemical sensing of the specific analyte. A wide range of substrates, including drugs and biomolecules, have been successfully confined into CP matrices for sensing applications. Several approaches and strategies have been proposed to coat very thin layers of imprinted CPs onto various substrates, such as electrodes and glass slides. Some of these methods include; (1) electropolymerization of an electroactive functional monomer, (2) drop-coating of a solution of a pre-prepared polymer with a CP, (3) preparation of composite membranes containing a conducting material (e.g., carbon nanotubes, graphite, or carbon black), MIP particles, and a binder (e.g., PVC), and (4) in situ chemical polymerization of a complex of a functional monomer and a template in solution. On comparing the various methods for MIP film preparation, MIP films prepared by electropolymerization have superior properties on adherence to the transducer surface, as well as simplicity and speed of

preparation. Moreover, electropolymerization enables easy control of the film thickness and morphology, results in high reproducibility, and gives the possibility of polymer preparation and operation in aqueous solution. During electropolymerization, the polymeric layer can be attached specifically via a simple process to a miniature sensing electrode that is easily prepared by cyclic voltammetry from bulk solutions of templates and conductive monomers. Conductive monomers as molecular imprinted materials have been used in the fabrication of microsensors and microfluidic systems. Thus, the twin objectives of high specificity and high sensitivity for a sensor can be realized by combining the concept of MIPs with the use of CPs. In this context, we describe in the following paragraphs how molecular imprinted conducting polymers (MICPs) can be used to prepare materials that act as transducers for the selective recognition and real-time detection of small molecule binding events. The most relevant reports pertaining to the use of pulsed amperometric detection for MICP-based sensors [547, 548].

With regards to the use of parent CP, PPy based MICPs have been extensively tried for sensor applications. Özcan and co-workers [549] described a paracetamol detection method based on molecularly imprinted PPy MEs. Although no detrimental effect of CPs on the recognition abilities of MIPs [550] has been reported thus far, this topic has not been explored in detail. The entrapment of MIP particles within electro synthesized PPy films or their anchoring on these films has also been proposed as a solution to improve the integration between MIPs and transducers. A combination of pyrrole and the functional group containing template was used for MIP-PPy films towards the electrochemical detection of halofuginone [550], phenothiazine [551], dapsone [551], clofibric acid [552], sulfadimethoxine [553] and flunixin [554]. MIP films were formed on the GCE or boron doped diamond electrode surfaces. Thin layers of MIP-PPy film were electrodeposited on the gold surface, and a 104 MHz surface aquatic sensor was developed for the detection of dopamine [555]. Quantum chemical calculations based on the DFT were performed to understand the nature of the interactions between the different templates and Py units of the MIP matrix. In the case of DA sensing, the interaction with Py is ascribed to an electrostatic interaction ( $\text{NH}_3^+$  -  $\pi$ ) between the protonated amine group and the Py aromatic ring. Also, the corresponding complex with DA was found to be the most energetically stable among the other templates considered in the investigation. The electrochemical behavior of a member of the tetracycline group of compounds, namely doxycycline was investigated [556] using MIP and non-imprinted PPy MEs. Chlorpyrifos (CPF)-templated molecular imprinted film was electrochemically synthesized on a pencil graphite electrode by electropolymerization of pyrrole in the presence of CPF. The fabricated ME was used as an impedimetric sensor for the determination of CPF using EIS [557]. A constant current technique was employed for the enantioselective detection of L-aspartic acid by using molecularly imprinted PPy films [558]. PPy can be combined with MIPs to impart catalytic effects to a system. This has been shown by Varghese et al. [559] who demonstrated the mechanistic aspects of a tyrosine

sensing event on an in situ copper oxide-modified molecular imprinted PPy-coated GCE (MIP-PPy GCE). The complexation mechanism used to explain the experimental findings takes into account the formation of both binary and ternary complexes of copper with tyrosine or phosphate, where an electrocatalytic mechanism invokes the formation of a copper(I) species (**Fig. 40**) [559].

**Fig. 40**

While fabricating sensors using MICPs, the morphology, doping levels and porosity of the resultant materials contribute to the selectivity of the target and sensitivity of the sensing process. When p-doping occurs for polymers such as PPy or PT, the cationic charges carried by the polymer backbones are counterbalanced by negative charges carried by anions. The size and characteristics of the dopant ions influence the sensor properties. The polymer network spacing as generated by the dopant ions controls the porosity of CPs. This effect has been proposed to form the basis of ISE. In the cases of bulk materials based MIPs, there can be a problem regarding the burial of the binding sites deep within the material, and as a result, the template is either permanently trapped or rebinding event is very slow due to long diffusion distances (especially for large templates). These problems are circumvented by introducing nanosized MIPs or using nanomaterials in the MIP formulation [560]. Nanosized materials provide much higher surface-to-volume ratio and thus a greater total surface area per weight of the material. These unique features of nanosized materials or nanostructured materials constitute advantageous such as improved template removal efficiency and faster rebinding capability due to better accessibility of recognition sites for the analyte as well as a lower mass-transfer resistance. Typically, MIP nanoparticles (MIP-NPs) exhibit several advantages as compared to bulk MIPs. Some functional components like magnetic materials or magnet nanomaterials are encapsulated into MICPs to result in functional component included MICPS to achieve the additional advantage from the functional components for MIP sensing characteristics. For an example, magnetic material included MIP will not only have magnetically susceptible characteristic, but also have selectivity for the guest molecules [561]. The concept of including a single functional component inclusion into MICPs can be extended to more than one functional components to synergistically derive the advantages for enhancing sensor characteristics. These advantageous features can be imparted by developing FCP based MIPs.

### **4.3. MIPs using FCPs**

The starting materials for the synthesis of FCP-based MIPs include pyrrole, aniline, and thiophene functionalized monomers, such as ethylenediamine tetra-*N*-(3-pyrrole-1-yl)propylacetamide, *N*-phenyl

ethylene diamines (NPEDMAs) and 3,4-ethylenedioxythiophene (EDOT), respectively, whose electropolymerization result in FCPs with largely improved properties. The synthesis of FCPs in the presence of a target molecule and polymer network formation condition leads to MICPs (**Fig. 41**) [562] and the MICPs can be integrated as sensitive layers in electrochemical sensors [563]. The use of FCPs as substrates that can also be chemically functionalized with the required probes gives rise to highly integrate sensing systems that possess both the recognition moieties and transducing properties required of a sensor. These materials possess high recognition specificity together with high sensitivity because they combine the properties of both MIPs and FCPs. As a consequence, the design and development of such materials in the field of sensors seems to be a promising approach for the selective and real-time recognition of small target molecules. An ideal sensor must be able to specifically detect very small amounts of a target. This necessitates the development of a more specific and more sensitive MICP layer. In particular, the functionalized probes present in the polymer matrix should be spatially well distributed and possess very high specific affinity towards the target in a given medium (polar or apolar). Thus, the choice of the chemical functionalities in the monomers appears to be essential. These functionalities are first involved during the association of monomers with the targets in pre-polymerization complexes, and again during the binding of targets with the polymer matrix. A strong interaction between the probe and target must then lead to an MICP matrix with highly specific imprints, and as a consequence, a very sensitive functionalized layer.

**Fig. 41**

MIP sensors using FCPs as sensitive membranes were constructed by direct electrochemical polymerization of aniline, pyrrole, thiophene, and their derivatives [564, 565]. Such MIP sensors offer advantages regarding the preparation of a chemosensitive layer and the sensor response performance, including efficiency of signal transduction, reproducibility, ease of manufacture, and control of layer thickness by electropolymerization. Compared with traditional MIPs, these MICPs have more compact and rigid structures that affect the imprinting efficiency of MIPs and sensor selectivity. The utilization of both conducting and nonconducting polymers prepared by electropolymerization of electroactive functional monomers, such as pristine and derivatized pyrrole, aminophenyl boronic acid, thiophene, porphyrin, aniline, phenylenediamine, phenol, and thiophenol, as MIPs was mentioned in a review [566]. A critical evaluation of the available literature on electro synthesized MIPs utilized as recognition elements in chemical sensors was also included in that review. However, in that review, only sensors were mentioned, and the impact and effect of functionalization on MIPs were not covered. Owing to their versatility and ability to participate in molecular recognition, these FCP based MIPs are finding a niche space in the field of molecular imprinting and sensing. In the fourth coming sections, we review the

literature on the use of various kinds of FCP-MIPs based on the parent polymers; PPY, PANI, and PT.

#### **4.3.1. MIP based on F-PPys**

##### **4.3.1.1. MIPs based on substituted PANIs**

The PPy derivative, ethylenediamine tetra-*N*-(3-pyrrole-1-yl)propyl acetamide, was used for the potentiostatic preparation of MIP films on carbon disc electrodes for the determination of selected metal cations, such as  $\text{Cu}^{2+}$  and  $\text{Hg}^{2+}$  [567]. In this monomer, four polymerizable Py moieties were covalently inserted into the EDTA skeleton towards improving both the rigidity and three-dimensional structure of the film. A proof-of-concept for the fabrication of microbial imprinted films from CP composite membranes was described. The imprinted films were prepared by absorbing pores onto the surface of GC electrodes and PPy/poly(3-methylthiophene) layers were then successively electrochemically deposited. Endospore binding could be detected either directly by monitoring changes in film susceptance or by following endospore germination. Despite the issues such as selectivity and calibration, the germination approach has been reported to be more sensitive and could be possibly exploited in sensor devices for detecting endospores [568].

##### **4.3.1.2. MIPs based on functional component included PPys**

The matrix structure of an electropolymerized Ppy film facilitates the doping with specific ions by entrapping the dopants in the film during its deposition onto an electrode surface. The properties of a PPy film, are dependent on the dopant and the electropolymerization condition. The overoxidized Ppy (o-PPy) film is porous and has large surface area favoring small molecule detection. Besides, during the overoxidation process, oxygen-containing groups such as carbonyl and carboxyl are introduced to the pyrrole unit, causing improvement of the perm-selective and antifouling properties of the sensor. The o-PPy based MIP has the special advantage that a complementary cavity can easily be created by extracting an anionic template molecule through overoxidation dedoping. Considering the requirements for in vivo sensing of DA, including sensitivity, selectivity, electrode size, and biocompatibility, o-PPy is a good candidate for MIP based sensing for DA. Consequently, the fabrication of o-PPy-MIP microelectrodes for in vitro validation, as well as for in vivo detection of DA in rat brain, was described. The principles of DA-imprinted o-PPy are shown in **Fig. 42**. Recognition was proposed to be due to hydrogen bond formation between the template (DA) and the PPy network [569]. A polymeric membrane-based ISE for the determination of L-AA was developed by Tonelli et al. [570] A sensor was fabricated by modifying a GCE with molecularly imprinted PPy synthesized by electropolymerization of the monomer in the presence of ascorbate. The performance of the MIP sensor was improved by subjecting the PPy

film to an oxidation treatment. An amperometric morphine sensor [571] has also been prepared using the MIP and doping concepts. The electrical conductivity of receptor layers allows the electrochemical detection of redox-active analytes and has been utilized for the detection of paracetamol bound to a PPy film [572]. Prabhakar et al. [573] fabricated a nucleic acid biosensor based on PPy-polyvinyl sulfonate film. Many chiral dopants and CPs have been used in the preparation of MIPs. Previous studies have reported that silicate-based chiral mesoporous materials, synthesized either by sol-gel and template synthesis or by molecular imprinting methods, facilitated enantioselective adsorption of chiral molecules [574]. For the preparation of chiral porous materials, including polymers and dendrimers, a variety of other imprinting approaches, involving the attachment of the chiral moieties framework, have been attempted [575].

### Fig. 42

A combination of MWNT/f-MWNT and PPY was used for the fabrication of MIP sensors [576-580]. Theoretically, some factors can have simultaneous effects on the MIP- analyte interaction and sensor characteristics. One of the major constrains in MIP design is the choice of optimal conditions for the development of MIPs. There is a need to select and optimize a multitude of variable parameters through polymer synthesis, template extraction, analyte rebinding and analytical determination that can influence the MIP characteristics. A good designs strategy needs to be evolved for the optimization of operating conditions of MIP processes. Multivariate or computational optimization methods have been used for the optimization of MIPs developed with MWNT-PPY combination [576-578]. A computational approach was used to screening the functional monomers and polymerization condition and solvent to arrive at a rational design for the fabrication of MWNT-PPY based electrochemical metoprolol (MTP) sensor [578]. According to the quantum mechanical calculations, the PPY –MWNT complex showed the highest binding energy to the template. DFT computational approach predicts that that PY/water combination was most suited to result in stable pre-polymerization adducts with MTP as the template. Similarly, a computational approach was used for screening functional monomers, polymerization conditions and solvent for the MWNT-Ppy based MIP sensors for 1,4-dihydroxyanthraquinone [577] and triamterene [576]. Electrochemical MIP sensor for tramadol based on the film composed of PPY and f-MWNT and the target template was developed [580]. The f-MWCNTs were used at the surface of the GCE to increase the surface area for the formation of the MIP film. Tetraethylortho silicate was used as cross-linker to form a polymeric network around the template through hydrogen bonds and ionic interactions. The –N–H group of the PPy units forms hydrogen bonds with the hydroxyl group of the tramadol molecules. The good performance of the MIP-sensor towards tramadol was explained based on the high conductivity of f-MWCNTs layer, large specific surface area and the porous nature of the imprinted film

to contain numerous recognition sites. In another work, an electrochemical sensor for ochratoxin A was fabricated by modifying the GCE surface with an MWCNTs-PPy based electropolymerized film [579]. In this sensor, the PPy was used for the formation of the MIP because it has the ability to form hydrogen bonds between the oxygen groups of ochratoxin A and the N–H group of PPy. A novel type of MIP-based electrochemical sensor was fabricated by successive electrodeposition of f-MWNTs (MWNT-COOH) and PPy in the presence of HCT onto a PGE surface [581].

G-PPy based MIP sensors have been reported for nitrate [582] and Bisphenol A [583]. A nitrate templated PPy- /G film was formed on the surface of GCE by electrochemical reduction of the GRO on GCE surface and electro-polymerizing a PPy film with a simultaneous nitrate doping [582]. The sensor was employed to detect nitrate levels in practical soil samples. The inclusion of G in MIP film contributed to high conductivity and hydrophobicity to cause enhancement of sensor performances. Graphene quantum dots (GQDs) are G sheets with sizes lesser than 100 nm. GQDs have excellent photoluminescence, good water solubility, and biocompatibility, and thus utilized in optical sensing platforms and bioimaging. An electrochemical MIP sensor was developed for the detection of bisphenol A based on PPy-GQDs composite [583]. The high sensitivity was attributed to the high electron transfer rate and good electrical conductivity of GQDs, while good selectivity was achieved through bisphenol-imprinted sites in the MIP-Py/GQDs composite.

ZnO has been extensively utilized as the sensing or support material in sensor fabrications due to its high refractive index, thermal stability, and high electron mobility. A fiber optic salivary cortisol sensor has been fabricated exploring lossy mode resonance (LMR) and MIP techniques [584]. LMR was generated by replacing the cladding of a highly multimode optical fiber with ZnO layer to result in the coupling of the evanescent wave at the fiber core/ZnO interface with the guided modes of the ZnO. The stages involved in the generation of MIP include; (a) the formation of the non-imprinted layer, removal of template and rebinding of analyte molecule and (b) diagrammatic representation of LMR probe. A photoelectrochemical MIP sensor for bilirubin, having good photochemical catalysis and molecular recognition capabilities, was fabricated based on the modification of MIP-Py film onto a porous titanium dioxide (PTT) surface by the molecular imprinting technique [585]. The photocurrent generation in the presence of bilirubin is attributed to the synergistic effect of PPy modified on PTT/ITO, lowering of the recombination of photogenerated electrons-holes and acceleration of the electron transfer. An electrochemical sensor was fabricated for paracetamol (PR) by successively electropolymerized a layer of Prussian blue (PB) and a layer of molecular imprinted PPy on the surface of a GCE [586]. The electrocatalytic property, PB has been utilized for the sensor fabrication. PR molecules were specifically adsorbed into the imprinted cavities of the outer layer of MIP. The inner layer of PB film was used as a

redox mediator to directly produce an electrochemical signal. The cavities in MIP layer not only specifically rebound the template molecule but also provided channels for electron transmission of PB, resulting in the increase of PR current. Carbon aerogel (CAG) is a kind of mesoporous carbon materials with an interconnected three-dimensional network structure and possesses high specific surface area, low density, suitable pore size distribution, excellent stability and distinguished electrical conductivity. The unique properties of the CAG along with the MIP-PPy were utilized to fabricate an electrochemical MIP sensor for the detection of DA [587]. The MIP-PPY was functionalized on the CAG substrate by the electropolymerization of pyrrole in the presence of the template molecules DA. DA was embedded in the PPy film by the strong hydrogen bonds formed between amino or hydroxyl groups of DA and N-H groups of PPy.

#### **4.3.1.3. MIPs based on biofunctionalized PPy**

The extent of chlorogenic acid (CGA) in coffee determines its aroma characteristics and the commercial value. A biomimetic complexation approach has been used for the fabrication of an electrochemical MIP sensor for CAG [588]. The MIP sensor for CGA was fabricated by modifying pencil graphite electrodes with MIP-PPy synthesized by electropolymerization of pyrrole monomer at constant potential in the presence of CGA. A possible mechanism for the binding effect of CGA in the MIP layer was envisaged involving the interaction of the CGA molecules with the PPy through hydrogen bonds formed between the hydrogen atom of the hydroxyl group of the CGA molecule and the nitrogen atom of the N-H group of the pyrrole units. Also, hydrogen bonds could also have resulted between the oxygen atom in the C=O group of CGA molecule and the hydrogen atom in the N-H group of the pyrrole unit. The sulfonate ( $-\text{SO}_3^-$ ) groups are known to be among the best dopants for Ppy. The sulfonate-rich compounds also have affinity to proteins such as, Ponceau S, Coomassie BB and Carrageenan. These aspects were considered in the design of molecular imprinted Ppy- protein-sensing films for the detection of a protein substrate, ricin toxin chain A (RTA) via substrate-dopant binding [589]. MIP- PPy sensing films were prepared by electropolymerization on array electrodes by cyclic voltammetry from a solution of pyrrole in PBS. The buffer was needed to preserve the conformation of immobilized RTA. The use of macromolecular dopants having high protein affinity was identified as the reason for specificity. The binding interactions between the flumequine (FLU) (a fluoroquinolone antibiotic) and PPy was predicted by DFT calculations and used as the basis for the fabrication of MIP shear horizontal surface acoustic wave sensor for FLU [590].

#### **4.3.1.4. MIPs based on nanostructured PPy**

Yang et al. [591] proposed an approach for the fabrication of surface molecularly imprinted monodisperse NWs that were capable of recognizing the template molecule. Unfortunately, their approach was devoid of enantioselective separating capability because the amino group of glutamic acid was immobilized on the pore walls of a silane-treated nanoporous alumina membrane. Therefore, it is critically significant to develop surface-imprinted nanomaterials that retain their enantioselectivity. As a solution to this problem, PPy NWs with an average diameter of ~100 nm and a length of few micrometers were successfully prepared by electrochemical polymerization [592]. This NWs consisted of an enantiomeric camphor sulfonic acid (D- or L-CSA) molecule acting as both the dopant and molecular imprinting pseudo template. Owing to their higher efficient surface area, PPy NWs have higher sensitivity and faster response times than bulky thin films. Both EIS and circular dichroism spectra were employed to demonstrate the enantioselective interactions between de-doped PPy NWs imprinted with CSA enantiomers (MIP-PPy) and chiral phenylalanine (D- or L-Phe). A simple, and cost effective method based on the chiral block copolymer (CBC)-based templating approach has also been reported to accomplish the well-organized chiral mesoporous structure of PPy and excellent selective chiral recognition properties. Chiral-Mesoporous-PPy (CMPPy) NPs were synthesized by templating CBCs of poly(ethylene oxide) (PEO) and chiral L- or D-glutamic acid [PEO-*b*-(L-/D-GluA)] and blocks of chiral L- or D-phenylalanine [PEO-*b*-(L-/D-Phe)] (**Fig. 43**) [593].

**Fig. 43**

#### **4.3.1.5. MIPs based on multicomponent included PPys**

MCNC materials possess complementary properties because of synergistic effects and thus increase the total performance of the sensing component. A composite MIP film composed of G and MWNT together has been prepared by electropolymerization of pyrrole on a G-MWCNTs NC coated GCE in the presence of rutin (i.e. quercetin-3-rhamnosylglucoside, RT) [594]. The netlike G-MWCNTs composite contributed to high conductivity and electrocatalytic activity. In an, another report, a composite MIP film composed of PPY, MWNTs, and BiCoPc (a binuclear phthalocyanine cobalt(II) sulfonate) was utilized for the fabrication MIP-sensor for metolcarb (MTMC) (an important N-methylcarbamate pesticide) [595]. BiCoPc was used in the MIP fabrication because of its desirable large p electron conjugated system, excellent electron storage and transfer ability, and electrocatalytic behavior. MIP-sensor was fabricated by the electrodeposition of the poly(o-aminophenol) (PoAP) membrane at the surface of the PPY-MWNTs-GC electrode in the presence of MTMC (**Fig. 44**). The active groups ( $-\text{NH}_3^+$ ) in PoAP are utilized to immobilize the template molecules during the positive potential scan. The good selectivity of PoAP-PPY-MWNTs-BiCoPc-GC electrode for MTMC was ascribed to the synergistic effect in the PPY-

MWNTs–BiCoPc functional layer and some selective binding sites in the imprinted PoAP membrane.

**Fig. 44**

An imprinted electrochemical sensor based on PPy-sulfonated graphene (PPy-SG)/hyaluronic acid-multiwalled carbon nanotubes (HA–MWCNTs) was developed for the sensitive detection of tryptamine. To improve the mechanical, electrical, and electrochemical properties of PPy, a PPy/SG composite was utilized. Owing to their high aspect ratio, ultra-low weight, high mechanical strength, high electrical conductivity, high thermal conductivity, and high surface-to-volume ratio, carboxylated MWNTs enhance the current response [596]. A high-performance sensor for the determination of levofloxacin (LEV) was fabricated based on a molecularly imprinted PPy ME incorporated with GF-AuNPs [597]. The GF-AuNPs dramatically promoted the electrooxidation of LEV on the electrode, whereas the molecularly imprinted PPy served as the recognition element for LEV. Before synthesis of the GF-AuNPs composite, the hydrophobic surface of GF was functionalized with the polyelectrolyte poly(diallyldimethylammonium chloride) (PDDA). The surface functionalization with PDDA not only increased the solubility of GF, but also allowed the further decoration with Au NPs. An efficient MIP recognition element in an electrochemical sensor was fabricated by directly electropolymerized OPD in the presence of quinoxaline-2-carboxylic acid (QCA). Furthermore, controllable electrochemical modification of a PPy/GO-binuclear phthalocyanine cobalt(II) sulfonate (PPY-GO-BiCoPc) functional composite on a GCE was achieved [598]. The results demonstrated that the dopants, GO and BiCoPc, significantly changed the surface morphology of the PPy film, and the MIP film was easily grown on the rough PPY-GO-BiCoPc surface (**Fig. 45**). A DFT-based computational approach was used for the selection of a functional monomer and suitable solvent to design MIPs with hydrochlorothiazide (HCT) as the template molecule. A MIP sensor was established on a microfluidic paper-based analytical device ( $\mu$ -PAD), and a visible light PEC sensing platform was established for the detection of pentachlorophenol (PCP) on an Au NP-decorated paper working electrode using PPy-functionalized ZnO NPs. A layer of PPy was grafted onto the ZnO surface through a simple electropolymerization method. After the removal of the template molecule from the resulting crosslinked PPy matrix, the recognition sites for PCP were generated, resulting in specific recognition and binding of PCP [599].

**Fig. 45**

#### **4.3.2. MIP based on F-PANIs**

##### **4.3.2.1. MIPs based on substituted PANIs**

A simpler and cost-effective approach to achieve closer integration between MIPs and F-PANI based transducers was demonstrated using a novel hybrid material prepared from *N*-phenyl ethylenediamine methacrylamide (NPEDMA), a bifunctional conjugated monomer containing acrylic and monomeric sites. A CP backbone containing PANI and polyacrylic functionalities was produced upon polymerization of NPEDMA (**Fig. 46**) [600, 601]. Utilizing the advantages of the bifunctionality in NPEDMA, an electrochemical sensor for catechol was constructed by grafting a layer of a catalytically active MIP over an electropolymerized layer of poly(NPEDMA) (**Fig. 46**) [602]. The sensors proved to be superior to electrodes prepared by the immobilization of MIP particles with essentially the same composition on the surface of an SPE. The efficient sensor performance was attributed to PANI chains acting as “molecular wires” resulting in closer contact between the catalytically active imprint sites and the CP layer, a phenomena not possible with an insulating polymer. Grafting of the MIP layer was achieved by irradiating the double-bond-bearing poly(NPEDMA) layer in the presence of *N,N'*-diethyldithiocarbamic acid benzyl ester. The converted portion of the pendant double bonds into functionalized groups contribute to the initiation of polymerization (**Fig. 46**). NPEDMA was also used to prepare coatings for microplate wells with thin layers of crosslinked polymers, as demonstrated by the preparation of a small library of MIPs imprinted with atrazine and the corresponding control polymers (NIPs) for quick screening and assays based on computational modeling [603]. Moreover, an electrochemical sensor was developed for detecting 17 $\beta$ -estradiol (E2) using an MIP-modified hybrid electrode containing NPEDMA. Conducting films were prepared on the surface of a Au electrode by electropolymerization of the aniline moiety of NPEDMA. An MIP layer was photochemically grafted over PANI via *N,N'*-diethyldithiocarbamic acid benzyl ester (iniferter) activation of the methacrylamide groups. Computational modeling was employed to select the most suitable monomer for the preparation of MIPs for E2 [604].

### Fig. 46

A double recognition strategy for DA based on a boronic acid-functionalized poly(aniline-co-anthranilic acid)-MIP composite (PANANA) has been reported for the prospective construction of a competitive sensor [605]. The reversible covalent cyclic ester between boronic acids and the phenolic hydroxyl groups of DA, as well as the specific cavities contained in the matrix of the imprinted polymer, were given as reasons for the high selectivity of this sensor. The vinyl groups on the PANANA surface enabled not only the conductive substrate but also resulted in template-imprinting sites on the material surface, providing more binding sites and fast association kinetics.

Poly(aniline-co-metaniolic acid) was prepared from a 1 : 3 molar ratio of ANI :*m*-aminobenzenesulfonic acid (MSAN) in the presence of progesterone template and an electrochemical sensor was constructed on a ITO surface [606]. Results from cyclic voltammetry revealed that the current density increased when the progesterone concentration increased from less than 1.0 pg mL<sup>-1</sup> to 100 pg mL<sup>-1</sup>. The progesterone in urine samples was tested. The recognition mechanism of the progesterone by the molecularly imprinted poly(ANI-co-MSAN) involves hydrogen bonding interaction between progesterone the –SOOH group in MSAN and –C=O groups in progesterone as well hydrophobic interaction through the aryl amine group of PANI and alkene group in progesterone. Electro-copolymers based on two monomers, ortho aminophenol (OAP) and aniline, were prepared in the presence of an organic pollutant, tris(2,3-dibromopropyl) isocyanurate (TBC) and an MIP sensor for TBC was fabricated [607]. OAP was selected as the multifunctional monomer for electro-polymerization because of its ease for electro-polymerization on various substrate materials and film forming capability with good chemical and mechanical stability. The concentration of TBC was monitored using differential pulse voltammetry. The cooperative involvement of the amino and hydroxyl groups on the OAP caused improved detection limit for the MIP sensor. The cyclic boronate complexes formed between the oronic acids and vicinal diols were reversibly dissociated and re-associated under acidic or basic conditions, respectively. This function of the boronic acid ligand has also been utilized to synthesize MIPs for vicinal diol-functionalized substrates, such as saccharides [608]. A boronate affinity-based oriented surface imprinting method was reported for facile preparation of glycoprotein-imprinted microplates. A template glycoprotein was first immobilized on a boronic acid-modified microplate through boronate affinity binding, and a thin layer of PANI was formed to cover the microplate surface via in-water self-copolymerization. After the template was removed using an acidic solution, 3D cavities that can rebind the template were obtained on the microplate surface. The prepared MIPs had all the favorable features of the previous boronate affinity-based molecular imprinting method [609].

#### **4.3.2.2. MIPs based on functional component included PANIs**

Roy et al. [610] reported a PANI-based molecularly imprinted biosensor for the detection of AA. However, the characteristics of this, such as stability, sensitivity, and reusability, were not satisfactory. These limitations could perhaps be overcome by adding large polymeric anions, such as pTSA, PSS, and polyvinyl sulfonate (PVSA), along with aniline during electropolymerization. This approach may enhance the charge neutrality of aniline during the reduction process, as well as improve sensor stability [611]. A molecularly imprinted PVSA-PANI composite-based sensor for *p*-nitrophenol detection has been reported recently [612]. The presence of PVSA in PANI resulted in increased conductivity, enhanced charge transfer characteristics, and stability of the PANI/ITO film. Briefly, the enhanced electrochemical

properties of the electrode were due to the secondary doping of PVSA (Fig. 47).

Fig. 47

Electrochemical MIP sensors were fabricated based on the PANI film included with Au NPs [613], Ni NPs [614] and G [615] for creatine, melamine and 2,4,6- trinitro toluene (TNT), respectively. Au NPs were modified with a composite capping monolayer consisting of electro polymerizable the aniline units and phenylboronic acid ligands that provided ligation sites for the association of different antibiotic substrates. The electropolymerization of the functionalized Au NPs in the presence of antibiotic substrates yielded imprinted NP composites carrying ligands that enabled the selective surface plasmon resonance (SPR) sensing of different antibiotics. For this purpose, electro polymerizable 4-thioaniline-modified Au NPs coated with a boronic acid-functionalized thiol ligand, 4-mercaptophenylboronic acid, were used for the preparation of MIP films for the SPR determination of a series of antibiotics bearing vicinal diol groups, including neomycin, kanamycin, and streptomycin. PANI@Au NC based MIP was fabricated using methacrylic acid (MAA) as monomers and melamine act as template molecules, then the MIP was prepared by the electrochemical deposition via cyclic voltammetry. The Au NPs inclusion not only improved the electrical conductivity but also has a significant electrocatalytic effect for Au@PANI based MIP melamine sensor [613]. G-PANI nanocomposites were prepared using an interfacial polymerization method [615]. Picric acid was used as the imprinting substrate. The removal of picric acid templates from the GN-PANI-molecularly imprinted polymer (G-PANI-MIP) film was done using acidic solvents to leave the imprinted cavities. The G-PANI nanocomposite act as p-donor sites to have effective interaction with TNT. The Ni@PANI NC film has been prepared by the chemical method to fabricate high conductivity electrodes *via* electrochemical deposition fabrication [614]. Typically, magnetic Ni@PANI NPs were firstly pre-adsorbed on the surface of GCE. Aniline and methacrylic acid (MAA) were used as the bifunctional monomers and creatinine acted as template molecules. Subsequently, the MIP was prepared by the electrochemical deposition via cyclic voltammetry. The reliability of this sensing method was validated using creatinine in urine samples. A fiber-optic MIP sensor for AA was developed using PANI–Ag nanocomposite film [616]. PANI–Ag nanocomposite was prepared by an in situ polymerization method, and the imprinted sites of AA were generated on the PANI–Ag nanocomposite. The sensing probe was further fabricated by coating a PANI–Ag–AA MIP layer over a 40 nm thick optical fiber. The AA sensing was based on localized surface plasmon resonance (LSPR) effect. As the AA molecules approached near the complementary binding sites in the MIP film, AA molecules are recognized and bound non-covalently with the sites, and cause changes in the effective dielectric nature of the sensing layer. The change in dielectric nature was monitored by the change in LSPR peak absorbance. Vitamin C in the tablets was determined to validate the reliability of the proposed LSPR based MIP probe.

#### 4.3.2.3. MIPs based on nanostructured PANIs

An electrochemical MIP sensor for paracetamol was constructed using conductive PANI NPs employing polymeric micelles as the nanoreactor [617]. The synthetic strategy involves the use of an amphiphilic acrylic copolymer containing both hydrophobic and hydrophilic segments and the self-assembly of micelles (Fig. 48). The aniline monomer and template molecules (paracetamol) were then adsorbed onto the polymeric micelles utilizing the electrostatic interaction, hydrogen bonding and hydrophobic interaction between aniline, paracetamol and polymeric micelle. Chemical oxidative polymerization resulted in the imprinting of the template into the polymer frame work. The large specific surface area owing to its nano-size and electrical conductivity of PANI chains resulted in good sensor performances.

Fig. 48

#### 4.3.2.4. MIPs based on multicomponent included PANIs

A magnetically controlled electrochemical MIP sensor was fabricated for the detection of insulin using multicomponent [618] Recognition sites to insulin were generated by surface polymerization on the ternary  $\text{Fe}_3\text{O}_4@\text{rGO}/\text{PANI}$  nanocomposites. The electromagnetic MIP not only provides multiple functionalized binding sites in the matrix to form hydrogen bonds, hydrophobic action and p-p stacking interaction with insulin, but also affords a promoting network for electron transfer. The selectivity towards insulin is attributed to the multiple recognition sites in the electromagnetic MIPs. Zhu et al. [619] also fabricated an electrochemical glutathione sensor based on the ternary  $\text{Fe}_3\text{O}_4@\text{rGO}/\text{PANI}$  nanocomposites. The molecular imprinting of the template was performed onto the surface of GCE under the magnetic field induction using the prepolymer, the template, and  $\text{Fe}_3\text{O}_4/\text{PANI}/\text{rGO}$  nanocomposites. The MIPs sensor was constructed by the electropolymerization with the assistance of magnetic field directed self-assembly approach. A chiral selective MIP sensor for AA was developed by the electropolymerization of aniline onto the surface of a carbon dots coated pencil graphite electrode surface in the presence of ferrocene sulfonic acid (FSA) [620]. FSA functions as the electron transport mediator and makes PANI in the self-doped state. The fabricated MIP sensor exhibited electro-catalytic performance due to the presence of carbon dots and PANI-FSA film provides the large electrochemically active surface and electrical conductivity. Besides, the functional groups in PANI-FSA facilitate non-covalent interactions i.e. electrostatic and hydrogen bonding attractions with the groups of the L-AA molecule (Scheme 2) and define the affinity and selectivity of the imprinted polymers towards L-AA.

A composite of protein-imprinted nanofibers based on PANI with the binding sites on the surface was reported [621]. PANI NFs were combined with  $\text{Fe}_3\text{O}_4@Au$  NPs and then functionalized with vinyl bonds, and copolymerization of these functional monomers was carried out to prepare the surface imprinted polymer. The MIP generated by this approach exhibited high loading capacity, good adsorption dynamics, and good binding selectivity owing to the specific interaction between the imprinted site and the target analyte, Lystein.

#### **4.3.3. MIPs based on F-PTs**

The utilization of computational methods in MIP design has permitted the prediction of functional monomer, molecular (typically electronic) structure and monomer-template interaction and forms the basis for the efficient preparation of high affinity polymers through a rational design protocol. Recent review details the various computational methods and the computational approach applied (molecular mechanics/molecular dynamics, semi-empirical quantum mechanics, ab initio quantum mechanics (Hartree-Fock, Moller-Plesset, etc.) or DFT) for the optimization and selection of functional monomer-target analyte to make efficient MIP [622]. Nano oligo/polythiophene film having pyrene-specific recognition sites was electrodeposited onto a gold surface based on the theoretical modeling studies that predict strong polar hydrogen (Hp)- the pi interactions between the polythiophene film and pyrene [623]. Specifically, the following chemical interactions between terthiophene and pyrene were envisaged: (i) gold-sulfur in the terthiophene ring (ii) gold- pi electrons in the terthiophene ring and (iii) terthiophene-terthiophene interactions in the form of van der Waals and electrostatic interactions.

A variety of functionalized thiophene derivatives composed of acidic or basic or hydrophobic functional groups were used to facilitate complimentary interactions with a specific target analyte (drugs, biomolecules, etc.) through the molecular imprinting approach [624]. A MIP sensor for the detection of melphalan was developed through electropolymerization of 3-thiophene acetic acid on either on the gold electrode or gold coated-EQCM electrode surface to imprint melphalan. Molecular simulation through DFT calculations, and experimental verification predicted a 1:4 ratio of template to monomer as the optimized stoichiometric non-covalent interactions [625]. The melphalan molecules are bound with non-covalent bonding with free carboxyl groups of 3-TAA. The concept of using two or more functional monomers was also tested for improving the selectivity towards the target molecule in the case of PT derivatives based MIPs. Sensitive layers based on PEDOT and molecular imprinted and non-imprinted poly(EDOT-co-3-thiophene acetic acid) were electro synthesized on gold substrates and used for the electrochemical detection of atrazine. These layers were characterized to study the effect of the chemical

functionalities and structural properties of these conducting polymers on the interaction with atrazine [626]. Pernites et al. [627] reported the fabrication of a MIP *via in-situ* electropolymerizations of the functional and crosslinking monomers terthiophene and carbazole and through non-covalent complexation with the template drugs naproxen, paracetamol, and theophylline (**Fig. 49(a,b)**). A quantitative electrochemical and electrochromic study (**Fig. 49(c)**) of the terthiophene and carbazole monomers (**Fig. 49(d)**) to form conjugated polymer network (CPN) films was also carried out.

**Fig. 49**

The use of an inorganic template was suggested to solve the problems associated with the application of MIPs in biological samples [628]. The functional monomer bis(2,2'-bithienyl)-(4-aminophenyl)methane allowed for  $\pi$ - $\pi$  stacking recognition of nitrotoluenes (NTs), including 2,4,6-trinitrophenol (TNP), TNT, 1,3,5-trinitrobenzene (TNB), and 2,4-dinitrotoluene (DNT) [629].

#### **4.3.4. MIPs based on polycarbazole and polyindole**

Selectivity is particularly important for sensors, especially those for chiral recognition. To address selectivity, Ho [630] designed a new amine-imide-type CP with improved imprinting efficiency. A chiral hybrid (obtained by hybridizing polymethacrylic acid with conducting polycarbazole by a covalent bond) based MIP sensor for L-phenylalanine (L-Phe) was fabricated by electrochemically crosslinking a pendant polymer precursor, poly[2-(N-carbazolyl)ethyl methacrylate-co-meth-acrylic acid] (PCEMMA), in one step. During the imprinting step, the electroactive carbazole groups in PCEMMA were cross-linked to the pendant polymer (PCEMMA) and stabilized the imprinted cavities without the use of an additional crosslinker. The polymethylacrylic acid in PCEMMA was used as a functional monomer to interact with the template; the flexibility of this group might balance the rigidity of the polycarbazole group, thereby improving the imprinted efficiency of the MIP. Instead of UV-light and photoinitiators, the potential of electropolymerized oxidation of PCEMMAs was used to initiate the polymerization. Moreover, the conductive polycarbazole, provides a very efficient matrix for hybrid MIP and contributes to the signal transport between the electrode and sensitive layer. [631].

DA detection was carried out using a composite of polyindole(Pin) /GQDs based MIP. Synthesis of PIn /GQDs - MIP involved i) preparation of Pin microspheres and ii) inclusion of GQD (prepared by the pyrolysis of citric acid) into a solution containing Pin and DA (**Fig. 50**) [632]. The nitrogen heteroatoms and oxygen containing groups incorporated into the PIn /GQDs composite attract DA molecules

effectively through hydrogen bonding interaction. The DA binding with PIn /GQDs – MIP is monitored through fluorescence quenching involving a low-affinity type (noncovalent interaction is off) and a high-affinity type (noncovalent interaction is on) by adjusting the pH. The dual-type interaction provided the possibility to adjust the binding interaction while keeping the specificity.

**Fig. 50**

## **5. Summary and perspectives**

It is apparent from the literature that the optical (absorption and/or emission) and electronic properties of CPs (e.g., PPys, PANIs, PTs, and PFs) can be dramatically modified or tuned through several functionalization strategies, and the number of functionalized conducting polymers (FCPs) are continuously being produced. Such FCPs represent one of the most useful chemical platforms for the design of sensors as they show improved sensor performance (selectivity and sensitivity) compared with pristine CPs. From the great number of publications, including the ~630 cited here, it is clear that the utilization of FCPs in sensors is a rapidly growing research area. Sensors have been fabricated mainly with PANI, PPy, PT, and PF-based FCPs and a few reports are also available on other class of CPs, such as polyacetylene and polycarbazole. We arranged the vast number of FCPs into four categories, substituted or derivatized FCPs (Category I), biofunctionalized FCPs (category II), NS-FCPs (Category III), and multicomponent FCPs (Category IV), based on their molecular architectures and functionalization strategies. We highlighted representative cases of the rational design of FCPs for the fabrication of sensors with improved properties, such as lower detection limits, enhanced sensitivity, specificity or selectivity for analytes, and enhanced stability. Prior knowledge of the pristine CPs and the changes in the properties of FCPs associated with functionalization form the basis and guidelines for enhancing the favorable characteristics of the sensors designed for a target analyte. The steady developments of FCPs for sensor applications over the last several years are due to the control and understanding of manifold synthetic reactions to build FCPs in any of the four categories mentioned in this review.

In particular, FCPs showed better solubility than CPs in common organic solvents (and in some cases water), and the improved processability provided the advantages for sensor fabrication. While chemically synthesized FCPs require film fabrication as an additional step in the sensor design, the electrochemical synthesis of FCPs avoids the post-film fabrication steps. Some of the functional group containing dopants impart processability and mechanical strength to the sensing film. Self-doped FCPs are resistant to the deterioration of the sensor performance, unlike externally doped FCPs where migration of the guest dopant molecules can occur. Self-doped CPs overcome the major drawbacks of

traditional CPs, such as poor solubility and loss of electrochemical activity in aqueous solution, especially at the physiological pH (~7.0). Self-doped CPs provide a biocompatible environment for the immobilization of enzymes in biosensors. Through incorporation of a functional chiral dopant, FCPs can also achieve new enantioselective properties. An electrically neutral analyte can function as a secondary dopant for the CP in combination with the primary functional dopant, and change the electronic, optical, or magnetic properties of the sensor material. The affinity of the CP backbone towards a gaseous analyte can be enhanced via the functional groups either on the polymer or on the dopant ion when gas sensors were fabricated with functional ion-included CPs. In sensors fabricated from FCPs prepared by the “grafting from” method, nanocomponents such as CNTs, NDs, and GF have been used as the substrate for grafting CP chains. Moreover, the properties of the grafted CPs were tuned by the grafting density and chemical composition of the CP chains. Importantly, synergistic properties derived from the nanocomponent(s) and the CP were exploited for improved sensor performance. One of the chief characteristics of substrate-grafted CPs is the stability of the CP layer on the substrate. Recently, CPs were hybridized with carbon nanostructured (CNS) materials either in their pristine or functionalized forms, and the combined optical, electrical, chemical, or electronic properties were used for chemical and biological sensing. CNS materials, such as CNTs, GF, fullerenes, and NDs, offer large surface areas, high electric conductivities, and can be tailored for sensor application through functionalization with CPs. The incorporation of CNS materials into CPs is effective for the detection of suitable analytes, especially gases, or in biosensors. The electron confinement caused by their nano dimensions provides unique directional pathways for the flow of charge carriers, making these materials especially suited for gas sensor applications. CPs interfaced with the CNS afforded high-performance sensors with enhanced sensitivity, lower detection limits, increased responses towards analytes, and selectivity towards relatively inert substances because of improved adsorption, catalytic, redox, luminescence, and transport characteristics. The combination of CPs and CNS has triggered burgeoning interest in gas sensing, biosensing, protein detection, DNA detection, immuosensing, and real-time detection of molecules released from living cells.

One of the main challenges in biosensor fabrication is the efficient translation of biological events (transduction). Biofunctionalized FCPs translate the interaction of the analyte with biological molecules into electrochemical, electroluminescent, gravimetric, or optical signals. The CP backbone in biofunctionalized FCPs enhances the quantity of bioreceptor units and acts as a signal transduction element, thus increasing the sensitivity and lowering the detection level of the analyte. The functional integration of biological entities with CPs is beneficially utilized for the development of biosensors. Various strategies, such as post-entrapment of the biomolecule within the CP matrix, doping the CP with biomolecules during polymerization, or covalent modification of CPs with the biomolecule, have been

utilized for the fabrication of biosensors with biofunctionalized FCPs. For example, the biofunctionalization of CPs via covalent modification has been carried out by peptide coupling of carboxylic groups in carboxylic acid-functionalized CPs and amines to create amide linkages.

Much efforts have been devoted towards the development of optical, electrochemical, and electrical biosensors and gas sensors using NS-FCPs. The functional groups on the surface of NS-FCPs have been utilized towards covalent attachment of specific receptors as well to immobilize NS-FCPs on electrodes for effective electrical contacts. The electrical transduction of 1-D NS-FCPs towards biological activities, such as the electrochemical reaction of biomolecules, antibody antigen interactions, or catalyzed reactions, was effectively exploited in several sensor designs. Electrochemical sensors exhibited exceptional sensing performance towards biomolecules and gases owing to their inherent high surface area and fast electron transport of the nanostructure and selectivity of the functional groups present in the FCPs. Another promising feature of NS-FCPs is that direct and label-free detection of analytes can be achieved. Research activities related to the use of NS-FCPs over the last 10 years has primarily been focused on nanowire and nanotube-functionalized derivatives of PPy, PT, and PANI. There is a great scope for extended research activities in this area to other functionalities and coupling chemistries for the incorporation of biomolecules with NS-FCPs.

The development of high-performance sensors has been the subject of tremendous research efforts over the last few years. Recently, sensor technologists have utilized multicomponent or multifunctional nanocomposites with CPs or FCPs to achieve ideal performance characteristics, such as good electron transduction, suitable physical or chemical environments for the immobilization of an enzyme, bioactivity, facile accessibility of the analyte, and a large surface area. Prospective multicomponent architectures were designed that demonstrated superior sensor performances compared with pristine CP or single-component sensors. The synergistic combination of the features of nanomaterials, CPs, and biomaterials provides great potential for the fabrication of high-performance sensors. The facile approaches available for synthesizing multicomponent nanocomposites are effectively utilized for the preparation of specific multicomponent FCPs with a proper selection of suitable components for improved sensor performance. For example, the combination of DNA-functionalized CPs and plasmonic NPs are utilized to develop optical sensors for the selective detection of biorecognition events. The judicious integration of FCPs with specifically tuned properties and multiple nanocomponents are therefore expected to provide promising materials for sensor applications. It is evident that the future development of such sophisticated materials lies in the parallel development of novel synthetic methods. However, a little research into one-step methodologies for the preparation of two- or multicomponent-incorporated CP or FCP nanocomposites has been carried out, and a significant challenge in the field

lies into the synthesis of multicomponent nanocomposites. The development of new sensing materials based on multicomponent CP or FCP nanocomposites will have a large impact on high-performance sensor systems and will help to resolving existing problems regarding miniaturization, multianalyte sensing, improving lifetime of the in vivo sensors, transduction-linked response time, signal generation, and processing techniques.

**Scheme 4** presents the comprehensive information on the utilization of different (substituted/derivitized, biofunctionalized, nanostructured and multi-component) categories of FCPS ( F-PPy, F-PANI, F-PT, F-PF, etc) for the fabrication of electrochemical, optical and other kinds of sensors. Electrochemical sensors were predominately fabricated using F-PPys, F-PANIs and F-PTs. Among them, nanostructured (Category III) and multicomponent (Category IV) based F-PPys, F-PANIs and F-PTs were used to a larger extent for electrochemical sensor fabrications over the other other two categories of FCPs. The smaller proportion of optical sensors fabricated using F-PPys, F-PANIs and F-PTs are calorimetric rather than light ON-OFF type. PANI matrix accommodates much easier functional modification with inclusion of dopant/functional components (including carbon nanostructures, metal/metal oxide NPs as compared to the other parent CPs(PPy, PT, PF etc). Interestingly, F-PFs are particularly used for light turn ON-OFF optical sensors. Although the basic structure of PF is electrically conductive, the optical/electro-optical characteristics of PFs are exploited for the fabrication of optical sensors. In the cases of electrochemical sensors, the synergistic properties of the multiple (more than two) components were effectively utilized for the improvement of sensor performances such as sensitivity and range of detection. However, there are not many studies that focused on the synergistic contributions of the co-included components towards augmenting the performances of optical sensors. Studies need to be focused on the exploration of the roles of multiple components towards enhancement of optical (light ON-OFF) sensor performances. Photoelectrochemical sensors (PECs) are emerging prominently because of their high sensitivities as compared to electrochemical sensors because of the decoupling of signal production and signal deduction processes. While signal is induced by light in PECs, signal measurement can be done electrochemically. Thus, PEC sensors offer the special advantage of dual mode detection of two independent analyte. However, there is a great demand on extensive researches for the utilization of FCPs towards fabrication of dual mode PEC sensors.

#### **Scheme 4**

In MICPs, the unique electronic and optical properties of CPs and the coexistence of a MIP framework and CP structure provide good scope for the incorporation of both selectivity and sensitivity in sensors. Thus, novel electrochemical and optical sensors can be designed using MICPs with improved

sensitivity (from CP) and superior selectivity (from MICP). Despite a large number of research papers in the field of general MIPs based on insulating materials, very little progress has been reported in the literature on the synthesis and application of MICPs. Importantly, a literature survey on the use of FCP-based MICPs revealed that the number of research contributions in this field is limited. This is evident from the comparison between the citations suggested in this review for FCP-based general electrochemical/optical sensors (~510 references) and those for FCP-based MIP sensors (~100 references). As FCPs can be synthesized in processable and soluble forms using various functional probes, it would be feasible to obtain judicious combinations of FCPs with specific functional probes to achieve good selectivity for the target (analyte), a MIP framework, and good transduction of signals using a CP backbone. These features could be utilized for the fabrication of sensors that to resolve some of the existing problems with the application of general MIP-based biosensors. It is envisioned that proper choice of a recognition group in an FCP for a target (analyte), optimization of the MIP and signal transduction (optical/electrochemical), processability in water or a polar solvent, and post or in situ immobilization of enzymes on the electrode surface would allow the fabrication of a high-performance sensor with good selectivity and sensitivity. Thus, integration of the beneficial features of FCPs into MIP sensors would pave the way for the commercial development of such sensors. Although important research progress is ongoing in this field, the utility of FCPs in MIP sensors is still in its infancy, and intensive research activities are expected in the years ahead.

In this review, several successful efforts on the use of FCPs to improve sensor performances, especially selectivity and sensitivity, have been highlighted. However, the absence of clear justifications for the choice of FCP, and the insufficient correlation between structural modifications in CPs and selection of an analyte constrain advancements in this research field. There are still a few important challenges in the use of FCPs for MIP and sensing applications. We believe that the compendium of techniques and platforms discussed in this review indicates that this research area is rapidly maturing at the intersection of disciplines such as nanotechnology and biotechnology. Continuous efforts are anticipated in the future towards the development of FCP-based sensing platforms to achieve real time and online monitoring of analytes, wireless sensors for biomedical applications, as well as multisensing lab-on chips to fabricate sensor devices with multi-operational modes (i.e., electrochemical and optical sensing).

In summary, we hope that this review will help inform readers about the advancements of FCPs in MIP and sensing applications, and also generate ideas for the development of innovative FCP-based sensing platforms for next generation sensors.

## 6. Acknowledgements

This work was supported by the Priority Research Centers Program through a National Research Foundation of Korea (NRF) grant funded by the Ministry of Education, Science, and Technology (2009–0093819).

ACCEPTED MANUSCRIPT

## 7. References

- [1] Lee K, Cho S, Park SH, Heeger AJ, Lee CW, Lee SH. Metallic transport in polyaniline. *Nature* 2006;441:65-8.
- [2] Bobacka J, Ivaska A, Lewenstam A. Potentiometric ion sensors. *Chem Rev* 2008;108:329-51.
- [3] Gerard M, Chaubey A, Malhotra BD. Application of conducting polymers to biosensors. *Biosens Bioelectron* 2002;17:345-59.
- [4] McQuade DT, Pullen AE, Swager TM. Conjugated polymer-based chemical sensors. *Chem Rev* 2000;100:2537-74.
- [5] Wolfbeis OS. Chemical sensors - survey and trends. *J Anal Chem* 1990;337:522-7.
- [6] Ates M. A review study of (bio) sensor systems based on conducting polymers. *Mater Sci Eng C* 2013;33:1853-9.
- [7] Bhadra S, Khastgir D, Singha NK, Lee JH. Progress in preparation, processing and applications of polyaniline. *Prog Polym Sci* 2009;34:783-810.
- [8] Janata J, Josowicz M. Conducting polymers in electronic chemical sensors. *Nat Mater* 2003;2:19-24
- [9] Kesik M, Akbulut H, Soylemez S, Cevher SC, Hizalan G, Udum YA, Endo T, Yamada S, Çırpan A, Yagci Y, Toppare L. Synthesis and characterization of conducting polymers containing polypeptide and ferrocene side chains as ethanol biosensors. *Polym Chem* 2014;5:6295-306.
- [10] Thomas SW, Joly GD, Swager TM. Chemical sensors based on amplifying fluorescent conjugated polymers. *Chem Rev* 2007;107:1339-86.
- [11] Bai H, Shi G. Gas sensors based on conducting polymers. *Sensors* 2007;7:267-307.
- [12] Bratov A, Abramova N, Ipatov A. Recent trends in potentiometric sensor arrays-A review. *Anal Chim Acta* 2010;678:149-59.
- [13] Barsan MM, Ghica ME, Brett CM. Electrochemical sensors and biosensors based on redox polymer/carbon nanotube modified electrodes: A review. *Anal Chim Acta* 2015;881:1-23.
- [14] Hoeben FJM, Jonkheijm P, Meijer EW, Schenning APHJ. About supramolecular assemblies of  $\pi$ -conjugated systems. *Chem Rev* 2005;105:1491-546.
- [15] Hui J, Prasad T, Reynolds JR, Schanze KS. Conjugated polyelectrolytes: synthesis, photophysics, and applications. *Angew Chem Int Ed* 2009;48:4300-16.
- [16] Liu B, Gaylord BS, Wang S, Bazan GC. Effect of chromophore-charge distance on the energy transfer properties of water-soluble conjugated oligomers. *J Am Chem Soc* 2003;125:6705-14.
- [17] Patil AO, Ikenoue Y, Basescu N, Colaneri N, Chen J, Wudl F, Heeger AJ. Self-doped conducting polymers. *Synth Met* 1987;20:151-9.
- [18] Phuong Le A, Huang TM, Chen PT, Yang ACM. Synthesis and optoelectronic behavior of

- conjugated polymer poly(3-hexylthiophene) grafted on multiwalled carbon nanotubes. *J Polym Sci* 2011;49:581-90.
- [19] Ghosh M, Maiti S, Dutta S, Das D, Das PK. Covalently functionalized single-walled carbon nanotubes at reverse micellar interface: a strategy to improve lipase activity. *Langmuir* 2012;28:1715-24.
- [20] Komathi S, Gopalan AI, Muthuchamy N, Lee KP. Polyaniline nanoflowers grafted onto nanodiamonds via a soft template-guided secondary nucleation process for high-performance glucose sensing. *RSC Adv* 2017;7:15342-51.
- [21] Stanke D, Hallensleben ML, Toppare L. Electrically conductive poly(methyl methacrylate-g-pyrrole) via chemical oxidative polymerization. *Synth Met* 1993;55:1108-13.
- [22] Muthuchamy N, Lee KP, Gopalan AI. Enhanced photoelectrochemical biosensing performances for graphene (2D)–Titanium dioxide nanowire (1D) heterojunction polymer conductive nanosponges. *Biosens Bioelectron* 2017;89:390-9.
- [23] Segal E, Tchoudakov R, Narkis M, Siegmann A, Wei Y. Polystyrene/polyaniline nanoblends for sensing of aliphatic alcohols. *Sensor Actuat B Chem* 2005;104:140-50.
- [24] Silverstein MS, Tai H, Sergienko A, Lumelsky Y, Pavlovsky S. Polyhipe: ipns, hybrids, nanoscale porosity, silica monoliths and ICP-based sensors. *Polymer* 2005;46:6682-94.
- [25] Matsuguchi M, Okamoto A, Sakai Y. Effect of humidity on NH<sub>3</sub> gas sensitivity of polyaniline blend films. *Sensor Actuat B Chem* 2003;94:46-52.
- [26] Kim JS, Sohn SO, Huh JS. Fabrication and sensing behavior of PVF<sub>2</sub> coated-polyaniline sensor for volatile organic compounds. *Sensor Actuat B Chem* 2005;108:409-13.
- [27] Watcharaphalakorn S, Ruangchuay L, Chotpattananont D, Sirivat A, Schwank J. Polyaniline/polyimide blends as gas sensors and electrical conductivity response to CO-N<sub>2</sub> mixtures. *Polym Int* 2005;54:1126-33.
- [28] Santhanam KSV, Sangoi R, Fuller L. A chemical sensor for chloromethanes using a nanocomposite of multiwalled carbon nanotubes with poly(3-methylthiophene). *Sensor Actuat B Chem* 2005;106:766-71.
- [29] Bongo M, Winther-Jensen O, Himmelberger S, Strakosas X, Ramuz M, Hama A, Stavrinidou E, Malliaras GG, Salleo A, Winther-Jensen B, Owens RM. PEDOT:gelatin composites mediate brain endothelial cell adhesion. *J Mater Chem B* 2013;1:3860-7.
- [30] Guimard NK, Gomez N, Schmidt CE. Conducting polymers in biomedical engineering. *Prog Polym Sci* 2007;32:876-921.
- [31] Rydzek G, Ji Q, Li M, Schaaf P, Hill JP, Boulmedais F, Ariga K. Electrochemical nanoarchitectonics and layer-by-layer assembly: From basics to future. *Nano Today* 2015;10:138-67.

- [32] Abe H, Liu J, Ariga K. Catalytic nanoarchitectonics for environmentally compatible energy generation. *Mater Today* 2016;19:12-8.
- [33] Ariga K, Li J, Fei J, Ji Q, Hill JP. Nanoarchitectonics for dynamic functional materials from atomic-/molecular-level manipulation to macroscopic action. *Adv Mater* 2016 28:1251-86.
- [34] Ariga K, Mori T, Nakanishi W, Hill JP. Solid surface vs liquid surface: nanoarchitectonics, molecular machines, and DNA origami. *Phys Chem Chem Phys* 2017;19:23658-76.
- [35] Komiyama M, Yoshimoto K, Sisido M, Ariga K. Chemistry can make strict and fuzzy controls for bio-systems: DNA nanoarchitectonics and cell-macromolecular nanoarchitectonics. *Bull Chem Soc Jpn* 2017;90:967-1004.
- [36] Ariga K, Malgras V, Ji Q, Zakaria MB, Yamauchi Y. Coordination nanoarchitectonics at interfaces between supramolecular and materials chemistry. *Coord Chem Rev* 2016;320:139-52.
- [37] Ariga K, Mori T, Hill JP. Interfacial nanoarchitectonics: lateral and vertical, static and dynamic. *Langmuir* 2013;29:8459-71.
- [38] Ariga K, Ito H, Hill JP, Tsukube H. Molecular recognition: from solution science to nano/materials technology. *Chem Soc Rev* 2012;41:5800-35.
- [39] Ariga K. Interfaces working for biology: Solving biological mysteries and opening up future nanoarchitectonics. *ChemNanoMat* 2016;2:333-43.
- [40] Omichi M, Asano A, Tsukuda S, Takano K, Sugimoto M, Saeki A, Sakamaki D, Onoda A, Hayashi T, Seki S. Fabrication of enzyme-degradable and size-controlled protein nanowires using single particle nano-fabrication technique. *Nat Commun* 2014;5:3718/1-8
- [41] Ikai T, Shimizu S, Kudo T, Maeda K, Kanoh S. Helical folding of  $\pi$ -conjugated polymers bearing glucose-linked biphenyl units in the main chain: application to circularly polarized luminescence materials. *Bull Chem Soc Jpn* 2017;90:910-8.
- [42] Kundu S, Patra A. Nanoscale strategies for light harvesting. *Chem Rev* 2016;117:712-57.
- [43] Truong MA, Nakano K. Syntheses and properties of ladder-type  $\pi$ -conjugated compounds containing a benzo [2, 1-b: 3, 4-b'] dithiophene skeleton. *Bull Chem Soc Jpn* 2016;89:1034-40.
- [44] Peng HS, Chiu DT. Soft fluorescent nanomaterials for biological and biomedical imaging. *Chem Soc Rev* 2015;44:4699-722.
- [45] Wolfbeis OS. An overview of nanoparticles commonly used in fluorescent bioimaging. *Chem Soc Rev* 2015;44:4743-68.
- [46] Yu J, Rong Y, Kuo CT, Zhou XH, Chiu DT. Recent advances in the development of highly luminescent semiconducting polymer dots and nanoparticles for biological imaging and medicine. *Anal Chem* 2016;89:42-56.
- [47] Wu C, Chiu DT. Highly fluorescent semiconducting polymer dots for biology and medicine. *Angew Chem Int Ed* 2013;52:3086-109.

- [48] Cheng HW, Stock P, Moeremans B, Baimpos T, Banquy X, Renner FU, Valtiner M. Characterizing the influence of water on charging and layering at electrified ionic-liquid/solid interfaces. *Adv Mater Interfaces* 2015;2:1500159/1-9
- [49] Asano A, Omichi M, Tsukuda S, Takano K, Sugimoto M, Saeki A, Seki S. Fabrication and arrangement of “clickable” nanowires by the single-particle nanofabrication technique. *J Phys Chem C* 2012;116:17274-9.
- [50] Seki S, Saeki A, Choi W, Maeyoshi Y, Omichi M, Asano A, Enomoto K, Vijayakumar C, Sugimoto M, Tsukuda S, Tanaka SI. Semiconducting Cross-Linked Polymer Nanowires Prepared by High-Energy Single-Particle Track Reactions. *J Phys Chem B* 2012;116:12857-63.
- [51] Goffri S, Müller C, Stingelin-Stutzmann N, Breiby DW, Radano CP, Andreasen JW, Thompson R, Janssen RA, Nielsen MM, Smith P, Siringhaus H. Multicomponent semiconducting polymer systems with low crystallization-induced percolation threshold. *Nature Mater* 2006;5:950-6.
- [52] Gopalan AI, Lee KP, Ragupathy D. Development of a stable cholesterol biosensor based on multi-walled carbon nanotubes-gold nanoparticles composite covered with a layer of chitosan-room-temperature ionic liquid network. *Biosens Bioelectron* 2009;24:2211-7.
- [53] Komathi S, Muthuchamy N, Lee KP, Gopalan AI. Fabrication of a novel dual mode cholesterol biosensor using titanium dioxide nanowire bridged 3D graphene nanostacks. *Biosens Bioelectron* 2016;84:64-71.
- [54] Manesh KM, Kim HT, Santhosh P, Gopalan AI, Lee KP. A novel glucose biosensor based on immobilization of glucose oxidase into multi-wall carbon nanotubes-polyelectrolyte-loaded electro-spun nanofibrous membrane. *Biosens Bioelectron* 2008;23:771-9.
- [55] Zampetti E, Pantalei S, Scalese S, Bearzotti A, De Cesare F, Spinella C, Macagnano A. Biomimetic sensing layer based on electrospun conductive polymer webs. *Biosens Bioelectron* 2011;26:2460-5.
- [56] Nguyen TD, Tran TH. Multicomponent nanoarchitectures for the design of optical sensing and diagnostic tools. *RSC Adv* 2014;4:916-42.
- [57] Gudiksen MS, Lauhon LJ, Wang J, Smith DC, Lieber CM. Growth of nanowire superlattice structures for nanoscale photonics and electronics. *Nature* 2002;415:617-20.
- [58] Ramanavicius A, Ramanaviciene A, Malinauskas A. Electrochemical sensors based on conducting polymer-polypyrrole. *Electrochim Acta* 2006;51:6025-37.
- [59] Deng Z, Stone DC, Thompson M. Characterization of polymer films of pyrrole derivatives for chemical sensing by cyclic voltammetry, X-ray photoelectron spectroscopy and vapor sorption studies. *Analyst* 1997;122:1129-38.
- [60] De Lacy Costello BPJ, Evans P, Guernion N, Ratcliffe NM, Sivanand PS, Teare GC. The synthesis of a number of 3-alkyl and 3-carboxy substituted pyrroles; their chemical

- polymerization onto poly(vinylidene fluoride) membranes, and their use as gas sensitive resistors. *Synth Met* 2000;114:181-8.
- [61] Alauzun J, Mehdi A, Reye C, Corriu RJP. Direct synthesis of bifunctional mesoporous organosilicas containing chelating groups in the framework and reactive functional groups in the channel pores. *J Mater Chem* 2007;17:349-56.
- [62] Brie M, Turcu R, Neamtu C, Pruneanu S. The effect of initial conductivity and doping anions on gas sensitivity of conducting polypyrrole films to NH<sub>3</sub>. *Sens Actuators B* 1996;37:119-22.
- [63] Pirsá S, Alizadeh N. A selective DMSO gas sensor based on nanostructured conducting polypyrrole doped with sulfonate anion. *Sens Actuators B* 2012;168:303-9.
- [64] Carquigny S, Sanchez JB, Berger F, Lakard B, Lallemand F. Ammonia gas sensor based on electrosynthesized polypyrrole films. *Talanta* 2009;78:199-206.
- [65] Paul S, Amalraj F, Radhakrishnan S. CO sensor based on polypyrrole functionalized with iron porphyrin. *Synth Met* 2009;159:1019-23.
- [66] Radhakrishnan S, Deshpande SD. Conducting polymers functionalized with phthalocyanine as nitrogen dioxide sensors. *Sensors* 2002;2:185-94.
- [67] Aradilla D, Estrany F, Aleman C. Polypyrrole derivatives as solvent vapor sensors. *RSC Adv* 2013;3:20545-58.
- [68] Aytaç S, Kuralay F, Boyacı İH, Unaleroglu C. A novel polypyrrole-phenylboronic acid based electrochemical saccharide sensor. *Sens Actuators B* 2011;160:405-11.
- [69] Fabregat G, Córdova-Mateo E, Armelin E, Bertran O, Alemán C. Ultrathin films of polypyrrole derivatives for dopamine detection. *J Phys Chem C* 2011;115:14933-41.
- [70] Izaoumen N, Bouchta D, Zejli H, Kaoutit ME, Stalcup AM, Temsamani KR. Electrosynthesis and analytical performances of functionalized poly (pyrrole/ $\beta$ -cyclodextrin) films. *Talanta* 2005;66:111-7.
- [71] Reynes O, Moutet JC, Royal G, Saint-Aman E. Electrochemical sensing of anions by (ferrocenylmethyl)trialkylammonium cations in homogeneous solution and in polymer films. *Electrochim Acta* 2004;49:3727-35.
- [72] Puangploy P, Smanmoo S, Surareungchai W. A new rhodamine derivative-based chemosensor for highly selective and sensitive determination of Cu<sup>2+</sup>. *Sens Actuators B* 2014;193:679-86
- [73] Taouil AE, Lallemand F, Melot JM, Husson J, Hihn JY, Lakard B. Effects of polypyrrole modified electrode functionalization on potentiometric pH responses. *Synth Met* 2010;160:1073-80.
- [74] Diaz AF, Kanazawa KK, Gardini GP. Electrochemical polymerization of pyrrole. *J Chem Soc Chem Commun* 1979;14:635-6.
- [75] Bibi S, Ullah H, Ahmad SM, Ali Shah AU, Bilal S, Tahir AA, Ayub K. Molecular and electronic structure elucidation of polypyrrole gas sensors. *J Phys Chem C* 2015;119:15994-6003.

- [76] Paul S, Joseph M. Polypyrrole functionalized with fepctsa for NO<sub>2</sub> sensor application. *Sens Actuators B* 2009;140:439-44.
- [77] Sizun T, Patois T, Bouvet M, Lakard B. Microstructured electrodeposited polypyrrole-phthalocyanine hybrid material, from morphology to ammonia sensing. *J Mater Chem* 2012;22:25246-53.
- [78] Pirsá S, Alizadeh N. Nanoporous conducting polypyrrole gas sensor coupled to a gas chromatograph for determination of aromatic hydrocarbons using dispersive liquid-liquid microextraction method. *IEEE Sensors J* 2011;11:3400-5.
- [79] Paul S, Chavan NN, Radhakrishnan S. Polypyrrole functionalized with ferrocenyl derivative as a rapid carbon monoxide sensor. *Synth Met* 2009;159:415-8.
- [80] Khan AA, Rao RA, Alam N, Shaheen S. Formaldehyde sensing properties and electrical conductivity of newly synthesized Polypyrrole-zirconium(IV) seleniodate cation exchange nanocomposite. *Sens Actuators B* 2015;211:419-27.
- [81] Prissanaroon-Ouajai W, Pigram PJ, Jones R, Sirivat A. A novel pH sensor based on hydroquinone monosulfonate-doped conducting polypyrrole. *Sens Actuators B* 2008;135:366-74.
- [82] Tavoli F, Alizadeh N. Electrically induced fluorescence Fe<sup>3+</sup> sensing behavior of nanostructured Tiron doped polypyrrole. *Anal Chim Acta* 2016;946:88-95.
- [83] Rounaghi GH, Razavipanah I, Vakili-Zarch MH, Ghanei-Motlagh M, Salavati MR. Electrochemical synthesis of Alizarin Red S doped polypyrrole and its applications in designing a novel silver (I) potentiometric and voltammetric sensor. *J Mol Liq* 2015;211:210-6.
- [84] Joshi A, Aswal DK, Gupta SK, Yakhmi JV, Gangal SA. ZnO-nanowires modified polypyrrole films as highly selective and sensitive chlorine sensors. *Appl Phys Lett* 2009;94:103115/1-3.
- [85] Hong L, Li Y, Yang M. Fabrication and ammonia gas sensing of palladium/polypyrrole nanocomposite. *Sens Actuators B* 2010;145:25-31.
- [86] Zhang J, Liu X, Wu S, Xu H, Cao B. One-pot fabrication of uniform polypyrrole/Au nanocomposites and investigation for gas sensing. *Sensors Actu B: Chem* 2013;186:695-700.
- [87] Tripathi KM, Kim T, Losic D, Tung TT. Recent advances in engineered graphene and composites for detection of volatile organic compounds (vocs) and non-invasive diseases diagnosis. *Carbon* 2016;110:97-129.
- [88] Sun J, Shu X, Tian Y, Tong Z, Bai S, Luo R, Li D, Liu CC. Facile preparation of polypyrrole-reduced graphene oxide hybrid for enhancing NH<sub>3</sub> sensing at room temperature. *Sens Actuators B* 2017;241:658-64.
- [89] Li Y, Jiao M, Yang M. In-situ grown nanostructured ZnO via a green approach and gas sensing properties of polypyrrole/ZnO nanohybrids. *Sens Actuators B* 2017;238:596-604.
- [90] Jain S, Karmakar N, Shah A, Kothari DC, Mishra S, Shimpi NG. Ammonia detection of 1-D

- zno/polypyrrole nanocomposite: Effect of CSA doping and their structural, chemical, thermal and gas sensing behavior. *Appl Surf Sci* 2017;396:1317-25.
- [91] Li Y, Ban H, Yang M. Highly sensitive NH<sub>3</sub> gas sensors based on novel polypyrrole-coated SnO<sub>2</sub> nanosheet nanocomposites. *Sens Actuators B* 2016;224:449-57.
- [92] Kaur A, Kumar R. Sensing of ammonia at room temperature by polypyrrole-tin oxide nanostructures: Investigation by Kelvin probe force microscopy. *Sensors Act A* 2016;245:113-8.
- [93] Joulazadeh M, Navarchian AH. Ammonia detection of one-dimensional nano-structured polypyrrole/metal oxide nanocomposites sensors. *Synth Metal* 2015;210:404-11.
- [94] Apetrei IM, Apetrei C. Application of voltammetric e-tongue for the detection of ammonia and putrescine in beef products. *Sens Actuators B* 2016;234:371-9.
- [95] Rad AS, Nasimi N, Jafari M, Shabestari DS, Gerami E. Ab-initio study of interaction of some atmospheric gases (SO<sub>2</sub>, NH<sub>3</sub>, H<sub>2</sub>O, CO, CH<sub>4</sub> and CO<sub>2</sub>) with polypyrrole (3ppy) gas sensor: DFT calculations. *Sens Actuators B* 2015;220:641-51.
- [96] Lin M. A dopamine electrochemical sensor based on gold nanoparticles/over-oxidized polypyrrole nanotube composite arrays. *RSC Adv* 2015;5:9848-51.
- [97] Zhou X, Ma P, Wang A, Yu C, Qian T, Wu S, Shen J. Dopamine fluorescent sensors based on polypyrrole/graphene quantum dots core/shell hybrids. *Biosens Bioelectron* 2015;64:404-10.
- [98] Marimuthu T, Mohamad S, Alias Y. Needle-like polypyrrole–nio composite for non-enzymatic detection of glucose. *Synth Met* 2015;207:35-41.
- [99] Periasamy AP, Roy P, Wu WP, Huang YH, Chang HT. Glucose oxidase and horseradish peroxidase like activities of cuprous oxide/polypyrrole composites. *Electrochim Acta* 2016;215:253-60.
- [100] Xing L, Rong Q, Ma Z. Non-enzymatic electrochemical sensing of hydrogen peroxide based on polypyrrole/platinum nanocomposites. *Sens Actuators B* 2015;221:242-7.
- [101] Yang Z, Zheng X, Zheng J. Facile synthesis of prussian blue/hollow polypyrrole nanocomposites for enhanced hydrogen peroxide sensing. *Ind Eng Chem Res* 2016;55:12161-6.
- [102] Nia PM, Meng WP, Alias Y. One-step electrodeposition of polypyrrole-copper nano particles for H<sub>2</sub>O<sub>2</sub> detection. *J Electrochem Soc* 2016;163:B8-14.
- [103] Said NR, Rezayi M, Narimani L, Manan NS, Alias Y. A novel potentiometric self-plasticizing polypyrrole sensor based on a bidentate bis-NHC ligand for determination of Hg (II) cation. *RSC Adv* 2015;5:76263-74.
- [104] Mahmoudian MR, Basirun WJ, Alias Y. A sensitive electrochemical Hg<sup>2+</sup> ions sensor based on polypyrrole coated nanospherical platinum. *RSC Adv* 2016;6:36459-66.
- [105] Seenivasan R, Chang WJ, Gunasekaran S. Highly sensitive detection and removal of lead ions in water using cysteine-functionalized graphene oxide/polypyrrole nanocomposite film electrode.

- ACS Appl Mater Interfaces 2015;7:15935-43.
- [106] Tabassum R, Gupta BD. Fiber optic manganese ions sensor using SPR and nanocomposite of ZnO–polypyrrole. *Sens Actuators B* 2015;220:903-9.
- [107] Dai H, Wang N, Wang D, Ma H, Lin M. An electrochemical sensor based on phytic acid functionalized polypyrrole/graphene oxide nanocomposites for simultaneous determination of Cd(II) and Pb(II). *Chem Eng J* 2016;299:150-5.
- [108] Li J, Lei W, Xu Y, Zhang Y, Xia M, Wang F. Fabrication of polypyrrole-grafted nitrogen-doped graphene and its application for electrochemical detection of paraquat. *Electrochim Acta* 2015;174:464-71.
- [109] Lee JS, Oh J, Kim SG, Jang J. Highly Sensitive and Selective Field-Effect-Transistor nonenzyme Dopamine Sensors Based on Pt/Conducting Polymer Hybrid Nanoparticles. *Small* 2015;11(20):2399-406.
- [110] Bidan G, Billon M, Galasso K, Livache T, Mathis G, Roget A, Torres-Rodriguez LM, Vieil E. Electropolymerization as a versatile route for immobilizing biological species onto surfaces: application to DNA biochips. *Appl Biochem Biotech* 2000;89:183-93.
- [111] Korri-Youssoufi H, Garnier F, Srivastava P, Godillot P, Yassar A. Toward bioelectronics: specific DNA recognition based on an oligonucleotide-functionalized polypyrrole. *J Am Chem Soc* 1997;119:7388-9.
- [112] Torres-Rodriguez LM, Roget A, Billon M, Bidan G, Livache T. Synthesis of a biotin functionalized pyrrole and its electropolymerization: toward a versatile avidin biosensor. *Chem Commun* 1998;1993-4.
- [113] Esmaili C, Abdi MM, Mathew AP, Jonoobi M, Oksman K, Rezayi M. Synergy effect of nanocrystalline cellulose for the biosensing detection of glucose. *Sensors* 2015;15:24681-97.
- [114] Gursoy SS, Uygun A, Tilki TJ. Synthesis and characterization of some N-substituted polypyrrole derivatives: towards glucose sensing electrodes. *Macromol Sci A* 2010;47:681-8.
- [115] Liu X, Neoh KG, Cen L, Kang ET. Enzymatic activity of glucose oxidase covalently wired via viologen to electrically conductive polypyrrole films. *Biosens Bioelectron* 2004;19:823-34.
- [116] Palod PA, Singh V. Improvement in glucose biosensing response of electrochemically grown polypyrrole nanotubes by incorporating crosslinked glucose oxidase. *Mater Sci Eng C* 2015;55:420-30.
- [117] Shamsipur M, Kazemi SH, Mousavi MF. Impedance studies of a nano-structured conducting polymer and its application to the design of reliable scaffolds for impedimetric biosensors. *Biosens Bioelectron* 2008;24:104-10.
- [118] Kaplan M, Kilic T, Guler G, Mandli J, Amine A, Ozsoz M. A novel method for sensitive microrna detection: Electropolymerization based doping. *Biosens Bioelectron* 2017;92:770-8.

- [119] Lê HQA, Chebil S, Makrouf B, Sauriat-Dorizon H, Mandrand B, Korri-Youssoufi H. Effect of the size of electrode on electrochemical properties of ferrocene-functionalized polypyrrole towards DNA sensing. *Talanta* 2010;81:1250-7.
- [120] Travas-Sejdic J, Peng H, Kilmaitin PA, Cannell MB, Bowmaker GA, Cooney RP, Soeller C. DNA sensor based on functionalized polypyrrole. *Synth Met* 2005;152:37-40.
- [121] Bidan G, Billon M, Calvo-Muñoz ML, Dupont-Fillard A. Bio-Assemblies onto Conducting Polymer Support: Implementation of DNA-Chips. *Mol Cryst Liq Cryst* 2004;418:255-70.
- [122] Dos Santos Riccardi C, Yamanaka H, Josowicz M, Kowalik J, Mizaikoff B, Kranz C. Label-Free DNA Detection Based on Modified Conducting Polypyrrole Films at Microelectrodes. *Anal Chem* 2006;78:1139-45.
- [123] Cosnier S, Ionescu RE, Herrmann S, Bouffier L, Demeunynck M, Marks RS. Electroenzymatic polypyrrole-intercalator sensor for the determination of West Nile virus cDNA. *Anal Chem* 2006;78:7054-7.
- [124] Peng H, Zhang L, Soeller C, Travas-Sejdic J. Conducting polymers for electrochemical DNA sensing. *Biomaterials* 2009;30:2132-48.
- [125] Santharaman P, Das M, Singh SK, Sethy NK, Bhargava K, Claussen JC, Karunakaran C. Label-free electrochemical immunosensor for the rapid and sensitive detection of the oxidative stress marker superoxide dismutase 1 at the point-of-care. *Sens Actuators B* 2016;236:546-53.
- [126] Seenivasan R, Maddodi N, Setaluri V, Gunasekaran S. An electrochemical immunosensing method for detecting melanoma cells. *Biosensor Bioelectron* 2015;68:508-15.
- [127] Lv X, Pang X, Li Y, Yan T, Cao W, Du B, Wei Q. Electrochemiluminescent immune-modified electrodes based on Ag<sub>2</sub>Se@cdse nanoneedles loaded with polypyrrole intercalated graphene for detection of CA72-4. *ACS Appl Mater Interfaces* 2014;7:867-72.
- [128] Zhang Z, Liang Y, Liang P, Li C, Fang S. Protein adsorption materials based on conducting polymers: polypyrrole modified with ω-(N-pyrrolyl)-octylthiol. *Polym Int* 2011;60:703-10.
- [129] Ionescu RE, Gondran C, Bouffier L, Jaffrezic-Renault N, Martelet C, Cosnier S. Label-free impedimetric immunosensor for sensitive detection of atrazine. *Electrochim Acta* 2010;55:6228-32.
- [130] Bourigua S, El Ichi S, Korri-Youssoufi H, Maaref A, Dzyadevych S, Jaffrezic-Renault N. Electrochemical sensing of trimethylamine based on polypyrrole-flavin-containing monooxygenase (FMO3) and ferrocene as redox probe for evaluation of fish freshness. *Biosens Bioelectron* 2011;28:105-11.
- [131] Özel AD, Dikici E, Bachas LG. Selectivity properties of corrin-doped polypyrrole film. *Monatsh Chem* 2013;144:781-91.
- [132] Ayenimo JG, Adeloju SB. Rapid amperometric detection of trace metals by inhibition of an

- ultrathin polypyrrole-based glucose biosensor. *Talanta* 2016;148:502-10.
- [133] Ayenimo JG, Adeloju SB. Inhibitive potentiometric detection of trace metals with ultrathin polypyrrole glucose oxidase biosensor. *Talanta* 2015;137:62-70.
- [134] Zhu B, Booth MA, Woo HY, Hodgkiss JM, Travas-Sejdic J. Label-Free, Electrochemical Quantitation of Potassium Ions from Femtomolar Levels. *Chem Asian J* 2015;10:2169-75.
- [135] Kwon OS, Park SJ, Jang J. A high-performance VEGF aptamer functionalized polypyrrole nanotube biosensor. *Biomaterials* 2010;31:4740-7.
- [136] Lee SH, Kwon OS, Song HS, Park SJ, Sung JH, Jang J, Park TH. Mimicking the human smell sensing mechanism with an artificial nose platform. *Biomaterials* 2012;33:1722-9.
- [137] Kwon OS, Hong TJ, Kim SK, Jeong JH, Hahn JS, Jang J. Hsp90-functionalized polypyrrole nanotube FET sensor for anti-cancer agent detection. *Biosens Bioelectron* 2010;25:1307-12.
- [138] Yoon H, Kim JH, Lee N, Kim BG, Jang J. A novel sensor platform based on aptamer-conjugated polypyrrole nanotubes for label-free electrochemical protein detection. *Chem Bio Chem* 2008;9:634-41.
- [139] Mao H, Zhang H, Liang J, Liu D, Wu S, Zhang Y, Zhang Y, Wu Q, Zhang G, Song XM. Preparation of poly (ionic liquids)-functionalized polypyrrole nanotubes and their electrocatalytic application to simultaneously determine dopamine and ascorbic acid. *J Mater Chem B* 2015;3:5310-7.
- [140] Yoon H, Ko S, Jang J. Field-effect-transistor sensor based on enzyme-functionalized polypyrrole nanotubes for glucose detection. *J Phys Chem B* 2008;112:9992-7.
- [141] Yoon H, Jang J. A field-effect-transistor sensor based on polypyrrole nanotubes coupled with heparin for thrombin detection. *Mol Cryst Liq Cryst* 2008;491:21-31.
- [142] Song HS, Kwon OS, Lee SH, Park SJ, Kim UK, Jang J, Park TH. Human taste receptor-functionalized field effect transistor as a human-like nanobioelectronic tongue. *Nano Lett* 2013;13:172-8.
- [143] Park JW, Lee C, Jang J. High-performance field-effect transistor-type glucose biosensor based on nanohybrids of carboxylated polypyrrole nanotube wrapped graphene sheet transducer. *Sens Actuators B* 2015;208:532-7.
- [144] Lin M, Hu X, Ma Z, Chen L. Functionalized polypyrrole nanotube arrays as electrochemical biosensor for the determination of copper ions. *Anal Chim Acta* 2012;746:63-9.
- [145] Ko S, Jang J. Controlled amine functionalization on conducting polypyrrole nanotubes as effective transducers for volatile acetic acid. *Biomacromolecules* 2007;8:182-7.
- [146] Yang X, Li L, Yan F. Polypyrrole/silver composite nanotubes for gas sensors. *Sensors Actuators B* 2010;145:495-500.
- [147] Xue M, Li F, Chen D, Yang Z, Wang X, Ji J. High-oriented polypyrrole nanotubes for next-

- generation gas sensor. *Adv Mater* 2016;28:8265-70.
- [148] Kwon OS, Park CS, Park SJ, Noh S, Kim S, Kong HJ, Bae J, Lee CS, Yoon H. Carboxylic acid-functionalized conducting-polymer nanotubes as highly sensitive nerve-agent chemiresistors. *Sci Rep* 2016;6:33724/1-7.
- [149] Hangarter CM, Bangar M, Mulchandani A, Myung NV. Conducting polymer nanowires for chemiresistive and FET-based bio/chemical sensors. *J Mater Chem* 2010;20:3131-40.
- [150] SeokáKwon O, JooáPark S. Highly sensitive and selective chemiresistive sensors based on multidimensional polypyrrole nanotubes. *Chem Commun* 2012;48:10526-8.
- [151] Wang Y, Jia W, Strout T, Schempf A, Zhang H, Li B, Cui J, Lei Y. Ammonia gas sensor using polypyrrole-coated TiO<sub>2</sub>/Zno Nanofibers. *Electroanalysis* 2009;21:1432-8.
- [152] Palod PA, Singh V. Facile synthesis of high density polypyrrole nanofiber network with controllable diameters by one step template free electropolymerization for biosensing applications. *Sens Actuators B* 2015;209:85-93.
- [153] Yang J, Cho M, Pang C, Lee Y. Highly sensitive non-enzymatic glucose sensor based on over-oxidized polypyrrole nanowires modified with Ni (OH)<sub>2</sub> nanoflakes. *Sens Actuators B* 2015;211:93-101.
- [154] Sasso L, Vedarethinam I, Emnéus J, Svendsen WE, Castillo-León J. Self-assembled diphenylalanine nanowires for cellular studies and sensor applications. *J Nanosci Nanotech* 2012;12:3077-83.
- [155] Ramanathan K, Bangar MA, Yun M, Chen W, Myung NV, Mulchandani A. Bioaffinity sensing using biologically functionalized conducting-polymer nanowire. *J Am Chem Soc* 2005;127:496-7
- [156] Bangar MA, Shirale DJ, Chen W, Myung NV, Mulchandani A. Single conducting polymer nanowire chemiresistive label-free immunosensor for cancer biomarker. *Anal Chem* 2009;81:2168-75
- [157] Liu P, Wu S, Zhang Y, Zhang H, Qin X. A fast response ammonia sensor based on coaxial ppy-PAN nanofiber yarn. *Nanomaterials* 2016;6:121/1-10.
- [158] Sharma A, Kumar A. Study of structural and electro-catalytic behaviour of amperometric biosensor based on chitosan/polypyrrole nanotubes-gold nanoparticles nanocomposites. *Synth Met* 2016;220:551-9.
- [159] Shrestha BK, Ahmad R, Mousa HM, Kim IG, Kim JI, Neupane MP, Park CH, Kim CS. High-performance glucose biosensor based on chitosan-glucose oxidase immobilized polypyrrole/Nafion/functionalized multi-walled carbon nanotubes bio-nanohybrid film. *J Colloid Interface Sci* 2016;482:39-47.
- [160] AL-Mokaram AM, Yahya R, Abdi MM, Mahmud HN. One-step electrochemical deposition of Polypyrrole-Chitosan-Iron oxide nanocomposite films for non-enzymatic glucose biosensor.

- Mater Lett 2016;183:90-3.
- [161] Sheng Q, Liu D, Zheng J. NiCo alloy nanoparticles anchored on polypyrrole/reduced graphene oxide nanocomposites for nonenzymatic glucose sensing. *New J Chem* 2016;40:6658-65.
- [162] Chen J, Sheng Q, Zheng J. Dispersed gold nanoparticles on nio coated with polypyrrole for non-enzymic amperometric sensing of glucose. *RSC Adv* 2015;5:105372-8.
- [163] Nia PM, Meng WP, Lorestani F, Mahmoudian MR, Alias Y. Electrodeposition of copper oxide/polypyrrole/reduced graphene oxide as a nonenzymatic glucose biosensor. *Sens Actuators B* 2015;209:100-8.
- [164] Gangadharan R, Anandan V, Zhang G. Optimizing the functionalization process for nanopillar enhanced electrodes with GOx/PPY for glucose detection. *Nanotechnology* 2008;19:395501/1-7.
- [165] Mao H, Ji C, Liu M, Sun Y, Liu D, Wu S, Zhang Y, Song XM. Hydrophilic polymer/polypyrrole/graphene oxide nanosheets with different performances in electrocatalytic applications to simultaneously determine dopamine and ascorbic acid. *RSC Adv* 2016;6:111632-9.
- [166] Wang Z, Ying Y, Li L, Xu T, Wu Y, Guo X, Wang F, Shen H, Wen Y, Yang H. Stretched graphene tented by polycaprolactone and polypyrrole net–bracket for neurotransmitter detection. *Appl Surf Sci* 2017;396:832-40.
- [167] Ke R, Zhang X, Wang L, Zhang C, Zhang S, Mao C, Niu H, Song J, Jin B, Tian Y. Electrochemiluminescence sensor based on graphene oxide/polypyrrole/cdse nanocomposites. *J Alloys Compd* 2015;622:1027-32.
- [168] Mao H, Liang J, Ji C, Zhang H, Pei Q, Zhang Y, Zhang Y, Hisaeda Y, Song XM. Poly (zwitterionic liquids) functionalized polypyrrole/graphene oxide nanosheets for electrochemically detecting dopamine at low concentration. *Mater Sci Eng C* 2016;65:143-50.
- [169] Mao H, Liang J, Zhang H, Pei Q, Liu D, Wu S, Zhang Y, Song XM. Poly (ionic liquids) functionalized polypyrrole/graphene oxide nanosheets for electrochemical sensor to detect dopamine in the presence of ascorbic acid. *Biosens Bioelectron* 2015;70:289-98.
- [170] Cui HF, Bai YF, Wu WW, He X, Luong JH. Modification with mesoporous platinum and poly (pyrrole-3-carboxylic acid)-based copolymer on boron-doped diamond for nonenzymatic sensing of hydrogen peroxide. *J Electroanal Chem* 2016;766:52-9.
- [171] Li L, Wang X, Liu G, Wang Z, Wang F, Guo X, Wen Y, Yang H. Reproducible preparation of a stable polypyrrole-coated-silver nanoparticles decorated polypyrrole-coated-polycaprolactone-nanofiber-based cloth electrode for electrochemical sensor application. *Nanotechnology* 2015;26:445704/1-11.
- [172] Qi C, Zheng J. Novel nonenzymatic hydrogen peroxide sensor based on Fe<sub>3</sub>O<sub>4</sub>/ppy/Ag nanocomposites. *J Electroanal Chem* 2015;747:53-8.

- [173] Nia PM, Lorestani F, Meng WP, Alias Y. A novel non-enzymatic H<sub>2</sub>O<sub>2</sub> sensor based on polypyrrole nanofibers–silver nanoparticles decorated reduced graphene oxide nano composites. *Appl Surf Sci* 2015;332:648-56.
- [174] Miodek A, Mejri N, Gomgnimbou M, Sola C, Korri-Youssoufi H. E-DNA sensor of *Mycobacterium tuberculosis* based on electrochemical assembly of nanomaterials (mwcnts/ppy/PAMAM). *Anal Chem* 2015;87:9257-64.
- [175] Spain E, Keyes TE, Forster RJ. Polypyrrole-gold nanoparticle composites for highly sensitive DNA detection. *Electrochim Acta* 2013;109:102-9.
- [176] Wilson J, Radhakrishnan S, Sumathi C, Dharuman V. Polypyrrole-polyaniline-Au (ppy-pani-Au) nano composite films for label-free electrochemical DNA sensing. *Sens Actuators B* 2012;171–172:216-22.
- [177] Radhakrishnan S, Sumathi C, Umar A, Jae Kim S, Wilson J, Dharuman V. Polypyrrole-poly(3,4-ethylenedioxythiophene)-Ag (ppy-PEDOT-Ag) nanocomposite films for label-free electrochemical DNA sensing. *Biosens Bioelectron* 2013;47:133-40.
- [178] Singh K, Solanki PR, Basu T, Malhotra BD. Polypyrrole/multiwalled carbon nanotubes-based biosensor for cholesterol estimation. *Polym Adv Technol* 2012;23:1084-91.
- [179] Zang S, Liu Y, Lin M, Kang J, Sun Y, Lei H. A dual amplified electrochemical immunosensor for ofloxacin: Polypyrrole film-Au nanocluster as the matrix and multi-enzyme-antibody functionalized gold nanorod as the label. *Electrochim Acta* 2013;90:246-53.
- [180] Arulraj AD, Devasenathipathy R, Chen SM, Vasantha VS, Wang SF. Femtomolar detection of mercuric ions using polypyrrole, pectin and graphene nanocomposites modified electrode. *J Colloid Interface Sci* 2016;483:268-74.
- [181] Sadrolhosseini AR, Naseri M, Kamari HM. Surface plasmon resonance sensor for detecting of arsenic in aqueous solution using polypyrrole-chitosan-cobalt ferrite nanoparticles composite layer. *Opt Commun* 2017;383:132-7.
- [182] Xiang C, Jiang D, Zou Y, Chu H, Qiu S, Zhang H, Xu F, Sun L, Zheng L. Ammonia sensor based on polypyrrole–graphene nanocomposite decorated with titania nanoparticles. *Ceram Int* 2015;41:6432-8.
- [183] Bangar MA, Hangarter CM, Yoo B, Rheem Y, Chen W, Mulchandani A, Myung NV. Magnetically assembled multisegmented nanowires and their applications. *Electroanalysis* 2009;21:61-7.
- [184] Khorami HA, Eghbali A, Keyanpour-Rad M, Vaezi MR, Kazemzad M. Ammonia sensing properties of (sno<sub>2</sub>-zno)/polypyrrole coaxial nanocables. *J Mater Sci* 2014;49:685-90.
- [185] Mane AT, Navale ST, Patil VB. Room temperature NO<sub>2</sub> gas sensing properties of DBSA doped ppy–WO<sub>3</sub> hybrid nanocomposite sensor. *Org Electron* 2015;19:15-25.
- [186] Nalage SR, Navale ST, Mane RS, Naushad M, Stadlar FJ, Patil VB. Preparation of camphor-

- sulfonic acid doped ppy–nio hybrid nanocomposite for detection of toxic nitrogen dioxide. *Synth Met* 2015;209:426-33.
- [187] Navale ST, Chougule MA, Patil VB, Mane AT. Highly sensitive, reproducible, selective and stable CSA-polypyrrole NO<sub>2</sub> sensor. *Synth Met* 2014;189:111-8.
- [188] Karmakar N, Fernandes R, Jain S, Patil UV, Shimpi NG, Bhat NV, Kothari DC. Room temperature NO<sub>2</sub> gas sensing properties of p-toluenesulfonic acid doped silver-polypyrrole nanocomposite. *Sens Actuators B* 2017;242:118-26.
- [189] Zou Y, Wang Q, Jiang D, Xiang C, Chu H, Qiu S, Zhang H, Xu F, Sun L, Liu S. Pd-doped TiO<sub>2</sub>@polypyrrole core-shell composites as hydrogen-sensing materials. *Ceram Int* 2016;42:8257-62.
- [190] Barkade SS, Pinjari DV, Singh AK, Gogate PR, Naik JB, Sonawane SH, Ashokkumar M, Pandit AB. Ultrasound assisted miniemulsion polymerization for preparation of polypyrrole-Zinc oxide (ppy/zno) functional latex for liquefied petroleum gas sensing. *Ind Eng Chem Res* 2013;52:7704-12.
- [191] Anwar N, Vagin M, Laffir F, Armstrong G, Dickinson C, McCormac T. Transition metal ion-substituted polyoxometalates entrapped in polypyrrole as an electrochemical sensor for hydrogen peroxide. *Analyst* 2012;137:624-30.
- [192] Baker CO, Huang X, Nelson W, Kaner RB. Polyaniline nanofibers: broadening applications for conducting polymers. *Chem Soc Rev* 2017;46:1510-25.
- [193] Pringsheim E, Terpetschnig E, Wolfbeis OS. Optical sensing of ph using thin films of substituted polyanilines. *Anal Chim Acta* 1997;357:247-52.
- [194] Tsai YT, Wen TC, Gopalan A. Tuning the optical sensing of ph by poly(diphenylamine). *Sens Actuators B* 2003;96:646-57.
- [195] Cankurtaran H, Yazici O, Dinc S, Karaman F. Humidity sensitive properties of electronically conductive poly(diphenylamine sulfonic acid) and its block copolymer and blends. *Int J Electrochem* 2013;8:3265-78.
- [196] Kumar P, Joseph A, Ramamurthy PC, Subramanian S. Lead ion sensor with electrodes modified by imidazole-functionalized polyaniline. *Microchim Acta* 2012;177:317-23.
- [197] Chamier J, Leaner J, Crouch AM. Photoelectrochemical determination of inorganic mercury in aqueous solutions. *Anal Chim Acta* 2010;661:91-6.
- [198] Hbaieb S, Amdouni N, Parrot-Lopez H, Kalfat R, Chevalier Y. Insulated molecular wires of polyaniline pseudopolyrotaxane. *New J Chem* 2011;35:36-40.
- [199] Mlika R, Hbaieb S, Ben Chaabene R, Chevalier Y, Kalfat R, Ben Ouada H. Electrochemical properties of gold electrodes functionalized by new pseudo-polyrotaxanes of polyaniline and chemically modified  $\beta$ -cyclodextrin inclusion complex. *Synth Met* 2012;162:186-92.

- [200] Philips MF, Gopalan AI, Lee KP. Development of a novel cyano group containing electrochemically deposited polymer film for ultrasensitive simultaneous detection of trace level cadmium and lead. *J Hazard Mater* 2012;237–8:46-54.
- [201] Athawale AA, Kulkarni MV. Polyaniline and its substituted derivatives as sensor for aliphatic alcohols. *Sens Actuators B* 2000;67:173-7.
- [202] Davis AP. Book Review: Boronic Acids in Saccharide Recognition. *Angew Chem Int Ed* 2007;119:5752-3.
- [203] Hansen JS, Christensen JB, Petersen JF, Hoeg-Jensen T, Norrild JC. Arylboronic acids: A diabetic eye on glucose sensing. *Sens Actuators B* 2012;161:45-79.
- [204] Bull SD, Davidson MG, vandenElsen JMH, Fossey JS, Jenkins ATA, Jiang YB, Kubo Y, Marken F, Sakurai K, Zhao J, James TD. Exploiting the Reversible Covalent Bonding of Boronic Acids: Recognition, Sensing, and Assembly. *Acc Chem Res* 2013;46:312-26.
- [205] Egawa Y, Seki T, Takahashi S, Anzai J. Electrochemical and optical sugar sensors based on phenylboronic acid and its derivatives. *Mater Sci Eng C* 2011;31:1257-64.
- [206] Qing G, Wang X, Jiang L, Fuchs H, Sun T. Saccharide-sensitive wettability switching on a smart polymer surface. *Soft Matter* 2009;5:2759-65.
- [207] Şenel M, Nergiz C, Dervisevic M, Çevik E. Development of amperometric glucose biosensor based on reconstitution of glucose oxidase on polymeric 3-aminophenyl boronic acid monolayer. *Electroanalysis* 2013;25:1194-200.
- [208] Ward Muscatello MM, Stunja LE, Asher SA. Polymerized crystalline colloidal array sensing of high glucose concentrations. *Anal Chem* 2009;81:4978-86.
- [209] Ivanova-Mitseva PK, Fragkou V, Lakshmi D, Whitcombe MJ, Davis F, Guerreiro A, Crayston JA, Ivanova DK, Mitsev PA, Piletska EV, Piletsky SA. Conjugated polymers with pendant iniferter units: versatile materials for grafting. *Macromolecules* 2011;44:1856-65.
- [210] Virji S, Kaner RB, Weiller BH. Hydrazine detection by polyaniline using fluorinated alcohol additives. *Chem Mater* 2005;17:1256-60.
- [211] Das M, Sarkar D. Effect of oxidizing agent on ammonia sensing of DBSA doped polyaniline nanocomposite thin film. *J Mater Sci Mater Electron* 2016;27:4109-19.
- [212] Duboriz I, Pud A. Polyaniline/poly(ethylene terephthalate) film as a new optical sensing material. *Sens Actuators B* 2014;190:398-407.
- [213] Chiam YS, Lim KS, Harun SW, Gan SN, Phang SW. Conducting polymer coated optical microfiber sensor for alcohol detection. *Sens Actuators A* 2014;205:58-62.
- [214] Mahato M, Adhikari B. Vapor phase sensing response of doped polyaniline-poly (vinyl alcohol) composite membrane to different aliphatic alcohols. *Synth Met* 2016;220:410-20.
- [215] Chen X, Wong CKY, Yuan CA, Zhang G. Impact of the functional group on the working range of

- polyaniline as carbon dioxide sensors. *Sens Actuators B* 2012;175:15-21.
- [216] Shukla SK, Demir MM, Govender PP, Tiwari A, Shukla SK. Optical fibre based non-enzymatic glucose sensing over Cu<sup>2+</sup>-doped polyaniline hybrid matrix. *Sens Actuators B* 2017;242:522-8.
- [217] Yang M, Kim DS, Yoon JH, Hong SB, Jeong SW, Yoo DE, Lee TJ, Lee SJ, Lee KG, Choi BG. Nanopillar films with polyoxometalate-doped polyaniline for electrochemical detection of hydrogen peroxide. *Analyst* 2016;141:1319-24.
- [218] Khesuoe MP, Okumu FO, Matoetoe MC. Development of a silver functionalised polyaniline electrochemical immunosensor for polychlorinated biphenyls. *Anal Meth* 2016;8:7087-95.
- [219] Kaisti M, Boeva Z, Koskinen J, Nieminen S, Bobacka J, Levon K. Hand-held transistor based electrical and multiplexed chemical sensing system. *ACS Sens* 2016;1:1423-31.
- [220] Nguyen HL, Cao HH, Nguyen DT, Nguyen VA. Sodium dodecyl sulfate doped polyaniline for enhancing the electrochemical sensitivity of mercury ions. *Electroanalysis* 2016;29:595-601.
- [221] Wu Q, Hu Z, Liu C, Wang X, Chen Y, Lu Y. Synthesis and optical properties of gallium phosphide nanotubes. *J Phys Chem B* 2005;109:19719-22.
- [222] Zhang T, Nix MB, Yoo BY, Deshusses MA, Myung NV. Electrochemically functionalized single-walled carbon nanotube gas sensor. *Electroanalysis* 2006;18:1153-8.
- [223] Lim JH, Phiboolsirichit N, Mubeen S, Deshusses MA, Mulchandani A, Myung NV. Electrical and gas sensing properties of polyaniline functionalized single-walled carbon nanotubes. *Nanotechnology* 2010;21:075502/1-7.
- [224] Yoo R, Kim J, Song MJ, Lee W, Noh JS. Nano-composite sensors composed of single-walled carbon nanotubes and polyaniline for the detection of a nerve agent simulant gas. *Sens Actuators B* 2015;209:444-8.
- [225] Yoo KP, Kwon KH, Min NK, Lee MJ, Lee CJ. Effects of O<sub>2</sub> plasma treatment on NH<sub>3</sub> sensing characteristics of multiwall carbon nanotube/polyaniline composite films. *Sens Actuators B* 2009;143:333-40.
- [226] Kar P, Choudhury A. Carboxylic acid functionalized multi-walled carbon nanotube doped polyaniline for chloroform sensors. *Sens Actuators B* 2013;183:25-33.
- [227] Yun J, Lim Y, Jang GN, Kim D, Lee SJ, Park H, Hong SY, Lee G, Zi G, Ha JS. Stretchable patterned graphene gas sensor driven by integrated micro-supercapacitor array. *Nano Energy* 2016;19:401-14.
- [228] Konwer S, Guha AK, Dolui SK. Graphene oxide-filled conducting polyaniline composites as methanol-sensing materials. *J Mater Sci* 2013;48:1729-39.
- [229] Varghese SS, Lonkar S, Singh KK, Swaminathan S, Abdala A. Recent advances in graphene based gas sensors. *Sens Actuators B* 2015;218:160-83.
- [230] Gavgani JN, Hasani A, Nouri M, Mahyari M, Salehi A. Highly sensitive and flexible ammonia

- sensor based on S and N co-doped graphene quantum dots/polyaniline hybrid at room temperature. *Sens Actuators B* 2016;229:239-48.
- [231] Zhang YH, Chen YB, Zhou KG, Liu CH, Zeng J, Zhang HL, Peng Y. Improving gas sensing properties of graphene by introducing dopants and defects: a first-principles study. *Nanotechnology* 2009;20:185504/1-8.
- [232] Bai S, Zhao Y, Sun J, Tian Y, Luo R, Li D, Chen A. Ultrasensitive room temperature NH<sub>3</sub> sensor based on a graphene–polyaniline hybrid loaded on PET thin film. *Chem Commun* 2015;51:7524-27.
- [233] Kumar V, Patil V, Apte A, Harale N, Patil P, Kulkarni S. Ultrasensitive gold nanostar–polyaniline composite for ammonia gas sensing. *Langmuir* 2015;31:13247-56.
- [234] Zhu G, Zhang Q, Xie G, Su Y, Zhao K, Du H, Jiang Y. Gas sensors based on polyaniline/zinc oxide hybrid film for ammonia detection at room temperature. *Chem Phys Lett* 2016;665:147-52.
- [235] Patil UV, Ramgir NS, Karmakar N, Bhogale A, Debnath AK, Aswal DK, Gupta SK, Kothari DC. Room temperature ammonia sensor based on copper nanoparticle intercalated polyaniline nanocomposite thin films. *Appl Surf Sci* 2015;339:69-74.
- [236] Itoh T, Matsubara I, Shin W, Izu N, Nishibori M. Preparation of layered organic-inorganic nanohybrid thin films of molybdenum trioxide with polyaniline derivatives for aldehyde gases sensors of several tens ppb level. *Sens Actuators B* 2008;128:512-20.
- [237] Itoh T, Matsubara I, Shin W, Izu N. Synthesis and characterization of layered organic/inorganic hybrid thin films based on molybdenum trioxide with poly(N-methylaniline) for VOC sensor. *Mater Lett* 2007;61:4031-4.
- [238] Sonker RK, Yadav BC, Sharma A, Tomar M, Gupta V. Experimental investigations on NO<sub>2</sub> sensing of pure zno and PANI–zno composite thin films. *RSC Adv* 2016;6:56149-58.
- [239] Ahmad S, Sultan A, Mohammad F. Rapid response and excellent recovery of a polyaniline/silicon carbide nanocomposite for cigarette smoke sensing with enhanced thermally stable DC electrical conductivity. *RSC Adv* 2016;6:59728-36.
- [240] Fathollahzadeh M, Hosseini M, Haghghi B, Kolahdouz M, Fathipour M. Fabrication of a liquid-gated enzyme field effect device for sensitive glucose detection. *Anal Chim Acta* 2016;924:99-105.
- [241] Hansen B, Hocevar MA, Ferreira CA. A facile and simple polyaniline-poly (ethylene oxide) based glucose biosensor. *Synth Met* 2016;222:224-31.
- [242] Rattanarat P, Teengam P, Siangproh W, Ishimatsu R, Nakano K, Chailapakul O, Imato T. An electrochemical compact disk-type microfluidics platform for use as an enzymatic biosensor. *Electroanalysis* 2015;27:703-12.
- [243] Zhang Y, Yang X, Gao Z. In situ polymerization of aniline on carbon quantum dots: a new

- platform for ultrasensitive detection of glucose and hydrogen peroxide. *RSC Adv* 2015;5:21675-80.
- [244] Ahammad AS, Al Mamun A, Akter T, Mamun MA, Faraezi S, Monira FZ. Enzyme-free impedimetric glucose sensor based on gold nanoparticles/polyaniline composite film. *J Solid State Electrochem* 2016;20:1933-9.
- [245] Sai-Anand G, Gopalan AI, Kang SW, Komathi S, Lee KP. One pot synthesis of new gold nanoparticles dispersed poly(2-aminophenyl boronic acid) composites for fabricating an affinity based electrochemical detection of glucose. *Sci Adv Mater* 2014;6:1356-64.
- [246] Yu Z, Li H, Zhang X, Liu N, Tan W, Zhang X, Zhang L. Facile synthesis of nico2o4@ polyaniline core-shell nanocomposite for sensitive determination of glucose. *Biosens Bioelectron* 2016;75:161-5.
- [247] Suea-Ngam A, Rattanarat P, Wongravee K, Chailapakul O, Srisa-Art M. Droplet-based glucosamine sensor using gold nanoparticles and polyaniline-modified electrode. *Talanta* 2016;158:134-41.
- [248] Ragupathy D, Gopalan AI, Lee KP, Manesh KM. Electro-assisted fabrication of layer-by-layer assembled poly(2,5-dimethoxyaniline)/phosphotungstic acid modified electrode and electrocatalytic oxidation of ascorbic acid. *Electrochem Commun* 2008;10:527-30.
- [249] Fang Y, Jiang Q, Deng M, Tian Y, Wen Q, Wang M. Preparation in-situ of carbon nanotubes/polyaniline modified electrode and application for ascorbic acid detection. *J Electroanal Chem* 2015;755:39-46.
- [250] Yang T, Yang R, Chen H, Nan F, Ge T, Jiao K. Electrocatalytic activity of molybdenum disulfide nanosheets enhanced by self-doped polyaniline for highly sensitive and synergistic determination of adenine and guanine. *ACS Appl Mater Interfaces* 2015;7:2867-72.
- [251] Gopalan AI, Lee KP, Manesh KM, Santhosh P, Kim JH, Kang JS. Electrochemical determination of dopamine and ascorbic acid at a novel gold nanoparticles distributed poly(4-aminothiophenol) modified electrode. *Talanta* 2007;71:1774-81.
- [252] Tezerjani MD, Benvidi A, Rezaeinasab M, Jahanbani S, Moshtaghioun SM, Youssefi M, Zarrini K. An impedimetric biosensor based on a composite of graphene nanosheets and polyaniline as a suitable platform for prostate cancer sensing. *Anal Meth* 2016;8:7507-15.
- [253] Zheng Q, Wu H, Shen Z, Gao W, Yu Y, Ma Y, Guang W, Guo Q, Yan R, Wang J, Ding K. An electrochemical DNA sensor based on polyaniline/graphene: high sensitivity to DNA sequences in a wide range. *Analyst* 2015;140:6660-70.
- [254] Yang Y, Zhang S, Kang M, He L, Zhao J, Zhang H, Zhang Z. Selective detection of silver ions using mushroom-like polyaniline and gold nanoparticle nanocomposite-based electrochemical DNA sensor. *Anal Biochem* 2015;490:7-13.

- [255] Ruecha N, Rodthongkum N, Cate DM, Volckens J, Chailapakul O, Henry CS. Sensitive electrochemical sensor using a graphene–polyaniline nanocomposite for simultaneous detection of Zn(II), Cd(II), and Pb(II). *Anal Chim Acta* 2015;874:40-8.
- [256] De Barros A, Ferreira M, Constantino CJ, Bortoleto JR, Ferreira M. Synergy between polyaniline and omt clay mineral in Langmuir–Blodgett films for the simultaneous detection of traces of metal ions. *ACS Appl Mater Interfaces* 2015;7:6828-34.
- [257] Khan A, Khan AA, Rahman MM, Asiri AM. High performance polyaniline/vanadyl phosphate (PANI–VOPO<sub>4</sub>) nano composite sheets prepared by exfoliation/intercalation method for sensing applications. *Eur Poly J* 2016;75:388-98.
- [258] Kulkarni MV, Kale BB. Studies of conducting polyaniline (PANI) wrapped-multiwalled carbon nanotubes (mwcnts) nanocomposite and its application for optical ph sensing. *Sens Actuators B* 2013;187:407-12.
- [259] Santhosh P, Manesh KM, Lee KP, Gopalan AI. Enhanced electrocatalysis for the reduction of hydrogen peroxide at new multiwall carbon nanotube grafted polydiphenylamine modified electrode. *Electroanalysis* 2006;18:894-903.
- [260] Santhosh P, Manesh KM, Gopalan A, Lee KP. Novel amperometric carbon monoxide sensor based on multi-wall carbon nanotubes grafted with polydiphenylamine-Fabrication and performance. *Sens Actuators B* 2007;125:92-9.
- [261] Shao D, Hu J, Chen C, Sheng G, Ren X, Wang X. Polyaniline multiwalled carbon nanotube magnetic composite prepared by plasma-induced graft technique and its application for removal of aniline and phenol. *J Phys Chem C* 2010;114:21524-30.
- [262] Santhosh P, Manesh KM, Gopalan A, Lee KP. Fabrication of a new polyaniline grafted multi-wall carbon nanotube modified electrode and its application for electrochemical detection of hydrogen peroxide. *Anal Chim Acta* 2006;575:32-8.
- [263] Manesh KM, Santhosh P, Komathi S, Kim NH, Park JW, Gopalan AI, Lee KP. Electrochemical detection of celecoxib at a polyaniline grafted multiwall carbon nanotubes modified electrode. *Anal Chim Acta* 2008;626:1-9.
- [264] Gopalan AI, Lee KP, Komathi S. Strategically functionalized carbon nanotubes as the ultrasensitive electrochemical probe for picomolar detection of sildenafil citrate (Viagra). *Biosens Bioelectron* 2011;26:3018-22.
- [265] Wang Z, Sun C, Vegesna G, Liu H, Liu Y, Li J, Zeng X. Glycosylated aniline polymer sensor: Amine to imine conversion on protein-carbohydrate binding. *Biosens Bioelectron* 2013;46:183-9.
- [266] Zhang Q, Prabhu A, San A, Al-Sharab JF, Levon K. A polyaniline based ultrasensitive potentiometric immunosensor for cardiac troponin complex detection. *Biosens Bioelectron* 2015;72:100-6.

- [267] Hu Y, Yang T, Li Q, Guan Q, Jiao K. Conjugated self-doped polyaniline-DNA hybrid as trigger for highly sensitive reagentless and electrochemical self-signal amplifying DNA hybridization sensing. *Analyst* 2013;138:1067-74.
- [268] Da Silva JSL, Oliveira MDL, deMelo CP, Andrade CAS. Impedimetric sensor of bacterial toxins based on mixed (Concanavalin A)/polyaniline films. *Colloids Surf B* 2014;117:549-54.
- [269] Caygill RL, Hodges CS, Holmes JL, Higson SPJ, Blair GE, Millner PA. Novel impedimetric immunosensor for the detection and quantitation of Adenovirus using reduced antibody fragments immobilized onto a conducting copolymer surface. *Biosens Bioelectron* 2012;32:104-10.
- [270] Fomo G, Waryo TT, Sunday CE, Baleg AA, Baker PG, Iwuoha EI. Aptameric recognition-modulated electroactivity of poly (4-styrenesulfonic acid)-doped polyaniline films for single-shot detection of tetrodotoxin. *Sensors* 2015;15:22547-60.
- [271] Steffens C, Manzoli A, Oliveira JE, Leite FL, Correa DS, Herrmann P, Sergio P. Bio-inspired sensor for insect pheromone analysis based on polyaniline functionalized AFM cantilever sensor. *Sens Actuators B* 2014;191:643-9.
- [272] Yoon H. Current trends in sensors based on conducting polymer nanomaterials. *Nanomaterials* 2013;3:524-49.
- [273] Talwar V, Singh O, Singh RC. ZnO assisted polyaniline nanofibers and its application as ammonia gas sensor. *Sens Actuators B* 2014;191:276-82.
- [274] Yin C, Duan G, Cai W. Polyaniline nanofibers and their self-assembly into a film to be used as ammonia sensor. *RSC Adv* 2016;6:103185-91.
- [275] Uh K, Kim T, Lee CW, Kim JM. A Precursor Approach to Electrospun Polyaniline Nanofibers for Gas Sensors. *Macromol Mater Eng* 2016;301:1320-6.
- [276] Wu DQ, Wu LL, Cui HC, Zhang HN, Yu JY. A rapid ammonia sensor based on lysine nanogel-sensitized PANI/PAN nanofibers. *J Mater Chem B* 2016;4:1520-7.
- [277] Pang Z, Nie Q, Wei A, Yang J, Huang F, Wei Q. Effect of In<sub>2</sub>O<sub>3</sub> nanofiber structure on the ammonia sensing performances of In<sub>2</sub>O<sub>3</sub>/PANI composite nanofibers. *J Mater Sci* 2017;52:686-95.
- [278] Guo Y, Wang T, Chen F, Sun X, Li X, Yu Z, Wan P, Chen X. Hierarchical graphene-polyaniline nanocomposite films for high-performance flexible electronic gas sensors. *Nanoscale* 2016;8:12073-80.
- [279] Mousavi S, Kang K, Park J, Park I. A room temperature hydrogen sulfide gas sensor based on electrospun polyaniline-polyethylene oxide nanofibers directly written on flexible substrates. *RSC Adv* 2016;6:104131-8.
- [280] Zhao J, Wu G, Hu Y, Liu Y, Tao X, Chen W. A wearable and highly sensitive CO sensor with a

- macroscopic polyaniline nanofiber membrane. *J Mater Chem A* 2015;3:24333-7.
- [281] Wang X, Wang J, Si Y, Ding B, Yu J, Sun G, Luo W, Zheng G. Nanofiber-net-binary structured membranes for highly sensitive detection of trace hcl gas. *Nanoscale* 2012;4:7585-92.
- [282] Wu S, Chen J, Tian Y, Tang X, Li W, Li J. Biofunctionalized dendritic polyaniline nanofiber for in situ amplified glucometer-based enzyme immunoassay of tumor marker. *Anal Methods* 2015;7:1843-8.
- [283] Anilkumar P, Jayakannan M. Hydroxyl-Functionalized Polyaniline Nanospheres: Tracing Molecular Interactions at the Nanosurface via Vitamin C Sensing. *Langmuir* 2008;24:9754-62.
- [284] Manesh KM, Santhosh P, Gopalan A, Lee KP. Electrospun poly(vinylidene fluoride)/poly(aminophenylboronic acid) composite nanofibrous membrane as a novel glucose sensor. *Anal Biochem* 2007;360:189-95.
- [285] Li G, Li Y, Peng H, Chen K. Synthesis of Poly(anilineboronic acid) nanofibers for electrochemical detection of glucose. *Macromol Rapid Commun* 2011;32:1195-9.
- [286] Lee JH, Hong HG. Nonenzymatic electrochemical sensing of hydrogen peroxide based on a polyaniline-mno<sub>2</sub> nanofiber-modified glassy carbon electrode. *J Appl Electrochem* 2015;45:1153-62.
- [287] Kim JH, Hong SG, Sun HJ, Ha S, Kim J. Precipitated and chemically-crosslinked laccase over polyaniline nanofiber for high performance phenol sensing. *Chemosphere* 2016;143:142-7.
- [288] Pandimurugan R, Thambidurai S. A seaweed–polyaniline nanofibre modified electrode for sensing of uric acid. *Anal Methods* 2015;7:10422-32.
- [289] Scagion VP, Mercante LA, Sakamoto KY, Oliveira JE, Fonseca FJ, Mattoso LH, Ferreira MD, Correa DS. An electronic tongue based on conducting electrospun nanofibers for detecting tetracycline in milk samples. *RSC Adv* 2016;6:103740-6.
- [290] Yari A, Saidikhah M. Trithiane silver-nanoparticles-decorated polyaniline nanofibers as sensing element for electrochemical determination of Adenine and Guanine in DNA. *J Electroanal Chem* 2016;783:288-94.
- [291] Hui N, Sun X, Song Z, Niu S, Luo X. Gold nanoparticles and polyethylene glycols functionalized conducting polyaniline nanowires for ultrasensitive and low fouling immunosensing of alpha-fetoprotein. *Biosens Bioelectron* 2016;86:143-9.
- [292] Banerjee S, Konwar D, Kumar A. Polyaniline nanofiber reinforced nanocomposite based highly sensitive piezoelectric sensors for selective detection of hydrochloric acid: Analysis of response mechanism. *Sens Actuators B* 2014;190:199-207.
- [293] Si Y, Wang X, Li Y, Chen K, Wang J, Yu J, Wang H, Ding BJ. Optimized colorimetric sensor strip for mercury(II) assay using hierarchical nanostructured conjugated polymers. *Mater Chem A* 2014;2:645-52.

- [294] Virji S, Kaner RB, Weiller BH. Hydrogen sensors based on conductivity changes in polyaniline nanofibers. *J Phys Chem B* 2006;13:22266-70.
- [295] Shirsat MD, Bangar MA, Deshusses MA, Myung NV, Mulchandani A. Polyaniline nanowires-gold nanoparticles hybrid network based chemiresistive hydrogen sulfide sensor. *Appl Phys Lett* 2009;94:083502/1-3.
- [296] Luo X, Lee I, Huang J, Yun M, Cui XT. Ultrasensitive protein detection using an aptamer-functionalized single polyaniline nanowire. *Chem Commun* 2011;47:6368-70.
- [297] Hui N, Chai F, Lin P, Song Z, Sun X, Li Y, Niu S, Luo X. Electrodeposited conducting polyaniline nanowire arrays aligned on carbon nanotubes network for high performance supercapacitors and sensors. *Electrochim Acta* 2016;199:234-41.
- [298] Ameen S, Akhtar MS, Shin HS. Nanocages-augmented aligned polyaniline nanowires as unique platform for electrochemical non-enzymatic glucose biosensor. *Appl Catal A* 2016;517:21-9.
- [299] Lee KP, Gopalan AI, Lee SH, Kim MS. Polyaniline and cyclodextrin based chiral nanobundles-functional materials having size and enantioselectivity. *Nanotechnology* 2006;17:375-80.
- [300] Sharma AL, Kumar P, Deep A. Highly sensitive glucose sensing with multi-walled carbon nanotubes - polyaniline composite. *Polym Plast Technol* 2012;51:1382-7.
- [301] Komathi S, Gopalan AI, Lee KP. Fabrication of a novel layer-by-layer film based glucose biosensor with compact arrangement of multi-components and glucose oxidase. *Biosens Bioelectron* 2009;24:3131-4.
- [302] Lee KP, Komathi S, Nam NJ, Gopalan AI. Sulfonated polyaniline network grafted multi-wall carbon nanotubes for enzyme immobilization, direct electrochemistry and biosensing of glucose. *Microchem J* 2010;95:74-9.
- [303] Gopalan AI, Lee KP, Ragupathy D, Lee SH, Lee JW. An electrochemical glucose biosensor exploiting a polyaniline grafted multiwalled carbon nanotube/perfluorosulfonate ionomer-silica nanocomposite. *Biomaterials* 2009;30:5999-6005.
- [304] Li R, Guo D, Ye J, Zhang M. Stabilization of Prussian blue with polyaniline and carbon nanotubes in neutral media for in vivo determination of glucose in rat brains. *Analyst* 2015;140:3746-52.
- [305] Zhang B, He Y, Liu B, Tang D. Nickel-functionalized reduced graphene oxide with polyaniline for non-enzymatic glucose sensing. *Microchim Acta* 2015;182(3-4):625-31.
- [306] Ghanbari K, Ahmadi F. Nio hedgehog-like nanostructures/Au/polyaniline nanofibers/reduced graphene oxide nanocomposite with electrocatalytic activity for non-enzymatic detection of glucose. *Anal Biochem* 2017;518:143-53.
- [307] Zhuang X, Tian C, Luan F, Wu X, Chen L. One-step electrochemical fabrication of a nickel oxide nanoparticle/polyaniline nanowire/graphene oxide hybrid on a glassy carbon electrode for use as a non-enzymatic glucose biosensor. *RSC Adv* 2016;6:92541-6.

- [308] Zheng W, Hu L, Lee LY, Wong KY. Copper nanoparticles/polyaniline/graphene composite as a highly sensitive electrochemical glucose sensor. *J Electroanal Chem* 2016;781:155-60.
- [309] Gopalan AI, Muthuchamy N, Komathi S, Lee KP. A novel multicomponent redox polymer nanobead based high performance non-enzymatic glucose sensor. *Biosens Bioelectron* 2016;84:53-63.
- [310] Kong FY, Li WW, Chen TT, Gu SX, Xu Q, Wang W. A paper disk equipped with graphene/polyaniline/Au nanoparticles/glucose oxidase biocomposite modified screen-printed electrode: Toward whole blood glucose determination. *Biosens Bioelectron* 2014;56:77-82.
- [311] Tang W, Li L, Zeng X. A glucose biosensor based on the synergistic action of nanometer-sized  $\text{TiO}_2$  and polyaniline. *Talanta* 2015;131:417-23.
- [312] Miao Z, Wang P, Zhong A, Yang M, Xu Q, Hao S, Hu X. Development of a glucose biosensor based on electrodeposited gold nanoparticles–polyvinylpyrrolidone–polyaniline nanocomposites. *J Electroanal Chem* 2015;756:153-60.
- [313] Chowdhury AD, Gangopadhyay R, De A. Highly sensitive electrochemical biosensor for glucose, DNA and protein using gold-polyaniline nanocomposites as a common matrix. *Sens Actuators B* 2014;190:348-56.
- [314] Ghanbari K, Babaei Z. Fabrication and characterization of non-enzymatic glucose sensor based on ternary  $\text{NiO}/\text{CuO}/\text{polyaniline}$  nanocomposite. *Anal Biochem* 2016;498:37-46.
- [315] Manesh KM, Santhosh P, Uthayakumar S, Gopalan AI, Lee KP. One-pot construction of mediatorless bi-enzymatic glucose biosensor based on organic-inorganic hybrid. *Biosens Bioelectron* 2010;25:1579-86.
- [316] Wu J, Yin L. Platinum nanoparticle modified polyaniline-functionalized boron nitride nanotubes for amperometric glucose enzyme biosensor. *ACS Appl Mater Interfaces* 2011;3:4354-62.
- [317] Homma T, Sumita D, Kondo M, Kuwahara T, Shimomura M. Amperometric glucose sensing with polyaniline/poly(acrylic acid) composite film bearing covalently-immobilized glucose oxidase: A novel method combining enzymatic glucose oxidation and cathodic  $\text{O}_2$  reduction. *J Electroanal Chem* 2014;712:119-23.
- [318] Granot E, Basnar B, Cheglakov Z, Katz E, Willner I. Enhanced bioelectrocatalysis using single-walled carbon nanotubes (swcnts)/polyaniline hybrid systems in thin-film and microrod structures associated with electrodes. *Electroanalysis* 2006;18:26-34.
- [319] Silva JV, Pimentel DM, Souto DEP, Luz R, de CS, Damos FS. Application of horseradish peroxidase/polyaniline/bis(2-aminoethyl) polyethylene glycol-functionalized carbon nanotube composite as a platform for hydrogen peroxide detection with high sensitivity at low potential. *J Solid State Electrochem* 2013;17:2795-804.
- [320] Lee KP, Gopalan AI, Komathi S. Direct electrochemistry of cytochrome c and biosensing for

- hydrogen peroxide on polyaniline grafted multi-walled carbon nanotube electrode. *Sens Actuators B* 2009;141:518-25.
- [321] Sheng Q, Wang M, Zheng J. A novel hydrogen peroxide biosensor based on enzymatically induced deposition of polyaniline on the functionalized graphene-carbon nanotube hybrid materials. *Sens Actuators B* 2011;160:1070-7.
- [322] Komathi S, Gopalan AI, Kim SK, SaiAnand G, Lee KP. Fabrication of horseradish peroxidase immobilized poly(N-[3-(trimethoxy silyl)propyl]aniline) gold nanorods film modified electrode and electrochemical hydrogen peroxide sensing. *Electrochim Acta* 2013;92:71-8.
- [323] Yang Z, Zheng X, Zheng J. A facile one-step synthesis of prussian blue/polyaniline/graphene oxide nanocomposites for electrochemical sensing of hydrogen peroxide. *Synth Met* 2016;221:153-8.
- [324] Hua MY, Lin YC, Tsai RY, Chen HC, Liu YC. A hydrogen peroxide sensor based on a horseradish peroxidase/polyaniline/carboxy-functionalized multiwalled carbon nanotube modified gold electrode. *Electrochim Acta* 2011;56:9488-95.
- [325] Gopalan AI, Komathi S, SaiAnand G, Lee KP. Nanodiamond based sponges with entrapped enzyme: A novel electrochemical probe for hydrogen peroxide. *Biosens Bioelectron* 2013;46:136-41.
- [326] Ding L, Su B. A non-enzymatic hydrogen peroxide sensor based on platinum nanoparticle–polyaniline nanocomposites hosted in mesoporous silica film. *J Electroanal Chem* 2015;736:83-7.
- [327] Yang Z, Zheng X, Zheng J. Non-enzymatic sensor based on a glassy carbon electrode modified with Ag nanoparticles/polyaniline/halloysite nanotube nanocomposites for hydrogen peroxide sensing. *RSC Adv* 2016;6:58329-35.
- [328] Bagherzadeh M, Mozaffari SA, Momeni M. Fabrication and electrochemical characterization of dopamine-sensing electrode based on modified graphene nanosheets. *Anal Methods* 2015;7:9317-23.
- [329] Komathi S, Gopalan AI, Lee KP. Nanomolar detection of dopamine at multi-walled carbon nanotube grafted silica network/gold nanoparticle functionalised nanocomposite electrodes. *Analyst* 2010;135:397-404.
- [330] Ghanbari K, Moloudi M. Flower-like ZnO decorated polyaniline/reduced graphene oxide nanocomposites for simultaneous determination of dopamine and uric acid. *Anal Biochem* 2016;512:91-102.
- [331] Govindasamy M, Chen SM, Mani V, Sathiyam A, Merlin JP, Al-Hemaid FM, Ali MA. Simultaneous determination of dopamine and uric acid in the presence of high ascorbic acid concentration using cetyltrimethylammonium bromide–polyaniline/activated charcoal composite. *RSC Adv*

- 2016;6:100605-13.
- [332] Hou T, Gai P, Song M, Zhang S, Li F. Synthesis of a three-layered  $\text{SiO}_2@Au$  nanoparticle@ polyaniline nanocomposite and its application in simultaneous electrochemical detection of uric acid and ascorbic acid. *J Mater Chem B* 2016;4:2314-21.
- [333] Kim TG, Ragupathy D, Gopalan AI, Lee KP. Electrospun carbon nanotubes-gold nanoparticles embedded nanowires: prosperous multi-functional nanomaterials. *Nanotechnology* 2010;21:134021/1-11.
- [334] Srivastava M, Srivastava SK, Nirala NR, Prakash R. A chitosan-based polyaniline-Au nanocomposite biosensor for determination of cholesterol. *Anal Methods* 2014;6:817-24.
- [335] Bai L, Yan B, Chai Y, Yuan R, Yuan Y, Xie S, Jiang L, He Y, Bai L, Yan B, Chai Y, Yuan R, Yuan Y, Xie S, Jiang L, He Y. An electrochemical aptasensor for thrombin detection based on direct electrochemistry of glucose oxidase using a functionalized graphene hybrid for amplification. *Analyst* 2013;138:6595-9.
- [336] Cui Y, Tang D, Liu B, Chen H, Zhang B, Chen G. Biofunctionalized dendritic polyaniline nanofibers for sensitive electrochemical immunoassay of biomarkers. *Analyst* 2012;137:1656-62.
- [337] Spain E, Keyes TE, Forster RJ. Vapour phase polymerised polyaniline-gold nanoparticle composites for DNA detection. *J Electroanal Chem* 2013;711:38-44.
- [338] Wang X, Liu W, Li C, Chu C, Wang S, Yan M, Yu J, Huang J. Synthesis of polyaniline using electrochemical polymerization and application in a sensitive DNA biosensor with  $[\text{Ru}(\text{bpy})_3]^{2+}$  functionalized nanoporous gold composite as label. *Monatsh Chem* 2013;144:1759-65.
- [339] Gangopadhyay R, Chowdhury AD, De A. Functionalized polyaniline nanowires for biosensing. *Sens Actuators B* 2012;171-172:777-85.
- [340] Hao Y, Zhou B, Wang F, Li J, Deng L, Liu YN. Construction of highly ordered polyaniline nanowires and their applications in DNA sensing. *Biosens Bioelectron* 2014;52:422-6.
- [341] Spain E, Kojima R, Kaner RB, Wallace GG, O'Grady J, Lacey K, Barry T, Keyes TE, Forster RJ. High sensitivity DNA detection using gold nanoparticle functionalized polyaniline nanofibres. *Biosens Bioelectron* 2011;26:2613-8.
- [342] Spricigo R, Dronov R, Rajagopalan KV, Lisdat F, Leimkuehler S, Scheller FW, Wollenberger U. Electrocatalytically functional multilayer assembly of sulfite oxidase and cytochrome c. *Soft Matter* 2008;4:972-8.
- [343] Wang L, Hua E, Liang M, Ma C, Liu Z, Sheng S, Liu M, Xie G, Feng W. Graphene sheets, polyaniline and aunps based DNA sensor for electrochemical determination of BCR/ABL fusion gene with functional hairpin probe. *Biosens Bioelectron* 2014;51:201-7.
- [344] Gopalan AI, Lee KP, Komathi S. Bioelectrocatalytic determination of nitrite ions based on polyaniline grafted nanodiamond. *Biosens Bioelectron* 2011;26:1638-43.

- [345] Gopalan AI, Ko KR, Lee SH, Komathi S, Veres M, Lee KP. Radiation induced preparation of new multifunctional nanobiowebs. *Radiat Phys Chem* 2012;81:1407-10.
- [346] Muchindu M, Waryo T, Arotiba O, Kazimierska E, Morrin A, Killard AJ, Smyth MR, Jahed N, Kgarebe B, Baker PGL, Iwuoha EI. Electrochemical nitrite nanosensor developed with amine- and sulphate-functionalised polystyrene latex beads self-assembled on polyaniline. *Electrochim Acta* 2010;55:4274-80.
- [347] Su Z, Liu Y, Zhang Y, Xie Q, Chen L, Huang Y, Fu Y, Meng Y, Li X, Ma M, Yao S. Thiol-ene chemistry guided preparation of thiolated polymeric nanocomposite for anodic stripping voltammetric analysis of Cd<sup>2+</sup> and Pb<sup>2+</sup>. *Analyst* 2013;138:1180-6.
- [348] Sai Anand G, Gopalan AI, Kang SW, Lee KP. Development of a surface plasmon assisted label-free calorimetric method for sensitive detection of mercury based on functionalized gold nanorods. *J Anal At Spectrom* 2013;28:488-98.
- [349] Ge S, Wu K, Zhang Y, Yan M, Yu J. Paper-based biosensor relying on flower-like reduced graphene guided enzymatically deposition of polyaniline for Pb<sup>2+</sup> detection. *Biosens Bioelectron* 2016;80:215-21.
- [350] Lin M, Liu Y, Sun Z, Zhang S, Yang Z, Ni C. Electrochemical immunoassay of benzo[a]pyrene based on dual amplification strategy of electron-accelerated Fe<sub>3</sub>O<sub>4</sub>/polyaniline platform and multi-enzyme-functionalized carbon sphere label. *Anal Chim Acta* 2012;722:100-6.
- [351] Ajayi RF, Sidwaba U, Feleni U, Douman SF, Tovide O, Botha S, Baker P, Fuku XG, Hamid S, Waryo TT, Vilakazi S. Chemically amplified cytochrome P450-2E1 drug metabolism nanobiosensor for rifampicin anti-tuberculosis drug. *Electrochim Acta* 2014;128:149-55.
- [352] Hasan M, Ansari MO, Cho MH, Lee M. Ammonia sensing and DC electrical conductivity studies of p-toluene sulfonic acid doped cetyltrimethylammonium bromide assisted V<sub>2</sub>O<sub>5</sub>@ polyaniline composite nanofibers. *J Indus Eng Chem* 2015;22:147-52.
- [353] Bairi VG, Bourdo SE, Sacre N, Nair D, Berry BC, Biris AS, Viswanathan T. Ammonia gas sensing behavior of tanninsulfonic acid doped polyaniline-tio<sub>2</sub> composite. *Sensors* 2015;15:26415-29.
- [354] Aussawasathien D, Sahasithiwat S, Menbangpung L, Teerawattananon C. Poly(o-anisidine)-polystyrene composite fibers via electrospinning process: Surface morphology and chemical vapor sensing. *Sens Actuators B* 2011;151:341-50.
- [355] Zhang T, Mubeen S, Yoo B, Myung NV, Deshusses MA. A gas nanosensor unaffected by humidity. *Nanotechnology* 2009;20:255501/1-5.
- [356] Heywang G, Jonas F. Poly(alkylenedioxythiophene)s - new, very stable conducting polymers. *Adv Mater* 1992;4:116-8.
- [357] Sotzing GA, Reynolds JR, Steel PJ. Poly(3,4-ethylenedioxythiophene) (PEDOT) prepared via electrochemical polymerization of EDOT, 2,2'-bis(3,4-ethylenedioxythiophene) (biedot), and their

- TMS derivatives. *Adv Mater* 1997;9:795-8.
- [358] Groenendaal L, Jonas F, Freitag D, Pielartzik H, Reynolds JR. Poly(3,4-ethylenedioxythiophene) and its derivatives: past, present, and future. *Adv Mater* 2000;12:481-94.
- [359] Dietrich M, Heinze J, Heywang G, Jonas F. Electrochemical and spectroscopic characterization of polyalkylenedioxythiophenes. *J Electroanal Chem* 1994;369:87-92.
- [360] Asplund M, von HH, Ingnas O. Composite biomolecule/PEDOT materials for neural electrodes. *Biointerphases* 2008;3:83-93.
- [361] Gonçalves VC, Balogh DT. Optical chemical sensors using polythiophene derivatives as active layer for detection of volatile organic compounds. *Sens Actuators B* 2012;162:307-12.
- [362] Gonçalves VC, Nunes BM, Balogh DT, Olivati CA. Detection of volatile organic compounds using a polythiophene derivative. *Physica status solidi* 2010;207:1756-9.
- [363] Nagarjuna G, Kumar A, Kokil A, Jadhav KG, Yurt S, Kumar J, Venkataraman D. Enhancing sensing of nitroaromatic vapours by thiophene-based polymer films. *J Mater Chem* 2011;21:16597-602.
- [364] Casalbore-Miceli G, Zanelli A, Girotto EM, Rinaldi AW, Rubira AF, Berlin A. Interactions between humidity and ferrocene-functionalized polythiophene. *Electrochim Acta* 2006;51:5268-73.
- [365] Zanuy D, Preat J, Perpète EA, Alemán C. Response of Crown Ether Functionalized Polythiophenes to Alkaline Ions. *J Phys Chem B* 2012;116:4575-83.
- [366] Liu B, Dai H, Bao Y, Du F, Tian J, Bai R. 2,6-substituted pyridine derivative-containing conjugated polymers: synthesis, photoluminescence and ion-sensing properties. *Polym Chem* 2011;2:1699-705.
- [367] Liu S, Tian J, Wang L, Luo Y, Sun X. Production of stable aqueous dispersion of poly(3,4-ethylenedioxythiophene) nanorods using graphene oxide as a stabilizing agent and their application for nitrite detection. *Analyst* 2011;136:4898-902.
- [368] Lin CY, Vasantha VS, Ho KC. Detection of nitrite using poly(3,4-ethylenedioxythiophene) modified spces. *Sens Actuators B* 2009;140:51-7.
- [369] Li TJ, Lin CY, Balamurugan A, Kung CW, Wang JY, Hu CW, Wang CC, Chen PY, Vittal R, Ho KC. Modification of glassy carbon electrode with a polymer/mediator composite and its application for the electrochemical detection of iodate. *Anal Chim Acta* 2012;737:55-63.
- [370] Jiang F, Yue R, Du Y, Xu J, Yang P. A one-pot green' synthesis of Pd-decorated PEDOT nanospheres for nonenzymatic hydrogen peroxide sensing. *Biosens Bioelectron* 2013;44:127-31.
- [371] Guo C, Li P, Pei M, Zhang G. A new polythiophene derivative-based fluorescent sensor for Co<sup>2+</sup>, Cu<sup>2+</sup>, Cd<sup>2+</sup>, and its complex with Cu<sup>2+</sup> for sensing homocysteine and glutathione. *Sens Actuators B* 2015;221:1223-8.
- [372] Li C, Shi G. Polythiophene-Based Optical Sensors for Small Molecules. *ACS Appl Mater*

- Interfaces 2013;5:4503-10.
- [373] Nie T, Lu L, Bai L, Xu J, Zhang K, Zhang O, Wen Y, Wu L. Simultaneous determination of folic acid and uric acid under coexistence of -ascorbic acid using a modified electrode based on poly (3,4-ethylenedioxythiophene) and functionalized single-walled carbon nanotubes composite. *Int J Electrochem Sci* 2013;8:7016-29.
- [374] Çiftçi H, Tamer U, Teker MŞ, Pekmez NÖ. An enzyme free potentiometric detection of glucose based on a conducting polymer poly (3-aminophenyl boronic acid-co-3-octylthiophene). *Electrochim Acta* 2013;90:358-65.
- [375] Kim DM, Shim YB. Disposable Amperometric Glycated Hemoglobin Sensor for the Finger Prick Blood Test. *Anal Chem* 2013;85:6536-43.
- [376] Liu G, Lan M, Liu W, Wu J, Ge J, Zhang H. Colorimetric detection of carbenicillin using cationic polythiophene derivatives. *Chinese J Polym Sci* 2013;31:1484-90.
- [377] Mazzotta E, Malitesta C, Margapoti E. Direct electrochemical detection of bisphenol A at PEDOT-modified glassy carbon electrodes. *Anal Bioanal Chem* 2013;405:3587-92.
- [378] Zhang L, Wen Y, Yao Y, Xu J, Duan X, Zhang G. Synthesis and characterization of pedot derivative with carboxyl group and its chemo/bio sensing application as nanocomposite, immobilized biological and enhanced optical materials. *Electrochim Acta* 2014;116:343-54.
- [379] Lai KF, Su WY, Chang WT, Cheng SH. The synergic effect of conducting polymer/ionic liquid composite electrodes on the voltammetric sensing of biomolecules. *Int J Electrochem Sci* 2013;8:7959-75.
- [380] Salgado R, delRio R, delValle MA, Armijo F. Selective electrochemical determination of dopamine, using a poly(3,4-ethylenedioxythiophene)/polydopamine hybrid film modified electrode. *J Electroanal Chem* 2013;704:130-6.
- [381] Yao Z, Bai H, Li C, Shi G. Colorimetric and fluorescent dual probe based on a polythiophene derivative for the detection of cysteine and homocysteine. *Chem Commun* 2011;47:7431-3.
- [382] Li C, Numata M, Bae AH, Sakurai K, Shinkai S. Self-assembly of supramolecular chiral insulated molecular wire. *J Am Chem Soc* 2005;127:4548-9.
- [383] Yao Z, Feng X, Hong W, Li C, Shi G. A simple approach for the discrimination of nucleotides based on a water-soluble polythiophene derivative. *Chem Commun* 2009;4696-8.
- [384] Yao Z, Li C, Shi G. Optically active supramolecular complexes of water-soluble achiral polythiophenes and folic acid: spectroscopic studies and sensing applications. *Langmuir* 2008;24:12829-35.
- [385] Huang BH, Geng ZR, Ma XY, Zhang C, Zhang ZY, Wang ZL. Lysosomal ATP imaging in living cells by a water-soluble cationic polythiophene derivative. *Biosens Bioelectron* 2016;83:213-20.
- [386] Li J, Li X, Zhang Y, Li R, Wu D, Du B, Zhang Y, Ma H, Wei Q. Electrochemiluminescence sensor

- based on cationic polythiophene derivative and NH<sub>2</sub>-graphene for dopamine detection. *RSC Adv* 2015;5:5432-7.
- [387] Ho HA, Béra-Abérem M, Leclerc M. Optical sensors based on hybrid DNA/conjugated polymer complexes. *Chem Eur J* 2005;11:1718-24.
- [388] Wang X, Zhao J, Guo C, Pei M, Zhang G. Simple hydrazide-based fluorescent sensors for highly sensitive and selective optical signaling of Cu<sup>2+</sup> and Hg<sup>2+</sup> in aqueous solution. *Sens Actuators B* 2014;193:157-65.
- [389] Wang L, Feng Q, Wang X, Pei M, Zhang G. A novel polythiophene derivative as a sensitive colorimetric and fluorescent sensor for anionic surfactants in water. *New J Chem* 2012;36:1897-901.
- [390] Yao Z, Ma W, Yang Y, Chen X, Zhang L, Lin C, Wu HC. Colorimetric and fluorescent detection of protamines with an anionic polythiophene derivative. *Org Biomol Chem* 2013;11:6466-9.
- [391] Liu M, Li B, Cui X. Anionic polythiophene derivative as peroxidase mimetics and their application for detection of hydrogen peroxide and glucose. *Talanta* 2013;115:837-41.
- [392] Das D, Kim DM, Park DS, Shim YB. A glucose sensor based on an aminophenyl boronic acid bonded conducting polymer. *Electroanalysis* 2011;23:2036-41.
- [393] Yao Z, Hu X, Huang B, Zhang L, Liu L, Zhao Y, Wu HC. Halochromism of a polythiophene derivative induced by conformational changes and its sensing application of carbon dioxide. *ACS Appl Mater Interfaces* 2013;5:5783-7.
- [394] Richardson-Burns SM, Hendricks JL, Foster B, Povlich LK, Kim DH, Martin DC. Polymerization of the conducting polymer poly(3,4-ethylenedioxythiophene) around living neural cells. *Biomaterials* 2007;28:1539-52.
- [395] Atta NF, Galal A, Ahmed RA. Voltammetric behavior and determination of isoniazid using PEDOT electrode in presence of surface active agents. *Int J Electrochem Sci* 2011;6:5097-113.
- [396] Tsakova V, Ilieva G, Filjova D. Role of the anionic dopant of poly (3, 4-ethylenedioxythiophene) for the electroanalytical performance: electrooxidation of acetaminophen. *Electrochim Acta* 2015;179:343-9.
- [397] Atta NF, Galal A, Ahmed RA. Simultaneous determination of catecholamines and serotonin on poly(3,4-ethylene dioxythiophene) modified Pt electrode in presence of sodium dodecyl sulfate. *J Electrochem Soc* 2011;158:F52-F60.
- [398] Si W, Lei W, Han Z, Zhang Y, Hao Q, Xia M. Electrochemical sensing of acetaminophen based on poly(3,4-ethylenedioxythiophene)/graphene oxide composites. *Sens Actuators B* 2014;193:823-9.
- [399] Tsai TH, Chen TW, Chen SM, Sarawathi R. Nickel, copper and manganese hexacyanoferrate with poly(3,4-ethylenedioxythiophene) hybrid film modified electrode for selectively determination

- of ascorbic acid. *Russ J Electrochem* 2012;48:291-301.
- [400] Nie T, Xu JK, Lu LM, Zhang KX, Bai L, Wen YP. Electroactive species-doped poly(3,4-ethylenedioxythiophene) films: Enhanced sensitivity for electrochemical simultaneous determination of vitamins B2, B6 and C. *Biosens Bioelectron* 2013;50:244-50.
- [401] Xu G, Li B, Cui XT, Ling L, Luo X. Electrodeposited conducting polymer PEDOT doped with pure carbon nanotubes for the detection of dopamine in the presence of ascorbic acid. *Sens Actuators B* 2013;188:405-10.
- [402] Si W, Lei W, Zhang Y, Xia M, Wang F, Hao Q. Electrodeposition of graphene oxide doped poly(3,4-ethylenedioxythiophene) film and its electrochemical sensing of catechol and hydroquinone. *Electrochim Acta* 2012;85:295-301.
- [403] Chiang CJ, Tsai KT, Lee YH, Lin HW, Yang YL, Shih CC, Lin CY, Jeng HA, Weng YH, Cheng YY, Ho KC, Dai CA. In situ fabrication of conducting polymer composite film as a chemical resistive CO<sub>2</sub> gas sensor. *Microelectron Eng* 2013;111:409-15.
- [404] Lin CY, Chen JG, Hu CW, Tunney JJ, Ho KC. Using a PEDOT:PSS modified electrode for detecting nitric oxide gas. *Sens Actuators B* 2009;140:402-6.
- [405] Aziz S, Chang DE, Doh YH, Kang CU, Choi KH. Humidity sensor based on PEDOT: PSS and Zinc Stannate nano-composite. *J Electron Mater* 2015;44:3992-9.
- [406] Wang F, Gu H, Swager TM. Carbon nanotube/polythiophene chemiresistive sensors for chemical warfare agents. *J Am Chem Soc* 2008;130:5392-3.
- [407] Nie T, Zhang O, Lu L, Xu J, Wen Y, Qiu X. Facile synthesis of poly(3,4-ethylenedioxythiophene)/graphene nanocomposite and its application for determination of nitrite. *Int J Electrochem Sci* 2013;8:8708-18.
- [408] Du X, Zhang Z, Zhang C, Zhang Y, Chen Q. One-step electrodeposition of poly (3, 4-ethylenedioxythiophene) on carboxylated multi-wall carbon nanotubes and its application in ascorbic acid sensing. *J Electroanal Chem* 2016;782:84-90.
- [409] Prathish KP, Carvalho RC, Brett CM. Electrochemical characterisation of poly (3, 4-ethylenedioxythiophene) film modified glassy carbon electrodes prepared in deep eutectic solvents for simultaneous sensing of biomarkers. *Electrochim Acta* 2016;187:704-13.
- [410] Dervisevic M, Senel M, Cevik E. Novel impedimetric dopamine biosensor based on boronic acid functional polythiophene modified electrodes. *Mater Sci Eng C* 2017;72:641-9.
- [411] Wang JY, Su YL, Wu BH, Cheng SH. Reusable electrochemical sensor for bisphenol A based on ionic liquid functionalized conducting polymer platform. *Talanta* 2016;147:103-10.
- [412] Bai S, Guo J, Sun J, Tang P, Chen A, Luo R, Li D. Enhancement of NO<sub>2</sub>-Sensing Performance at Room Temperature by Graphene-Modified Polythiophene. *Ind Eng Chem Res* 2016;55(19):5788-94.

- [413] Dunst K, Jurków D, Jasiński P. Laser patterned platform with PEDOT–graphene composite film for NO<sub>2</sub> sensing. *Sens Actuators B* 2016;229:155-65.
- [414] Abasıyanık MF, Şenel M. Immobilization of glucose oxidase on reagentless ferrocene-containing polythiophene derivative and its glucose sensing application. *J Electroanal Chem* 2010;639:21-6.
- [415] Kuwahara T, Oshima K, Shimomura M, Miyauchi S. Immobilization of glucose oxidase and electron-mediating groups on the film of 3-methylthiophene/thiophene-3-acetic acid copolymer and its application to reagentless sensing of glucose. *Polymer* 2005;46:8091-7.
- [416] Liu M, Luo C, Peng H. Electrochemical DNA sensor based on methylene blue functionalized polythiophene as a hybridization indicator. *Talanta* 2012;88:216-21.
- [417] Olowu RA, Ndangili PM, Baleg AA, Ikpo CO, Njomo N, Baker P, Iwuoha E. Spectroelectrochemical dynamics of dendritic poly(propyleneimine)-polythiophene star copolymer aptameric 17 $\beta$ -estradiol biosensor. *Int J Electrochem Sci* 2011;6:1686-708.
- [418] Uygun A. DNA hybridization electrochemical biosensor using a functionalized polythiophene. *Talanta* 2009;79:194-8.
- [419] Kang SK, Kim JH, An J, Lee EK, Cha J, Lim G, Park YS, Chung DJ. Synthesis of polythiophene derivatives and their application for electrochemical DNA sensor. *Polym J* 2004;36:937-42.
- [420] Lin P, Luo X, Hsing IM, Yan F. Organic electrochemical transistors integrated in flexible microfluidic systems and used for label-free DNA sensing. *Adv Mater* 2011;23:4035-40.
- [421] Wen Y, Xu J, Liu M, Li D, Lu L, Yue R, He H. A vitamin C electrochemical biosensor based on one-step immobilization of ascorbate oxidase in the biocompatible conducting poly(3,4-ethylenedioxythiophene)-lauroylsarcosinate film for agricultural application in crops. *J Electroanal Chem* 2012;674:71-82.
- [422] Donovan KC, Arter JA, Pilolli R, Cioffi N, Weiss GA, Penner RM. Virus-Poly(3,4-ethylenedioxythiophene) composite films for impedance-based biosensing. *Anal Chem* 2011;83:2420-4.
- [423] Ma F, Rehman A, Liu H, Zhang J, Zhu S, Zeng X. Glycosylation of quinone-fused polythiophene for reagentless and label-free detection of E. Coli. *Anal Chem* 2015;87:1560-8.
- [424] Daprà J, Lauridsen LH, Nielsen AT, Rozlosnik N. Comparative study on aptamers as recognition elements for antibiotics in a label-free all-polymer biosensor. *Biosens Bioelectron* 2013;43:315-20.
- [425] Winther-Jensen O, Kerr R, Winther-Jensen B. Alcohol vapour detection at the three phase interface using enzyme-conducting polymer composites. *Biosens Bioelectron* 2014;52:143-6.
- [426] Moczko E, Istamboulie G, Calas-Blanchard C, Rouillon R, Noguer T. Biosensor employing screen-printed PEDOT:PSS for sensitive detection of phenolic compounds in water. *J Polym Sci Part A Polym Chem* 2012;50:2286-92.

- [427] Kannan B, Williams DE, Laslau C, Travas-Sejdic J. A highly sensitive, label-free gene sensor based on a single conducting polymer nanowire. *Biosens Bioelectron* 2012;35:258-64.
- [428] Sekine J, Luo SC, Wang S, Zhu B, Tseng HR, Yu H. Functionalized Conducting Polymer Nanodots for Enhanced Cell Capturing: the Synergistic Effect of Capture Agents and Nanostructures. *Adv Mater* 2011;23:4788-92.
- [429] Kwon OS, Park SJ, Lee JS, Park E, Kim T, Park HW, You SA, Yoon H, Jang J. Multidimensional Conducting Polymer Nanotubes for Ultrasensitive Chemical Nerve Agent Sensing. *Nano Lett* 2012;12:2797-802.
- [430] Zhang Y, Liu S, Wang L, Luo Y, Tian J, Asiri AM, Al-Youbi AO, Sun X. Novel use of poly(3,4-ethylenedioxythiophene) nanoparticles for fluorescent nucleic acid detection. *ACS Comb Sci* 2012;14:191-6.
- [431] Hocevar MA, Fabregat G, Armelin E, Ferreira CA, Alemán C. Nanometric polythiophene films with electrocatalytic activity for non-enzymatic detection of glucose. *Eur Poly J* 2016;79:132-9.
- [432] Zhang K, Xu J, Zhu X, Lu L, Duan X, Hu D, Dong L, Sun H, Gao Y, Wu Y. Poly (3, 4-ethylenedioxythiophene) nanorods grown on graphene oxide sheets as electrochemical sensing platform for rutin. *J Electroanal Chem* 2015;739:66-72.
- [433] Özcan A, İlkbaşı S. Preparation of poly (3, 4-ethylenedioxythiophene) nanofibers modified pencil graphite electrode and investigation of over-oxidation conditions for the selective and sensitive determination of uric acid in body fluids. *Anal Chim Acta* 2015;891:312-20.
- [434] Rajaram R, Anandhakumar S, Mathiyarasu J. Electrocatalytic oxidation of NADH at low overpotential using nanoporous poly (3, 4)-ethylenedioxythiophene modified glassy carbon electrode. *J Electroanal Chem* 2015;746:75-81.
- [435] Zhou H, Tang Y, Zhai J, Wang S, Tang Z, Jiang L. Enhanced photoelectrochemical detection of bioaffinity reactions by vertically oriented Au nanobranches complexed with a biotinylated polythiophene derivative. *Sensors* 2009;9:1094-107.
- [436] Wu L, Xu J, Lu L, Yang T, Gao Y. Fabrication of nanostructured PEDOT clusters using  $\beta$ -cyclodextrin as substrate and applied for simultaneous determination of hyperoside and shikonin. *Colloids Surf A Physicochem Eng Asp* 2015;482:203-12.
- [437] Moghaddam HM, Malkeshi H. Self-assembly synthesis and ammonia gas-sensing properties of ZnO/Polythiophene nanofibers. *J Mater Sci Mater Electron* 2016;27:8807-15.
- [438] Park E, Kwon OS, Park SJ, Lee JS, You S, Jang J. One-pot synthesis of silver nanoparticles decorated poly(3,4-ethylenedioxythiophene) nanotubes for chemical sensor application. *J Mater Chem* 2011;22:1521-6.
- [439] Satapathi S, Kokil A, Venkatraman BH, Li L, Venkataraman D, Kumar J. Sensitive detection of nitroaromatics with colloidal conjugated polymer nanoparticles. *IEEE Sensors J* 2013;13:2329-

33.

- [440] Shaik M, Rao VK, Sinha AK, Murthy KS, Jain R. Sensitive detection of nitrogen dioxide gas at room temperature using poly (3, 4-ethylenedioxythiophene) nanotubes. *J Environ Chem Eng* 2015;3:1947-52.
- [441] Cheng YH, Kung CW, Chou LY, Vittal R, Ho KC. Poly(3,4-ethylenedioxythiophene) (PEDOT) hollow microflowers and their application for nitrite sensing. *Sens Actuators B* 2014;192:762-8.
- [442] Zuo Y, Xu J, Zhu X, Duan X, Lu L, Gao Y, Xing H, Yang T, Ye G, Yu Y. Poly (3, 4-ethylenedioxythiophene) nanorods/graphene oxide nanocomposite as a new electrode material for the selective electrochemical detection of mercury (II). *Synth Met* 2016;220:14-9.
- [443] Wang JY, Chen LC, Ho KC. Synthesis of redox polymer nanobeads and nanocomposites for glucose biosensors. *ACS Appl Mater Interfaces* 2013;5:7852-61.
- [444] Wisitsoraat A, Pakapongpan S, Sriprachuabwong C, Phokharatkul D, Sritongkham P, Lomas T, Tuantranont A. Graphene-PEDOT:PSS on screen printed carbon electrode for enzymatic biosensing. *J Electroanal Chem* 2013;704:208-13.
- [445] Strakosas X, Sessolo M, Hama A, Rivnay J, Stavrinidou E, Malliaras GG, Owens RM. A facile biofunctionalisation route for solution processable conducting polymer devices. *J Mater Chem B* 2014;2:2537-45.
- [446] Santhosh P, Manesh KM, Uthayakumar S, Komathi S, Gopalan AI, Lee KP. Fabrication of enzymatic glucose biosensor based on palladium nanoparticles dispersed onto poly(3,4-ethylenedioxythiophene) nanofibers. *Bioelectrochem* 2009;75:61-6.
- [447] Xiao X, Wang M, Li H, Si P. One-step fabrication of bio-functionalized nanoporous gold/poly(3,4-ethylenedioxythiophene) hybrid electrodes for amperometric glucose sensing. *Talanta* 2013;116:1054-9.
- [448] Hui N, Wang W, Xu G, Luo X. Graphene oxide doped poly (3, 4-ethylenedioxythiophene) modified with copper nanoparticles for high performance nonenzymatic sensing of glucose. *J Mater Chem B* 2015;3:556-61.
- [449] Krzyczmonik P, Socha E, Skrzypek S. Immobilization of glucose oxidase on modified electrodes with composite layers based on poly (3, 4-ethylenedioxythiophene). *Bioelectrochemistry* 2015;101:8-13.
- [450] Demirci S, Emre FB, Ekiz F, Oğuzkaya F, Timur S, Tanyeli C, Toppare L. Functionalization of poly-SNS-anchored carboxylic acid with Lys and PAMAM: surface modifications for biomolecule immobilization/stabilization and bio-sensing applications. *Analyst* 2012;137:4254-61.
- [451] Kakhki S, Barsan MM, Shams E, Brett CMA. New robust redox and conducting polymer modified electrodes for ascorbate sensing and glucose biosensing. *Electroanalysis* 2013;25:77-84.
- [452] Yao Y, Wen Y, Xu J, Zhang L, Duan XJ. Application of commercial poly(3,4-

- ethylenedioxythiophene):poly(styrene sulfonate) for electrochemical sensing of dopamine. Serbian Chem Soc 2013;78:1397-411.
- [453] Atta NF, Galal A, El-Ads EH. Gold nanoparticles-coated poly(3,4-ethylene-dioxythiophene) for the selective determination of sub-nano concentrations of dopamine in presence of sodium dodecyl sulfate. *Electrochim Acta* 2012;69:102-11.
- [454] Choe JE, Ahmed MS, Jeon S. Trouble free dopamine sensing by palladium nanoparticles fabricated poly (3, 4-ethylenedioxythiophene) functionalized graphene. *J Electrochem Soc* 2016;163:B113-8.
- [455] Huang Y, Bu L, Wang W, Qin X, Li Z, Huang Z, Fu Y, Su X, Xie Q, Yao S. One-pot preparation of uricase-poly(thiophene-3-boronic acid)-Ptnano composites for high-performance amperometric biosensing of uric acid. *Sens Actuators B* 2013;177:116-23.
- [456] Siao HW, Chen SM, Lin KC. Electrochemical study of PEDOT-PSS-MDB-modified electrode and its electrocatalytic sensing of hydrogen peroxide. *J Solid State Electrochem* 2011;15:1121-8.
- [457] Chen Y, Gai P, Jin L, Zhu D, Tian D, Abdel-Halim ES, Zhang J, Zhu JJ. Fabrication of PEDOT nanowhiskers for electrical connection of the hemoglobin active center for H<sub>2</sub>O<sub>2</sub> electrochemical biosensing. *J Mater Chem B* 2013;1:3451-7.
- [458] Wen Y, Duan X, Xu J, Yue R, Li D, Liu M, Lu L, He H. One-step electrosynthesis of poly(3,4-ethylenedioxy-thiophene)-ethylsulfate matrix for fabricating vitamin C electrochemical biosensor and its determination in commercial juices. *J Solid State Electrochem* 2012;16:3725-38.
- [459] Dutse SW, Yusof NA, Ahmad H, Hussein MZ, Zainal Z. DNA-based biosensor for detection of *Ganoderma boninense*, an oil palm pathogen utilizing newly synthesized ruthenium complex [Ru(phen)<sub>2</sub>(qtpy)]<sup>2+</sup> based on a PEDOT-PSS/Ag nanoparticles modified electrode. *Int J Electrochem Sci* 2013;8:11048-57.
- [460] Spain E, Keyes TE, Forster RJ. DNA sensor based on vapor polymerized pedot films functionalized with gold nanoparticles. *Biosens Bioelectron* 2013;41:65-70.
- [461] Radhakrishnan S, Sumathi C, Dharuman V, Wilson J. Gold nanoparticles functionalized poly(3,4-ethylenedioxythiophene) thin film for highly sensitive label free DNA detection. *Anal Methods* 2013;5:684-9.
- [462] Zhang Y, Li Z, Cheng Y, Lv X. Colorimetric detection of microrna and rnase H activity in homogeneous solution with cationic polythiophene derivative. *Chem Commun* 2009;3172-4.
- [463] Kim S, Oh WK, Jeong YS, Jang J. Dual-functional poly(3,4-ethylenedioxythiophene)/mno<sub>2</sub> nanoellipsoids for enhancement of neurite outgrowth and exocytosed biomolecule sensing in PC12 cells. *Adv Funct Mater* 2013;23:1947-56.
- [464] Gao YS, Xu JK, Lu LM, Zhu XF, Wang WM, Yang TT, Zhang KX, Yu YF. A label-free electrochemical immunosensor for carcinoembryonic antigen detection on a graphene platform

- doped with poly (3, 4-ethylenedioxythiophene)/Au nanoparticles. RSC Adv 2015;5:86910-8.
- [465] Sriprachuabwong C, Karuwan C, Wisitsorrat A, Phokharatkul D, Lomas T, Sritongkham P, Tuantranont A. Inkjet-printed graphene-PEDOT:PSS modified screen printed carbon electrode for biochemical sensing. J Mater Chem 2012;22:5478-85.
- [466] Phongphut A, Sriprachuabwong C, Wisitsoraat A, Tuantranont A, Prichanont S, Sritongkham P. A disposable amperometric biosensor based on inkjet-printed Au/PEDOT-PSS nanocomposite for triglyceride determination. Sens Actuators B 2013;178:501-7.
- [467] Pires NMM, Dong T, Hanke U, Hoivik N. Integrated optical microfluidic biosensor using a polycarbazole photodetector for point-of-care detection of hormonal compounds. J Biomed Opt 2013;18:097001/1-8.
- [468] Lange U, Mirsky VM. Chemosensitive nanocomposite for conductometric detection of hydrazine and NADH. Electrochim Acta 2011;56:3679-84.
- [469] Sundari PA, Manisankar P. Development of ultrasensitive surfactants doped poly(3,4-ethylenedioxythiophene)/multiwalled carbon nanotube sensor for the detection of pyrethroids and an organochlorine pesticide. J Appl Electrochem 2011;41:29-37.
- [470] Chauhan N, Chawla S, Pundir CS, Jain U. An electrochemical sensor for detection of neurotransmitter-acetylcholine using metal nanoparticles, 2D material and conducting polymer modified electrode. Biosen Bioelectron 2017;89:377-83.
- [471] Xu F, Liu Y, Xie S, Wang L. Electrochemical preparation of a three dimensional PEDOT-cuxo hybrid for enhanced oxidation and sensitive detection of hydrazine. Anal Methods 2016;8:316-25.
- [472] Guo X, Jian J, Lin L, Zhu H, Zhu S. O<sub>2</sub> plasma-functionalized swcnts and PEDOT/PSS composite film assembled by dielectrophoresis for ultrasensitive trimethylamine gas sensor. Analyst 2013;138:5265-73.
- [473] Jian J, Guo X, Lin L, Cai Q, Cheng J, Li J. Gas-sensing characteristics of dielectrophoretically assembled composite film of oxygen plasma-treated SWCNTs and PEDOT/PSS polymer. Sens Actuators B 2013;178:279-88.
- [474] Zampetti E, Pantalei S, Muzyczuk A, Bearzotti A, De Cesare F, Spinella C, Macagnano A. A high sensitive NO<sub>2</sub> gas sensor based on PEDOT-PSS/TiO<sub>2</sub> nanofibers. Sens Actuators B 2013;176:390-8.
- [475] Lin Y, Huang L, Chen L, Zhang J, Shen L, Chen Q, Shi W. Fully gravure-printed NO<sub>2</sub> gas sensor on a polyimide foil using WO<sub>3</sub>-PEDOT: PSS nanocomposites and Ag electrodes. Sens Actuators B 2015;216:176-83.
- [476] Gavvani JN, Dehsari HS, Hasani A, Mahyari M, Shalamzari EK, Salehi A, Taromi FA. A room temperature volatile organic compound sensor with enhanced performance, fast response and recovery based on N-doped graphene quantum dots and poly (3, 4-ethylenedioxythiophene)–

- poly (styrenesulfonate) nanocomposite. RSC Adv 2015;5:57559-67.
- [477] Choi KH, Sajid M, Aziz S, Yang BS. Wide range high speed relative humidity sensor based on PEDOT: PSS–PVA composite on an IDT printed on piezoelectric substrate. Sensors Act A Phys 2015;228:40-9.
- [478] Taccola S, Greco F, Zucca A, Innocenti C, De Julián Fernández C, Campo G, Sangregorio C, Mazzolai B, Mattoli V. Characterization of free-standing PEDOT:PSS/Iron oxide nanoparticle composite thin films and application as conformable humidity sensors. ACS Appl Mater Interfaces 2013;5:6324-32.
- [479] Ishii O, Kakehata R, Kutsuzawa N, Okuzaki H. Application of magnetic ribbon coated with poly(3,4-ethylenedioxy-thiophene)/poly(4-styrenesulfonate) to a wireless humidity sensor. IEEJ Trans Elec Electron Eng 2012;7(S1):S190-2.
- [480] Tung TT, Castro M, Feller JF, Kim TY, Suh KS. Hybrid film of chemically modified graphene and vapor-phase-polymerized PEDOT for electronic nose applications. Organic Electron 2013;14:2789-94.
- [481] Wang F, Yang Y, Swager TM. Molecular recognition for high selectivity in carbon nanotube/polythiophene chemiresistors. Angew Chem Int Ed 2008;47:8394-6.
- [482] Gao Y, Li J, Yang X, Xiang Q, Wang K. Electrochemiluminescence Biosensor Based on PEDOT-PSS- Graphene Functionalized ITO Electrode. Electroanalysis 2014;26:382-8.
- [483] Wang Q, Yun Y. A nanomaterial composed of cobalt nanoparticles, poly(3,4-ethylenedioxythiophene) and graphene with high electrocatalytic activity for nitrite oxidation. Microchim Acta 2012;177:411-8.
- [484] Zuo J, Zhang Z, Jiao J, Pang H, Zhang D, Ma H. Sensitive and selective nitrite sensor based on phosphovanadomolybdates H<sub>6</sub>[p<sub>10</sub>o<sub>9</sub>v<sub>3</sub>o<sub>40</sub>], poly (3, 4-ethylenedioxythiophene) and Au nanoparticles. Sens Actuators B 2016;236:418-24.
- [485] Peteu SF, Whitman BW, Galligan JJ, Swain GM. Electrochemical detection of peroxynitrite using hemin–PEDOT functionalized boron-doped diamond microelectrode. Analyst 2016;141:1796-806.
- [486] Ding L, Zhai J, Bond AM, Zhang J. Polystyrenesulfonate doped poly(hydroxymethyl-3,4-ethylenedioxythiophene) stabilized Au nanoparticle modified glassy carbon electrode as a reusable sensor for mercury(II) detection in chloride media. J Electroanal Chem 2013;704:96-101.
- [487] Tarabella G, Villani M, Calestani D, Mosca R, Iannotta S, Zappettini A, Coppedè N. A single cotton fiber organic electrochemical transistor for liquid electrolyte saline sensing. J Mater Chem 2012;22:23830-4.
- [488] Lin KC, Wu TH, Chen SM. A highly sensitive persulfate sensor based on a hybrid nanocomposite

- with silicomolybdate doping poly (3, 4-ethylenedioxythiophene) on multi-walled carbon nanotubes. *RSC Adv* 2015;5:59946-52.
- [489] Sun B, Long YZ, Liu SL, Huang YY, Ma J, Zhang HD, Shen G, Xu S. Fabrication of curled conducting polymer microfibrillar arrays via a novel electrospinning method for stretchable strain sensors. *Nanoscale* 2013;5:7041-5.
- [490] Ranjith KS, Kumar RR. Facile construction of vertically aligned zno nanorod/PEDOT: PSS hybrid heterojunction-based ultraviolet light sensors: efficient performance and mechanism. *Nanotechnology* 2016;27:095304/1-10.
- [491] Festin N, Plesse C, Pirim P, Chevrot C, Vidal F. Electro-active Interpenetrating Polymer Networks actuators and strain sensors: Fabrication, position control and sensing properties. *Sens Actuators B* 2014;193:82-8.
- [492] Dwivedi AK, Prasad KM, Trivedi V, Iyer PK. Interaction of heme proteins with anionic polyfluorene: insights into physiological effects, folding events, and inhibition activity. *ACS Appl Mater Interfaces* 2012;4:6371-7.
- [493] Dwivedi AK, Saikia G, Iyer PK. Aqueous polyfluorene probe for the detection and estimation of Fe<sup>3+</sup> and inorganic phosphate in blood serum. *J Mater Chem* 2011;21:2502-7.
- [494] Wu X, Xu B, Tong H, Wang L. Highly selective and sensitive detection of cyanide by reaction-based conjugated polymer chemosensor. *Macromolecules* 2011;44:4241-8.
- [495] Heeger PS, Heeger AJ. Making sense of polymer-based biosensors. *Proc Natl Acad Sci* 1999;96:12219-21.
- [496] Saikia G, Iyer PK. A Remarkable Superquenching and Superdequenching Sensor for the Selective and Noninvasive Detection of Inorganic Phosphates in Saliva. *Macromolecules* 2011;44:3753-8.
- [497] Li P, Zhao Y, Yao L, Nie H, Zhang M. A simple, selective, fluorescent iron(III) sensing material based on peripheral carbazole. *Sens Actuators B* 2014;191:332-6.
- [498] Ibrahimova V, Eda Kocak M, Önal AM, Tuncel D. Optical and electronic properties of fluorene-based copolymers and their sensory applications. *J Polym Sci Part A Polym Chem* 2013;51:815-23.
- [499] Li L, He F, Wang X, Ma N, Li L. Reversible pH-responsive fluorescence of water-soluble polyfluorenes and their application in metal ion detection. *ACS Appl Mater Interfaces* 2012;4:4927-33.
- [500] Wu CS, Lin YJ, Chen Y. A fluorene-based material containing triple azacrown ether groups: synthesis, characterization and application in chemosensors and electroluminescent devices. *Org Biomol Chem* 2014;12:1419-29.
- [501] Li D, Li H, Liu M, Chen J, Ding J, Huang X, Wu H. A novel D- $\pi$ -A conjugated polymer

- chemosensor based on benzo[c] [1,2,5] selenadiazole for highly selective and sensitive recognition of mercury (II) ions. *Macromol Chem Phys* 2014;215:82-9.
- [502] Wu X, Xu B, Tong H, Wang L. Meta-linked and para-linked water-soluble poly(arylene ethynylene)s with amino acid side chains: Effects of different linkage on Hg<sup>2+</sup> ion sensing properties in aqueous media. *J Polym Sci Part A Polym Chem* 2012;50:1521-9.
- [503] Zhou XH, Yan JC, Pei J. Exploiting an imidazole-functionalized polyfluorene derivative as a chemosensory material. *Macromolecules* 2004;37:7078-80.
- [504] Álvarez-Díaz A, Salinas-Castillo A, Camprubí-Robles M, Costa-Fernández JM, Pereiro R, Mallavia R, Sanz-Medel A. Conjugated polymer microspheres for "turn-off"/"turn-on" fluorescence optosensing of inorganic ions in aqueous media. *Anal Chem* 2011;83:2712-8.
- [505] Lv F, Feng X, Tang H, Liu L, Yang Q, Wang S. Development of film sensors based on conjugated polymers for copper (II) ion detection. *Adv Funct Mater* 2011;21:845-50.
- [506] Wu CS, Liu CT, Chen Y. Multifunctional copolyfluorene containing pendant benzimidazolyl groups: applications in chemical sensors and electroluminescent devices. *Polym Chem* 2012;3:3308-17.
- [507] Chakraborty C, Bera MK, Samanta P, Malik S. Selective detection of cyanide by a polyfluorene-based organoboron fluorescent chemodosimeter. *New J Chem* 2013;37:3222-8.
- [508] Hu J, Zhang G, Geng Y, Liu S. Micellar nanoparticles of coil-rod-coil triblock copolymers for highly sensitive and ratiometric fluorescent detection of fluoride ions. *Macromolecules* 2011;44:8207-14.
- [509] Wang H, Peng Z, Long Y, Chen H, Yang Y, Li N, Liu F. A simple and reusable fluorescent sensor for heme proteins based on a conjugated polymer-doped electrospun nanofibrous membrane. *Talanta* 2012;94:216-22.
- [510] Yan M, Gao W, Ge S, Ge L, Chu C, Yu J, Song X, Hou S. A novel conjugated polyfluorene: synthesis, characterization and application in label-free ECL immunoassays for biomarker detection. *J Mater Chem* 2012;22:5568-73.
- [511] Li Q, Sun K, Chang K, Yu J, Chiu DT, Wu C, Qin W. Ratiometric luminescent detection of bacterial spores with terbium chelated semiconducting polymer dots. *Anal Chem* 2013;85:9087-91.
- [512] He C, He Q, Deng C, Shi L, Zhu D, Fu Y, Cao H, Cheng J. Turn on fluorescence sensing of vapor phase electron donating amines via tetraphenylporphyrin or metallophenylporphyrin doped polyfluorene. *Chem Commun* 2010;46:7536-8.
- [513] Zhang J, Xing B, Song J, Zhang F, Nie C, Jiao L, Liu L, Lv F, Wang S. Associated analysis of DNA methylation for cancer detection using CCP-based FRET technique. *Anal Chem* 2014;86:346-50.

- [514] Shi J, Cai L, Pu KY, Liu B. Synthesis and characterization of water-soluble conjugated glycopolymer for fluorescent sensing of concanavalin A. *Chem Asian J* 2010;5:301-8.
- [515] Shi H, Xiujie C, Liu S, Xu H, An Z, Ouyang L, Tu Z, Zhao Q, Fan Q, Wang L, Huang W. Hyper-branched phosphorescent conjugated polyelectrolytes for time-resolved heparin sensing. *ACS Appl Mater Interfaces* 2013;5:4562-8.
- [516] Pu KY, Liu B. A multicolor cationic conjugated polymer for naked-eye detection and quantification of heparin. *Macromolecules* 2008;41:6636-40.
- [517] Jiang J, Zhang C, Lin W, Liu Y, Liu S, Xu Y, Zhao Q, Huang W. Long-lived phosphorescent Iridium (iii) complexes conjugated with cationic polyfluorenes for heparin sensing and cellular imaging. *Macromol Rapid Commun* 2015;36:640-6.
- [518] Xu Q, An L, Yu M, Wang S. Design and synthesis of a new conjugated polyelectrolyte as a reversible pH sensor. *Macromol Rapid Commun* 2008;29:390-5.
- [519] Dong L, Deng C, He C, Shi L, Fu Y, Zhu D, Cao H, He Q, Cheng J. Highly sensitive vapor detection of amines with fluorescent conjugated polymer: A novel lasing turn-on sensory mechanism. *Sens Actuators B* 2013;180:28-34.
- [520] Wu X, Xu B, Tong H, Wang L. Phosphonate-functionalized polyfluorene film sensors for sensitive detection of iron(III) in both organic and aqueous media. *Macromolecules* 2010;43:8917-23.
- [521] Roeser J, Heinrich B, Bourgogne C, Rawiso M, Michel S, Hubscher-Bruder V, Arnaud-Neu F, Mery S. Dendronized polymers with silver and mercury cations recognition: complexation studies and polyelectrolyte behavior. *Macromolecules* 2013;46:7075-85.
- [522] Qin C, Wu X, Tong H, Wang L. High solubility and photoluminescence quantum yield water-soluble polyfluorenes with dendronized amino acid side chains: Synthesis, photophysical, and metal ion sensing properties. *J Mater Chem* 2010;20:7957-64.
- [523] Qin C, Wu X, Gao B, Tong H, Wang L. Amino acid-functionalized polyfluorene as a water-soluble Hg<sup>2+</sup> chemosensor with high solubility and high photoluminescence quantum yield. *Macromolecules* 2009;42:5427-9.
- [524] Wang X, Wang G, Liang F, Wang Y, Wei X, Feng L, Zhang L. Highly sensitive and selective chemosensors for D-fructose based on electrostatic interaction in aqueous solution. *Sens Actuators B* 2012;171-172:486-91.
- [525] Bao B, Ma M, Zai H, Zhang L, Fu N, Huang W, Wang L. Conjugated polymer nanoparticles for label-free and bioconjugate-Recognized DNA sensing in serum. *Adv Sci* 2015;2:1400009/1-6.
- [526] Wasin T, Enomoto K, Sakurai T, Padalkar VS, Cheng HL, Tang MT, Horio A, Sakamaki D, Omichi M, Saeki A, Kikuchi K. Fabrication of "clickable" polyfluorene nanowires with high aspect ratio as biological sensing platforms. *ACS Sens* 2016;1:766-74.
- [527] Ding W, Zhang H, Xu J, Wen Y, Zhang J, Liu H, Yao Y, Zhang Z. Development of solution-

- dispersible hyperbranched conjugated polymer nanoparticles for Fe<sup>3+</sup> fluorescent detection and their application in logic gate. *J Polym Sci A Polym Chem* 2016;54:3694-700.
- [528] Chiu YC, Chen Y, Kuo CC, Tung SH, Kakuchi T, Chen WC. Synthesis, morphology, and sensory applications of multifunctional rod-coil-coil triblock copolymers and their electrospun nanofibers. *ACS Appl Mater Interfaces* 2012;4:3387-95.
- [529] Sakai R, Nagai A, Tago Y, Sato S, Nishimura Y, Arai T, Satoh T, Kakuchi T. Fluorescence turn-on sensing of anions based on disassembly process of urea-functionalized poly(phenylenebutadiynylene) aggregates. *Macromolecules* 2012;45:4122-27.
- [530] Lou X, Zeng Q, Zhang Y, Wan Z, Qin J, Li Z. Functionalized polyacetylenes with strong luminescence: "turn-on" fluorescent detection of cyanide based on the dissolution of gold nanoparticles and its application in real samples. *J Mater Chem* 2012;22:5581-6.
- [531] Pourghaz Y, Dongare P, Thompson DW, Zhao Y. Click functionalized poly(p-phenylene ethynylene)s as highly selective and sensitive fluorescence turn-on chemosensors for Zn<sup>2+</sup> and Cd<sup>2+</sup> ions. *Chem Commun* 2011;47:11014-6.
- [532] Whitcombe MJ, Chianella I, Larcombe L, Piletsky SA, Noble J, Porter R, Horgan A. The rational development of molecularly imprinted polymer-based sensors for protein detection. *Chem Soc Rev* 2011;40:1547-71.
- [533] Whitcombe MJ, Alexander C, Vulfson EN. Imprinted polymers: versatile new tools in synthesis. *Synlett* 2000;911-23.
- [534] Zhang HQ, Ye L, Mosbach K. Non-covalent molecular imprinting with emphasis on its application in separation and drug development. *J Mol Recognit* 2006;19:248-59.
- [535] Whitcombe MJ, Lakshmi D. Imprinted polymers. In: Cosnier S, Karyakin A, editors, *Electropolymerization: Concepts, Materials and Applications*. Weinheim: Wiley-VCH 2010. p. 133-51.
- [536] Chen LX, Xu SF, Li JH. Recent advances in molecular imprinting technology: current status, challenges and highlighted applications. *Chem Soc Rev* 2011;40:2922-42.
- [537] Alexander C, Andersson HS, Andersson LI, Ansell RJ, Kirsch N, Nicholls IA, O'Mahony J, Whitcombe MJ. Molecular imprinting science and technology: A survey of the literature for the years up to and including 2003. *J Mol Recognit* 2006;19:106-80.
- [538] Subrahmanyam S, Karim K, Piletsky SA. Computational approaches in the design of synthetic receptors. In *Designing receptors for the next generation of biosensors* Springer, Berlin, Heidelberg 2012;12:131-65.
- [539] Kunath S, Marchyk N, Haupt K, Feller KH. Multi-objective optimization and design of experiments as tools to tailor molecularly imprinted polymers specific for glucuronic acid. *Talanta* 2013;105:211-8.

- [540] Le Jeune J, Spivak DA. Chiral effects of alkyl-substituted derivatives of N,O-bismethacryloyl ethanolamine on the performance of one monomer molecularly imprinted polymers (omnimips). *Anal Bioanal Chem* 2007;389:433-40.
- [541] Wulff G. The covalent and other stoichiometric approaches. In: Yan M, editor. *Molecularly imprinted materials: science and technology*. Boca Raton: CRC press 2005. p. 59-92.
- [542] Qi PP, Wang JC, Wang LD, Li Y, Jin J, Su F, Tian YZ, Chen JP. Molecularly imprinted polymers synthesized via semi-covalent imprinting with sacrificial spacer for imprinting phenols. *Polymer* 2010;51:5417-5423.
- [543] Kirsch N, Whitcombe MJ. The semi-covalent approach. In: Yan M, editor. *Molecularly imprinted materials: science and technology*. Boca Raton: CRC press 2005. p. 93-122.
- [544] Conrad II PG, Shea KJ. The use of metal coordination for controlling the microenvironment of imprinted polymers. In: Yan M, editor. *Molecularly imprinted materials: science and technology*. Boca Raton: CRC press 2005. p. 123-80.
- [545] Mayes AG, Whitcombe MJ. Synthetic strategies for the generation of molecularly imprinted organic polymers. *Adv Drug Deliv Rev* 2005;57:1742-78.
- [546] Sardesai NP, Barron JC, Rusling JF. Carbon nanotube microwell array for sensitive electrochemiluminescent detection of cancer biomarker proteins. *Anal Chem* 2011;83:6698-703
- [547] Ramanaviciene A, Ramanavicius A. Pulsed amperometric detection of DNA with an ssdna/polypyrrole-modified electrode. *Anal Bioanal Chem* 2004;379:287-93.
- [548] Ramanaviciene A, Finkelsteinas A, Ramanavicius A. Basic electrochemistry meets nanotechnology: Electrochemical preparation of artificial receptors based on a nanostructured conducting polymer, polypyrrole. *J Chem Educ* 2006;83:1212-4.
- [549] Özcan L, Sahin M, Sahin Y. Electrochemical preparation of a molecularly imprinted polypyrrole-modified pencil graphite electrode for determination of ascorbic acid. *Sensors* 2008;8:5792-805.
- [550] Ramanavicius A, Oztekin Y, Balevicius Z, Kausaite-Mikstimiene A, Krikstolaityte V, Baleviciute I, Ratautaite V, Ramanaviciene A. Conducting and electrochemically generated polymers in sensor design (mini review). *Procedia Eng* 2012;47:825-8.
- [551] Nezhadali A, Rouki Z, Nezhadali M. Electrochemical preparation of a molecularly imprinted polypyrrole modified pencil graphite electrode for the determination of phenothiazine in model and real biological samples. *Talanta* 2015;144:456-65.
- [552] Schweiger B, Kim J, Kim YJ, Ulbricht M. Electropolymerized molecularly imprinted polypyrrole film for sensing of clofibrac acid. *Sensors* 2015;15:4870-89.
- [553] Turco A, Corvaglia S, Mazzotta E. Electrochemical sensor for sulfadimethoxine based on molecularly imprinted polypyrrole: Study of imprinting parameters. *Biosens Bioelectron* 2015;63:240-7.

- [554] Radi AE, Abd El-Ghany N, Wahdan T. Voltammetric determination of flunixin on molecularly imprinted polypyrrole modified glassy carbon electrode. *J Anal Methods Chem* 2016;2016:5296582/1-7.
- [555] Maouche N, Ktari N, Bakas I, Fourati N, Zerrouki C, Seydou M, Maurel F, Chehimi MM. A surface acoustic wave sensor functionalized with a polypyrrole molecularly imprinted polymer for selective dopamine detection. *J Mol Recognit* 2015;28:667-78.
- [556] Gürler B, Özkorucuklu SP, Kir E. Voltammetric behavior and determination of doxycycline in pharmaceuticals at molecularly imprinted and non-imprinted overoxidized polypyrrole electrodes. *J Pharm Biomed Anal* 2013;84:263-8.
- [557] Uygun ZO, Dilgin Y. A novel impedimetric sensor based on molecularly imprinted polypyrrole modified pencil graphite electrode for trace level determination of chlorpyrifos. *Sens Actuators B* 2013;188:78-84.
- [558] Syritski V, Reut J, Menaker A, Gyurcsányi RE, Öpik A. Electrosynthesized molecularly imprinted polypyrrole films for enantioselective recognition of L-aspartic acid. *Electrochim Acta* 2008;53:2729-36.
- [559] Saumya V, Prathish KP, Dhanya S, Rao TP. Mechanistic aspects of tyrosine sensing on an in situ copper oxide modified molecularly imprinted polypyrrole coated glassy carbon electrode. *J Electroanal Chem* 2011;663:53-8.
- [560] Wackerlig J, Schirhagl R. Applications of molecularly imprinted polymer nanoparticles and their advances toward industrial use: a review. *Anal Chem* 2015;88:250-61.
- [561] Chen L, Li B. Application of magnetic molecularly imprinted polymers in analytical chemistry. *Anal Methods* 2012;4:2613-21.
- [562] Pardieu E, Cheap H, Vedrine C, Lazerges M, Lattach Y, Garnier F, Remita S, Pernelle C. Molecularly imprinted conducting polymer based electrochemical sensor for detection of atrazine. *Anal Chim Acta* 2009;649:236-45.
- [563] Lattach Y, Garnier F, Remita S. Influence of chemical and structural properties of functionalized polythiophene-based layers on electrochemical sensing of atrazine. *Chem Phys Chem* 2012;13:281-90.
- [564] Yin XL, Ding JJ, Zhang S, Kong JL. Enantioselective sensing of chiral amino acids by potentiometric sensors based on optical active polyaniline films. *Biosens Bioelectron* 2006;21:2184-7.
- [565] Okuno H, Kitano T, Yakabe H, Kishimoto M, Deore BA, Siigi H, Nagaoka T. Characterization of overoxidized polypyrrole colloids imprinted with l-lactate and their application to enantioseparation of amino acids. *Anal Chem* 2002;74:4184-90.
- [566] Sharma PS, Pietrzyk-Le A, D'Souza F, Kutner W. Electrochemically synthesized polymers in

- molecular imprinting for chemical sensing. *Anal Bioanal Chem* 2012;402:3177-204.
- [567] Buica GO, Bucher B, Moutet JM, Royal G, Saint-Aman E, Ungureanu EM. Voltammetric sensing of mercury and copper cations at poly(EDTA-like) film modified electrode. *Electroanalysis* 2009;21:77-86.
- [568] Namvar A, Warriner K. Microbial imprinted polypyrrole/poly(3-methylthiophene) composite films for the detection of *Bacillus* endospores. *Biosens Bioelectron* 2007;22:2018-24.
- [569] Tsai TC, Han HZ, Cheng CC, Chen LC, Chang HC, Chen JJJ. Modification of platinum microelectrode with molecularly imprinted over-oxidized polypyrrole for dopamine measurement in rat striatum. *Sens Actuators B* 2012;171–172:93-101.
- [570] Tonelli D, Ballarin B, Guadagnini L, Mignani A, Scavetta E. A novel potentiometric sensor for L-ascorbic acid based on molecularly imprinted polypyrrole. *Electrochim Acta* 2011;56:7149-54.
- [571] Yeh WM, Ho KC. Amperometric morphine sensing using a molecularly imprinted polymer-modified electrode. *Anal Chim Acta* 2005;542:76-82.
- [572] Özcan L, Sahin Y. Determination of paracetamol based on electropolymerized-molecularly imprinted polypyrrole modified pencil graphite electrode. *Sens Actuators B* 2007;127:362-9.
- [573] Prabhakar N, Arora K, Singh S, Pandey MK, Singh H, Malhotra BD. Polypyrrole-polyvinyl sulphonate film based disposable nucleic acid biosensor. *Anal Chim Acta* 2007;589:6-13.
- [574] Álvaro M, Benitez M, Das D, Ferrer B, García H. Synthesis of chiral periodic mesoporous silicas (chimo) of mcm-41 type with binaphthyl and cyclohexadiyl groups incorporated in the framework and direct measurement of their optical activity. *Chem Mater* 2004;16:2222-8.
- [575] Wang B, Chi C, Shan W, Zhang YH, Ren N, Yang WL, Tang Y. Chiral mesostructured silica nanofibers of MCM-41. *Angew Chem Int Ed* 2006;45:2088-90.
- [576] Nezhadali A, Mojarrab M. Fabrication of an electrochemical molecularly imprinted polymer triamterene sensor based on multivariate optimization using multi-walled carbon nanotubes. *J Electroanal Chem* 2015;744:85-94.
- [577] Nezhadali A, Senobari S, Mojarrab M. 1, 4-dihydroxyanthraquinone electrochemical sensor based on molecularly imprinted polymer using multi-walled carbon nanotubes and multivariate optimization method. *Talanta* 2016;146:525-32.
- [578] Nezhadali A, Mojarrab M. Computational design and multivariate optimization of an electrochemical metoprolol sensor based on molecular imprinting in combination with carbon nanotubes. *Anal Chim Acta* 2016;924:86-98.
- [579] Pacheco JG, Castro M, Machado S, Barroso MF, Nouws HP, Delerue-Matos C. Molecularly imprinted electrochemical sensor for ochratoxin A detection in food samples. *Sens Actuators B* 2015;215:107-12.
- [580] Deiminiat B, Rounaghi GH, Arbab-Zavar MH. Development of a new electrochemical imprinted

- sensor based on poly-pyrrole, sol-gel and multiwall carbon nanotubes for determination of tramadol. *Sens Actuators B* 2017;238:651-9.
- [581] Nezhadali A, Mojarrab M. Computational study and multivariate optimization of hydrochlorothiazide analysis using molecularly imprinted polymer electrochemical sensor based on carbon nanotube/polypyrrole film. *Sens Actuators B* 2014;190:829-37.
- [582] Pan P, Miao Z, Yanhua L, Linan Z, Haiyan R, Pan K, Linpei P. Preparation and evaluation of a stable solid state ion selective electrode of polypyrrole/electrochemically reduced graphene/glassy carbon substrate for soil nitrate sensing. *Int J Electrochem Sci* 2016;11:4779-93.
- [583] Tan F, Cong L, Li X, Zhao Q, Zhao H, Quan X, Chen J. An electrochemical sensor based on molecularly imprinted polypyrrole/graphene quantum dots composite for detection of bisphenol A in water samples. *Sens Actuators B* 2016;233:599-606.
- [584] Usha SP, Shrivastav AM, Gupta BD. A contemporary approach for design and characterization of fiber-optic-cortisol sensor tailoring LMR and zno/PPY molecularly imprinted film. *Biosens Bioelectron* 2017;87:178-86.
- [585] Zhang C, Bai W, Yang Z. A novel photoelectrochemical sensor for bilirubin based on porous transparent tio<sub>2</sub> and molecularly imprinted polypyrrole. *Electrochim Acta* 2016;187:451-6.
- [586] Dai Y, Li X, Lu X, Kan X. Voltammetric determination of paracetamol using a glassy carbon electrode modified with Prussian Blue and a molecularly imprinted polymer, and ratiometric read-out of two signals. *Microchim Acta* 2016;183:2771-8.
- [587] Yang Z, Liu X, Wu Y, Zhang C. Modification of carbon aerogel electrode with molecularly imprinted polypyrrole for electrochemical determination of dopamine. *Sens Actuators B* 2015;212:457-63.
- [588] Koirala K, Sevilla FB, Santos JH. Biomimetic potentiometric sensor for chlorogenic acid based on electrosynthesized polypyrrole. *Sens Actuators B* 2016;222:391-6.
- [589] Komarova E, Aldissi M, Bogomolova A. Design of molecularly imprinted conducting polymer protein-sensing films via substrate-dopant binding. *Analyst* 2015;140:1099-106.
- [590] Ktari N, Fourati N, Zerrouki C, Ruan M, Seydou M, Barbaut F, Nal F, Yaakoubi N, Chehimi MM, Kalfat R. Design of a polypyrrole MIP-SAW sensor for selective detection of flumequine in aqueous media. Correlation between experimental results and DFT calculations. *RSC Adv* 2015;5:88666-74.
- [591] Yang HH, Zhang SQ, Tan F, Zhuang ZX, Wang XR. Surface molecularly imprinted nanowires for biorecognition. *J Am Chem Soc* 2005;127:1378-9.
- [592] Huang JY, Wei ZX, Chen JC. Molecular imprinted polypyrrole nanowires for chiral amino acid recognition. *Sens Actuators B* 2008;134:573-8.

- [593] Paik P, Gedanken A, Mastai Y. Chiral-mesoporous-polypyrrole nanoparticles: Its chiral recognition abilities and use in enantioselective separation. *J Mater Chem* 2010;20:4085-93.
- [594] Yang L, Yang J, Xu B, Zhao F, Zeng B. Facile preparation of molecularly imprinted polypyrrole-graphene-multiwalled carbon nanotubes composite film modified electrode for rutin sensing. *Talanta* 2016;161:413-8.
- [595] Kong LJ, Pan MF, Fang GZ, He XL, Xia YQ, Wang S. Electrochemical sensor based on a bilayer of PPY–MWCNTs–BiCoPc composite and molecularly imprinted P o AP for sensitive recognition and determination of metolcarb. *RSC Adv* 2015;5:11498-505.
- [596] Xing XR, Liu S, Yu JH, Lian WJ, Huang JD. Electrochemical sensor based on molecularly imprinted film at polypyrrole-sulfonated graphene/hyaluronic acid-multiwalled carbon nanotubes modified electrode for determination of tryptamine. *Biosens Bioelectron* 2012;31:277-83.
- [597] Wang F, Zhu L, Zhang J. Electrochemical sensor for levofloxacin based on molecularly imprinted polypyrrole-graphene-gold nanoparticles modified electrode. *Sens Actuators B* 2014;192:642-7
- [598] Yang Y, Fang G, Wang X, Pan M, Qian H, Liu H, Wang S. Sensitive and selective electrochemical determination of quinoxaline-2-carboxylic acid based on bilayer of novel poly(pyrrole) functional composite using one-step electro-polymerization and molecularly imprinted poly(o-phenylenediamine). *Anal Chim Acta* 2014;806:136-43
- [599] Sun G, Wang P, Ge L, Yu J, Ge S, Yan M. Photoelectrochemical sensor for pentachlorophenol on microfluidic paper-based analytical device based on the molecular imprinting technique. *Biosens Bioelectron* 2014;56:97-103
- [600] Lakshmi D, Bossi A, Whitcombe MJ, Chianella I, Fowler SA, Subrahmanyam S, Piletska EV, Piletsky SA. Electrochemical sensor for catechol and dopamine based on a catalytic molecularly imprinted polymer-conducting polymer hybrid recognition element. *Anal Chem* 2009;81:3576-84.
- [601] Lakshmi D, Whitcombe MJ, Davis F, Chianella I, Piletska EV, Guerreiro A, Subrahmanyam S, Brito PS, Fowler SA, Piletsky SA. Chimeric polymers formed from a monomer capable of free radical, oxidative and electrochemical polymerization. *Chem Commun* 2009;2759-61.
- [602] Berti F, Todros S, Lakshmi D, Whitcombe MJ, Chianella I, Ferroni M, Piletsky SA, Turner APF, Marrazza G. Quasi-monodimensional polyaniline nanostructures for enhanced molecularly imprinted polymer-based sensing. *Biosens Bioelectron* 2010;26:497-503.
- [603] Lakshmi D, Akbulut M, Ivanova-Mitseva PK, Whitcombe MJ, Piletska EV, Karim K, Güven O, Piletsky SA. Computational design and preparation of mips for atrazine recognition on a conjugated polymer-coated microtiter plate. *Ind Eng Chem Res* 2013;52:13910-6.
- [604] Des Azevedo S, Lakshmi D, Chianella I, Whitcombe MJ, Karim K, Ivanova-Mitseva PK, Subrahmanyam S, Piletsky SA. Molecularly imprinted polymer-hybrid electrochemical sensor for the detection of  $\beta$ -estradiol. *Ind Eng Chem Res* 2013;52:13917-23.

- [605] Gu L, Jiang XY, Liang Y, Zhou TS, Shi GY. Double recognition of dopamine based on a boronic acid functionalized poly(aniline-co-anthranilic acid)-molecularly imprinted polymer composite. *Analyst* 2013;138:5461-9.
- [606] Lee MH, O'Hare D, Guo HZ, Yang CH, Lin HY. Electrochemical sensing of urinary progesterone with molecularly imprinted poly(aniline-co-metanilic acid)s. *J Mater Chem B* 2016;4:3782-7.
- [607] Ma X, Liu J, Wu D, Wang L, Zhang Z, Xiang S. Ultrasensitive sensing of tris (2, 3-dibromopropyl) isocyanurate based on the synergistic effect of amino and hydroxyl groups of a molecularly imprinted poly (o-aminophenol) film. *New J Chem* 2016;40:1649-54.
- [608] Frasconi M, Tel-Vered R, Riskin M, Willner I. Surface plasmon resonance analysis of antibiotics using imprinted boronic acid-functionalized Au nanoparticle composites. *Anal Chem* 2010;82:2512-9.
- [609] Bi X, Liu Z. Facile preparation of glycoprotein-imprinted 96-well microplates for enzyme-linked immunosorbent assay by boronate affinity-based oriented surface imprinting. *Anal Chem* 2014;86:959-66
- [610] Roy AK, Nisha V, Dhand C, Malhotra BD. Molecularly imprinted polyaniline film for ascorbic acid detection. *J Mol Recognit* 2011;24:700-6.
- [611] Güven O. Radiation-induced conductivity control in polyaniline blends/composites. *Radiat Phys Chem* 2007;76:1302-7.
- [612] Roy AC, Nisha VS, Dhand C, Ali MA, Malhotra BD. Molecularly imprinted polyaniline-polyvinylsulfonic acid composite based sensor for para-nitrophenol detection. *Anal Chim Acta* 2013;777:63-71.
- [613] Rao H, Chen M, Ge H, Lu Z, Liu X, Zou P, Wang X, He H, Zeng X, Wang Y. A novel electrochemical sensor based on Au@PANI composites film modified glassy carbon electrode binding molecular imprinting technique for the determination of melamine. *Biosens Bioelectron* 2017;87:1029-35.
- [614] Rao H, Lu Z, Ge H, Liu X, Chen B, Zou P, Wang X, He H, Zeng X, Wang Y. Electrochemical creatinine sensor based on a glassy carbon electrode modified with a molecularly imprinted polymer and a Ni@polyaniline nanocomposite. *Microchim Acta* 2017;184:261-9.
- [615] Shi L, Hou AG, Chen LY, Wang ZF. Electrochemical sensor prepared from molecularly imprinted polymer for recognition of TNT. *Polym Composite* 2015;36:1280-5.
- [616] Shrivastav AM, Usha SP, Gupta BD. A localized and propagating SPR, and molecular imprinting based fiber-optic ascorbic acid sensor using an in situ polymerized polyaniline-Ag nanocomposite. *Nanotechnology* 2016;27:345501/1-16.
- [617] Luo J, Sun J, Huang J, Liu X. Preparation of water-compatible molecular imprinted conductive polyaniline nanoparticles using polymeric micelle as nanoreactor for enhanced paracetamol

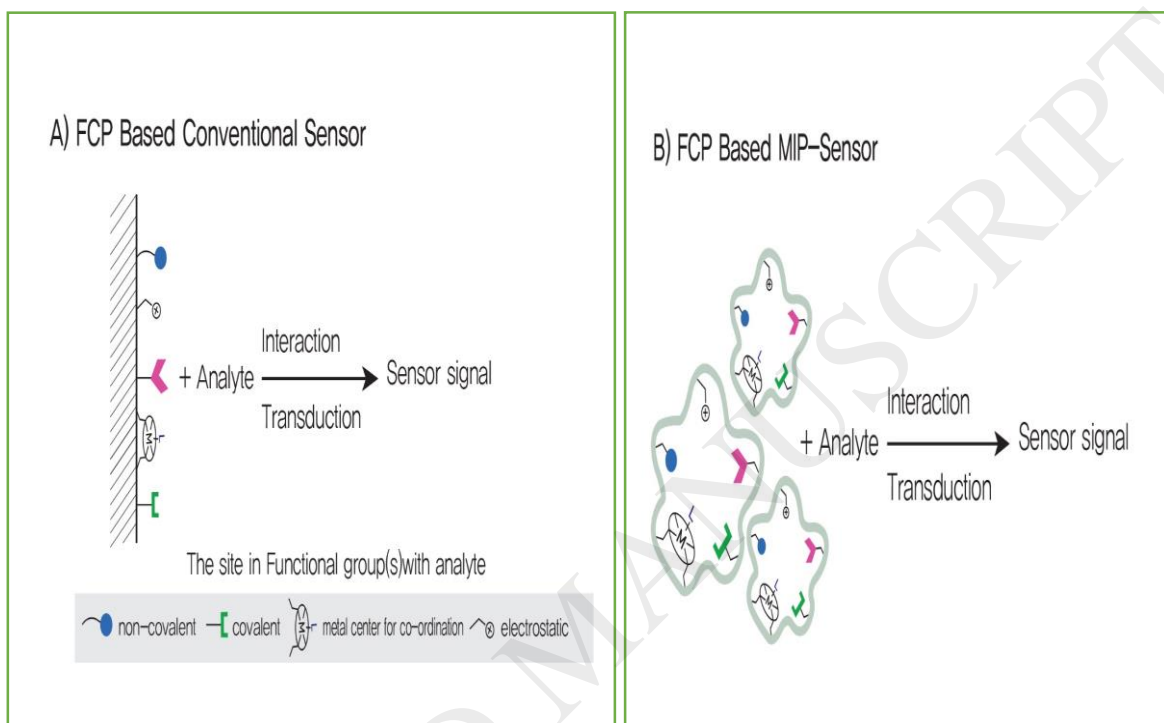
- detection. *Chem Eng J* 2016;283:1118-26.
- [618] Zhu W, Xu L, Zhu C, Li B, Xiao H, Jiang H, Zhou X. Magnetically controlled electrochemical sensing membrane based on multifunctional molecularly imprinted polymers for detection of insulin. *Electrochim Acta* 2016;218:91-100.
- [619] Zhu W, Jiang G, Xu L, Li B, Cai Q, Jiang H, Zhou X. Facile and controllable one-step fabrication of molecularly imprinted polymer membrane by magnetic field directed self-assembly for electrochemical sensing of glutathione. *Anal Chim Acta* 2015;886:37-47.
- [620] Pandey I, Jha SS. Molecularly imprinted polyaniline-ferrocene-sulfonic acid-Carbon dots modified pencil graphite electrodes for chiral selective sensing of D-Ascorbic acid and L-Ascorbic acid: A clinical biomarker for preeclampsia. *Electrochim Acta* 2015;182:917-28.
- [621] Li Y, Bin Q, Lin Z, Chen Y, Yang H, Cai Z, Chen G. Synthesis and characterization of vinyl-functionalized magnetic nanofibers for protein imprinting. *Chem Commun* 2015;51:202-5
- [622] Cowen T, Karim K, Piletsky S. Computational approaches in the design of synthetic receptors—A review. *Anal Chim Acta* 2016;936:62-74.
- [623] Tiu BD, Krupadam RJ, Advincula RC. Pyrene-imprinted polythiophene sensors for detection of polycyclic aromatic hydrocarbons. *Sensors Act B: Chem* 2016;228:693-701.
- [624] Huynh TP, Sharma PS, Sosnowska M, D'Souza F, Kutner W. Functionalized polythiophenes: Recognition materials for chemosensors and biosensors of superior sensitivity, selectivity, and detectability. *Prog Polym Sci* 2015;47:1-25.
- [625] Singh AK, Singh M. QCM sensing of melphalan via electropolymerized molecularly imprinted polythiophene films. *Biosens Bioelectron* 2015;74:711-7.
- [626] Lattach Y, Fourati N, Zerrouki C, Fournion JM, Garnier F, Pernelle C, Remita S. Molecularly imprinted surface acoustic wave sensors: The synergy of electrochemical and gravimetric transductions in chemical recognition. *Electrochim Acta* 2012;73:36-44
- [627] Pernites R, Ponnampati R, Felipe MJ, Advincula R. Electropolymerization molecularly imprinted polymer (E-MIP) SPR sensing of drug molecules: Pre-polymerization complexed terthiophene and carbazole electroactive monomers. *Biosens Bioelectron* 2011;26:2766-71.
- [628] Mehdinia A, Aziz-Zanjani MO, Ahmadifar M, Jabbari A. Design and synthesis of molecularly imprinted polypyrrole based on nanoreactor SBA-15 for recognition of ascorbic acid. *Biosens Bioelectron* 2013;39:88-93.
- [629] Huynh TP, Sosnowska M, Sobczak JW, Kc CB, Nesterov VN, D'Souza F, Kutner W. Simultaneous chronoamperometry and piezoelectric microgravimetry determination of nitroaromatic explosives using molecularly imprinted thiophene polymers. *Anal Chem* 2013;85:8361-8.
- [630] Chen PY, Vittal R, Nien PC, Liou GS, Ho KC. A novel molecularly imprinted polymer thin film as

biosensor for uric acid. *Talanta* 2010;80:1145-51.

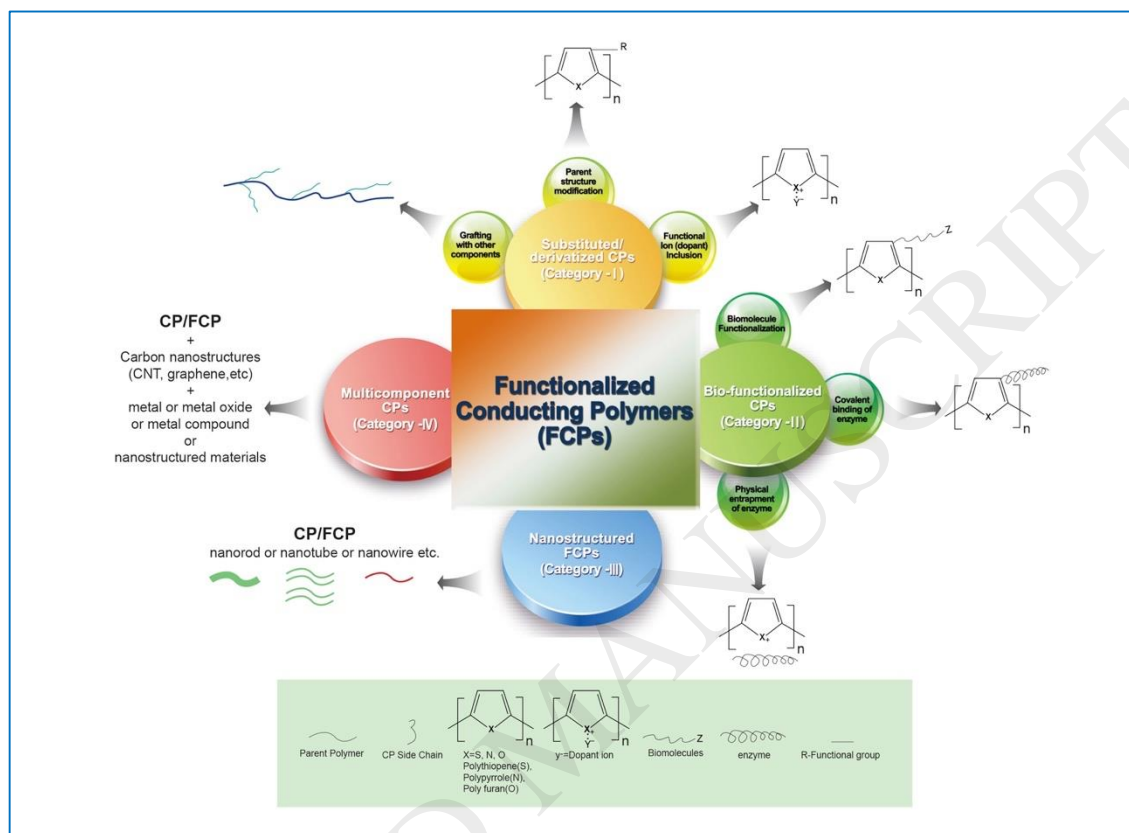
- [631] Chen Y, Chen L, Bi RL, Xu L, Liu Y. A potentiometric chiral sensor for L-Phenylalanine based on crosslinked polymethylacrylic acid-polycarbazole hybrid molecularly imprinted polymer. *Anal Chim Acta* 2012;754:83-90.
- [632] Zhou X, Wang A, Yu C, Wu S, Shen J. Facile synthesis of molecularly imprinted graphene quantum dots for the determination of dopamine with affinity-adjustable. *ACS Appl Mater Interfaces* 2015;7:11741-7.

ACCEPTED MANUSCRIPT

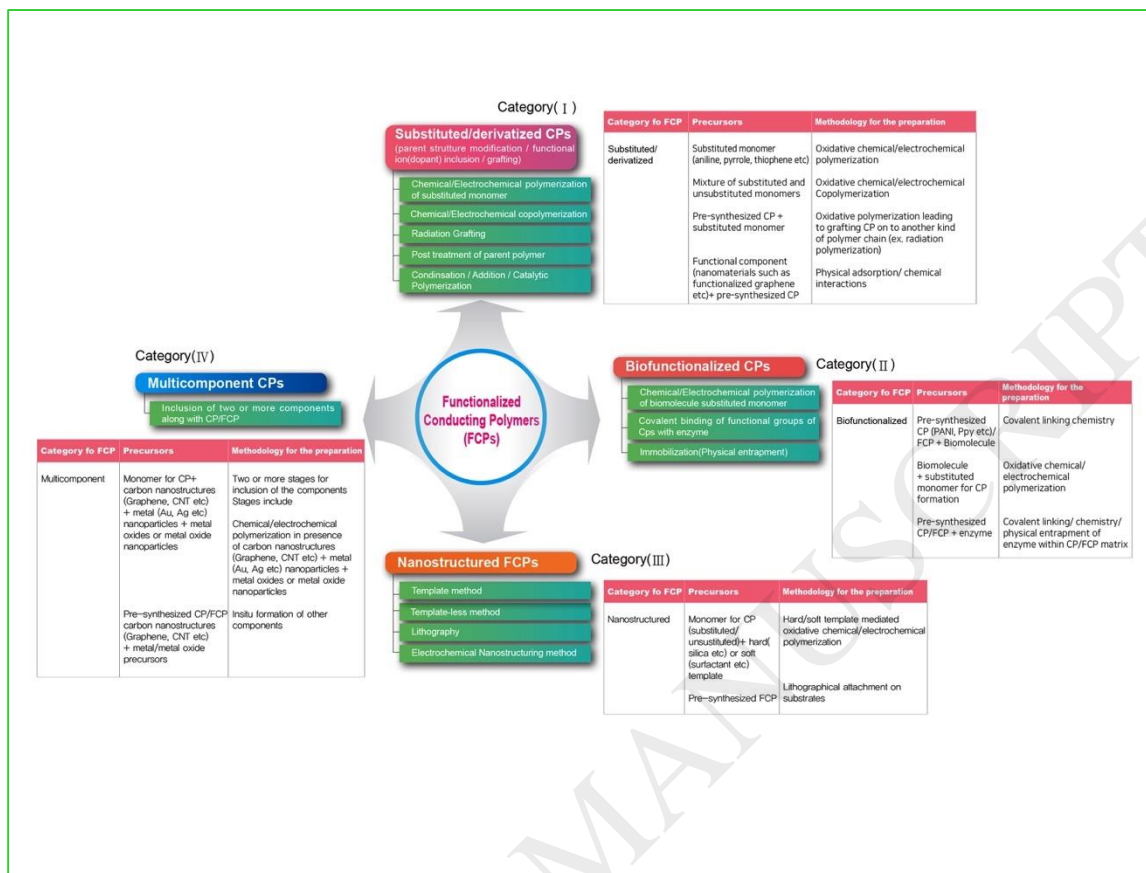
## Schemes and Figures



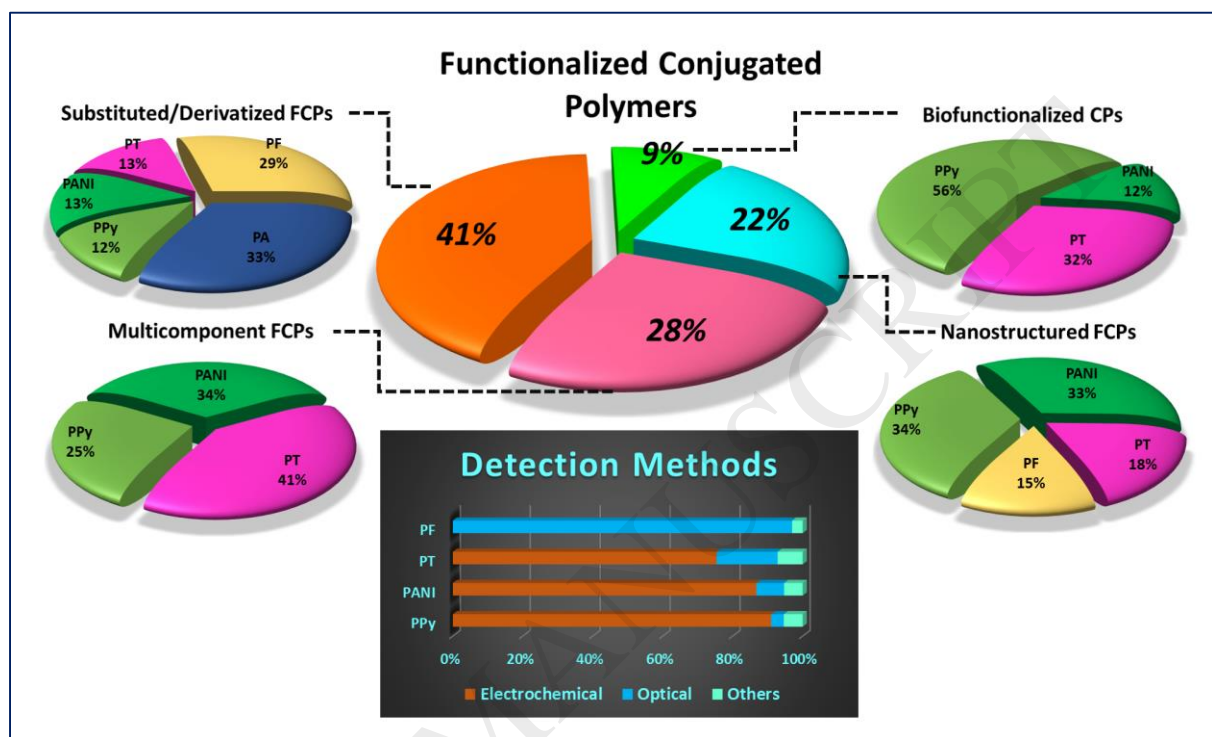
**Scheme 1. Basic operational principles detailing the interactions between sensor matrix and the analyte for the (A) FCP based conventional and (B) MIP sensors.**



**Scheme 2. Categories of FCPs with selected parent structures and functionalization routes.**



**Scheme 3. General strategies for the preparation of FCPs and brief details (associated tables).**



**Scheme 4. Comprehensive details of FCP based sensors for different categories and signal transduction modes.**

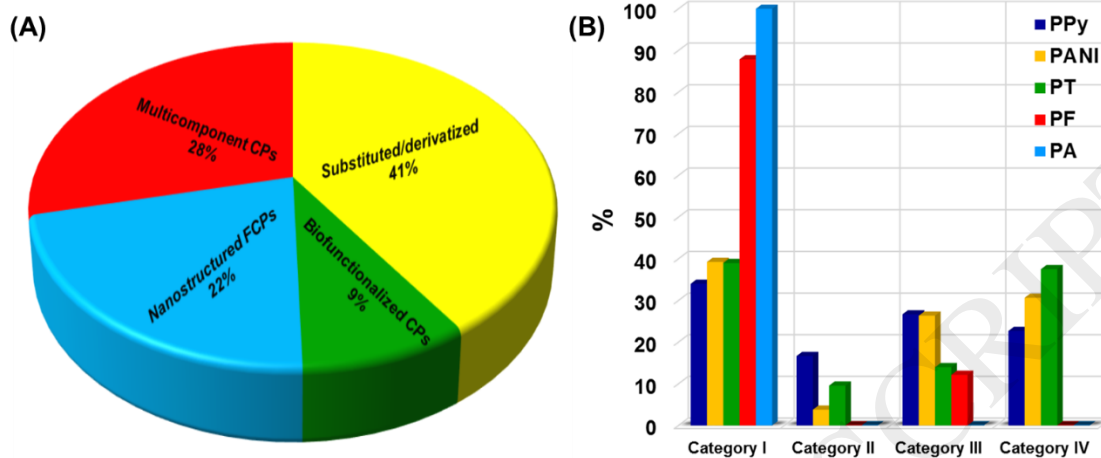


**Fig. 1.** (A) Pie chart showing the distribution of publications among the four categories of FCPs; (B) The bar chart showing the distribution of publications based on PPy, PANI, PT, PF and PA

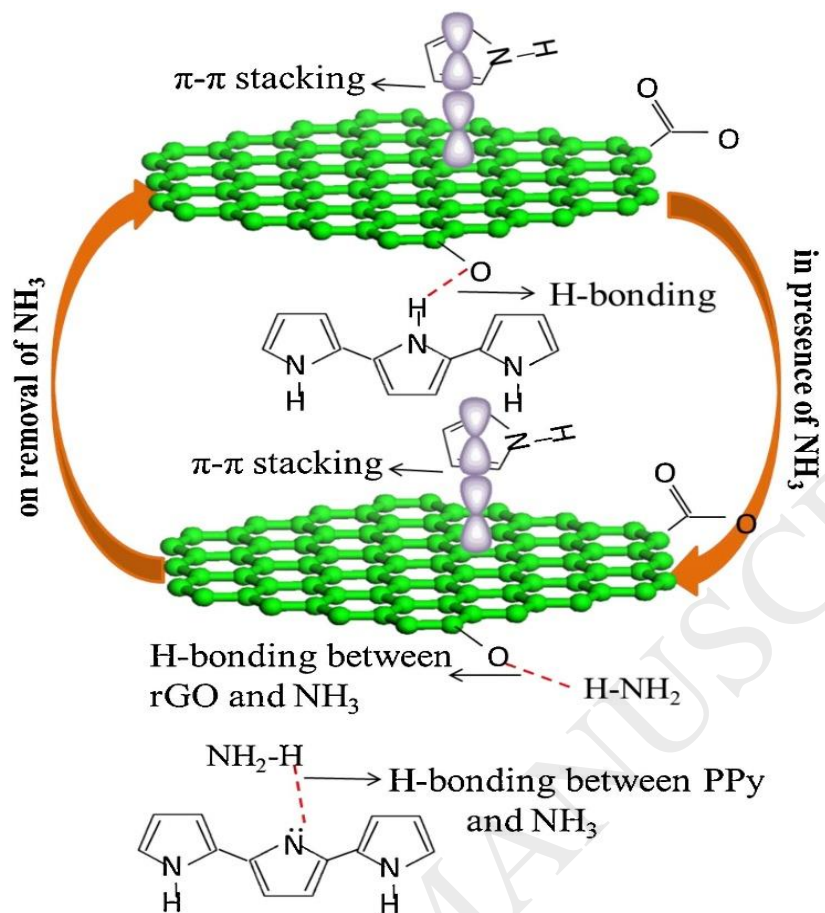


**Fig. 2.** Schematic presentation depicting interaction of  $\text{NH}_3$  with PPy/rGO hybrid. [88], Copyright 2017 (Reprinted with permission from Elsevier Ltd.).

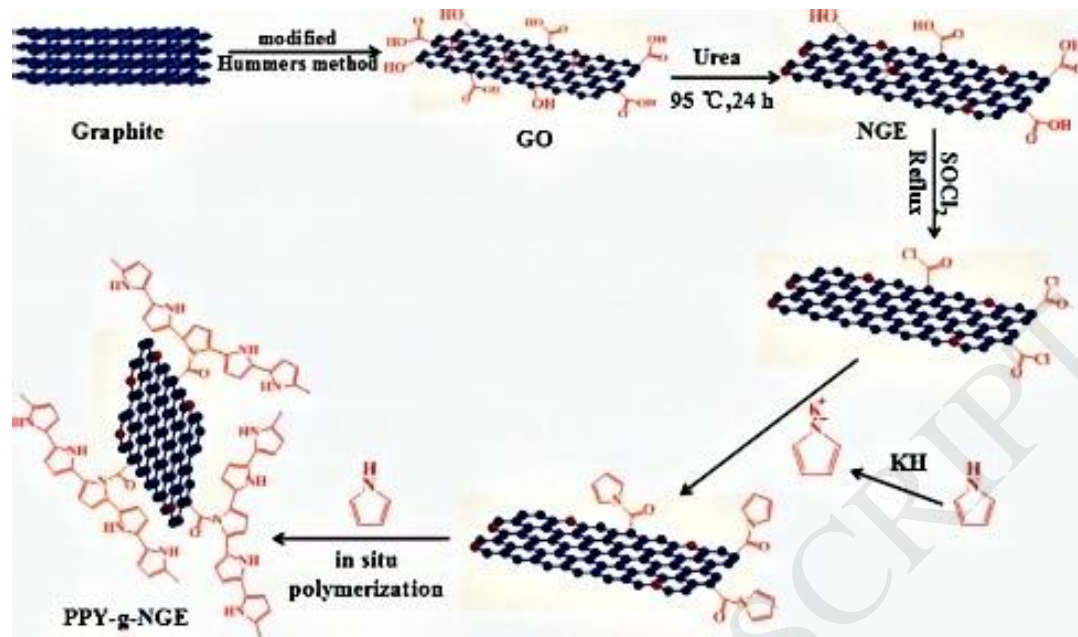


**Fig. 3.** The proposed formation scheme of PPY-g-NGE composite. The red dots in the structure stand for the nitrogen atoms doped in graphene. [108], Copyright 2015 (Reprinted with permission from Elsevier Ltd.).

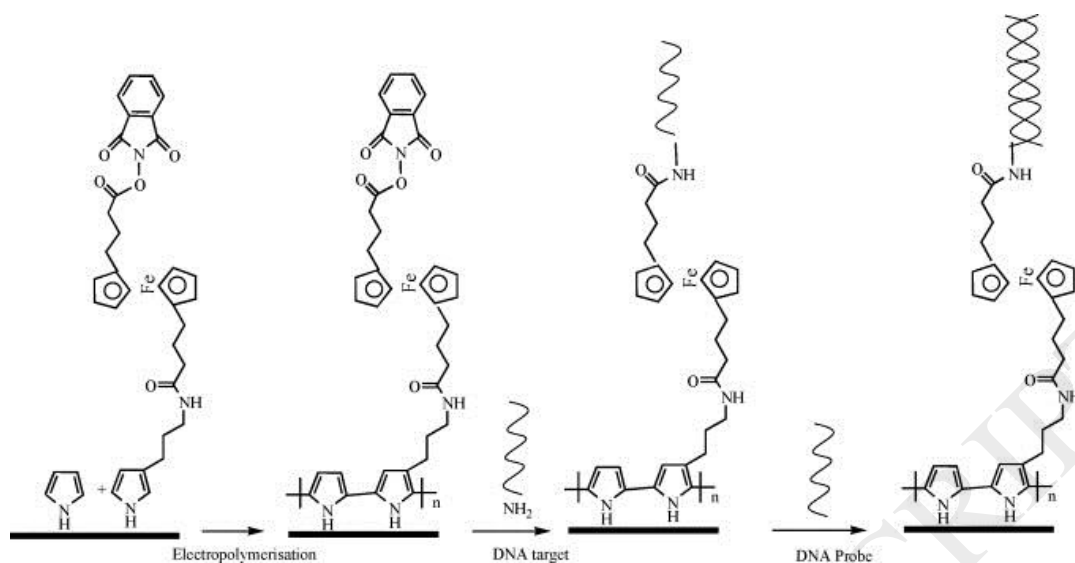


**Fig. 4.** Synthetic strategy for the construction of the biosensors by electrochemical copolymerization reaction followed by covalent attachment of DNA probe and hybridization of the DNA target. [119], Copyright 2011 (Reprinted with permission from Elsevier Ltd.).

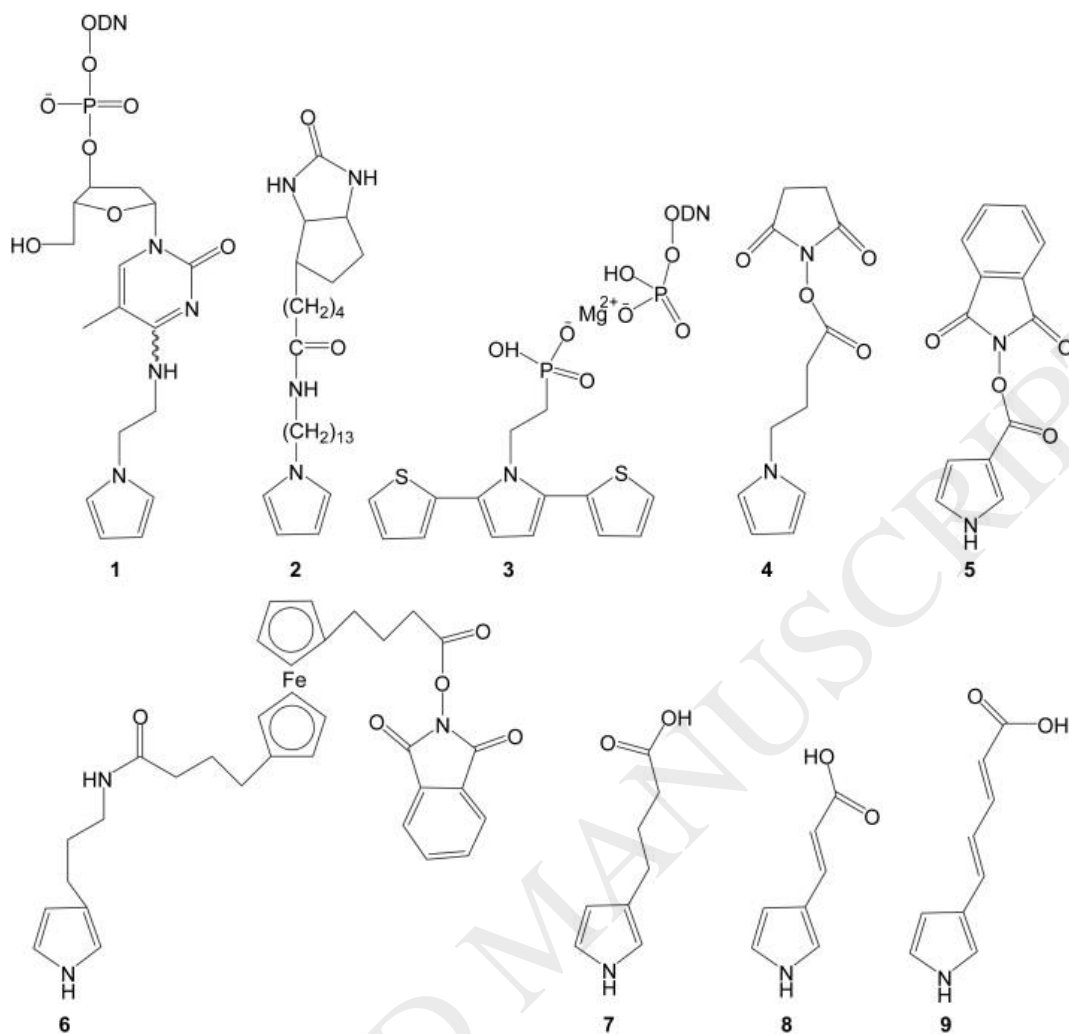


**Fig. 5.** Structures of functionalized pyrrole monomers for DNA sensors. [124], Copyright 2009 (Reprinted with permission from Elsevier Ltd.).

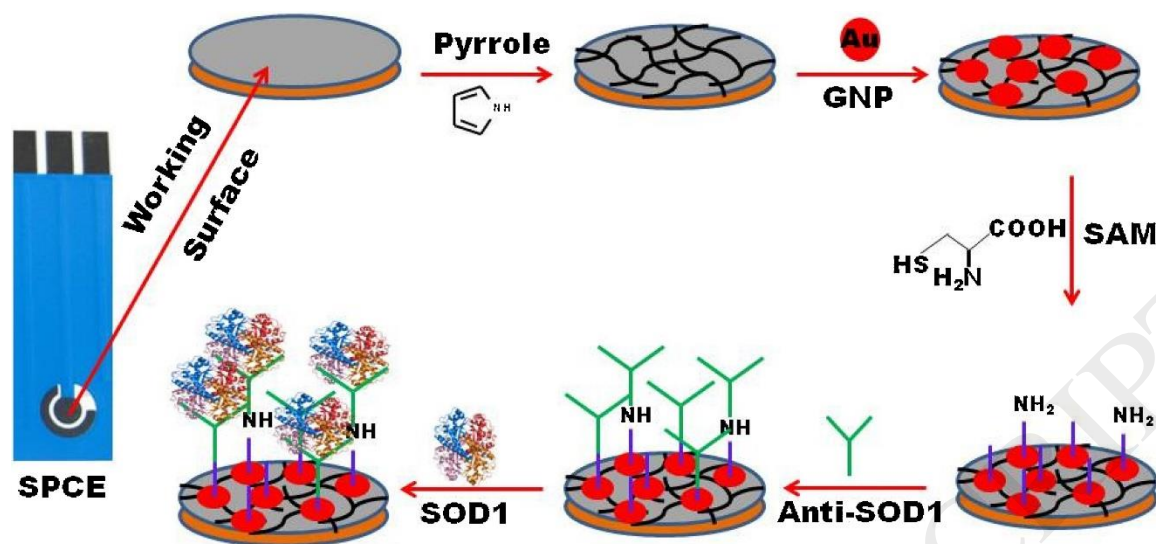


**Fig. 6.** Schematic representation of the label-free SOD1 immunosensor. [125], Copyright 2016 (Reprinted with permission from Elsevier Ltd.).

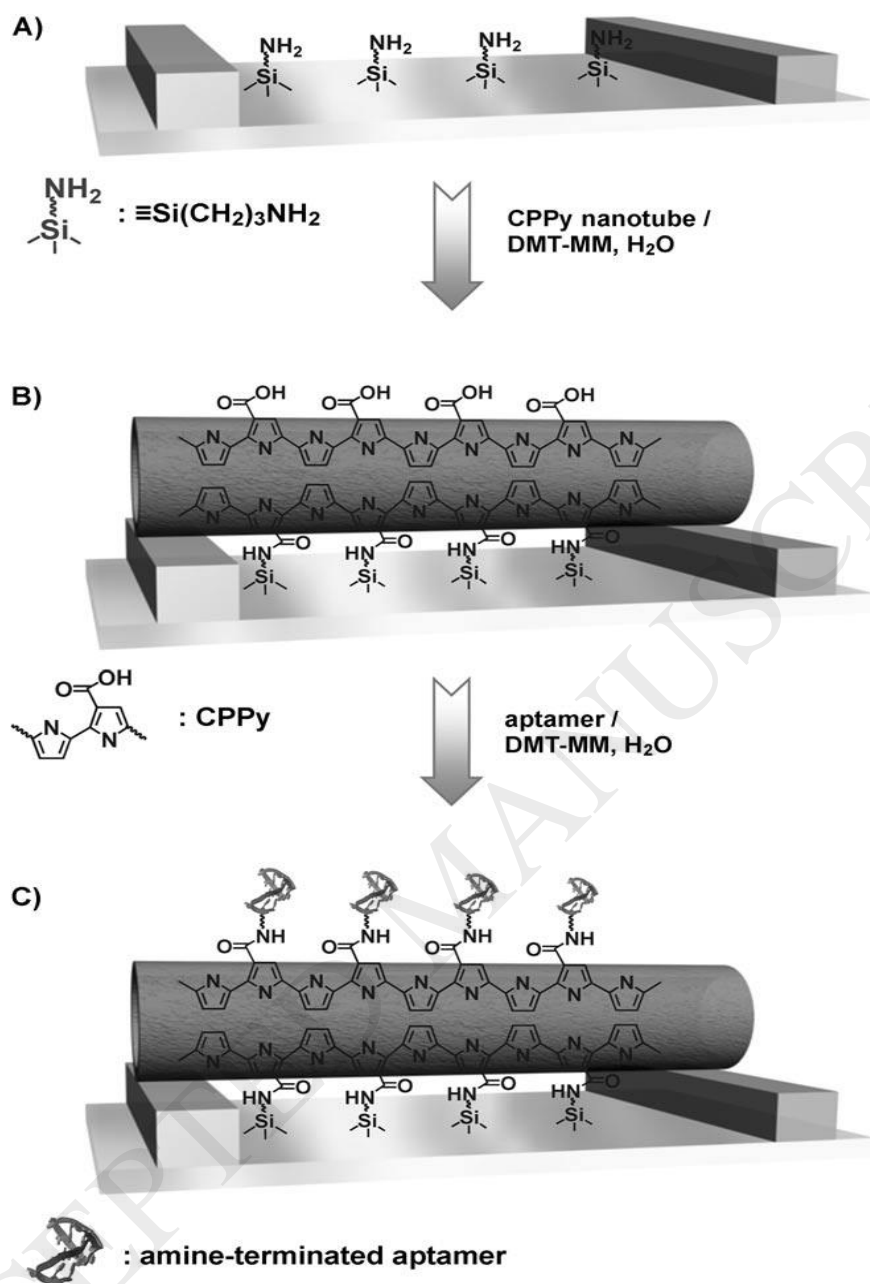


**Fig. 7.** Fabrication of PPy-COOH NTs as bioreceptors for detection of thrombin proteins. [138], Copyright 2008 (Reprinted with permission from Wiley-VCH publishers).

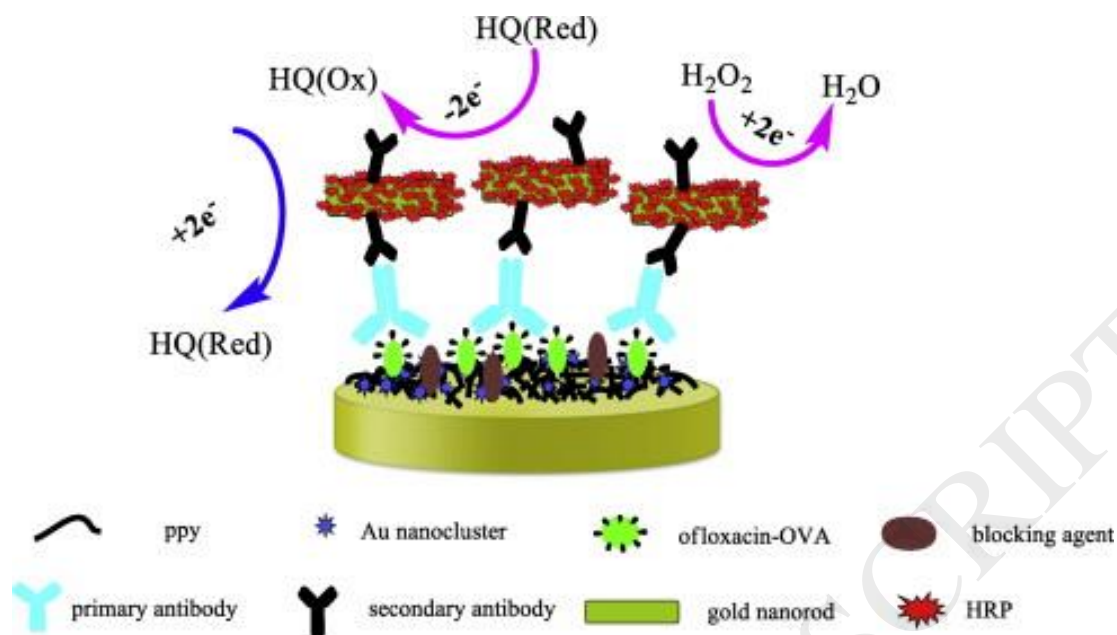


**Fig. 8.** Schematic representation of the OFL electrochemical immunosensor using Au nanoclusters/PPy/GCE as the substrate and multi-HRP-GNR-Ab<sub>2</sub> bioconjugates as the label with the aid of electron mediator (QH) and the addition of H<sub>2</sub>O<sub>2</sub>. [175], Copyright 2013 (Reprinted with permission from Elsevier Ltd.).

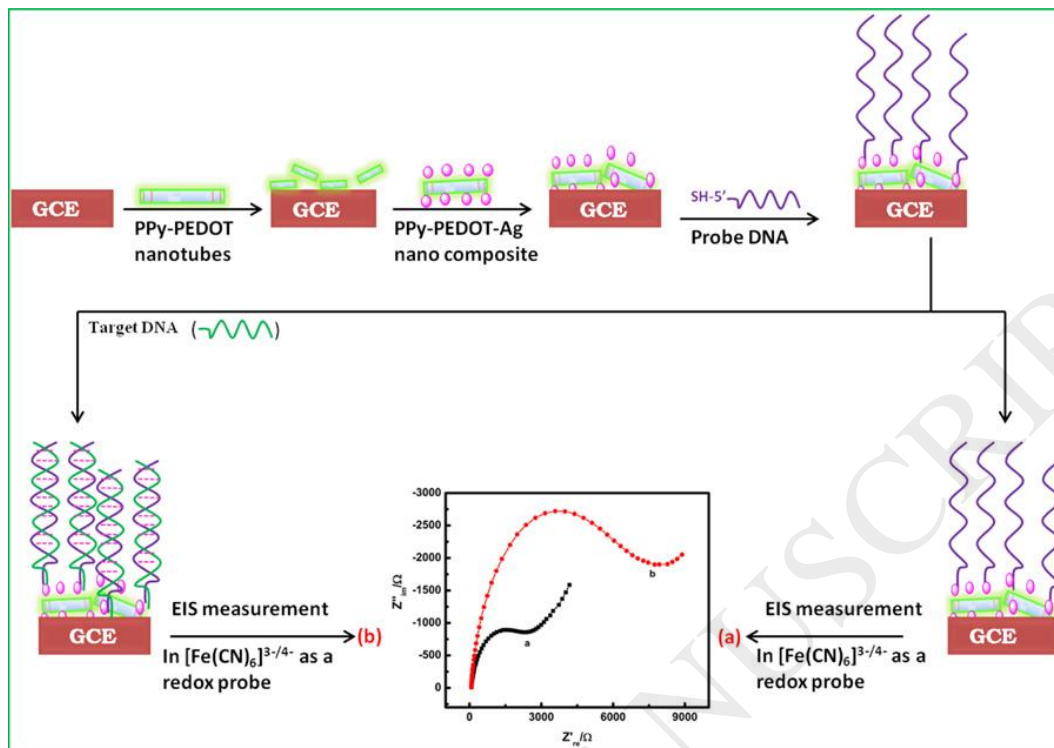


**Fig. 9.** Schematic illustration of the fabrication of PPy-PEDOT-Ag-S-ssDNA and the DNA hybridization sensing. [177], Copyright 2013 (Reprinted with permission from Elsevier Ltd.).

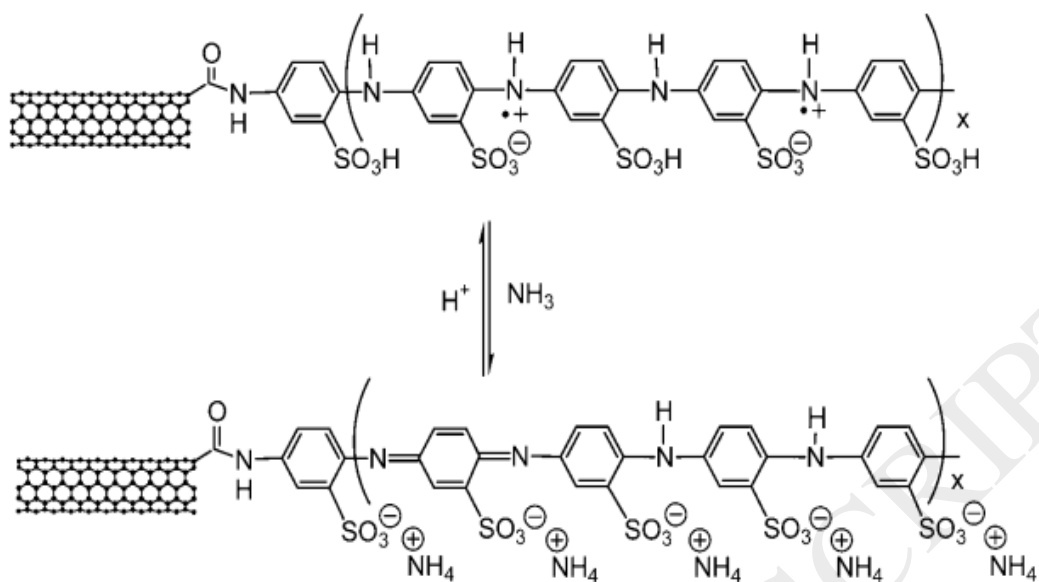


**Fig. 10.** Interaction of SWNT-PABS with  $\text{NH}_3$ . [221], Copyright 2004 (Reprinted with permission from the American Chemical Society).

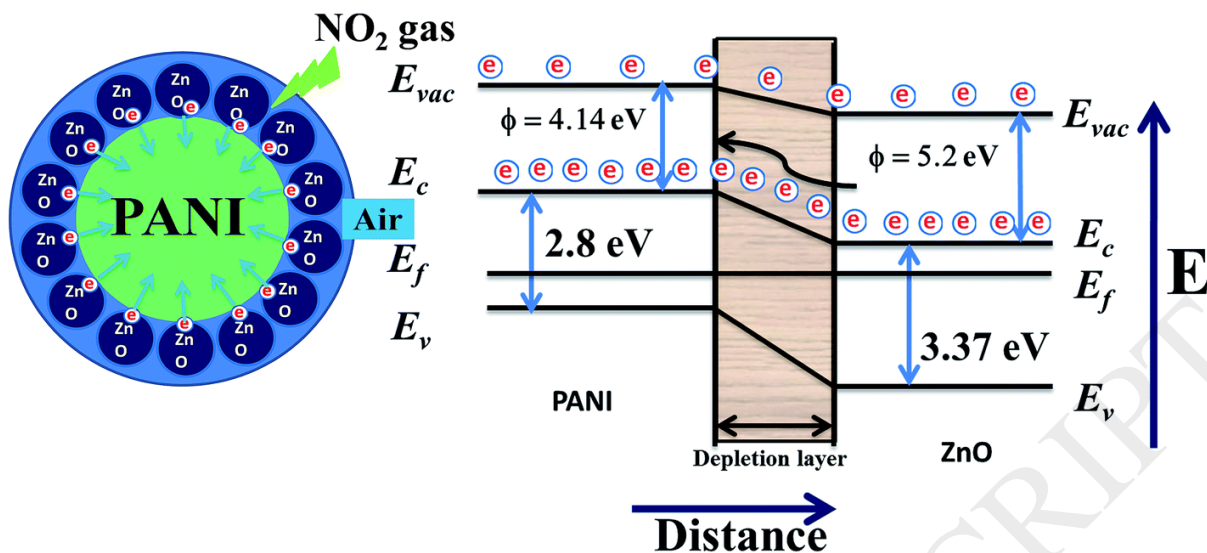


**Fig. 11.** Schematic diagram of the proposed mechanism of NO<sub>2</sub> sensing of ZnO/PANI heterojunctions. [238], Copyright 2016 (Reprinted with permission from the Royal Society of Chemistry).

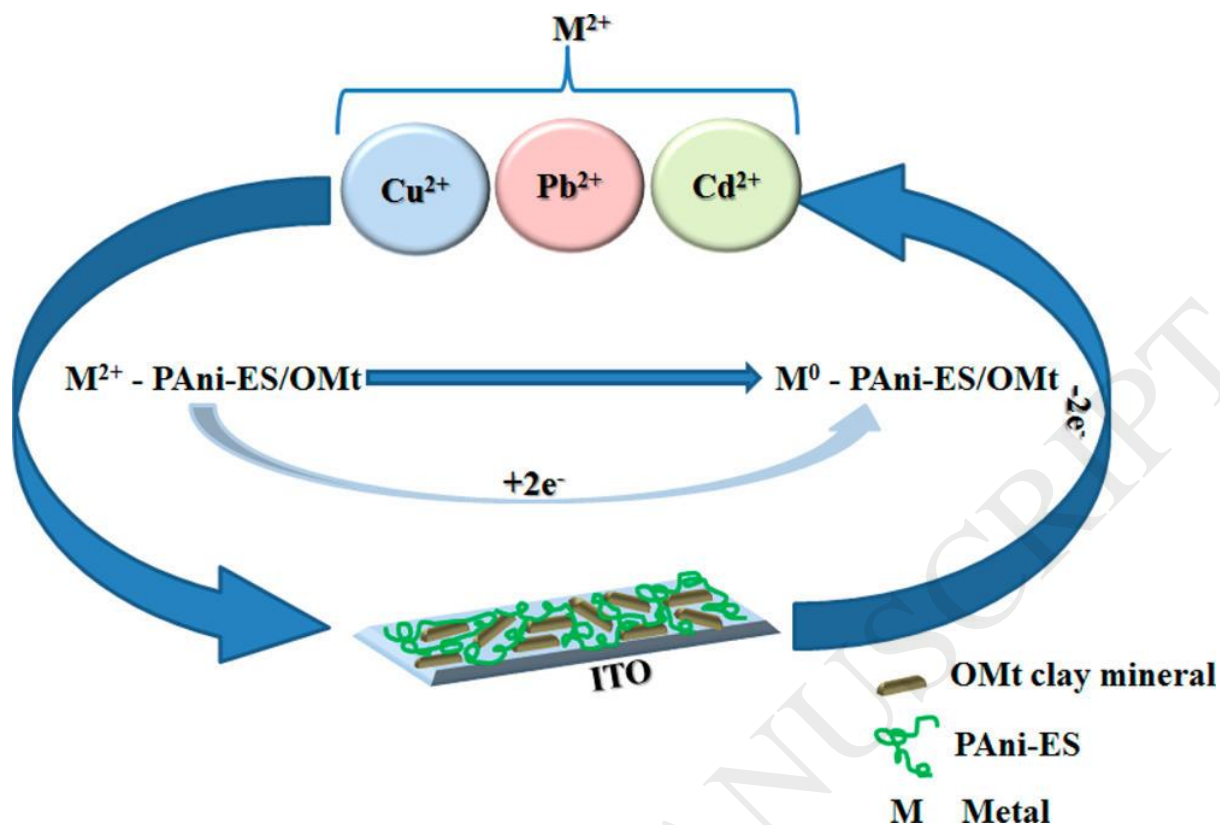


**Fig. 12.** Mechanism behind detection of metal ions with the LB films, for the case of the PANI-ES/OMt film. The HCl electrolyte solution should contain one of the three metal ions ( $\text{Cu}^{2+}$ ,  $\text{Pb}^{2+}$ , and  $\text{Cd}^{2+}$ ). [256], Copyright 2015 (Reprinted with permission from the American Chemical Society).

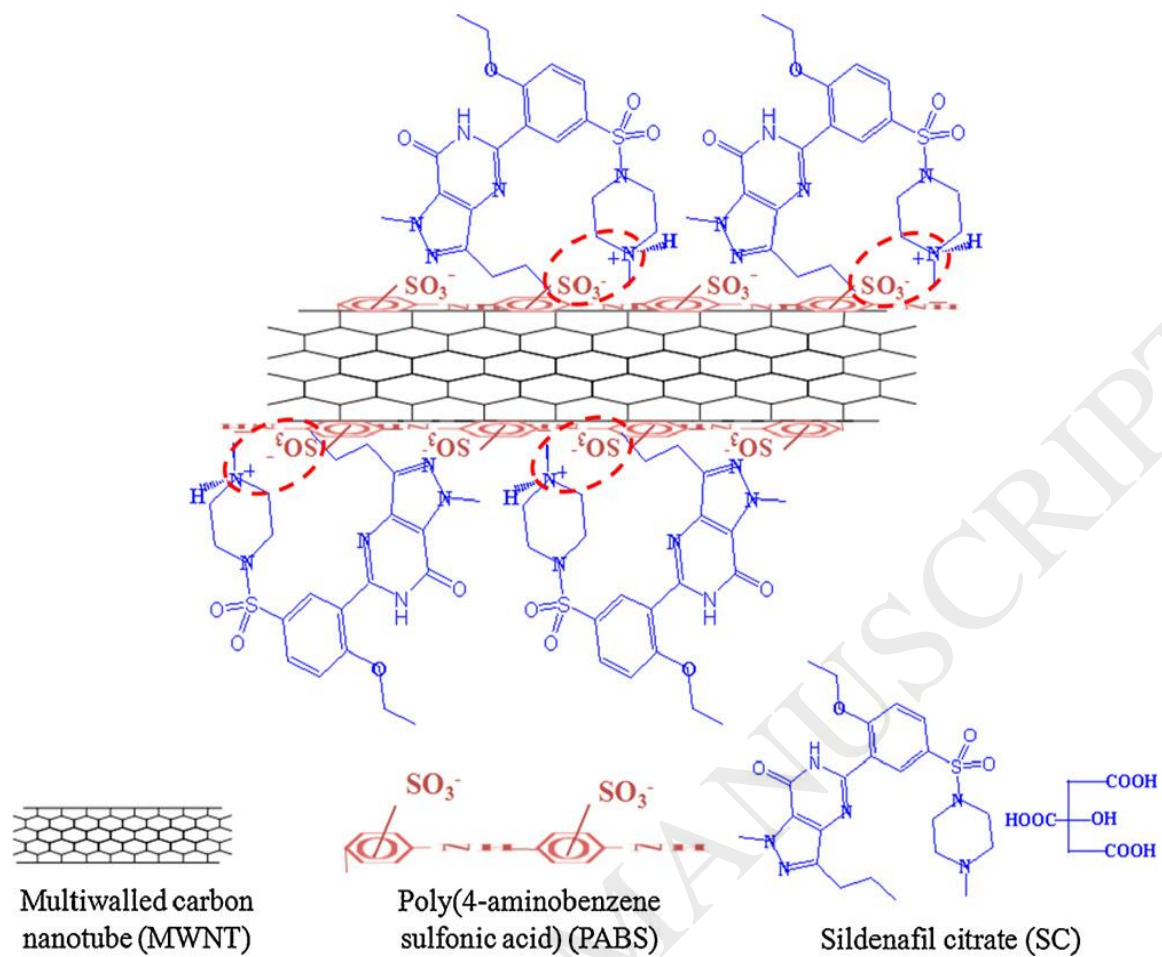


**Fig. 13.** Scheme showing Interactions of SC with MWNT-g-PABS. [264], Copyright 2011 (Reprinted with permission from Elsevier Ltd.).

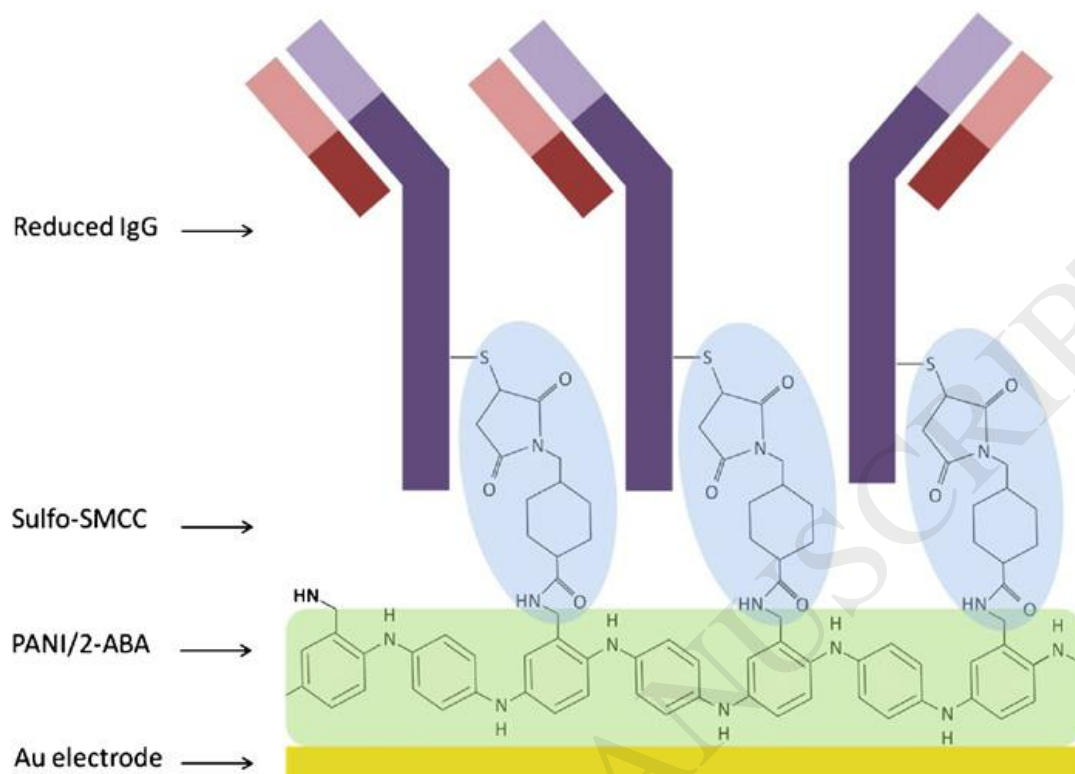


**Fig. 14.** Schematic representation of PANI/2-ABA/sulfo-SMCC/reduced IgG immunosensor. [269], Copyright 2012 (Reprinted with permission from Elsevier Ltd.).

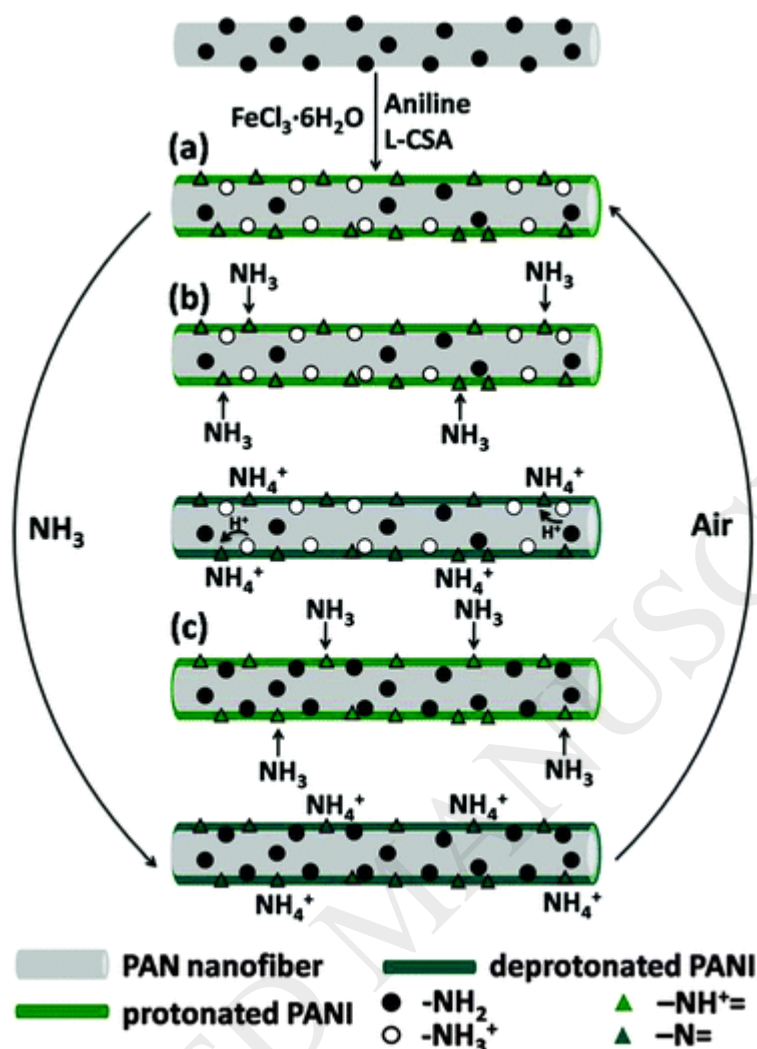


**Fig. 15.** Schematic model of the three steps for the sensitization mechanism of the prepared nanofiber sensor: (a) PANI was synthesized on the surface of PAN nanofibers, at the same time,  $-\text{NH}_2$  and  $-\text{N}=\text{}$  were converted into  $-\text{NH}_3^+$  and  $-\text{NH}^+=$ , respectively, because of L-CSA; (b)  $\text{NH}_3$  contacted with the surface of the NC fibers,  $\text{NH}_3$  reacted with  $-\text{NH}^+=$  to form  $-\text{N}=\text{}$ , then  $\text{H}^+$  of  $-\text{NH}_3^+$  transferred to  $-\text{N}=\text{}$ ; (c)  $\text{NH}_3$  reacted with the new formed  $-\text{NH}^+=$ . [276], Copyright 2016 (Reprinted with permission from the Royal Society of Chemistry).

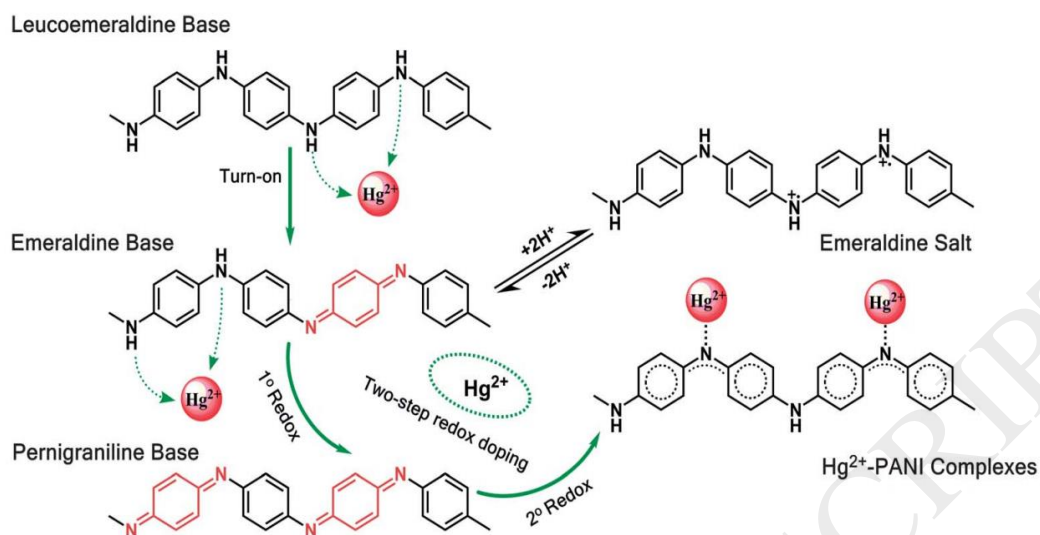


**Fig. 16.** Schematic illustration of the sensing mechanism of PANI-LB probes upon exposure to  $\text{Hg}^{2+}$  ions in aqueous solution. [293], Copyright 2014 (Reprinted with permission from the Royal Society of Chemistry).

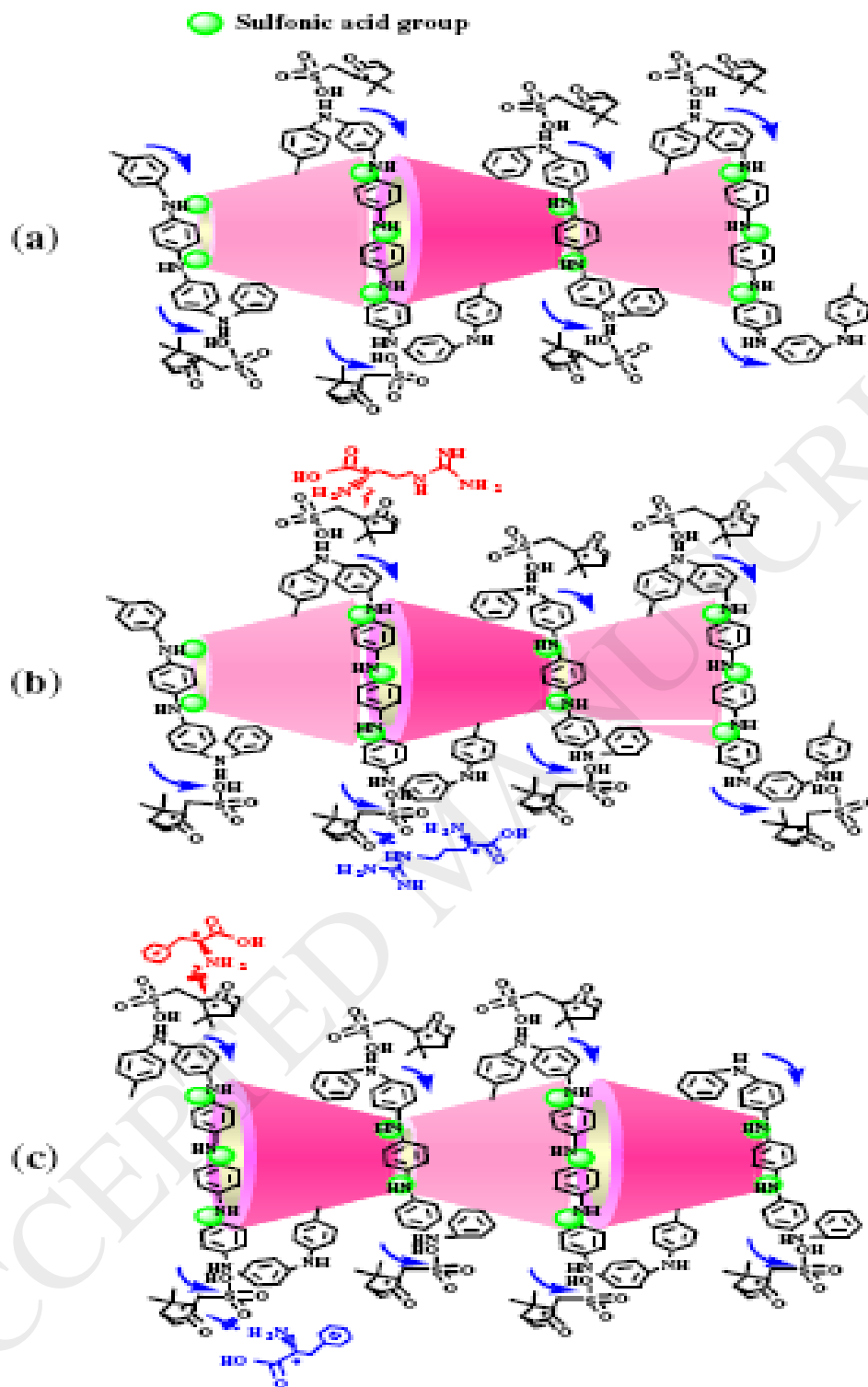


**Fig. 17.** (a) Probable structure of PANI chiral nanobundles (C-PANI-CDS-NB; intertwined helical polyaniline chains over the interconnected  $\beta$ -cyclodextrin sulfate (CDS) nanotubes), (b) chiral discrimination using C-PANI-CDS-NB for phenylalanine, (c) bulky phenyl group preventing enantiodiscrimination using C-PANI-CDS-NB. [299], Copyright 2006 (Reprinted with permission from IOP science publishers).

ACCEPTED MANUSCRIPT

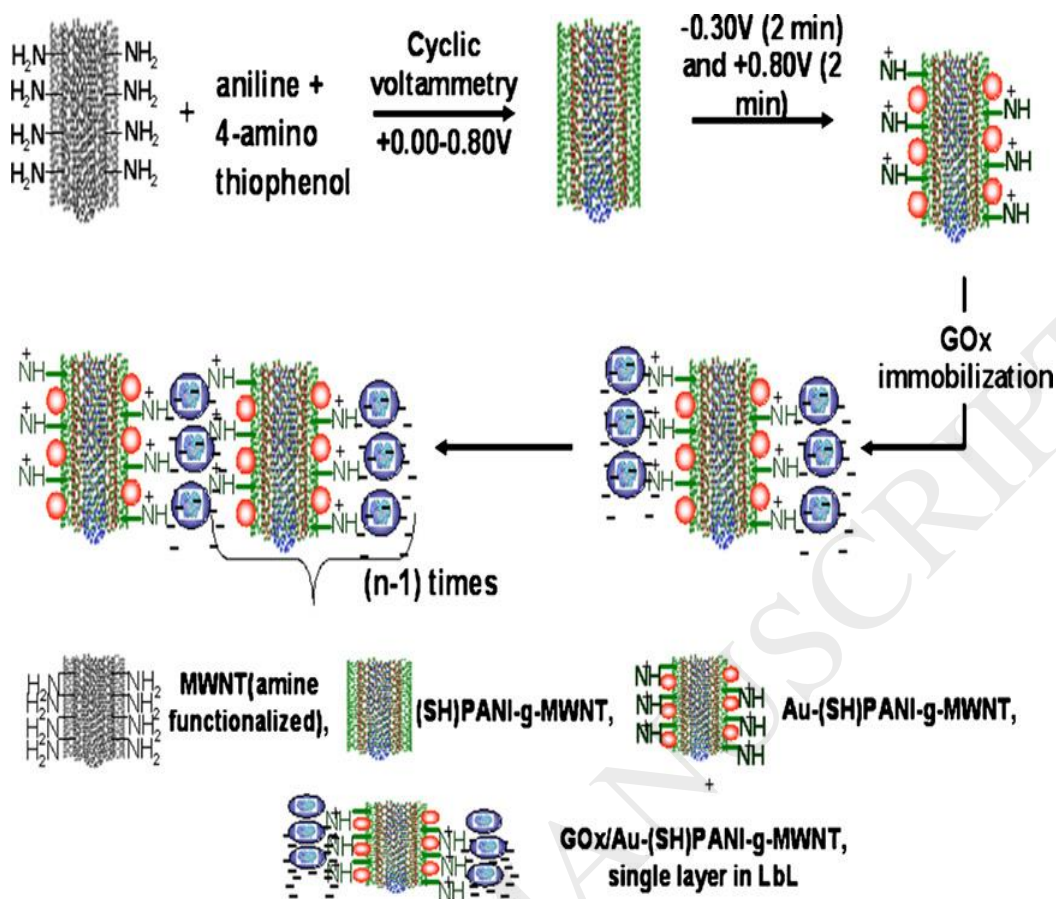


**Fig. 18.** Schematic showing the fabrication of LbL based biosensor comprising of multi-components, MWNT, PANI(SH), Au particles and GOx. [301], Copyright 2009 (Reprinted with permission from Elsevier Ltd.).

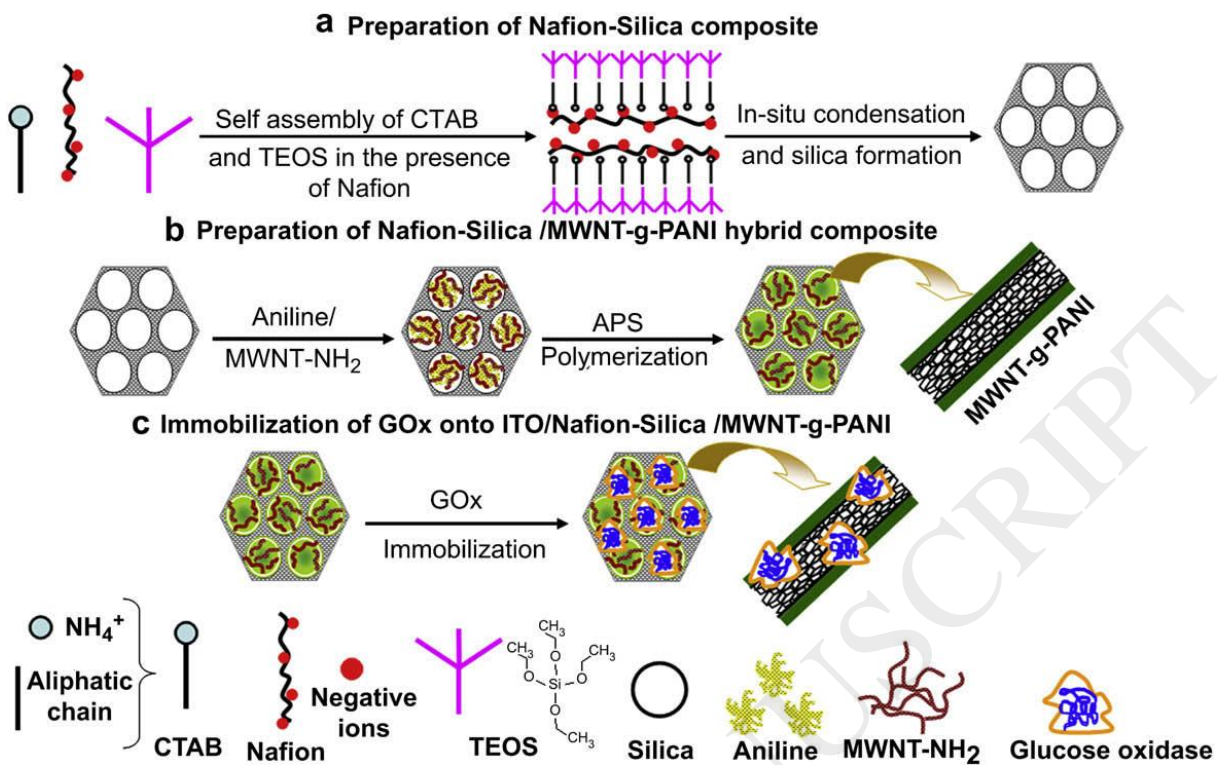


**Fig. 19.** Schematic showing the fabrication of Nafion-silica/MWNT-g-PANI/GOx biosensor. [303], Copyright 2009 (Reprinted with permission from Elsevier Ltd.).

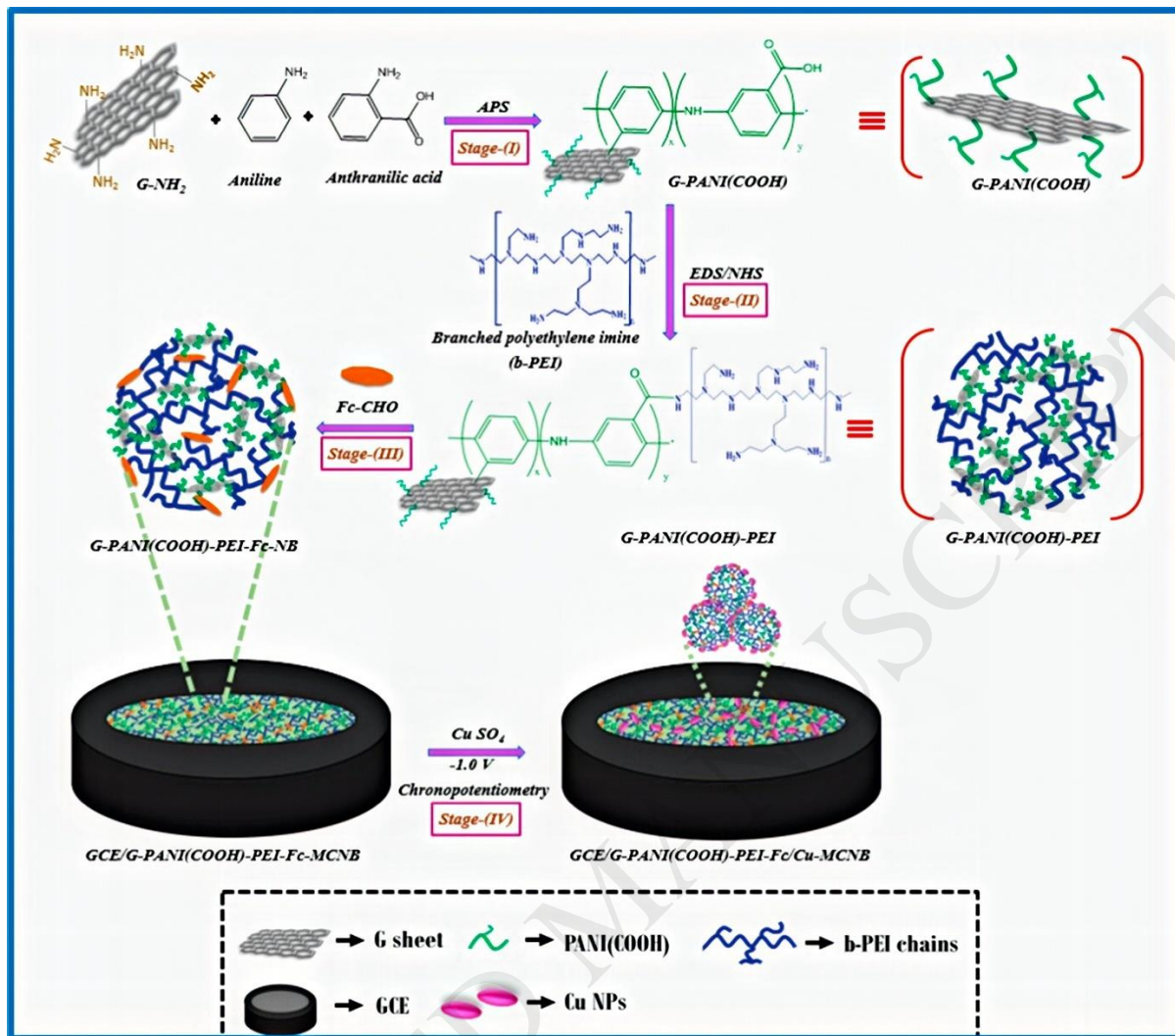


**Fig. 20.** Stages in the preparation of G-PANI(COOH)-PEI-Fc/Cu-MCNB/GCE based NEG sensor. Stage-(I); Grafting poly(aniline-co-anthranilic acid) chains onto G-NH<sub>2</sub> (G-PANI(COOH)); Stage-(II); Covalent linking of -COOH groups in G-PANI(COOH) with -NH<sub>2</sub> groups in b-PEI; Stage-(III); Network formation via cross-linking of G-PANI(COOH) with Fc-CHO and Stage-(IV) Electrodeposition of Cu NPs on to G-PANI(COOH)-PEI-Fc/GCE. [309], Copyright 2016 (Reprinted with permission from Elsevier Ltd.).

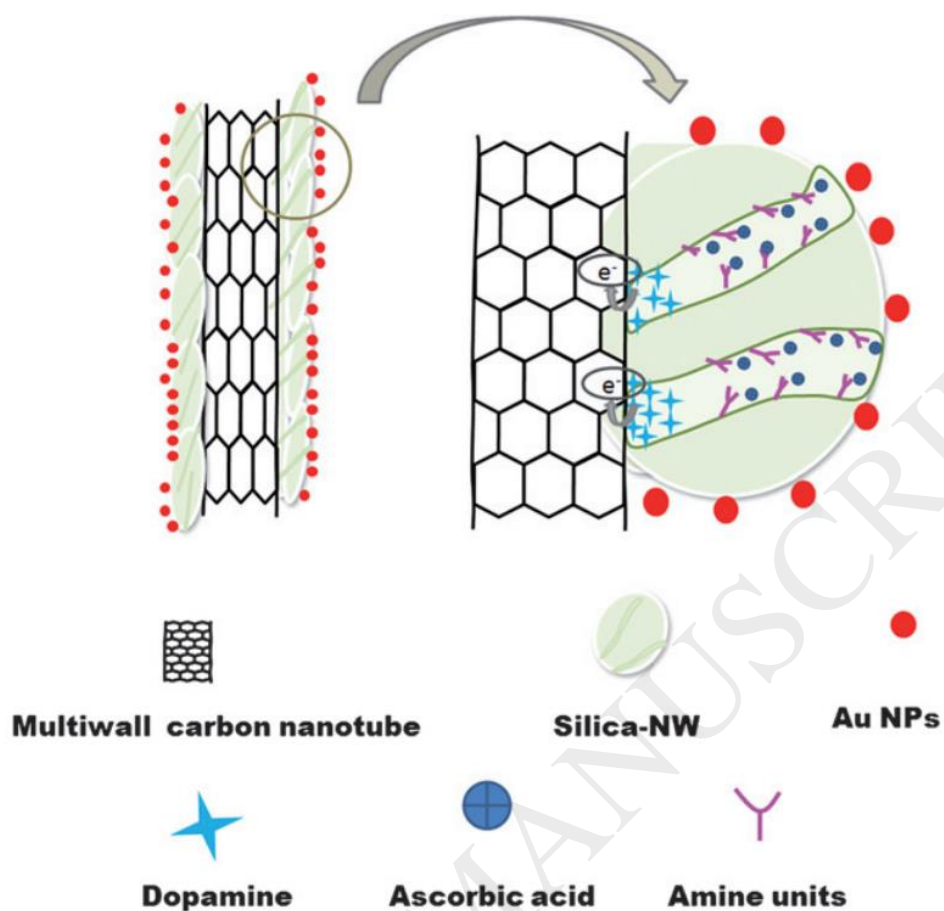


**Fig. 21.** Propable mechanism for the discrimination of AA and DA at MWNT-g-silica-NW/Au NPs. [329], Copyright 2010 (Reprinted with permission from the Royal Society of Chemistry).

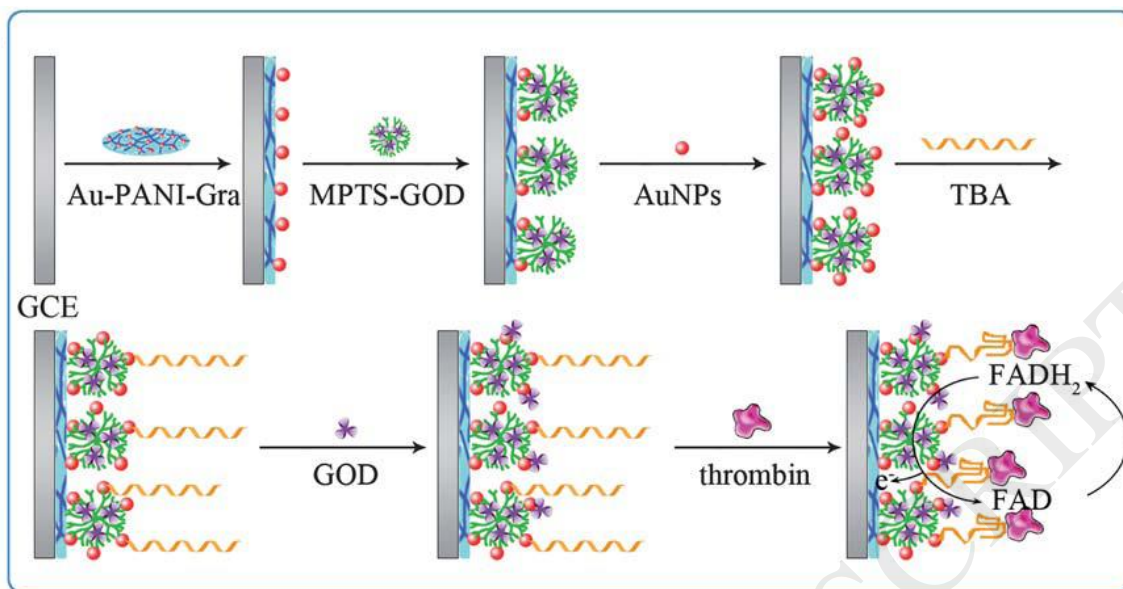
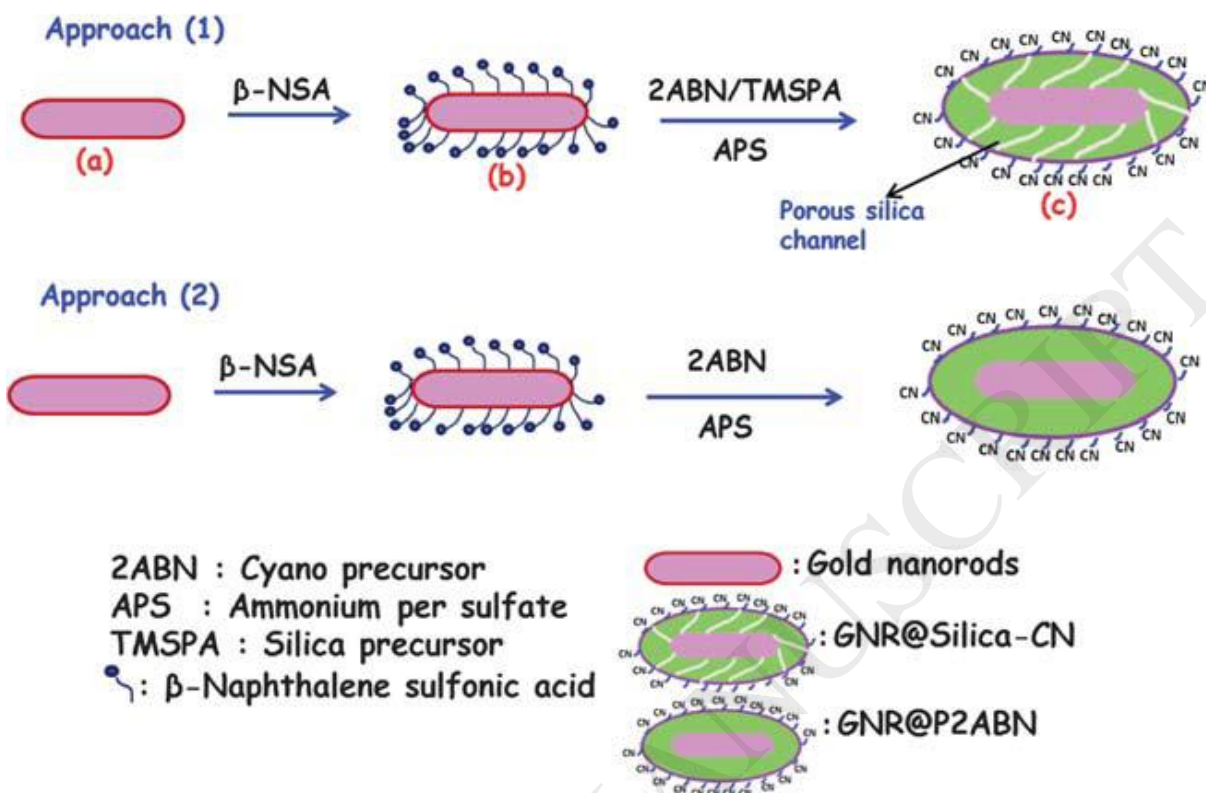
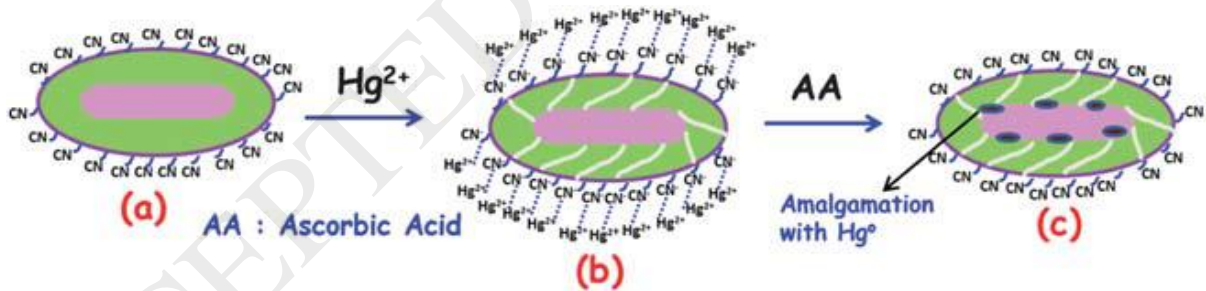


**Fig. 22.** Schematic Illustration of the stepwise aptasensor fabrication. [335], Copyright 2013 (Reprinted with permission from the Royal Society of Chemistry).

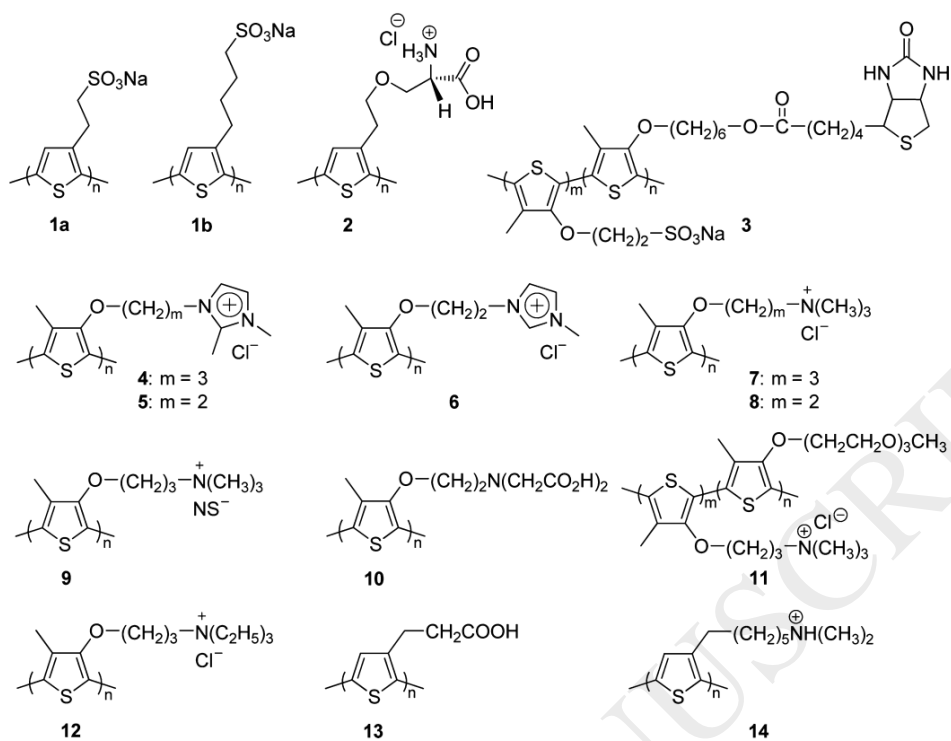
(A)



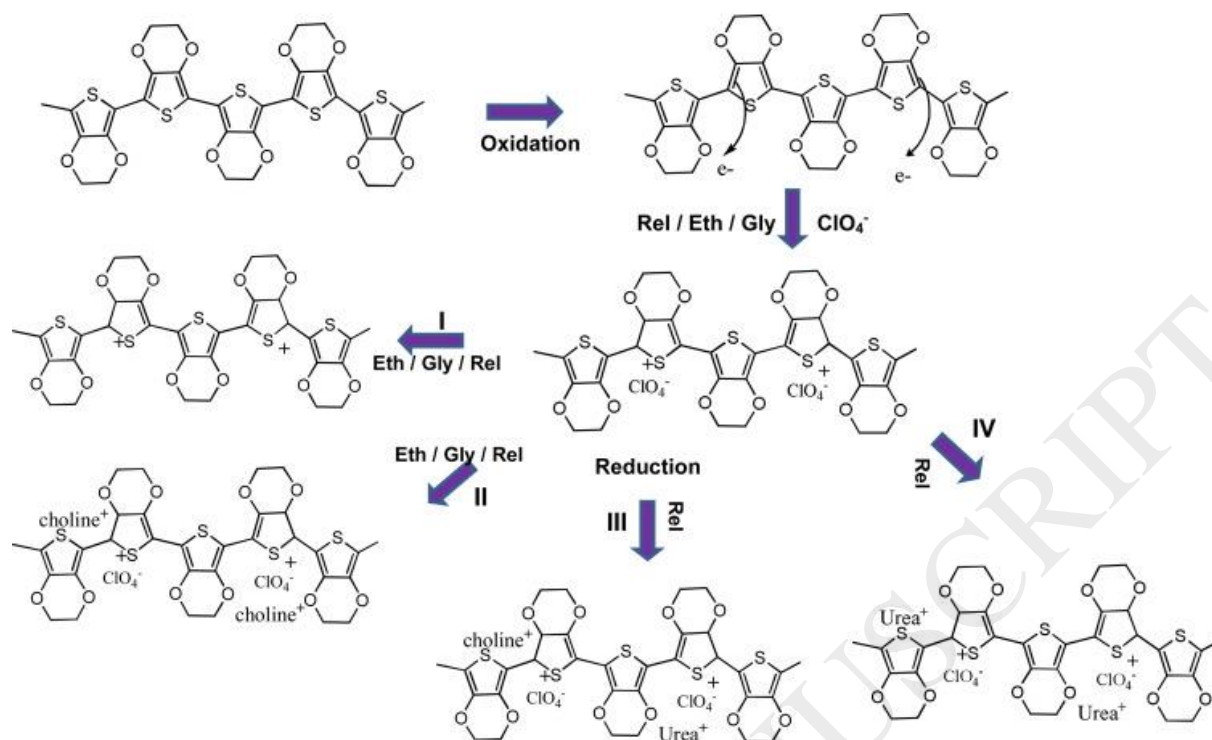
(B)



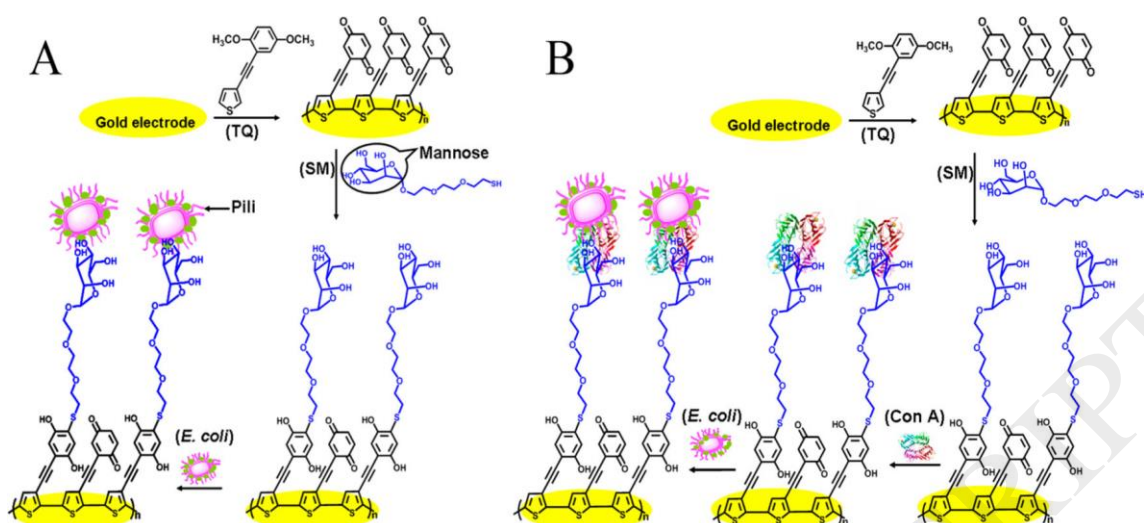
**Fig. 23.** (A) Stages in the preparation of 1) GNR@silica-CN and 2) GNR@P2ABN; (B) Mechanism of  $Hg^{2+}$  sensing. [348], Copyright 2013 (Reprinted with permission from the Royal Society of Chemistry)



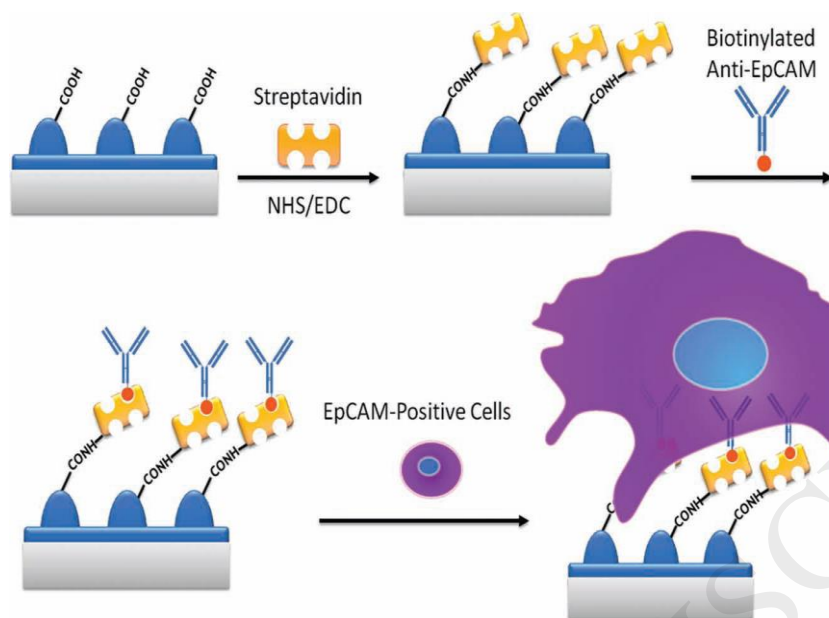
**Fig. 24.** Chemical structures of typical water-soluble PTs. [372], Copyright 2013 (Reprinted with permission from the American Chemical Society).



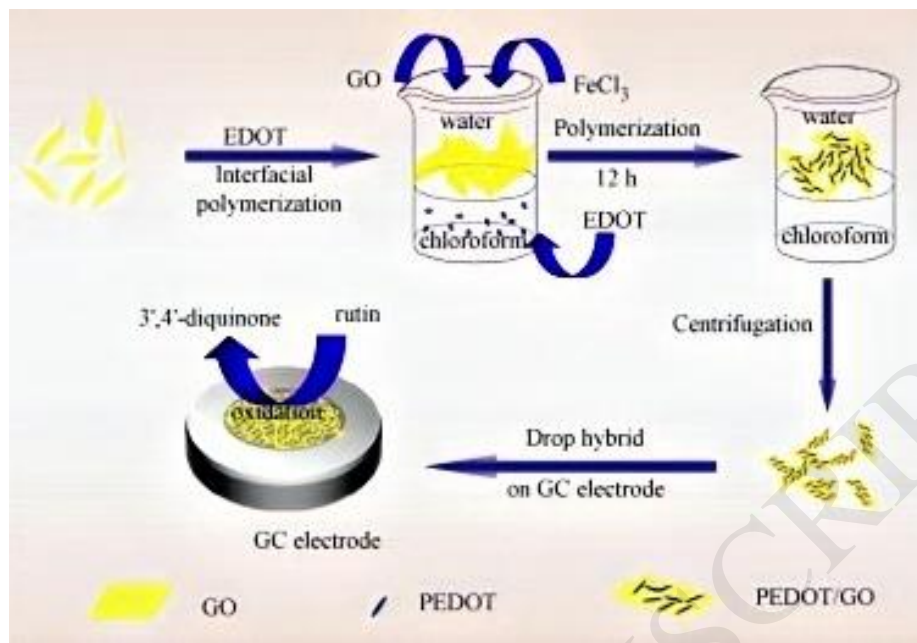
**Fig. 25.** Plausible pathways for doping/dedoping in ethaline, glyceline and reline based eutectics; (i) Pathways I and II applicable for ethaline/glyceline (ii) pathways I, II, III, IV applicable for reline. [409], Copyright 2016 (Reprinted with permission from Elsevier Ltd.).



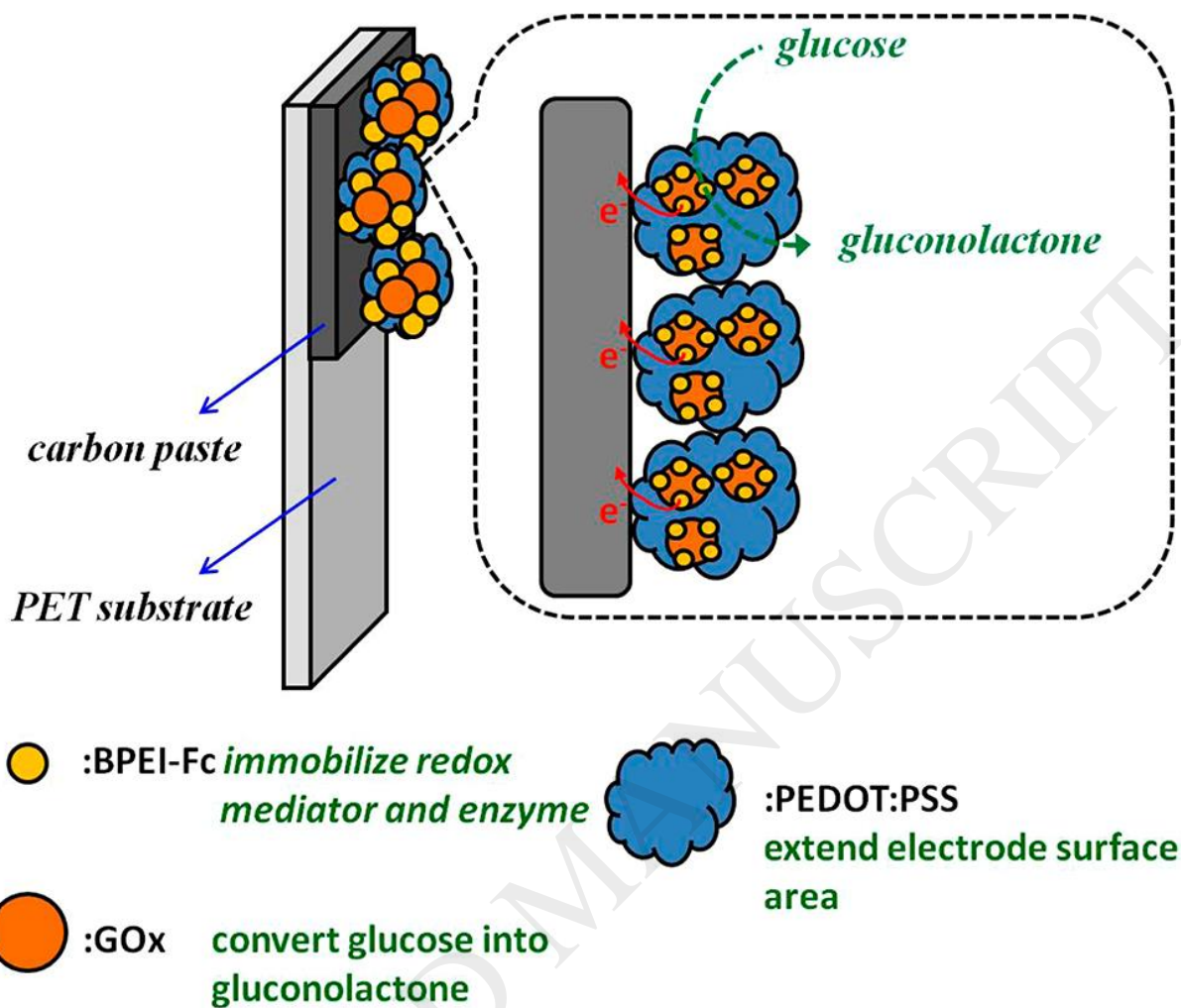
**Fig. 26.** Schematic representation of different modes of *E. coli* detection used in this work: (A) a direct *E. coli* detection using Pili-Mannose binding and (B) a Con A-mediated *E. coli* detection using LPS-Mannose binding. [423], Copyright 2015 (Reprinted with permission from the American Chemical Society)



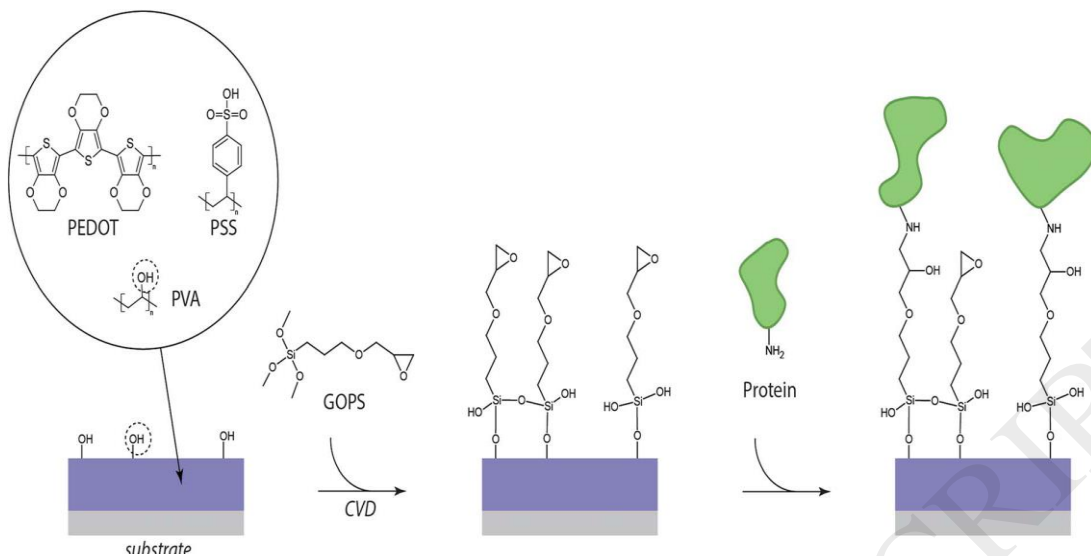
**Fig. 27.** Representation of bioconjugating epithelial cellular adhesion molecule antibody (anti-EpCAM) onto PEDOT nanodots and films. [428], Copyright 2011 (Reprinted with permission from Wiley-VCH publishers).



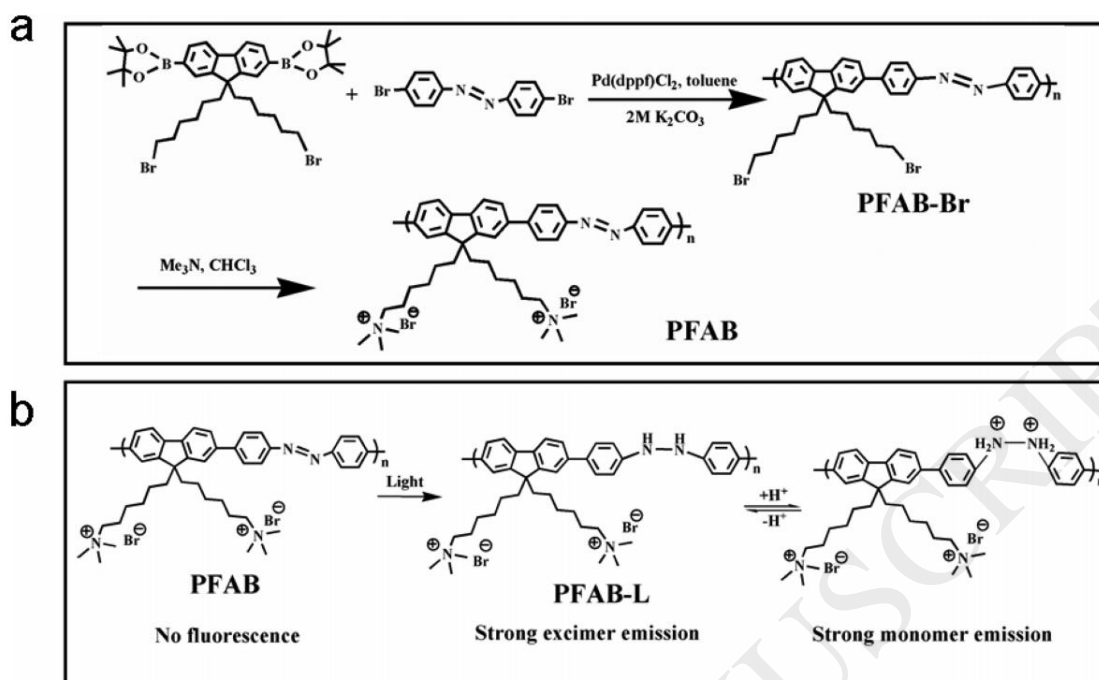
**Fig. 28.** The process of synthesis of PEDOT/GO nanocomposites, and the fabricating procedures of PEDOT/GO electrode. [432], Copyright 2016 (Reprinted with permission from Elsevier Ltd.).



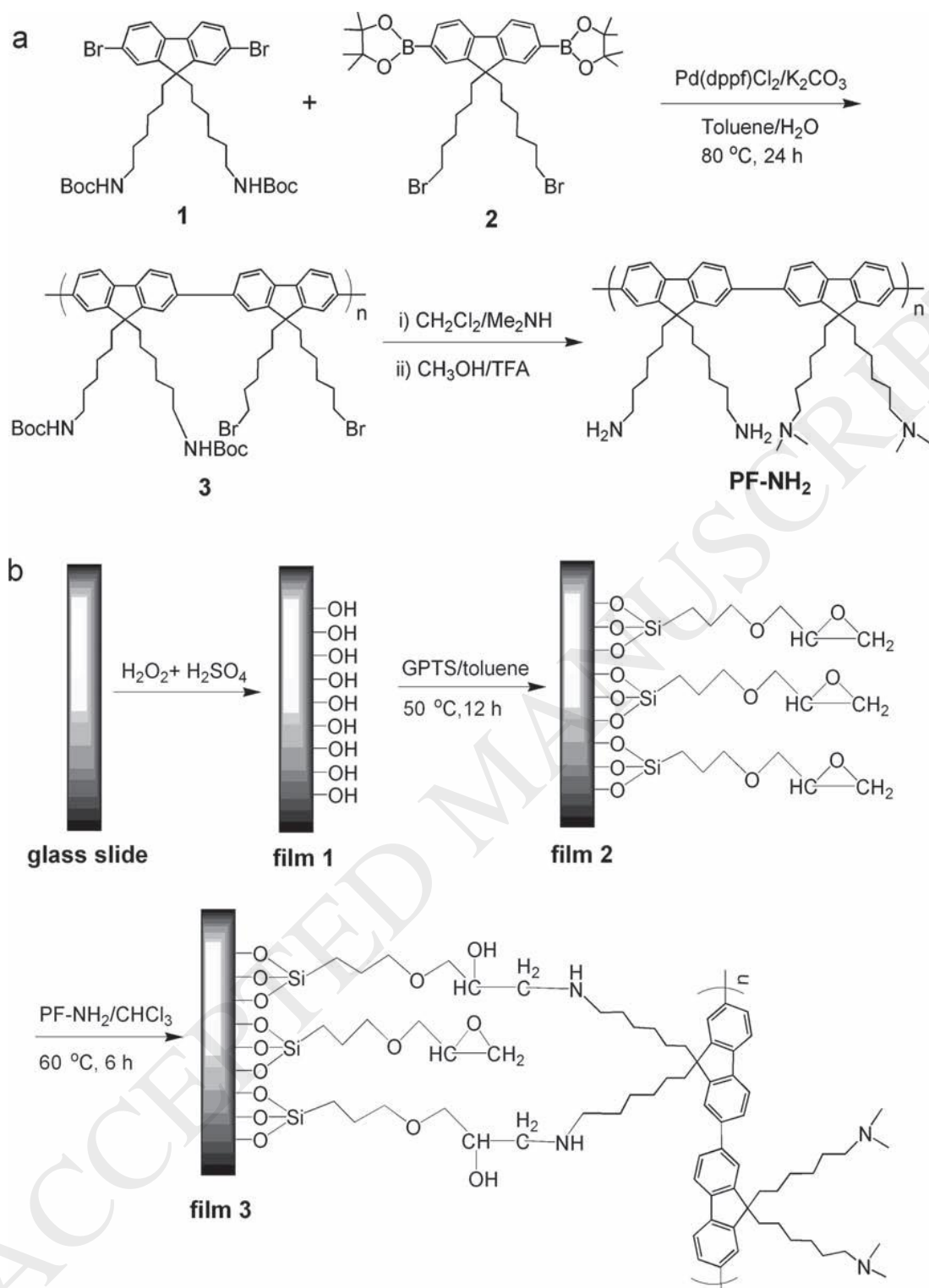
**Fig. 29.** Schematic diagram of the BPEI-Fc/PEDOT:PSS/GOx/SPCE. [443], Copyright 2013 (Reprinted with permission from the American Chemical Society).



**Fig. 30.** Reaction scheme for biofunctionalization of PEDOT:PSS by incorporation of PVA. [445], Copyright 2014 (Reprinted with permission from the Royal Society of Chemistry).



**Fig. 31.** (a) Synthesis routine of polymer PFAB and (b) Photoreduction and pH-responsive mechanism of PFAB. [499], Copyright 2012 (Reprinted with permission from the American Chemical Society).



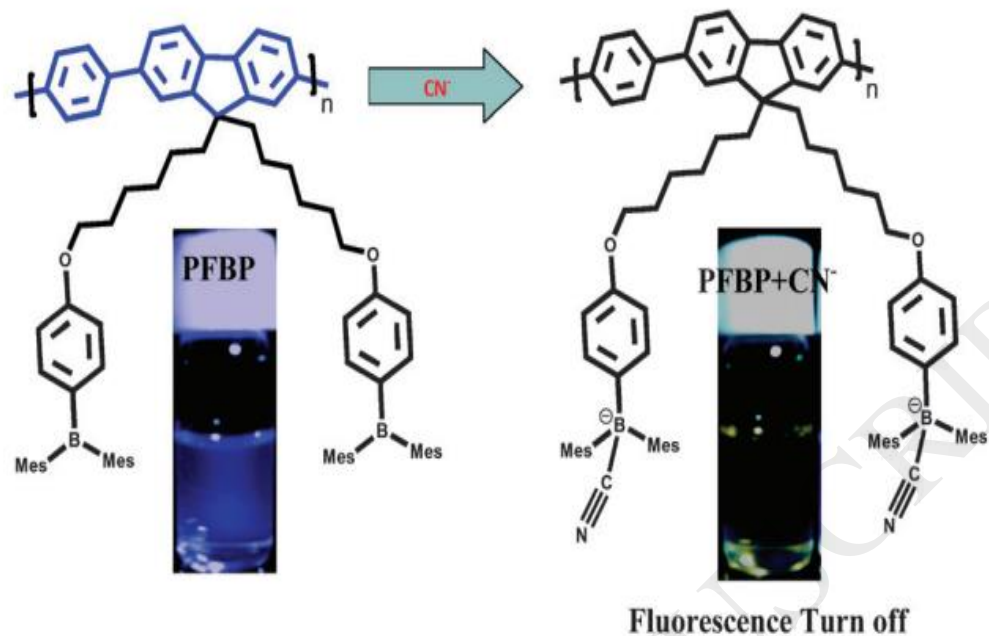


**Fig. 33.** Mechanism of the cyanide attack at the boron centre of the polymer PFBP and the change observed Under UV light at 365 nm. [507], Copyright 2013 (Reprinted with permission from the Royal Society of Chemistry).

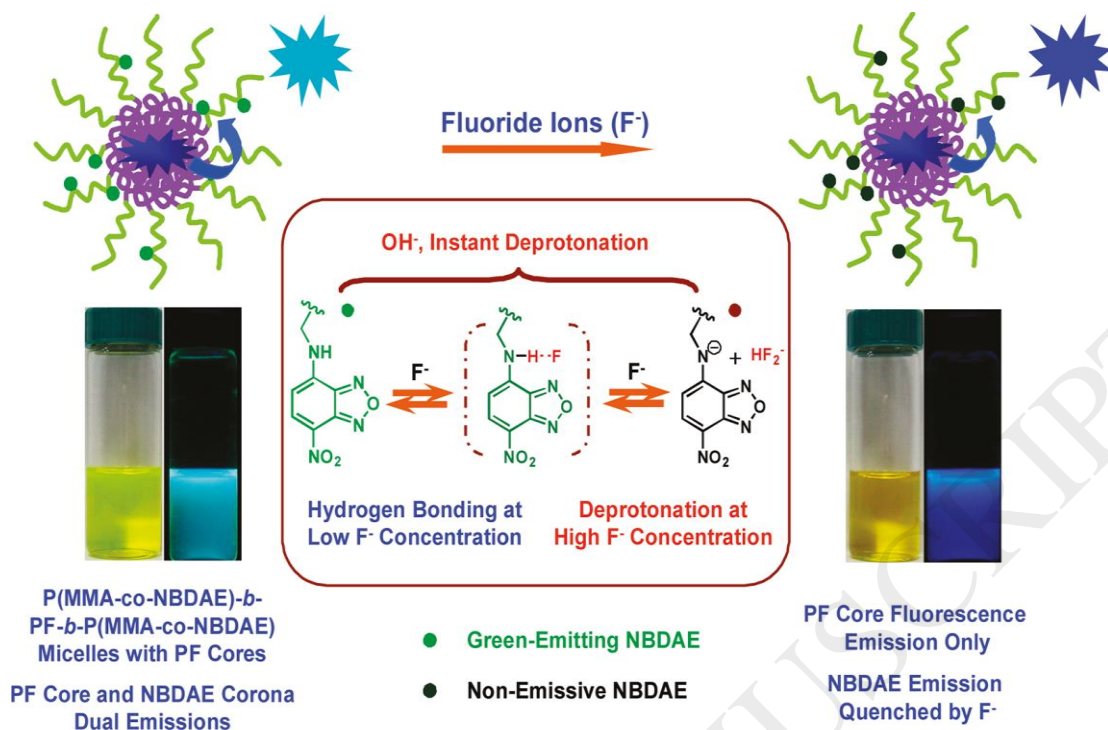


**Fig. 34.** Schematic Illustration of P(MMA-co-NBDAE)-b-PF-b-P(MMA-co-NBDAE) Triblock Copolymer Micelles Consisting of Blue-Emitting Polyfluorene (PF) Cores and Green-Emitting P(MMA-co-NBDAE) Coronas, Which Can Serve as Ratiometric Fluorescent Probes for Fluoride Ions. [508], Copyright 2011 (Reprinted with permission from the American Chemical Society).

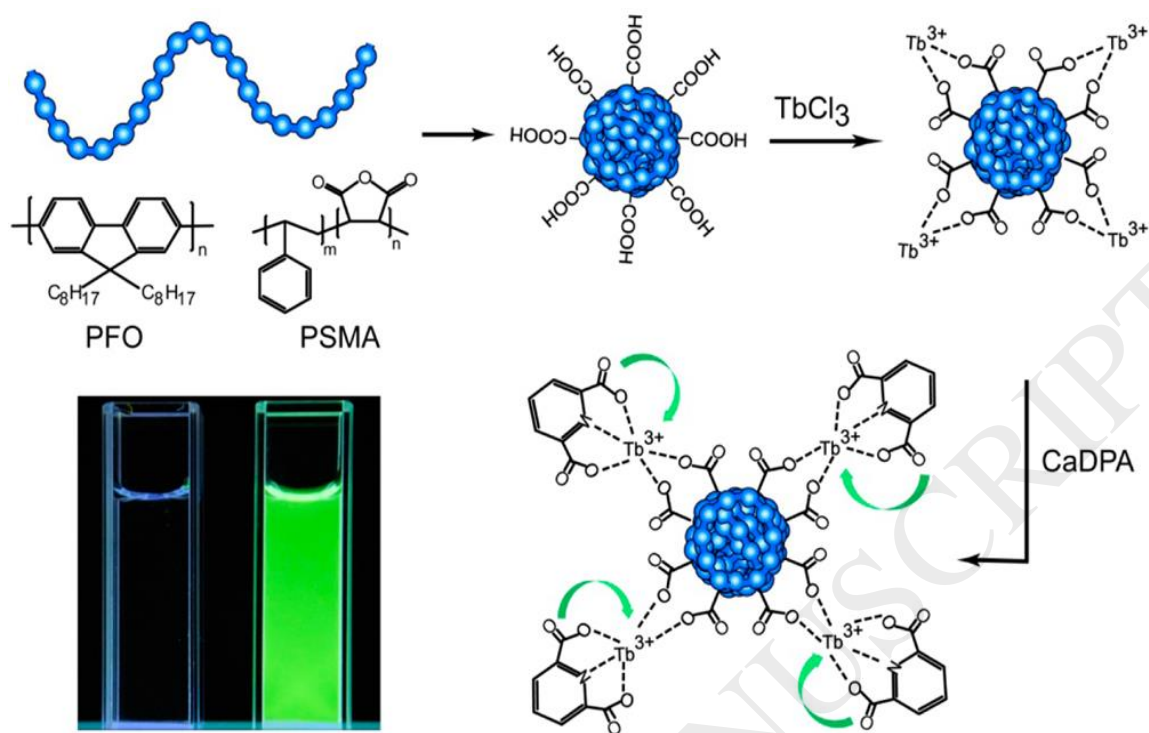


**Fig. 35.** Ratiometric Detection of CaDPA with Terbium Chelated PFO Dots. [511], Copyright 2013 (Reprinted with permission from the American Chemical Society).

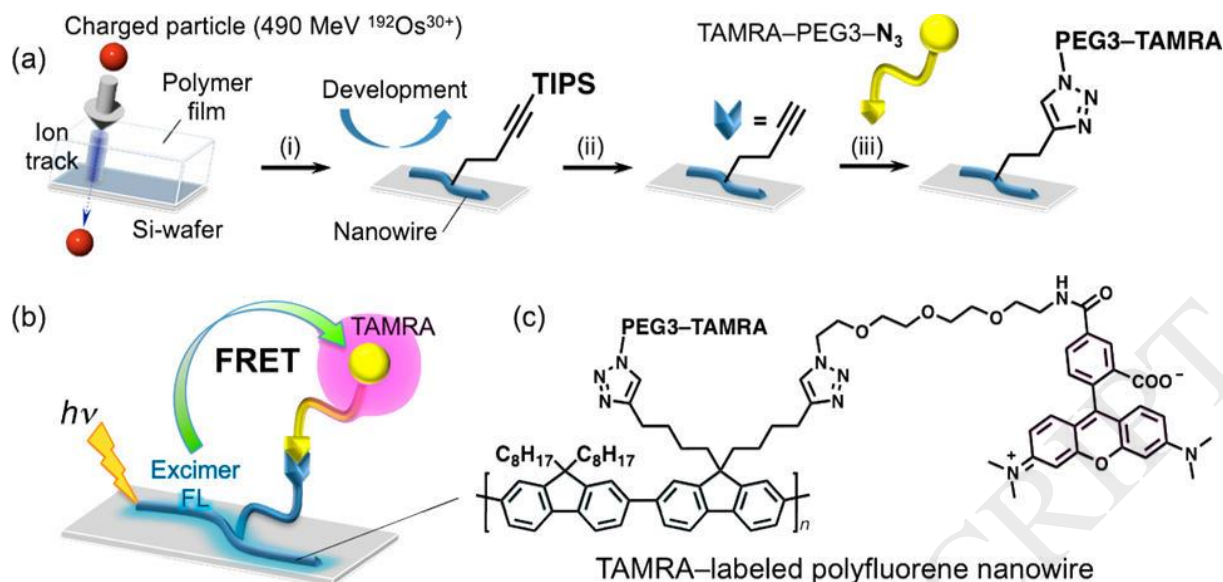


**Fig. 36.** (a) Schematic illustrations of TAMRA-labeled polyfluorene nanowire fabrication by the SPNT: (i) High-energy charged particles induce nonhomogeneous cross-linking reactions along the “single” particle trajectories in a polymer film. The area unexposed to charged particles are subsequently developed with appropriate solvent, the remaining cross-linked sections then transform into nanowires with one end bound to the Si-wafer surface; (ii) Deprotection of TIPS Sacetylenes with TBAF to give alkyne ( $-\text{C}\equiv\text{CH}$ ) groups; (iii) Nanowire surface functionalization via copper-catalyzed alkyne-azide click reaction. (b) Schematic function of the FRET-based nanowire platform. (c) Chemical structure of the TAMRA-labeled polyfluorene nanowire. [526], Copyright 2016 (Reprinted with permission from the American Chemical Society).

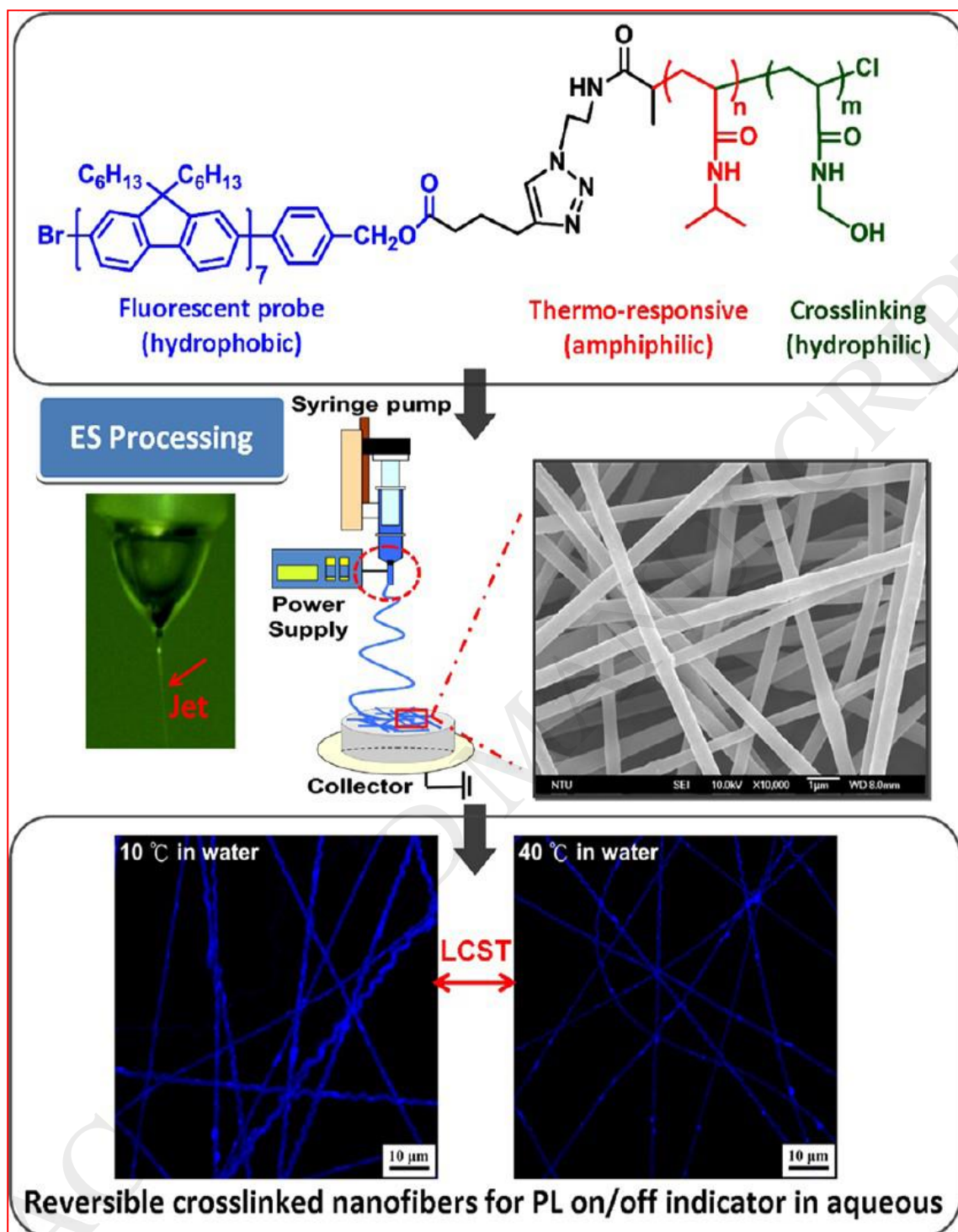


**Fig. 37.** Design of multifunctional sensory ES nanofibers from conjugated Rod-Coil-Coil triblock copolymers. [528], Copyright 2012 (Reprinted with permission from the American Chemical Society).

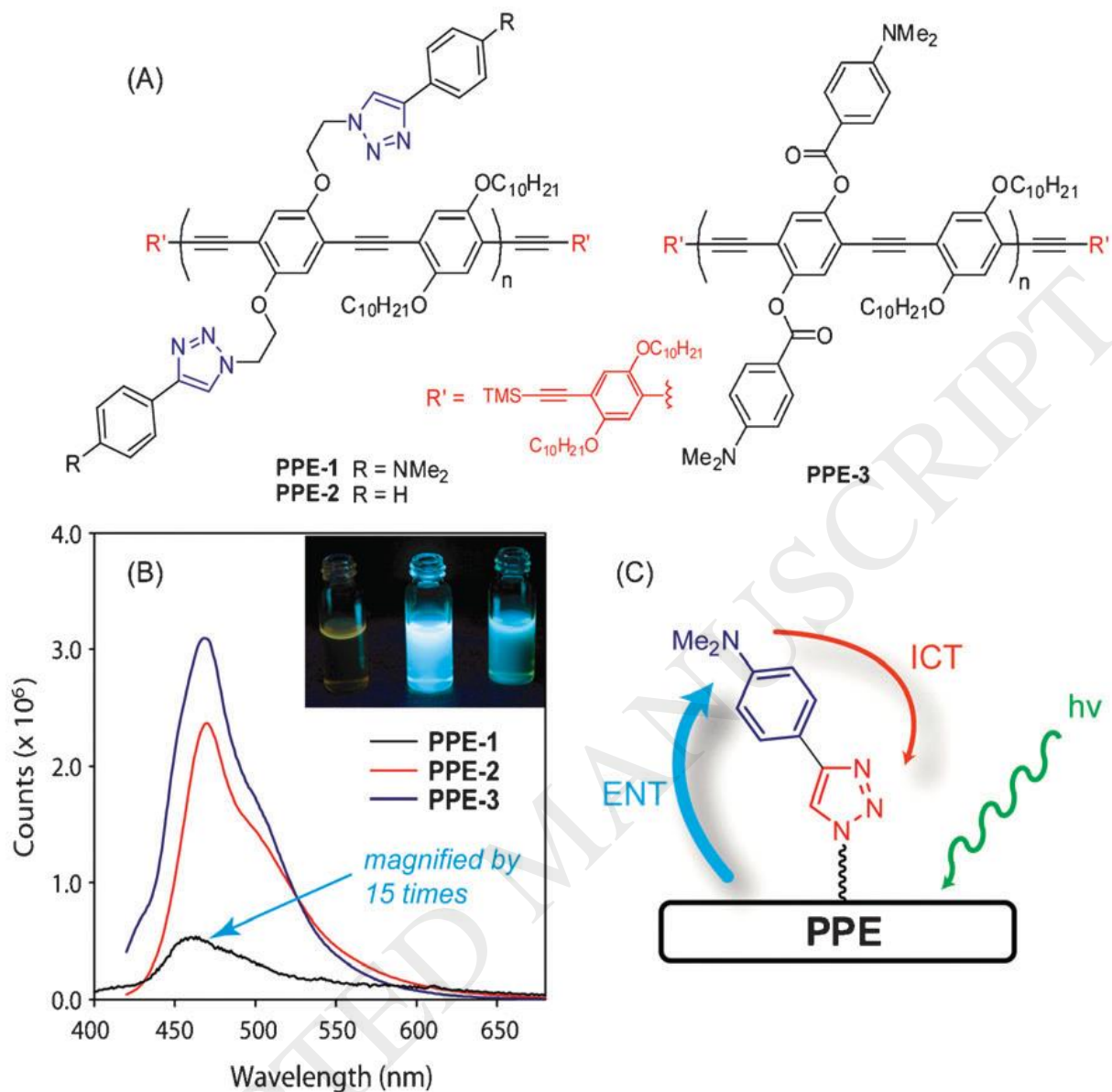


**Fig. 38.** (A) Molecular structures, and (B) fluorescence spectra of PPE-1, PPE-2, and PPE-3. Inset: photographic images of THF solutions of PPE-1 (left), PPE-2 (middle), and PPE-3 (right) under the irradiation of a UV lamp. (C) Proposed fluorescence quenching mechanism for PPE-1. [531], Copyright 2011 (Reprinted with permission from the Royal Society of Chemistry).

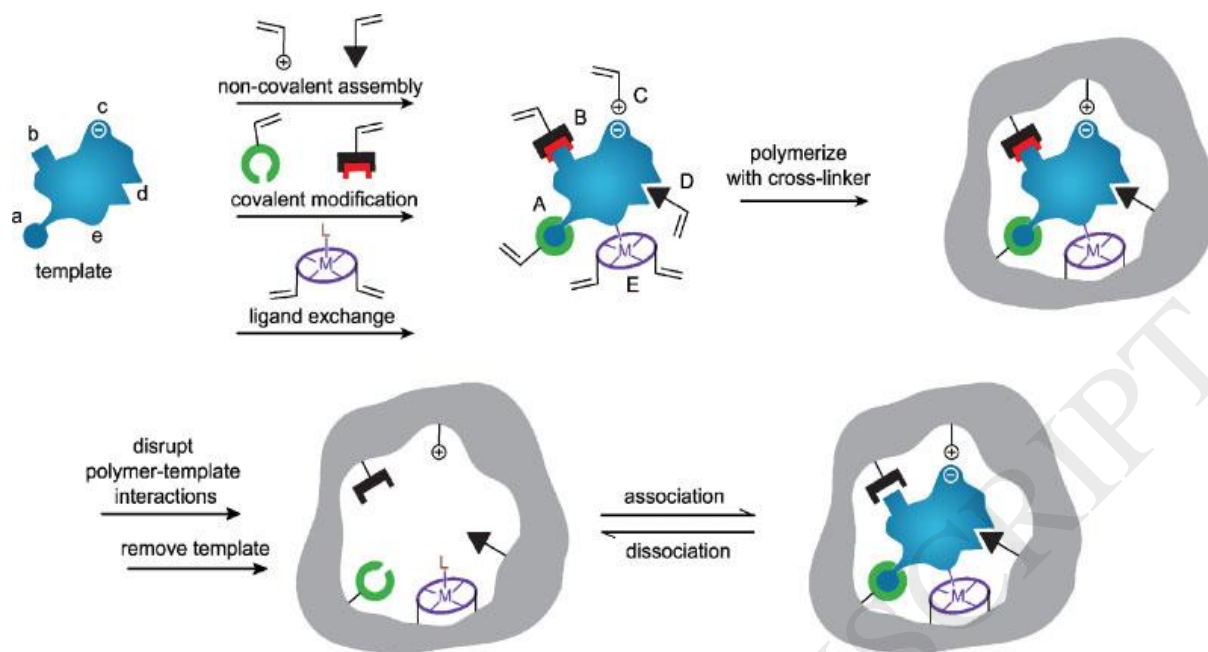


**Fig. 39.** Schematic representation of the molecular imprinting process. Details of descriptions can be referred from Ref [537], Copyright 2006 (Reprinted with permission Wiley-VCH publishers).

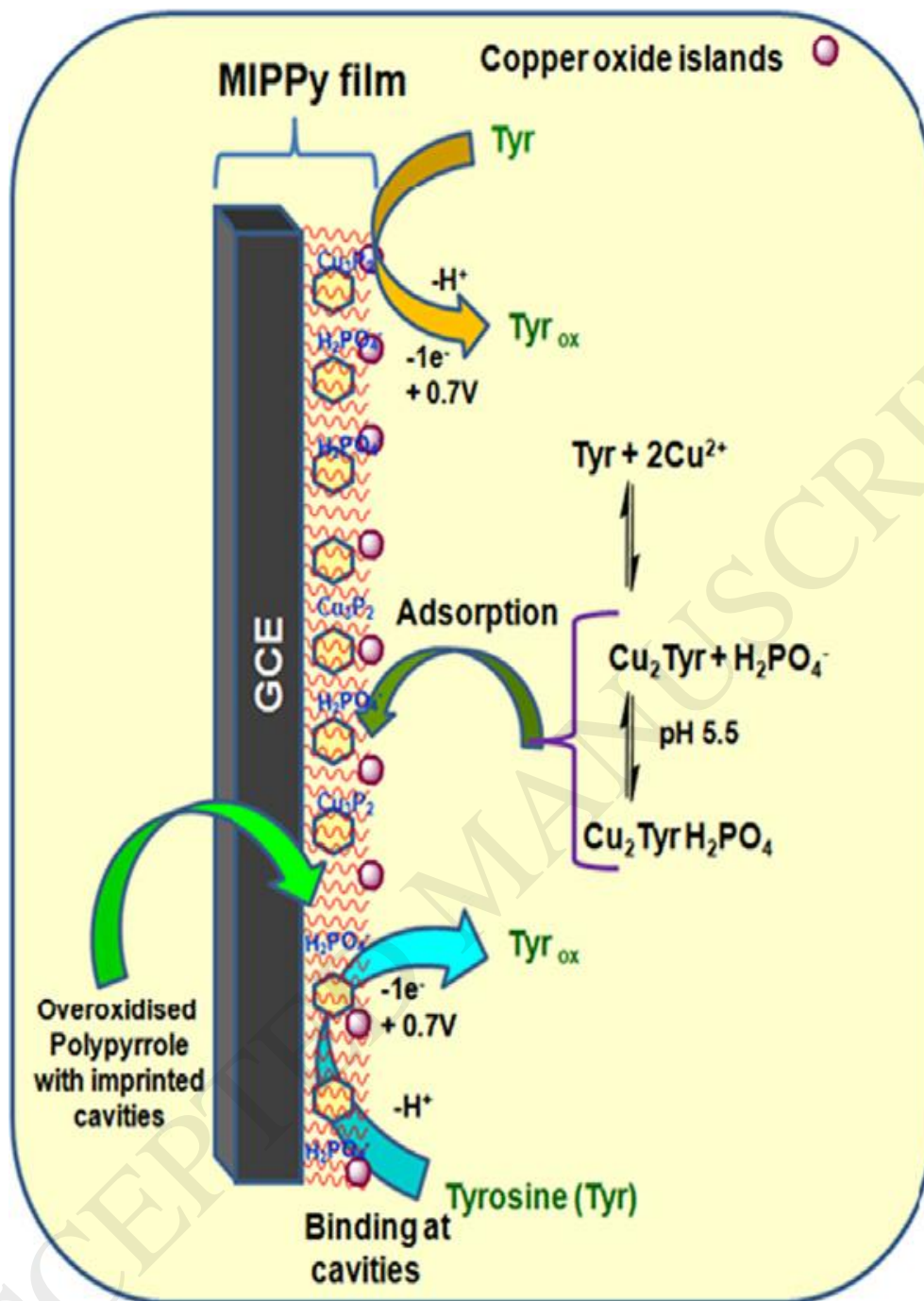


**Fig. 40.** Schematic diagram of the chemical and electro chemical equilibria of tyrosine occurring at in situ copper oxide modified MIPPy electrode – solution interface. [559], Copyright 2011 (Reprinted with permission from Elsevier Ltd.).

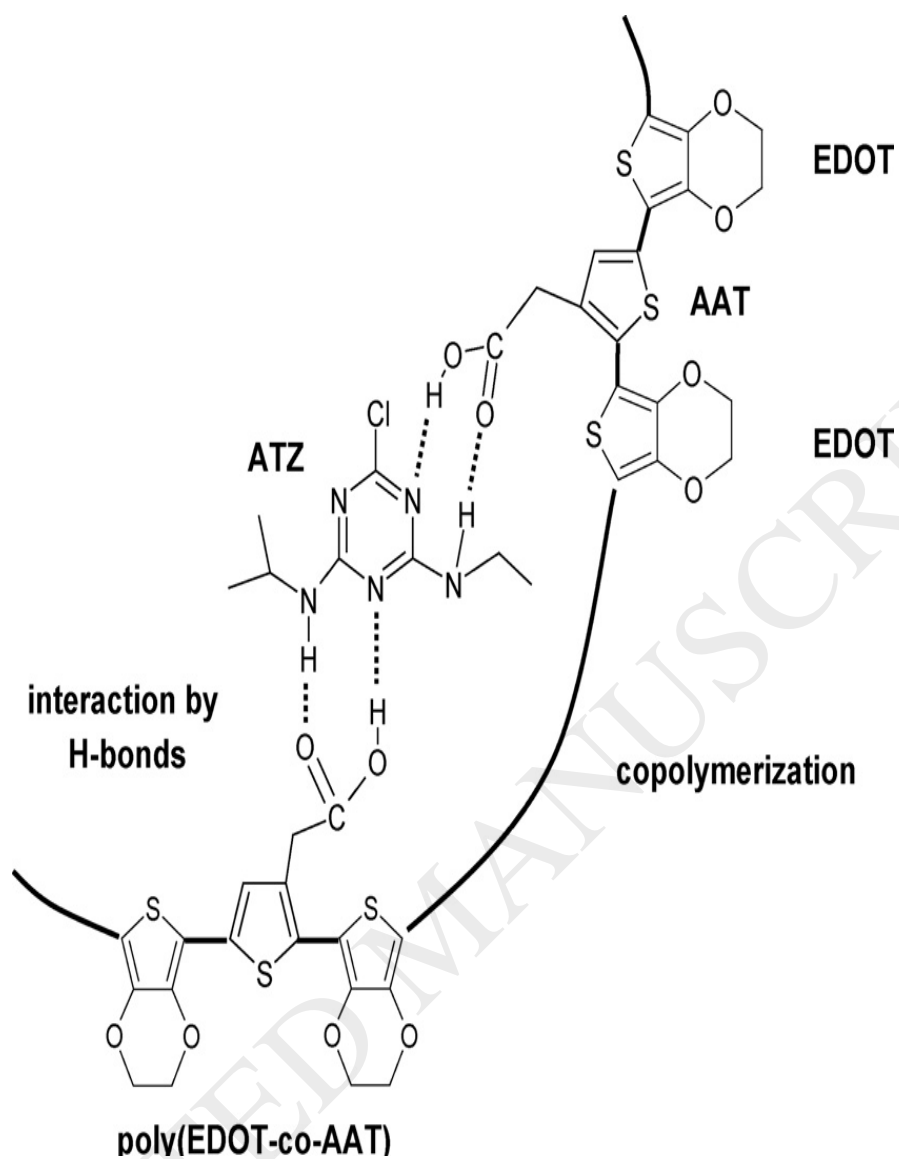


**Fig. 41.** Schematic representation of poly(EDOT-co-AAT) copolymerization after the establishment of H-bonds between AAT and ATZ in a prepolymerization complex. [562], Copyright 2009 (Reprinted with permission from Elsevier Ltd.).

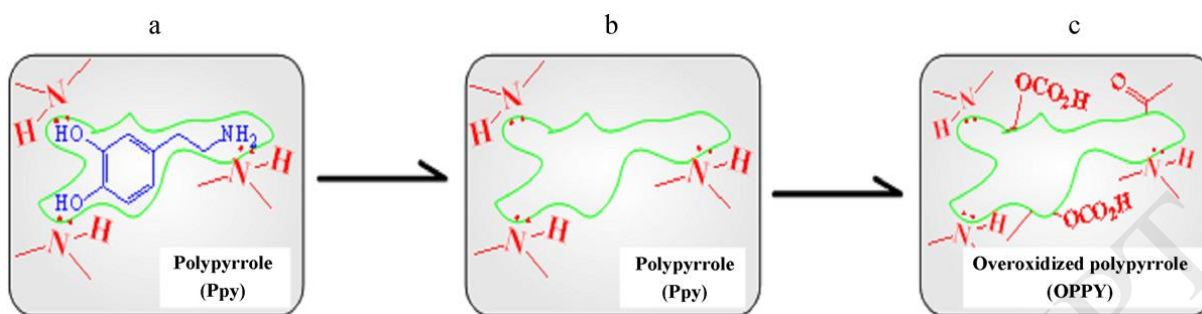


**Fig. 42.** Schematic representation of the fabricated process of molecular imprinting of OPPy on a platinum substrate. (a) Electro-polymerization of DA-imprinted PPy films on platinum substrate, (b) the extraction of template molecules DA and (c) the formation of OPPy through the over-oxidation. [569], Copyright 2012 (Reprinted with permission from Elsevier Ltd.).

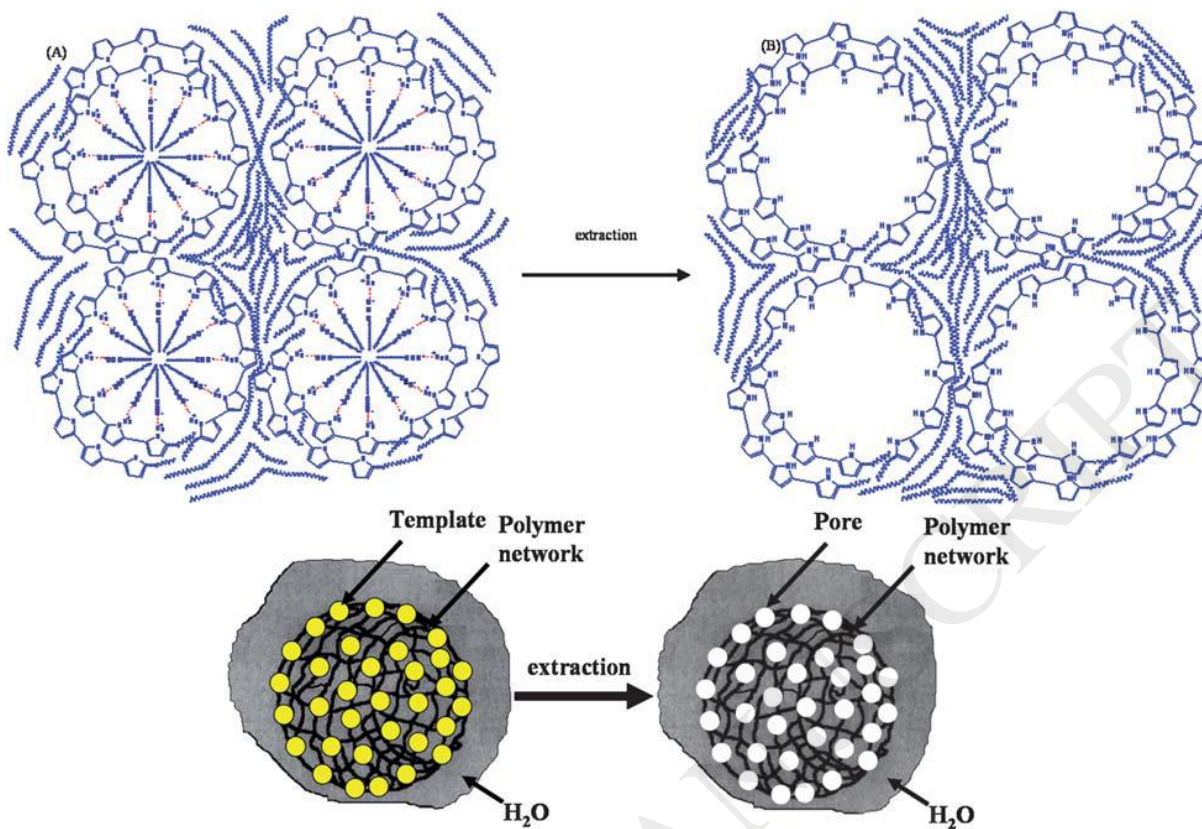


**Fig. 43.** (A) Templating of chiral block copolymers (CBCs) for synthesizing the CMPPy, and electrostatic interaction between negatively charged carboxylic groups of CBC molecules and protonated imine nitrogens of polypyrrole (PPy), (B) after extraction of CBCs from the mesopores. [593], Copyright 2010 (Reprinted with permission from the Royal Society of Chemistry).

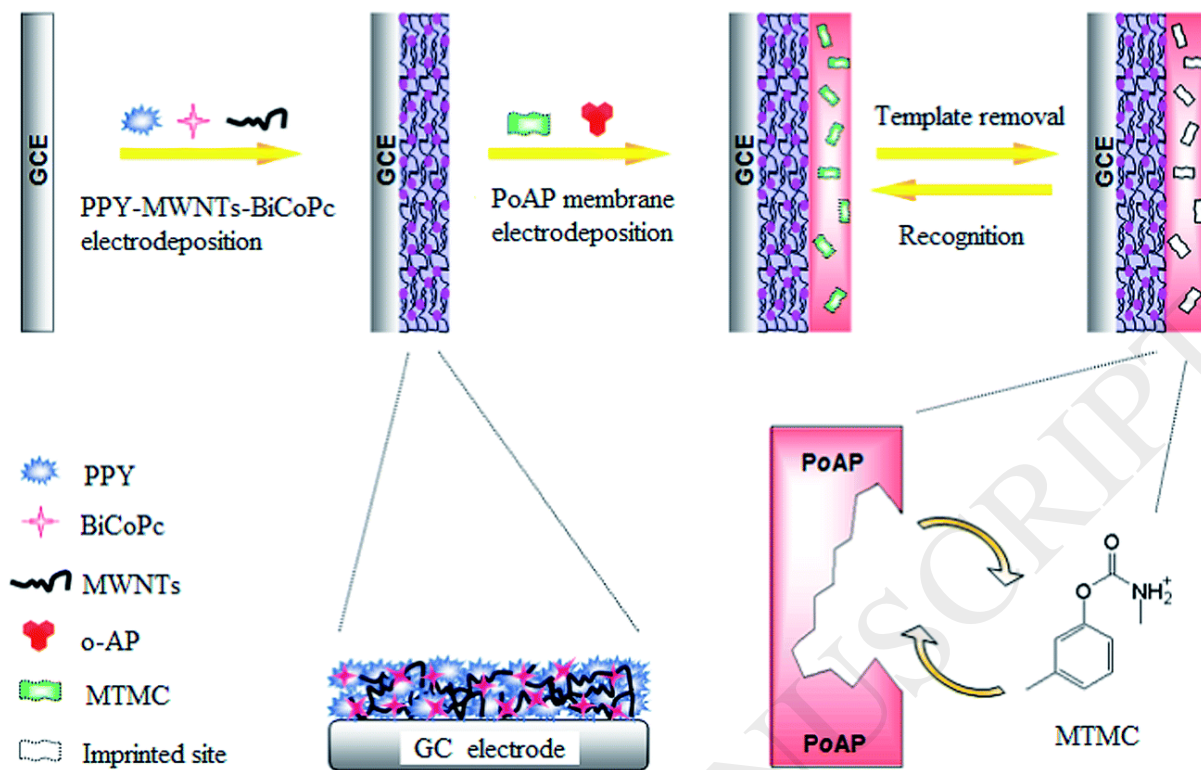


**Fig. 44.** Preparation procedure for the imprinted PPY-MWNTs-BiCoPc-GC electrode. [595], Copyright 2015 (Reprinted with permission from the Royal Society of Chemistry).

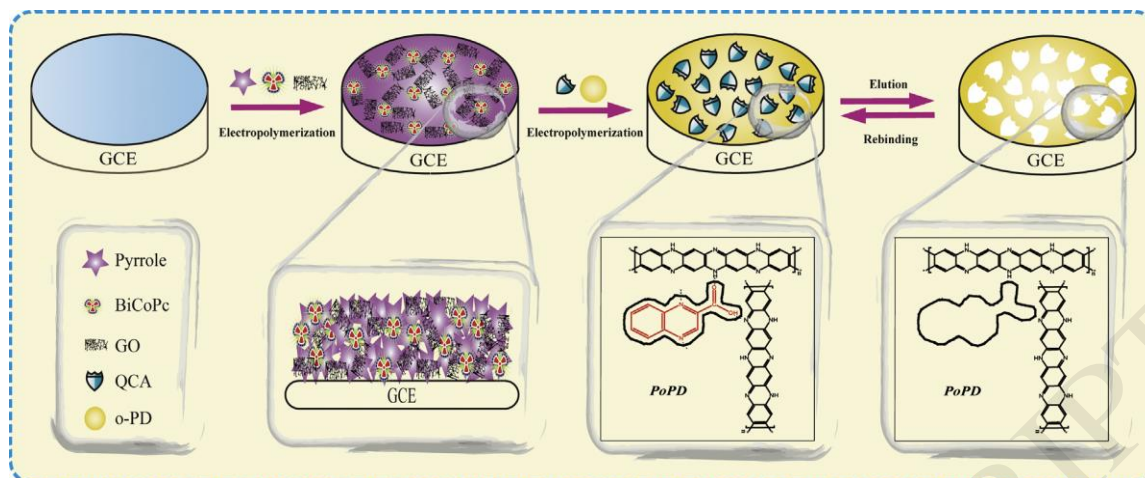


**Fig. 45.** Schematic representation of the MIP/PPY-GO-BiCoPc/GCE fabrication process. [598], Copyright 2011 (Reprinted with permission from Elsevier Ltd.).

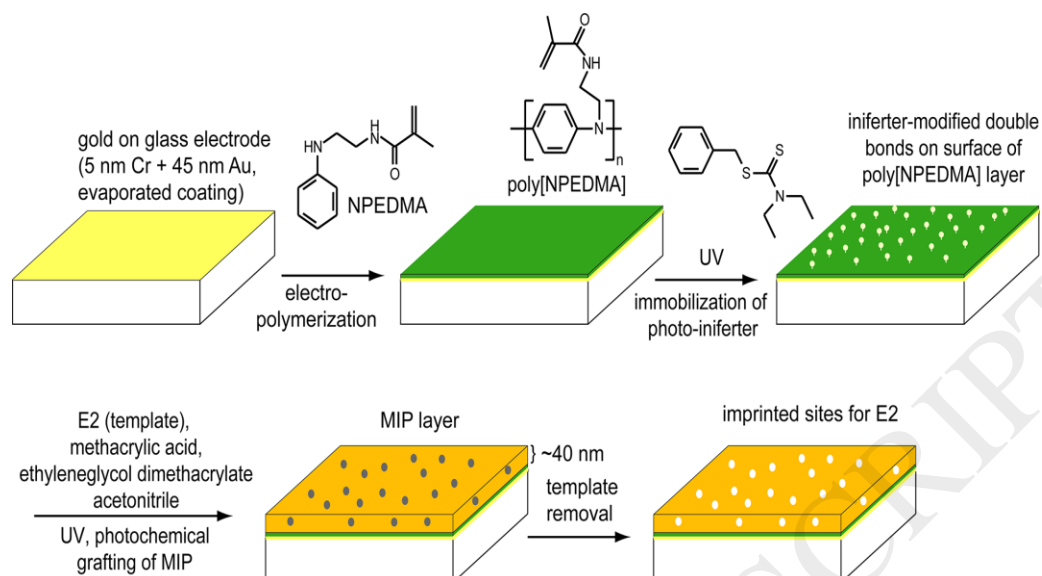


**Fig. 46.** Schematic diagram of steps followed during the development of MIP hybrid sensor for E2. N-phenylethylene diamine methacrylamide (NPEDMA). [600], Copyright 2013 (Reprinted with permission from the American Chemical Society).

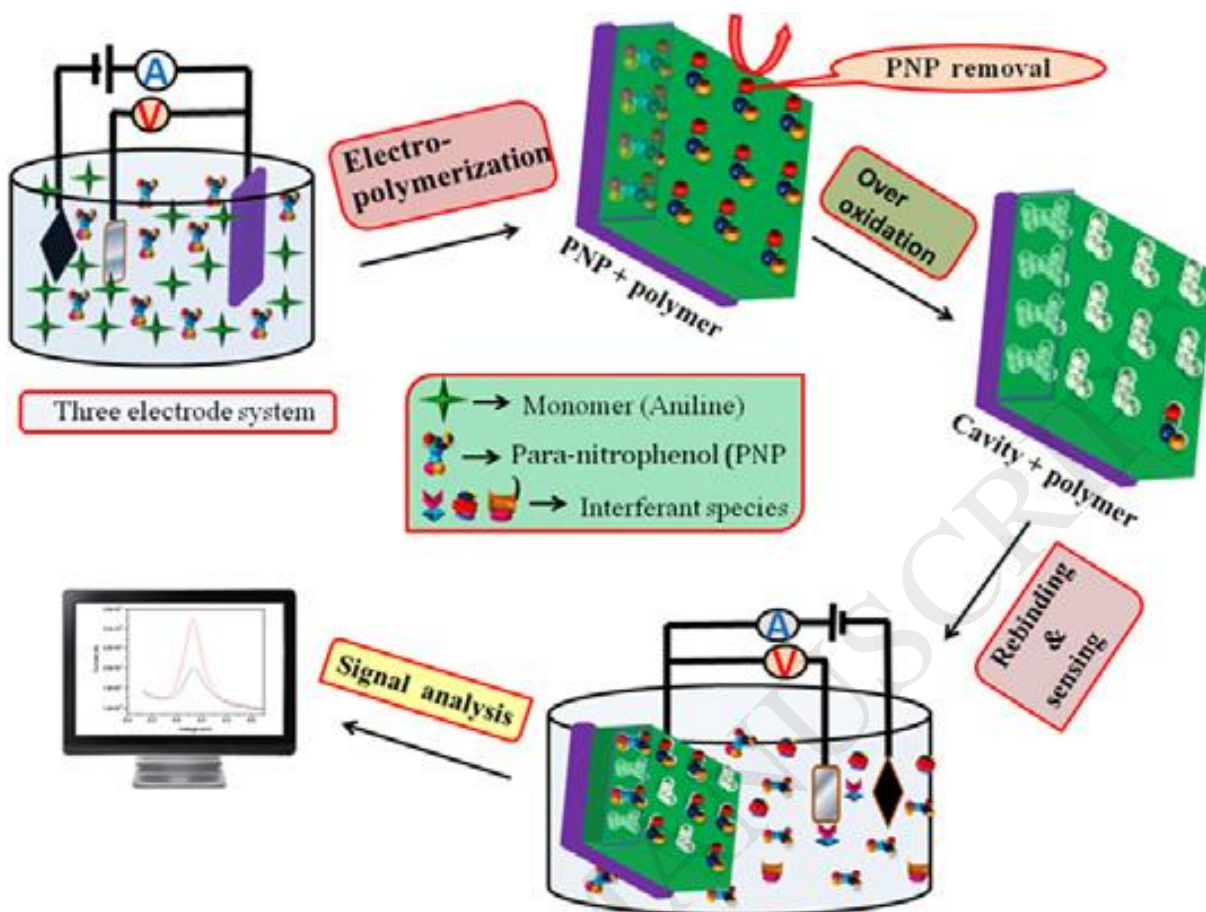


**Fig. 47.** Molecularly imprinted polyaniline-polyvinyl sulphonic acid (PVSA) composite based sensor for para-nitrophenol detection. [612], Copyright 2013 (Reprinted with permission from Elsevier Ltd.).

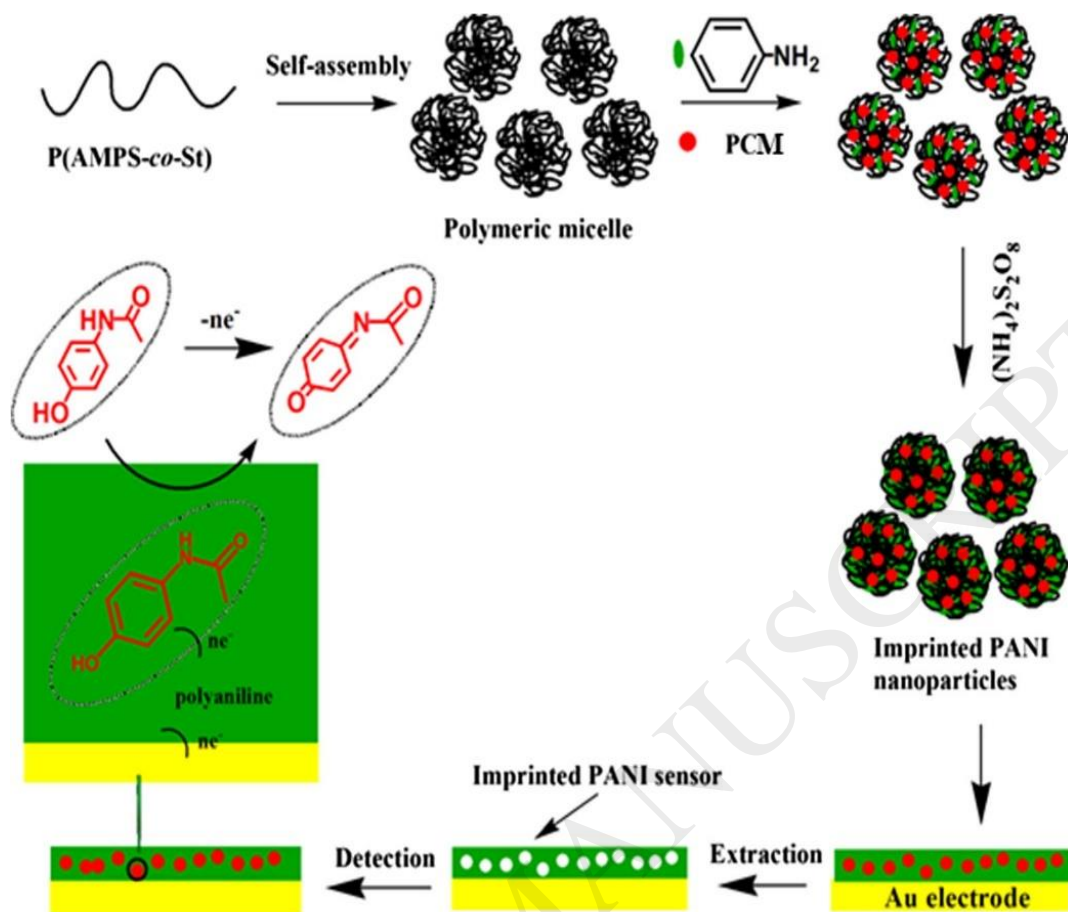


**Fig. 48.** Schematic illustration of the synthesis of molecular imprinted PANI NPs using polymeric micelle as nanoreactor and the fabrication of imprinted PANI sensor. [617], Copyright 2016 (Reprinted with permission from Elsevier Ltd.).

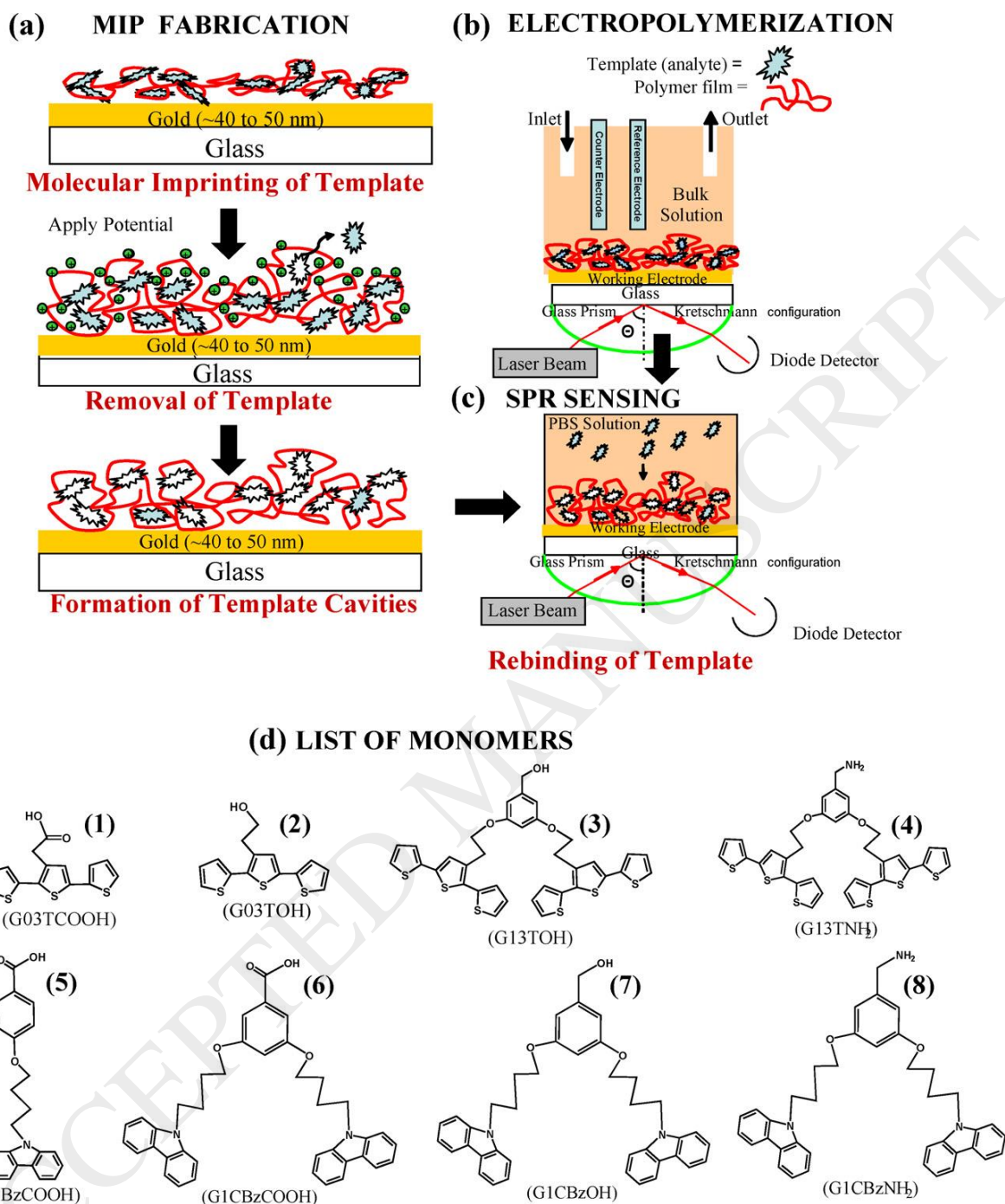


**Fig. 49.** (a) Sensor film fabrication by molecular imprinting and template removal by constant potential wash at 0.4V (versus Ag/AgCl). (b) ESPR in situ set-up for electropolymerization and (c) SPR sensing of the imprinted guest molecule using (d) different monomers of poly(terthiophene), G0 3T-COOH (1), G0 3T-OH (2), G1 3T-OH (3), G1 3T-NH<sub>2</sub> (4) and of poly(carbazole), G0 CBz-COOH (5), G1 CBz-COOH (6), G1 CBz-OH (7), G1 CBz-NH<sub>2</sub> (8). [627], Copyright 2011 (Reprinted with permission from Elsevier Ltd.).

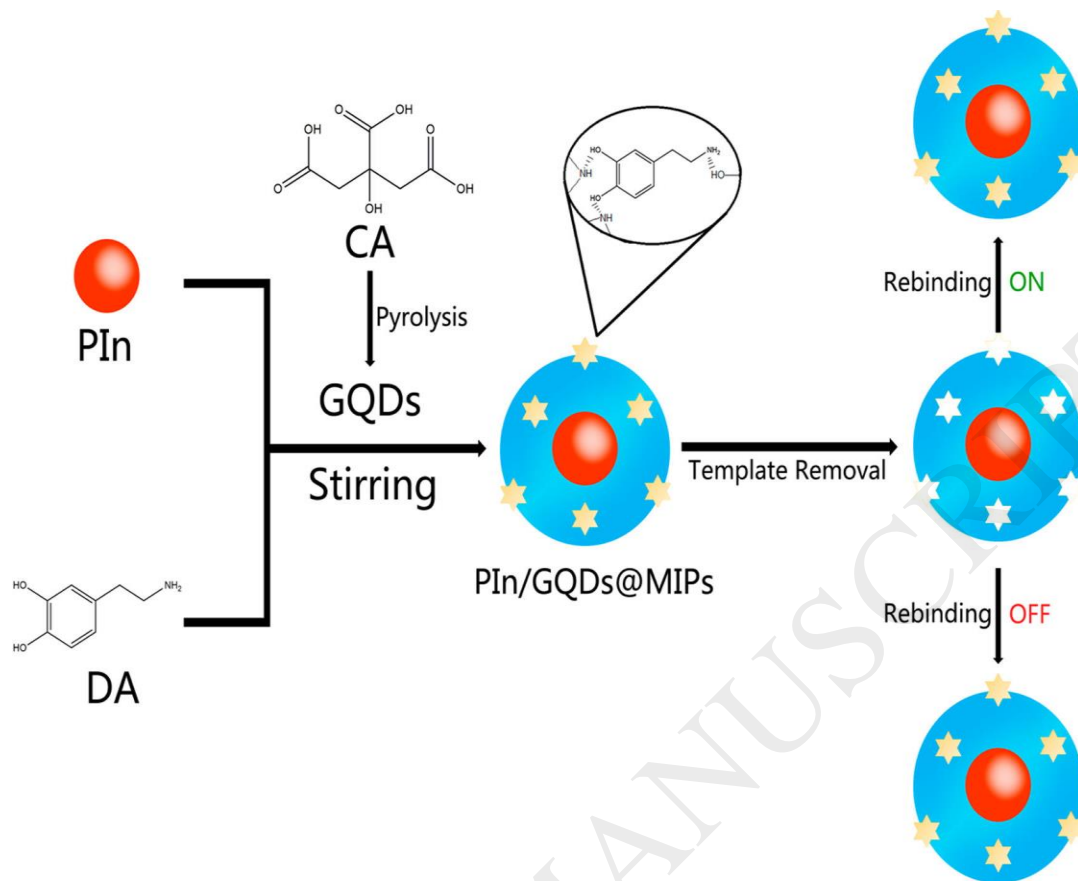


**Fig. 50.** Illustration of the preparation of PIn/GQDs@MIPs. [622], Copyright 2015 (Reprinted with permission from the American Chemical Society)

**Table 1. Functionalized polypyrroles (PPy) for sensors and related details: Functionalization approach, name of F-PPy, type of sensor (based on analyte), analyte(s) name, detection technique, role of F-PPy for sensing and sensor performances.**

Mode of Parent structure functionalization/modification	Name of FCP (abbreviation) or functional structure in the FCP	Type of sensor (Analyte)	Specific analyte(s)	Detection method/Technique	Function/Role of F-PPy for sensing*	Sensor performances* (LR and DL)	Ref
Substituted / derivatized	3-alkyl substituted PPy	Chemical (Gas)	Hexane, toluene, water, acetonitrile, triethylamine, butanal, methanol, ethanol, butan-1-ol, hexan-1-ol, and nonan-1-ol	acoustic wave	Secondary oxidation process-good sensitivity to non-polar vapour- chain length of alkyl group influences the sensitivity to non-polar solvent	-	[60]
	PPy functionalized with 5,10,15,20-tetraphenyl-21H,23H-porphyrin iron(III) chloride	Electrochemical (Gas)	CO	Resistance	Interaction of CO with central iron atom and subsequent electronic charge transport from FeTPPCI to PPy.	-	[65]
	PPy functionalized with copper thalocyanine	Electrochemical (Gas)	Methanol, NH <sub>3</sub> , and NO <sub>2</sub>	Resistance	Charge transfer complex formation between thalocyanine and NO <sub>2</sub>	-	[66]
	Poly(N-2(cyanoethyl)pyrrole) (PNCEPy), Poly (N-2-cyano methyl pyrrole) (PNCMPy)	Chemical (Gas)	Gas molecules of different solvents (i.e., water, methanol, acetonitrile, and chloroform)	Quantum mechanical calculation	Sensing depends on functional group in the FCP and not on length of alkyl group	-	[67]
	3-(1 <i>H</i> -pyrrol-1-yl)phenyl boronic acid-substituted PPy	Electrochemical (Sugar)	Saccharides	Potentiometry	Complexation with saccharides	<u>D-Glu</u> LR = 0.25-1.25 mM	[68]

						DL = 0.17 mM D-fructose LR = 0.05-0.52 mM DL = 0.008 mM	
	PNCEPy and Poly(N-methyl) pyrrole (PNMPy)	Electrochemical (Neurotransmitter)	DA	CV	Flexibility of cyanoethyl groups and the dipole of the cyano groups favour vanderwalls interaction and dipole induction with DA LR = 100 $\mu$ M to 10 mM	-	[69]
	PPy/ $\beta$ -cyclodextrin	Electrochemical (Neurotransmitters)	Polyhydroxyphenyls and neurotransmitters (epinephrine, metanephrine, and l-dopa (l-3,4-dihydroxyphenylalanine))	CV	Complexation capability of PPy/ $\beta$ -CD- $\beta$ -CD forms inclusion complex	-	[70]
	Ferrocenylmethyl trialkylammonium derivatives of PPy	Electrochemical/optical (Ion)	Dihydrogenphosphate and adenosine triphosphate (ATP) anions	DPV and Fluorescence "turn on"	Ion pairing interactions with alkyl ammonium groups and complexation through ferrocenium center	-	[71]
	Rhodamine derivative of PPy	Electrochemical (Ion)	Cu <sup>2+</sup>	Potentiometry	-	LR = 0.4–10 $\mu$ M DL = 280 nM	[72]
	Poly(11-N-pyrrolylundecanoic) acid and poly(N-undecylpyrrole)	Electrochemical (Ion)	Protons (pH)	Potentiometry	-COOH groups are sensitive to pH changes	LR = 4-9	[73]
Functional ion-dopant inclusion	Phthalocyanine doped PPy	Electrochemical (Gas)	NO <sub>2</sub>	Conductivity	Interaction of NO <sub>2</sub> with sulfonic acid derivatized phthalocyanine and withdrawl of electron from the CP backbone	-	[76]
	N-sulfonated cobalt phthalocyanines doped Ppy	Electrochemical (Gas)	NH <sub>3</sub>	EIS	-	-	[77]
	Dodecylsulfate (DS)-doped Ppy	Chemical	Benzene, ethyl	Liquid-liquid	Interaction of aromatic hydrocarbons	LR = 15-150 $\mu$ g	[78]

		(Gas)	benzene, toluene, and 1,3,5-trimethylbenzene	micro extraction	leads to $\pi$ - $\pi$ electron donor- acceptor complex formation	mL <sup>-1</sup> (all analytes)	
	ferrocenylmethyltrimethyl ammonium iodide (FTMA-I) doped PPy	Electrochemical (Gas)	CO	Resistance	Interaction of CO with -NH groups and withdrawal of electron to create mobile positive charge/polaron	DL = 100 ppm	[79]
	PPy-zirconium(IV)selenoiodate cation exchange NC	Electrochemical (Gas)	Formaldehyde	Conductivity	Interaction between oxygen atom of formaldehyde and carbocation of PPy chains	-	[80]
	Hydroquinone sulfonate (HQS)-doped PPy	Electrochemical (Ion)	Proton (pH)	Potentiometry	Protonation of -NH <sub>2</sub> groups	-	[81]
	Tiron doped PPy	fluorescence (Ion)	Fe <sup>3+</sup>	Fluorescence	-	LR = $5.0 \times 10^{-8}$ - $1.0 \times 10^{-6}$ mol L <sup>-1</sup>	[82]
	Alizarin Red S doped PPy	Electrochemical (Ion)	Ag <sup>+</sup>	Potentiometry and Voltammetry	Complexation between Ag <sup>+</sup> and Alizarin Red S	LR = $5.0 \times 10^{-8}$ - $6.3 \times 10^{-3}$ M and $9.2 \times 10^{-10}$ - $2.8 \times 10^{-6}$ M DL = $2.5 \times 10^{-8}$ M and $4.6 \times 10^{-10}$ M	[83]
Functional compound inclusion	PPy (PPy)-reduced graphene oxide (rGO) hybrid	Electrochemical (Gas)	NH <sub>3</sub>	Resistance	$\pi$ stacking and hydrogen bonding interaction between PPy and rGO	LR = 1 ppm - 10 ppm	[88]
	PPy/ZnO nanohybrid	Electrochemical (Gas)	NH <sub>3</sub>	Resistance	Diffusion of analyte gas within the 3D ZnO-PPy nanostructure	-	[89]
	PPy/ZnO NC	Electrochemical (Gas)	NH <sub>3</sub>	Resistance	Effective charge transfer and extended delocalization of $\pi$ -electrons	LR = 5 ppm-120 ppm	[90]
	PPy-coated SnO <sub>2</sub> NCs	Electrochemical (Gas)	NH <sub>3</sub>	Resistance	Polymerization conditions influence the sensor properties	LR = 1-10.7 ppm DL = 257 ppb	[91]
	PPy-tin oxide hybrid	Electrochemical (Gas)	NH <sub>3</sub>	Kelvin probe force microscopy (KPFM)	Faster sensor response is due to nucleation of charge compensating sites/di-ole interfaces	-	[92]
	PPy/metal oxide NCs	Electrochemical	NH <sub>3</sub>	Resistance	Nanotubular morphology facilitates	LR = 10-80 ppm	[93]

	(Gas)				adsorption/desorption		
Bisphthalocyanine and PPy	Electrochemical (Gas)	NH <sub>3</sub> and Putrescine	Voltammetry	Coordination interaction between Fe and nitrogen atoms of NH <sub>3</sub>	DL = 1.85 μM (NH <sub>3</sub> ) and 0.34 μM (putrescine)	[94]	
Au NPs/over-oxidized PPy (o-PPy) composite	Electrochemical (Biomolecule)	DA	SWV	Increased surface area by Au NPs and electrostatic interactions	LR = 25 nM - 2.5 μM	[96]	
PPy/Graphene quantum dots (GQD) core/shell composite	Fluorescent sensors (Biomolecule)	DA	Fluorescent intensity	Synergistic effect from Lamellar arrangement of G, conductivity of PPy and biocompatibility	LR = 5-8000 nM DL = 10 pM	[97]	
PPy-NiO NC	Electrochemical (Biomolecule)	Glu	CA	High surface area of NiO and conductivity of PPy	LR = 0.01-0.50 mM and 1-20 mM DL = 0.33 and 5.77 μM	[98]	
PPy/Cu <sub>2</sub> O NC	Electrochemical (Biomolecule)	Glu	CV	Good stability of Cu <sub>2</sub> O/PPy electrode over a wider potential window	-	[99]	
PPy/Pt NC	Electrochemical (Biomolecule)	H <sub>2</sub> O <sub>2</sub>	CA	-	LR = 500–6300 μm DL = 0.6 μm	[100]	
Prussian blue/hollow PPy (PB/H-PPy) NCs	Electrochemical (Biomolecule)	H <sub>2</sub> O <sub>2</sub>	Amperometry	Catalytic activity improvement by PB and large surface area of hollow structure of PPy	LR = 5.0 μM to 2.775 mM DL = 1.6 μM	[101]	
PPy-Cu NPs composite	Electrochemical (Biomolecule)	H <sub>2</sub> O <sub>2</sub>	CA	A combination of electro reduction and chemical reduction involving PPy and Cu ions	LR = 0.2 mM to 1 mM DL = 0.9 μm	[102]	
PPy/bidentate bis-N heterocyclic ligand	Electrochemical (Ion)	Hg <sup>2+</sup>	Nernstian response	Selective complexation between Hg <sup>2+</sup> and the ligand functionalized PPy	LR = 1.0 × 10 <sup>-6</sup> to 1.0 × 10 <sup>-2</sup> M DL = 2.5 × 10 <sup>-7</sup> M	[103]	
PPy coated with Pt NPs	Electrochemical (Ion)	Hg <sup>2+</sup>	DPV	Increased conductivity by Pt and pores in the PPy/Pt NC	LR = 5 to 500 nM DL = 0.27 nM	[104]	
Cysteine-Functionalized GO/PPy NC	Electrochemical (Ion)	Pb <sup>2+</sup>	DPV	High affinity to Pb <sup>2+</sup> and good electron transfer properties of rGO	LR = 1.4-28 ppb, 28-280 ppb and 280-14 000 ppb	[105]	
PPy-ZnO NC	Optical (Ion)	Mn <sup>2+</sup>		Shift in the resonance wavelength by ZnO	-	[106]	

	Phytic acid functionalized PPy/GO NC	Electrochemical (Ion)	Cd <sup>2+</sup> and Pb <sup>2+</sup>	DPV	Synergistic effective form the negative charges on phytic acid and high surface area of rGO	LR = 5-150 µg/L	[107]
Grafted PPy	PPy-grafted N-doped G (PPY-g-NGE)	Electrochemical (herbicides)	Paraquat (PQ)	DPV	Covalent bonding between PPy and NGE	LR = 5.00 × 10 <sup>-8</sup> to 2.00 × 10 <sup>-6</sup> M DL = 41 nM and 58 nM	[108]
	Immobilized Pt particle decorated conducting-polymer (3-carboxylate PPy) NPs	Electrochemical (Biomolecule)	DA	FET	π-π interactions and electrocatalysis by Pt		[109]
Biofunctionalized PPy	PPy-cellulose nanocrystal composite	Electrochemical (Biomolecule)	Glu		Synergistic effects	DL = 50 ± 10 µM	[113]
	N-(p-benzoic acid)PPy (NpbPPy)/GOx	Electrochemical (Biomolecule)	Glu	Amperometry	-	LR = 0 - 9.2 M DL = 1x10 <sup>-6</sup> M	[114]
	Functionalization of PPy with (N-(2-carboxyl-ethyl)-N'-(4-vinylbenzyl)-4,4'-bipyridinium dichloride (CVV)/GOx	Electrochemical (Biomolecule)	Glu	CV and Amperometry	Electron transfer mediation of CVV between the electrode and enzyme	LR = 0-20 mM	[115]
	PPy NT/GOx	Electrochemical (Biomolecule)	Glu	Amperometry	Electrostatic interaction involving the negative charge at the end of pedant groups	LR = 0.2-13 mM DL = 50 µM	[116]
	Cyt-C/α-COOH-PPy	Electrochemical (Biomolecule)	H <sub>2</sub> O <sub>2</sub>	EIS	Under applied negative potentials , interaction between cyt-C and negatively charged polymer surface	LR = 1-200 µmol <sup>-1</sup> DL = 0.25 µmol <sup>-1</sup>	[117]
	Ribonucleic acids (RNAs)-PPy	Electrochemical (Oligonucleotide)	microRNA (mir-21)	EIS	Increased hybridization due to doping of antimir-21	DL = 0.17 nM	[118]
	Copolymer of 1-(Pthalimidyl butanate)-1-N-(3-butyl pyrrole) butamide) ferrocene and pyrrole	Electrochemical (Oligonucleotide)	DNA	CV	Electrochemical property of ferrocenyl group	Detection limit = 0.05 fmol	[119]
	Oligonucleotides (ODNs) grafted poly(pyrrole-co-4-(3-pyrrolyl)butanoic acid	Electrochemical (Oligonucleotide)	DNA	EIS and CV	-	-	[120]
	Biotinylated pyrrole derivative	Optical (Oligonucleotide)	DNA	SPR imaging ECL	Electroconductivity of the PPy derivatives was exploited to trigger the electrochemiluminescence of the	-	[121]

					DNA sequence labeled with a luminol derivative		
2,5-bis(2-thienyl)- <i>N</i> -(3-phosphorylpropyl)pyrrole modified with phosphoric acid (pTPTC3-PO <sub>3</sub> H <sub>2</sub> ) films	Optical (virus)	Short target DNA (18- and 27-mer)	label-free CV		Increase of negative charges at the barrier due to the formation of the double helix during hybridization and variation of spacer length from polymer backbone	DL = 1.82x10 <sup>-21</sup> molL <sup>-1</sup>	[122]
Redox acridone derivative (RAD)/PPy derivative film containing <i>N</i> -hydroxysuccinimide groups	Electrochemical (Virus)	West Nile virus cDNA	Amperometry		Hybridization between two oligonucleotides (dsDNA-ssDNA) through "fishing" out the duplex	DL = 90 fM	[123]
Self-assembled monolayers (SAMs) of Au NPs (GNPs)-PPy and biofunctionalized with monoclonal anti-SOD1 antibody	Electrochemical (immunosensor)	Superoxide dismutase 1	CV		Eliminates the need for secondary antibody	LR = 0.5 nM - 5 μM, DL = 0.5 nM	[125]
Amino-functionalized silica NPs ( <i>n</i> -SiNPs)-PPy NC	Electrochemical (immunosensor)	Melanocortin 1 receptor (MC1R) antigen and anti-MC1R antibody (MC1R-Ab)	CV		-	-	[126]
PPy intercalated G	Electrochemiluminescence (immunosensor)	CA72-4 (the tumor biomarker)	ECL intensity		Good conductivity, catalytic activity and large surface area of the NC	LR = 10 <sup>-4</sup> to 20 U/mL DL = 2.1 × 10 <sup>-5</sup> U/mL	[127]
PPy functionalized with ω-( <i>N</i> -pyrrolyl)-octylthiol	Optical (Protein)	Bovine serum albumin (BSA)	SPR		Blocking behaviour	-	[128]
<i>N</i> -substituted nitrilotriacetic acid (NTA) PPy film (PNTA)	Electrochemical (Herbicide)	Atrazine	EIS		P(NTA) enabled successive coordination of Cu <sup>2+</sup> and histidine tagged IgG atrazine antibody by affinity interactions	LR = 10 pg mL <sup>-1</sup> - 1 μg mL <sup>-1</sup> DL = 10 pg mL <sup>-1</sup>	[129]
Ferrocenyl-substituted PPy	Electrochemical (Ion)	Trimethylamine (fish freshness)	EIS and Amperometry		Electrochemical oxidation signal of the ferrocenyl groups	LR = 0.4 - 80 μg mL <sup>-1</sup> DL = 0.4 μg mL <sup>-1</sup>	[130]
PPy-containing vitamin B <sub>12</sub>	Electrochemical (Ion)	Thiocyanate	Potentiometry		Cobalt coordination with anions of interest	LR = upto 1.0x10 <sup>-4</sup> M	[131]

						DL = $1 \times 10^{-5}$ M	
	Ultrathin PPy-GOx	Electrochemical (Ions)	Hg <sup>2+</sup> , Cu <sup>2+</sup> , Pb <sup>2+</sup> and Cd <sup>2+</sup>	Amperometry	-	LR = 0.48-3.3 $\mu$ M (Hg <sup>2+</sup> ), 1.5-10 $\mu$ M (Cu <sup>2+</sup> ), 1.6-7.7 $\mu$ M (Pb <sup>2+</sup> ), and 4-26 $\mu$ M (Cd <sup>2+</sup> ).	[133]
	Ultrathin PPy-GOx	Electrochemical (Ions)	Cu <sup>2+</sup> , Hg <sup>2+</sup> , Cd <sup>2+</sup> and Pb <sup>2+</sup> ion	Potentiometry	Interaction between thiol group of GOx and metal ions	LR = Cu <sup>2+</sup> (0.079-16 $\mu$ M), Hg <sup>2+</sup> (0.025-5 $\mu$ M), Pb <sup>2+</sup> (0.10-15 $\mu$ M) and Cd <sup>2+</sup> (0.04-62 $\mu$ M)	[132]
	PPy/K <sup>+</sup> -specific G-rich aptamer	Electrochemical (Ion)	K <sup>+</sup>	EIS	Guanin rich base increases the K <sup>+</sup> sensitivity	LR = 20 fM - 1 mM, DL = 14.7 fM	[134]
Nanostructured F-PPy	PPy-COOH NTs biofunctionalized with heparin	Electrochemical (Protein)	Thrombin	Current/resistance	Decrease in the charge carrier density of PPy-COOH NTs by screening the negative charge of heparin.	-	[141]
	Amine-terminated thrombin aptamers bound PPy-COOH NTs	Electrochemical (Protein)	Thrombin	Drain to source current	Dipole-dipole or dipole-charge interactions between thrombin and the aptamer-conjugated polymer chains	-	[138]
	PPy-COOH NTs biofunctionalized with Hsp 90 aminoacid residues	Electrochemical (Protein)	Heat shock protein 90 (Hsp90)	Liquid-ion gated FET current change	Affinity between Hsp90 and Hsp90 inhibitors	-	[137]
	PPy-COOH NTs Anti-Vascular Endothelial Growth Factor (VEGF) RNA aptamer conjugated	Electrochemical (Virus)	VEGF	Resistance	VEGF (target molecule) plays the role of gate dielectric of the p-type FET sensor	DL = 400 fM	[135]
	Poly(ionic liqs.) functionalized PPy NTs (PILs/PPyNTs)	Electrochemical (Biomolecule)	DA and AA	DPV	Good electrocatalytic and surface charge properties	DL = 1.8 mM (DA) and 5.0 mM (AA)	[139]
	rGO-carboxylated PPy (C-PPy) NT	Electrochemical	Glu	FET	C-PPy act as the conducting channel	DL = 1 nM	[143]

		(Biomolecule)			and good interface with G		
GOx functionalized pyrrole-3-carboxylic acid (P3CA) NTs	Electrochemical (Biomolecule)	Glu	Liquid-ion gated FET – drain to source current	-	LR = 0.5-20 mM	[140]	
Receptor protein, hTAS2R38, functionalized PPy-COOH NTs	Electrochemical (taste)	Tastants (Nanobioelectronic tongue (nbe-tongue))	Liquid-ion gated FET – drain to source current	Signal transduction generated through covalent interaction between taste receptor and PPy-COOH NTs	-	[142]	
PPy-COOH NTs conjugated hOR3A1 (nanobioelectronic nose (nbe-nose))	Electrochemical (Odor)	Taste receptors	Current	Increase in the contact area between target molecules and PPy-COOH NTs result a higher density of polaron or bipolaron on the backbone of the PPy-COOH NTs.	DL = 0.02 parts per trillion (ppt)	[136]	
Polyamine-modified PPy open NTs (PPy-NH <sub>2</sub> NTs)	Electrochemical (Gas)	Acetic acid	Resistance	Negatively charged acetate anion compensate the positive charges on the polymer backbone and resultant polarons/bipolarons to result increase in conductivity	-	[145]	
PPy/Ag composite NTs	Electrochemical (Gas)	NH <sub>3</sub>	Resistance	Ag particles provide electron traps and augment uniform diffusion of NH <sub>3</sub> .	-	[146]	
High-oriented single crystal PPy NTs	Electrochemical (Gas)	NH <sub>3</sub>	Resistance	High surface area of PPy-NT and intermolecular interactions	DL = 0.05 ppb	[147]	
PPy-COOH NT transducers	Electrochemical (Gas)	di-Me methylphosphate (DMMP)	Chemiresistive sensing	Hydrogen bonding interactions	DL = 0.5 ppb	[148]	
High density PPy NF	Electrochemical (Biomolecule)	Glu	Amperometry	Good affinity between PPy NF and Glu	LR = 125 μM-11.25 mM	[152]	
PPy NW modified nickel hydroxide nanoflakes (nf-Ni(OH) <sub>2</sub> @oPPyNW)	Electrochemical (Biomolecule)	Glu	CA	The NF surface provides high loading condition for electrocatalytics Ni(OH) <sub>2</sub> flake.	LR = 0.001-4.863 mM DL = 0.3 μM	[153]	
Diphenylalanine peptide NWs (PNWs) functionalized PPy	Electrochemical (Biomolecule)	DA	Amperometry	-	-	[154]	

	Avidin- and streptavidin functionalized PPy NW	Electrochemical (Oligonucleotide)	biotin-DNA,	FET resistance	-	LR = 1-100 nM	[155]
	Covalently linked PPy NWs with cancer antigen (CA 125) antibody	Electrochemical (Cancer antigen)	CA 125	FET conductance	Electrical transduction	LR = upto 1000 U/mL DL = 1 U/mL	[156]
Multicomponents	CS-PPy-NTs/Au NCs	Electrochemical (Biomolecule)	Glu	Amperometry	CS offers biocompatibility to GOx, PPy NT promotes electron transfer and Au attributes to electrocatalysis	LR = 3-230 $\mu$ M DL = 3.10 $\mu$ M	[158]
	PPy (PPy)-Nafion (Nf)-functionalized multi-walled carbon NTs (fMWCNTs) NC	Electrochemical (Biomolecule)	Glu	Amperometry	Nf provides electrochemical stability and good dispersion of fMWCNTs	LR = up to 4.7 mM DL = 5 $\mu$ M	[159]
	PPy-CS-Iron oxide NC	Electrochemical (Biomolecule)	Glu	Amperometry	-	LR = 1-16 mM DL = 234 $\mu$ M	[160]
	NiCo alloy NPs/PPy/rGO NCs	Electrochemical (Biomolecule)	Glu	Amperometry	Electrocatalytic properties by CoOH/Co <sub>2</sub> and NiOOH/Ni(OH) <sub>2</sub>	LR = 0.5 $\mu$ M-4.1 mM DL = 0.17 $\mu$ M	[161]
	Au NPs on NiO coated PPy	Electrochemical (Biomolecule)	Glu	Amperometry	Cyclic mediation redox process involving NiO, Ni(OH) <sub>2</sub> and Glu	LR = 0.5 $\mu$ M to 1.7 mM DL = 0.15 $\mu$ M	[162]
	Cu <sub>x</sub> O/PPy/rGO/GCE NC	Electrochemical (Biomolecule)	Glu	Amperometry	Synerstic contribution from Cu <sub>x</sub> O, PPy and rGO	LR = 0.1-100 mM DL = 0.03 $\mu$ M	[163]
	Gold Nanopillar-functionalized with PPy/GOx	Electrochemical (Biomolecule)	Glu	Amperometry	-	LR = 2.5 – 150 mM	[164]
	Hydrophillic polymers (HPs)/PPy/GO	Electrochemical (Biomolecule)	DA and AA	DPV	Synergistic role of the different hydrophilic groups in HPs and chemical properties	DA LR = 6 – 13 $\mu$ M and 32 – 60 $\mu$ M DL = 0.408 $\mu$ M and 1.025 $\mu$ M AA LR = 150–220 $\mu$ M and 300 – 440 $\mu$ M	[165]

						DL = 0.659 $\mu$ M and 1.962 $\mu$ M	
	rGO/PDDA/PCL@PPy NCs	Electrochemical (Biomolecule)	DA	DPV	Electrochemical conductivity improvement because of good dispersion of rGO into PCL@PPy network	LR = 4 $\mu$ M to 690 $\mu$ M DL = 0.34 $\mu$ M	[166]
	GO/PPy/CdSe NC	Electrochemiluminescence (Biomolecule)	DA	ECL	Reaction between CdSe and sulphate ion radicals, generated by the interaction between GO and PPy	LR = 0.01-16 nM DL = 0.004 nM	[167]
	Poly(zwitterionic liquids) functionalized PPy/GO nanosheets	Electrochemical (Biomolecule)	DA	DPV	The negative charged group in the pendant part of IL and intermolecular charge transfer	DL = 17.3 nM LR = 40-1220 nM	[168]
	Poly(ionic liquids) functionalized PPy/GO nanosheets (PILs/PPy/GO)	Electrochemical (Biomolecule)	DA and AA		Synergistic effects of GO with a lamella structure, conducting of PPy and biocompatibility of IL.		[169]
	Poly(3-carboxylic acid) based on dendrimer boron doped diamond	Electrochemical (Biomolecule)	H <sub>2</sub> O <sub>2</sub>	Amperometry	Minimum electrode fouling	LR = 5 $\mu$ M ~ 49 mM DL = 2 $\mu$ M	[170]
	Fe <sub>3</sub> O <sub>4</sub> /PPy/Ag NCs	Electrochemical (Biomolecule)	H <sub>2</sub> O <sub>2</sub>	Amperometry	Synergistic contributions from the components of NC	LR = 5 $\mu$ M to 11.5 mM DL = 1.7 $\mu$ M	[172]
	Ag@PPy/Polycaprolactum@PPy	Electrochemical (Biomolecule)	H <sub>2</sub> O <sub>2</sub>	Amperometry	Synergistic effect of the components	LR = 0.01mM to 3.5mM DL = 1 $\mu$ M	[171]
	AMP-PPyNFs-AgNPs-rGO	Electrochemical (Biomolecule)	H <sub>2</sub> O <sub>2</sub>	Amperometry	NFs provide high surface area for reduction of H <sub>2</sub> O <sub>2</sub>	LR = 0.1-5 mM DL = 1.099 $\mu$ M	[173]
	MWCNTs-PPy-PAMAM-Fc NC	Electrochemical (Oligonucleotide)	DNA	CV and SWV	Nonspecific interactions provided by wrapping of MWCNTs with PPy and functionalization of PAMAM	DL = 0.3 fM	[174]
	DNA hybridized integrated PPy-Au NP composite	Electrochemical (Oligonucleotide)	DNA	CA	-	LR = 150 pM – 1 $\mu$ M	[175]
	Thiolated probe DNA immobilized Ag NPs-functionalized PPy-PANI NTs	Electrochemical (Oligonucleotide)	DNA	DPV	Combination of PPy-PANI and Au NPs increased the conductance	LR = 1x10 <sup>-6</sup> M – 1x10 <sup>-13</sup> M DL = 1.0x10 <sup>-3</sup> M	[176]

HS-ssDNA immobilized Ag NPs-functionalized PPy-PEDOT NTs	Electrochemical (Oligonucleotide)	DNA	EIS	Combination of high surface area, conductivity and catalytic efficiency was achieved through multicomponents	-	[177]
ChOx/ChEt immobilized PPy-MWNT NC	Electrochemical (Biomolecule)	cholesterol	DPV	PPy-MWNT accept electrons from oxidation of ChEt and ChOx-Effective charges facilitate the electrical contact between enzyme and electrode	DL = 0.04 mM	[178]
Multienzyme-antibody functionalized gold nanorod (GNR)- PPy film	Electrochemical (antibiotic)	Ofloxacin	CV	Au-clusters/PPy captures large amount of OFL-antigen and GNRs-allow the loading of large number of HRP molecules	LR = 0.08 – 410 ng/L DL = 0.03 ng/L	[179]
PPy/Pectin/G NCs	Electrochemical (Ion)	Hg <sup>2+</sup>	DPV	Interaction between PPy and pectin	DL = 4 fM	[180]
PPy-CS-cobalt ferrite NPs composite layer	(Ion)	Ar(V)	SPR	Defects induced ferromagnetism	DL = 0.001 ppm	[181]
TiO <sub>2</sub> @PPy-G nanoplates (GN) NC	Electrochemical (Gas)	NH <sub>3</sub>	Resistance	p-n junction formation between PPy and GN and large surface area of the NC	-	[182]
Multisegmented Au-PPy-Ni-Au NWs	Electrochemical (Gas)	NH <sub>3</sub>	Resistance	Magnetic dipole interactions between Ni segment of the NW and electrode	DL = 75 ppm	[183]
SnO <sub>2</sub> -ZnO/PPy coaxial nanocables	Electrochemical (Gas)	NH <sub>3</sub>	Resistance	Interaction between positive charges along PPy chains and surrounding environment resulted increase in conductivity	LR = 10 - 85 ppm	[184]
CSA doped PPy-NiO hybrid NC	Electrochemical (Gas)	NO <sub>2</sub>	Resistance	Creation of more active sites for gas adsorption	LR = 66-100% ppm	[186]
DBSA doped PPy-WO <sub>3</sub> hybrid NC	Electrochemical (Gas)	NO <sub>2</sub>	Resistance	-	LR = 5-100 ppm	[185]

	p-TSA doped silver-PPy NC	Electrochemical (Gas)	NO <sub>2</sub>	Resistance	Porous structure and faster charge transfer	LD = 5 ppm	[188]
	Pd-doped TiO <sub>2</sub> @PPy core-shell composites	(Gas)	H <sub>2</sub>	Resistance	-	LR = 0.005 to 2.5 vol% DL = 0.001vol%	[189]
	Zinc oxide-incorporated PPy (PPy/ZnO) - ultrasound assisted in situ miniemulsion polymerization	Electrochemical (Gas)	LPG	Resistance	Generation of p-n junction	-	[190]
	Zinc oxide-incorporated PPy (PPy/ZnO) - ultrasound assisted in situ miniemulsion polymerization	Electrochemical (Biomolecule)	H <sub>2</sub> O <sub>2</sub>	Amperometry	Inner sphere electron transfer involving Fe(II)/(III)	-	[191]

\*If available in the reference paper

LR- Linear Range; DL – Detection Limit

AA – ascorbic acid; CA – Chrono amperometry; CV – Cyclic voltammetry; DA – Dopamine; DPV – Differential pulse voltammetry; ECL – Electro chemiluminescence; EIS – Electrochemical impedance spectroscopy; FET – Field effect transistor; Glu – Glucose; SPR – Surface Plasmon resonance; SWSV – square wave stripping voltammetry

Table 2. Cross-sectional details on the signal transduction mode based sensors utilizing the four functionalization categories of polypyrroles(F-PPys)

Sensor signal transduction mode	Mode of Parent structure functionalization/ modification	Name of FCP (abbreviation) or functional structure in the FCP	Specific analyte(s)
Electrochemical	Substituted derivatized	PPy functionalized with 5,10,15,20-tetraphenyl-21H,23H-porphyrin iron(III) chloride	CO[65]
		PPy functionalized with copper thalocyanine	Methanol, NH <sub>3</sub> , and NO <sub>2</sub> [66]
		3-(1 <i>H</i> -pyrrol-1-yl)phenyl boronic acid-substituted PPy	Saccharides[68]
		PNCEPy and Poly(N-methyl) pyrrole (PNMPy)	DA [69]
		PPy/ $\beta$ -cyclodextrin	Polyhydroxyphenyls and neurotransmitters (epinephrine, metanephrine, and l-dopa (l-3,4-dihydroxyphenylalanine)) [70]
		Ferrocenylmethyl trialkylammonium derivatives of PPy	Dihydrogenphosphate and adenosine triphosphate (ATP) anions[71]
		Rhodamine derivative of PPy	Cu <sup>2+</sup> [72]
	Poly(11-N-pyrrolylundecanoic) acid and poly(N-undecylpyrrole)	Protons (pH) [73]	
	Functional ion-dopant inclusion	Phthalocyanine doped PPy	NO <sub>2</sub> [76]
		N-sulfonated cobalt phthalocyanines doped Ppy	NH <sub>3</sub> [77]
		ferrocenylmethyltrimethyl ammonium iodide (FTMA-I) doped PPy	CO[79]
		PPy-zirconium(IV)selenoiodate cation exchange NC	Formaldehyde[80]
		Hydroquinone sulfonate (HQS)-doped PPy	Proton (pH) [81]
	Functional compound inclusion	Alizarin Red S doped PPy	Ag <sup>+</sup> [83]
		PPy (PPy)-reduced graphene oxide (rGO) hybrid	NH <sub>3</sub> [88]
		PPy/ZnO nanohybrid	NH <sub>3</sub> [89]
		PPy/ZnO NC	NH <sub>3</sub> [90]
		PPy-coated SnO <sub>2</sub> NCs	NH <sub>3</sub> [91]
		PPy-tin oxide hybrid	NH <sub>3</sub> [92]
	PPy/metal oxide NCs	NH <sub>3</sub> [93]	
	Bisphthalocyanine and PPy	NH <sub>3</sub> and Putrescine[94]	

		Au NPs/over-oxidized PPy (o-PPy) composite	DA[96]
		PPy-NiO NC	Glu[98]
		PPy/Cu <sub>2</sub> O NC	Glu[99]
		PPy/Pt NC	H <sub>2</sub> O <sub>2</sub> [100]
		Prussian blue/hollow PPy (PB/H-PPy) NCs	H <sub>2</sub> O <sub>2</sub> [101]
		PPy-Cu NPs composite	H <sub>2</sub> O <sub>2</sub> [102]
		PPy/bidentate bis-N heterocyclic ligand	Hg <sup>2+</sup> [103]
		PPy coated with Pt NPs	Hg <sup>2+</sup> [104]
		Cysteine-Functionalized GO/PPy NC	Pb <sup>2+</sup> [105]
		Phytic acid functionalized PPy/GO NC	Cd <sup>2+</sup> and Pb <sup>2+</sup> [107]
	Grafted PPy	PPy-grafted N-doped G (PPY-g-NGE)	Paraquat (PQ) [108]
		Immobilized Pt particle decorated conducting-polymer (3-carboxylate PPy) NPs	DA[109]
	Biofunctionalized PPy	PPy-cellulose nanocrystal composite	Glu[113]
		N-(p-benzoic acid)PPy (NpbPPy)/GOx	Glu[114]
		Functionalization of PPy with (N-(2-carboxyl-ethyl)-N'-(4-vinylbenzyl)-4,4'-bipyridinium dichloride (CVV)/GOx	Glu[115]
		PPy NT/GOx	Glu[116]
		Cyt-C/α-COOH-PPy	H <sub>2</sub> O <sub>2</sub> [117]
		Ribonucleic acids (RNAs)-PPy	microRNA (mir-21) [118]
		Copolymer of 1-(Pthalimidyl butanate)-1-N-(3-butyl pyrrole) butamide) ferrocene and pyrrole	DNA[119]
		Oligonucleotides (ODNs) grafted poly(pyrrole-co-4-(3-pyrrolyl)butanoic acid	DNA[120]
		Redox acridone derivative (RAD)/PPy derivative film containing N-hydroxysuccinimide groups	West Nile virus cDNA[123]
		Self-assembled monolayers (SAMs) of Au NPs (GNPs)-PPy and biofunctionalized with monoclonal anti-SOD1 antibody	Superoxide dismutase [125]
		Amino-functionalized silica NPs (n-SiNPs)-PPy NC	Melanocortin 1 receptor (MC1R) antigen and anti-MC1R antibody (MC1R-Ab) [126]
		PPy intercalated G	CA72-4 (the tumor biomarker) [127]
		N-substituted nitrilotriacetic acid (NTA) PPy film (PNTA)	Atrazine[128]
		Ferrocenyl-substituted PPy	Trimethylamine (fish freshness) [129]
		PPy-containing vitamin B <sub>12</sub>	Thiocyanate [130]
		Ultrathin PPy-GOx	Hg <sup>2+</sup> , Cu <sup>2+</sup> , Pb <sup>2+</sup> and Cd <sup>2+</sup> [131]
		Ultrathin PPy-GOx	Cu <sup>2+</sup> , Hg <sup>2+</sup> , Cd <sup>2+</sup> and Pb <sup>2+</sup> ion [132]

		PPy/K <sup>+</sup> -specific G-rich aptamer	K <sup>+</sup> [133]	
Nanostructured F-PPy		PPy-COOH NTs biofunctionalized with heparin	Thrombin[141]	
		Amine-terminated thrombin aptamers bound PPy-COOH NTs	Thrombin[138]	
		PPy-COOH NTs biofunctionalized with Hsp 90 aminoacid residues	Heat shock protein 90 (Hsp90) [137]	
		PPy-COOH NTs Anti-Vascular Endothelial Growth Factor (VEGF) RNA aptamer conjugated	VEGF[135]	
		Poly(ionic liqs.) functionalized PPy NTs (PILs/PPyNTs)	DA and AA[139]	
		rGO-carboxylated PPy (C-PPy) NT	Glu[143]	
		GOx functionalized pyrrole-3-carboxylic acid (P3CA) NTs	Glu[140]	
		Receptor protein, hTAS2R38, functionalized PPy-COOH NTs	Tastants (Nanobioelectronic tongue (nbe-tongue)) [142]	
		PPy-COOH NTs conjugated hOR3A1 (nanobioelectronic nose (nbe-nose))	Taste receptors[136]	
		Polyamine-modified PPy open NTs (PPy-NH <sub>2</sub> NTs)	Acetic acid[145]	
		PPy/Ag composite NTs	NH <sub>3</sub> [146]	
		High-oriented single crystal PPy NTs	NH <sub>3</sub> [147]	
		PPy-COOH NT transducers	di-Me methylphosphonate (DMMP) [148]	
		High density PPy NF	Glu[152]	
		PPy NW modified nickel hydroxide nanoflakes (nf-Ni(OH) <sub>2</sub> @oPPyNW)	Glu[153]	
		Diphenylalanine peptide NWs (PNWs) functionalized PPy	DA[154]	
		Avidin- and streptavidin functionalized PPy NW	biotin-DNA, [155]	
		Covalently linked PPy NWs with cancer antigen (CA 125) antibody	CA 125[156]	
	Multicomponents		CS-PPy-NTs/Au NCs	Glu[158]
			PPy (PPy)-Nafion (Nf)-functionalized multi-walled carbon NTs (fMWCNTs) NC	Glu[159]
		PPy-CS-Iron oxide NC	Glu[160]	
		NiCo alloy NPs/PPy/rGO NCs	Glu[161]	
		Au NPs on NiO coated PPy	Glu[162]	
		Cu <sub>2</sub> O/PPy/rGO/GCE NC	Glu[163]	
		Gold Nanopillar-functionalized with PPy/GOx	Glu[164]	
		Hydrophilic polymers (HPs)/PPy/GO	DA and AA[165]	
		rGO/PDDA/PCL@PPy NCs	DA[166]	
		Poly(zwitterionic liquids) functionalized PPy/GO nanosheets	DA[168]	
		Poly(ionic liquids) functionalized PPy/GO nanosheets (PILs/PPy/GO)	DA and AA[169]	
		Poly(3-carboxylic acid) based on dendrimer boron doped diamond	H <sub>2</sub> O <sub>2</sub> [170]	
		Fe <sub>3</sub> O <sub>4</sub> /PPy/Ag NCs	H <sub>2</sub> O <sub>2</sub> [172]	

		Ag@PPy/Polycaprolactum@PPy	H <sub>2</sub> O <sub>2</sub> [171]
		AMP-PpyNFs-AgNPs-rGO	H <sub>2</sub> O <sub>2</sub> [173]
		MWCNTs-PPy-PAMAM-Fc NC	DNA[174]
		DNA hybridized integrated PPy-Au NP composite	DNA[175]
		Thiolated probe DNA immobilized Ag NPs-functionalized PPy-PANI NTs	DNA[176]
		HS-ssDNA immobilized Ag NPs-functionalized PPy-PEDOT NTs	DNA[177]
		ChOx/ChEt immobilized PPy-MWNT NC	cholesterol[178]
		Multienzyme-antibody functionalized gold nanorod (GNR)- PPy film	Ofloxacin[179]
		PPy/Pectin/G NCs	Hg <sup>2+</sup> [180]
		PPy-CS-cobalt ferrite NPs composite layer	Ar(V) [181]
		TiO <sub>2</sub> @PPy-G nanoplates (GN) NC	NH <sub>3</sub> [182]
		Multisegmented Au-PPy-Ni-Au NWs	NH <sub>3</sub> [183]
		SnO <sub>2</sub> -ZnO/PPy coaxial nanocables	NH <sub>3</sub> [184]
		CSA doped PPy-NiO hybrid NC	NO <sub>2</sub> [186]
		DBSA doped PPy-WO <sub>3</sub> hybrid NC	NO <sub>2</sub> [185]
		p-TSA doped silver-PPy NC	NO <sub>2</sub> [188]
		Pd-doped TiO <sub>2</sub> @PPy core-shell composites	H <sub>2</sub> [189]
		Zinc oxide-incorporated PPy (PPy/ZnO) - ultrasound assisted in situ miniemulsion polymerization	LPG[190]
		Zinc oxide-incorporated PPy (PPy/ZnO) - ultrasound assisted in situ miniemulsion polymerization	H <sub>2</sub> O <sub>2</sub> [191]
Optical	Functional compound inclusion	PPy-ZnO NC	Mn <sup>2+</sup> [106]
	Biofunctionalized PPy	Biotinylated pyrrole derivative	DNA[121]
		2,5-bis(2-thienyl)-N-(3-phosphorylpropyl)pyrrole modified with phosphoric acid (pTPTC3-PO <sub>3</sub> H <sub>2</sub> ) films	Short target DNA (18- and 27-mer) [122]
		PPy functionalized with ω-(N-pyrrolyl)-octylthiol	Bovine serum albumin (BSA) [128]
Others	Substituted derivatized	3-alkyl substituted PPy	Hexane, toluene, water, acetonitrile, triethylamine, butanal, methanol, ethanol, butan-1-ol, hexan-1-ol, and nonan-1-ol[60]
		Poly(N-2(cyanoethyl)pyrrole) (PNCEPy), Poly (N-2-cyano methyl pyrrole) (PNCMPy)	Gas molecules of different solvents (i.e., water, methanol, acetonitrile, and chloroform) [67]

	Functional ion-dopant inclusion	Dodecylsulfate (DS)-doped Ppy	Benzene, ethyl benzene, toluene, and 1,3,5-trimethylbenzene[78]
		Tiron doped PPy	Fe <sup>3+</sup> [82]
	Functional compound inclusion	PPy/Graphene quantum dots (GQD) core/shell composite	DA[97]
	Multicomponents	GO/PPy/CdSe NC	DA[167]

\*If available in the reference paper

AA – ascorbic acid; DA – Dopamine; Glu – Glucose

**Table 3. Functionalized polyanilines (F-PANI) for sensors and related details: Functionalization approach, name of F-PANI, type of sensor (based on analyte), analyte(s) name, detection technique, role of F-PANI for sensing and sensor performances.**

Mode of Parent structure functionalization/modification	Name of FCP (abbreviation) or functional structure in the FCP	Type of sensor (Analyte)	Specific analyte(s)	Detection method/Technique	Function/Role of FCP for sensing*	Sensor performances* (LR and DL)	Ref
Substituted / derivatized PANI	Poly(2-Bromo aniline), Poly(2-Chloro aniline), Poly(3-Chloro aniline), Poly(4-Chloro aniline), Poly(o-toluidine), Poly(m-toluidine), Poly(p-toluidine), Poly(N-methyl aniline) (PNMA) and Poly (diphenyl amine)	Optical (Ion)	Proton (pH)	UV	Transformation of blue emeraldine base to protonated emeraldine green form	-	[193]
	Poly(diphenyl amine) (PDPA)	Optical (Ion)	pH	UV	Difference in redox characteristics of PDPA as compared to PANI	LR = 2-13 pH	[194]
	Poly(diphenyl aminesulfonic acid) (PDSA)	Electrochemical (Ion)	Humidity	EIS	Ion transport via doped ions	LR = 0 - 95% RH	[195]
	Imidazole substituted PANI	Electrochemical (Ion)	Pb <sup>2+</sup>	DPV	Complexation with IMPANI	DL = 20 ngmL <sup>-1</sup> (carbon paste) DL = 2 ngmL <sup>-1</sup> (carbon)	[196]
	Rhodamine 6G derivative(RS) of PANI	Photo Electrochemical (Ion)	Hg <sup>2+</sup>	Photo voltage measurement	Photon excitation of electron from the RS-Hg <sup>2+</sup> complex.	LR = 10-150 µg L <sup>-1</sup> DL = 0.2 µg L <sup>-1</sup>	[197]
	PANI-pseudo-polyrotaxane (PANI-β-CDpNH <sub>2</sub> )	Electrochemical (Ion)	Pb <sup>2+</sup>	EIS	PANI conformational changes and spatial hindrances by Pb <sup>2+</sup>	DL = 31 ppm	[199, 198]
	Poly(diphenylamine-co-2-aminobenzonitrile) (P(DPA-co-2ABN))	Electrochemical (Ion)	Cd <sup>2+</sup> and Pb <sup>2+</sup>	DPV	CN <sup>-</sup> groups in PDPA film coordinate with heavy metal ions(Cd <sup>2+</sup> and Pb <sup>2+</sup> ) and improved the preconcentration	LR Cd <sup>2+</sup> = 1.26–907.8 ppm Pb <sup>2+</sup> = 0.26–58.73 ppm DL Cd <sup>2+</sup> = 0.255 ppm Pb <sup>2+</sup> = 0.165 ppm	[200]

	PNMA, Poly (N-ethyl aniline), Poly (2,3 dimethyl aniline), Poly (2,5 dimethyl aniline) and Poly (diphenyl amine)	Electrochemical (ion)	pH	Resistance	Sensing is governed by chain length of alcohol, its chemical structure and structural arrangements of polymeric chains	-	[201]
Functional ion-dopant inclusion	PANI doped with hexafluoroisopropanol (HFIP)	Electrochemical (Gas)	Hydrazine	Resistance	Interactions between HFIP and hydrazine results in conductance changes- HF was proposed to be generated through the exchange of fluorine atoms on HFIP with hydrogen from hydrazine	-	[210]
	Dodecylbenzene sulphonic acid (DBSA)/Potassium dichromate PANI	Electrochemical (Gas)	NH <sub>3</sub>	Resistance	Multiple oxidation state of dichromate	-	[211]
	PANI-HCl with polyethylene terphthalate	Optical (Gas)	NH <sub>3</sub>	UV	oxidation degree of PANI – the analyte extracts the dopant from the sensor film and withdraws protons from the PANI chains	LR = 5 – 200 ppm and 200 – 920 ppm	[212]
	Diocetyl sodium sulfosuccinate doped PANI	Optical (Gas)	Various alcohols	Optical spectrum analyze (microfiber)	Optical responses associated with the changes in refractive index of microfiber and number of alkyl substituent of alcohol	-	[213]
	Doped PANI-poly(vinyl alcohol) composite membrane	Electrochemical (Gas)	Aliphatic alcohols	Resistance	Structural order alignment between PANI and PVA result in interaction with –OH group of alcohols	-	[214]
	Sulfonated PANI (SPAN)	-	CO <sub>2</sub>	Molecular model	-	LR = [10 <sup>2</sup> , 10 <sup>4</sup> ] ppm	[215]
	Cupric ion doped PANI (Cu <sup>2+</sup> /PANI) hybrid	Optical (Biomolecule)	Glu	O-dianisidine indicator- UV-visible spectroscopy	Oxidative interaction between Glu and Cu <sup>2+</sup>	LR = 50 mg/dL - 200 mg/dL	[216]
	Polyoxometalate-(POM) doped PANI	Electrochemical (Biomolecule)	H <sub>2</sub> O <sub>2</sub>	Flow injection	Multiple redox reaction of POM	LR = 0.1 mM – 20 mM	[217]
	NPs (Ag NPs)-doped PANI (PANI)	Electrochemical immunosensor (Biomolecule)	Polychlorinated biphenyl (PCB)	SWV	Enamine formation through interaction with glutaraldehyde and changing to amine form upon addition of antibody	LR= 0.2 -1.2 ng mL <sup>-1</sup> DL= 0.063 ng mL <sup>-1</sup>	[218]
PANI doped with dinonylnaphthalene	Electrochemical	K <sup>+</sup>	Prift voltage	-	-	[219]	

	sulfonic acid (PANI-DNNSA)	(Ion)		shift			
	Sodium dodecyl sulfate doped PANI	Electrochemical (Ion)	Hg <sup>2+</sup>	Square wave anodic stripping voltammetry	Adsorption of Hg <sup>2+</sup> ions at pH 4.5 onto PANI-SDS film	DL = 2.4 nM	[220]
Functional component inclusion	SWNTs-poly(m-aminophenyl sulfonic acid) (PMABS)	Electrochemical (Gas)	NH <sub>3</sub>	Resistance	Proton transfer from self-doped PMABS to result in zwitter ionic form	-	[222]
	PANI-SWNTs	Electrochemical (Gas)	NH <sub>3</sub>	Resistance	NH <sub>3</sub> adsorption onto polymer and withdrawal of protons from -N-H sites to form -NH <sub>4</sub> <sup>+</sup> and deprotonation in PANI	LR = 50 ppb - 30 ppm	[222]
	PANI-SWNTs	Electrochemical (Gas)	NH <sub>3</sub> , NO <sub>2</sub> , and H <sub>2</sub> S	FET Resistance	Deprotonation of N <sup>+</sup> -H sites of the PANI emeraldine salt to form NH <sub>4</sub> <sup>+</sup> conductivity changes with the transfer of $\pi$ electrons from PANI to NO <sub>2</sub>	-	[223]
	SWNT and PANI	Electrochemical (Gas)	Dimethyl-methyl-phosphonate (DMMP)	Mass flow controller - Resistance	Adsorption of DMMP at interface between SWNT and PANI-electron transfer and resistance changes	LR = 1 ppm - 5 ppm	[224]
	Plasma-treated MWNT/PANI (pf MWNT/PANI)	Electrochemical (Gas)	NH <sub>3</sub>	FET Resistance	Formation of hydrogen bonds between polar NH <sub>3</sub> molecules and oxygen contain defects of MWNT-binding through defective sites in CNT	LR = 0-100 ppm	[225]
	PANI/ carboxylic acid-functionalized MWNT (c-MWNT) (PANI/ c-MWNT)	Electrochemical (Vapour)	Chloroform	Resistance	Dipole interactions of PANI with chloroform molecules facilitated the electron delocalization and charge transport and decreased the resistance change in the oxidation state of PANI-MWNT composite	-	[226]
	PANI-wrapped MWNT	Electrochemical (Gas)	NO <sub>2</sub>	Integrated micro-supercapacit	Patterned G and enhancement of hole concentration	-	[227]

				or (MSC). Voltametric capacitance			
PANI/GO composite	Electrochemical (Vapour)	Methanol	Resistance	Hydrogen bonding interaction between methanol and the polymer chain	LR = 100-500 ppm	[228]	
S and N co-doped GQD/PANI hybrid	Electrochemical (Gas)	NH <sub>3</sub>	Resistance	Reversible acid-base doping- dedoping processes. QCD enhances the interaction between NH <sub>3</sub> and PANI	Detection range = 50 ppB - 1 ppm	[230]	
rGO-PANI hybrid	Electrochemical (Gas)	NH <sub>3</sub>	Resistance	Large surface area of NC enhanced adsorption/desorption of NH <sub>3</sub> , high electron carrier mobility and electron transfer between rGO and PANI	-	[232]	
Gold-PANI Composite	Electrochemical (Gas)	NH <sub>3</sub>	Resistance	Semi-covalent dative bond between Au and PANI	LR = 20 ppm – 250 ppm	[233]	
PANI/ZnO hybrid	Electrochemical (Gas)	NH <sub>3</sub>	Resistance	Porous structure of NR and high aspect ratio of ZnO NR, ZnO and PANI form p-n junction	Detection range = 10 – 50 ppm	[234]	
Cu NP-PANI NC	Electrochemical (Gas)	NH <sub>3</sub>	Resistance	Protonation-deprotonation process	Detection range = 10 – 100 ppm	[235]	
[(PANIS) <sub>x</sub> MoO <sub>3</sub> ] organic-inorganic layered composite	Electrochemical (Gas)	Acetaldehyde	Resistance	Adsorption of aldehyde molecules into the hybrid interlayers and molecular size of aldehyde	-	[236]	
PNMA/MoO <sub>3</sub> organic-inorganic layered composite	Electrochemical (Gas)	Formaldehyde	Resistance	Adsorption of aldehyde molecules into the (PNMA)/MoO <sub>3</sub> interlayers.	-	[237]	
PANI-ZnO NC	Electrochemical (Gas)	NO <sub>2</sub>	Resistance	Formation of ZnO-PANI hetero junction nanostructures	-	[238]	
PANI/Silicon carbide (Pani/SiC) NC	Electrochemical (Gas)	Cigarette smoke sensor	DC electrical conduction	High surface area PANI coated SiC and improved adsorption-desorption process	-	[239]	
Carboxylated MWNT-PANI NC (MWCNTCOOH/PAn)	Electrochemical (Biomolecule)	Glu	Liquid-gated enzyme field effect device	Electrostatic interaction between GOx and PANI	DL= ~0.5 μM	[240]	
PANI-poly(ethylene oxide) (PEO) NC	Electrochemical	Glu	CA	-	LR = 1 to 10 mM	[241]	

		(Biomolecule)				DL = 0.82 mM	
G-PANI (G-PANI) NC	Electrochemical (Biomolecule)	Glu	Electrochemical compact disk (eCD) platform	Shift in potential for glucose oxide due to electrocatalytic property	LR = 1 to 10 mM DL = 0.29 mM		[242]
PANI with carbon quantum dots (QCDs)	Optical (Biomolecule)	Glu and H <sub>2</sub> O <sub>2</sub>	Fluorescence intensity	Synergistic effects from PANI and CQDs	LR = 0.90 – 270 $\mu$ M DL = 0.90 $\mu$ M		[243]
Au NPs/PANI composite	Electrochemical (Biomolecule)	Glu	EIS	Charge transfer between Au and PANI	LR = 0.3-10 mM DL = 0.1 mM		[244]
PAPBA/Au NC	Electrochemical (Biomolecule)	Glu	CV	Electrocatalytic activity due to synergistic properties of boronic groups and Au NPs- faster electron transfer by Au NPs	LR = 1 - 28 mM		[245]
NiCo <sub>2</sub> O <sub>4</sub> @PANI core-shell NC	Electrochemical (Biomolecule)	Glu	CA	Effective electron conducting channel and shortening electron transfer path	DL = 0.3833 $\mu$ M		[246]
Au-PANI NC	Electrochemical (Biomolecule)	D-glucosamine	Droplet microfluidic system	-	LR = 0.5-5mM DL = 0.45 mM		[247]
Poly(2,5-dimethoxyaniline) and phosphotungstic acid	Electrochemical (Biomolecule)	AA	CV	Presence of tungsten atoms in between layers of PDMA resulted faster mediation of electrons	-		[248]
CNT/PANI-CME	Electrochemical (Biomolecule)	AA	CV and DPV	CNT improved electrochemical stability of PANI	LR= $1.0 \times 10^{-6}$ mol L <sup>-1</sup> to $4.5 \times 10^{-4}$ mol L <sup>-1</sup> , DL= $1.0 \times 10^{-7}$ mol L <sup>-1</sup>		[249]
SPAN- MoS <sub>2</sub> NC	Electrochemical (Biomolecule)	Adenine and Guanine	DPV	Electrochemical repulsion between SPAN and MoS <sub>2</sub> and $\pi$ - $\pi^*$ stacking effect	<u>Adenine</u> LR = 0.05 – 100 $\mu$ M DL = 3 nm <u>Guanine</u> LR = 0.05 – 100 $\mu$ M DL = 5 nm		[250]
Poly (4-amino thiophenol) (PAT) with	Electrochemical	AA and DA	DPV	Preferential oxidation of AA ahead of	<u>AA</u>		[251]

	Au NPs	(Biomolecule)			DA	LR = 10 - 50 $\mu$ M DA LR = 10 - 50 $\mu$ M	
	PANI-GO NC	Electrochemical (Oligonucleotide)	Prostate cancer cells and DNA	EIS	DNA hybridization with PANI-GO NC	LR=1.0 $\times 10^{-16}$ M to 1.0 $\times 10^{-8}$ M DL=3.3 $\times 10^{-17}$ M	[252]
	PANI-G nanosheet composites	Electrochemical (Oligonucleotide)	DNA	EIS	$\pi$ - $\pi^*$ stacking interaction and electrostatic interaction	Detection range = 0.01 – 1 $\mu$ M	[253]
	AgNPs@PANI NC	Electrochemical (Oligonucleotide)	DNA/Ag <sup>+</sup>	EIS	Electrostatic interaction between PANI and DNA cysteine-Ag <sup>+</sup> complex formation	LR=0.01-100nM DL=10pM	[254]
	G-PANI NC	Electrochemical (ions)	Zn(II), Cd(II), and Pb(II)	SWASV	Improved electron transport pathway and electron transfer kinetics	DL = 1.0 $\mu$ g L <sup>-1</sup> (for Zn(II)) 0.1 $\mu$ g L <sup>-1</sup> (Cd(II) and Pb(II))	[255]
	PANI-ES/Clay NC	Electrochemical (Ions)	Cd <sup>2+</sup> , Pb <sup>2+</sup> and Cu <sup>2+</sup>	SWASV	$\pi$ - $\pi$ and electrostatic interactions	LR = 20 – 120 $\mu$ g/L DL = 0.263 $\mu$ g/L (Cd <sup>2+</sup> ) DL = 0.232 $\mu$ g/L (Pb <sup>2+</sup> ) DL = 0.211 $\mu$ g/L (Cu <sup>2+</sup> )	[256]
	PANI/vanadyl phosphate (PANI-VOPO <sub>4</sub> ) composite	Electrochemical (Ion)	Pb <sup>2+</sup>	Current-Potential response	Large area covered by Pb <sup>2+</sup> ions, intermolecular and intramolecular interactions of PANI-VOPO <sub>4</sub> composite	LR = 2.0 nM-2.0 mM DL = $\sim 1.36 \pm 0.05$ nM	[257]
	Sulfonic acid doped PANI-wrapped MWNTs	Optical (Ion)	pH	UV	-	LR = 1–12 pH	[258]
Grafted PANIs	MWNT-g-PDPA	Electrochemical (Biomolecule)	CO and H <sub>2</sub> O <sub>2</sub>	Amperometry	-	LR = 10 - 200 ppm (CO) LR = 1 - 21 mM (H <sub>2</sub> O <sub>2</sub> )	[259, 260]
	MWNT-g-PANI	Electrochemical (Biomolecule)	H <sub>2</sub> O <sub>2</sub>	Amperometry	-	LR = 1 - 20 $\times 10^{-8}$ M DL = 1 nM	[262]

	MWNTs-g-PANI	Electrochemical (Drug)	Celecoxib (CEL)	DPV	Synergistic contribution of the MWNTs and PANI for effective preconcentration of CEL at the electrode surface	DL = $1 \times 10^{-11}$ M	[263]
	Poly(4-aminobenzene sulfonic acid) (PABS) grafted MWNTs (MWNT-g-PABS)	Electrochemical (Drug)	Sildenafil citrate (SC)	SWAdSV	Electrostatic interactions between sulfonic acid groups in MWNT-g-PABS and protonated SC	LR = $1 \times 10^{-11}$ – $0.896 \times 10^{-4}$ M; DL = $0.469 \times 10^{-11}$ M	[264]
Biofunctionalization	Mannosilated PANI (manno-PANI)	Electrochemical (Biomolecule)	Concanavaline (Con A)	EIS	Con A-mannose interactions cause partial deprotonation of PANI	LR = 3-15 nM DL = 0.12 nM	[265]
	PANI/dinonylnaphthalenesulfonic acid (PANI/DNNSA)	Electrochemical immunosensor	troponin I-T-C (Tn I-T-C)	Potentiometry	Prevention of non-specific binding	DL = < 5 pg/mL or 56 fM	[266]
	SPAN-ssDNA	Electrochemical (Oligonucleotide)	dsDNA (cauliflower mosaic virus 35S)	CV	Interaction of SPAN-dsDNA or ssDNA caused conformational changes	LR = $1 \times 10^{-14}$ – $1 \times 10^{-8}$ molL <sup>-1</sup> DL = $2.3 \times 10^{-15}$ molL <sup>-1</sup>	[267]
	Con A lectin functionalized PANI	Electrochemical (Bacterial toxin)	Lipopolysaccharide from Escherichia coli and lipoteichoic acid from Staphylococcus aureus	EIS	Con A interacts with either LPS from E. coli or the LTA from S. aureus	-	[268]
	Polyclonal antibody fragments cleaved by 2-mercaptoethylamine onto a functionalized PANI matrix containing 2-aminobenzylamine	Electrochemical (Virus)	Serotypes of Ad, Ad5, and Ad3, virus particles	EIS	Changes in the charge transfer resistance	-	[269]
	C//PANI+/PSSA-glu-NH <sub>2</sub> -Apt	Electromechanical (toxin)	Tetrodotoxin	EIS	Electron transport between the biomolecule and electrode surface	DL = 0.199 ng·mL <sup>-1</sup>	[270]
	PANI functionalized AFM cantilever	Electromechanical (Hormone)	insect pheromone 2-heptanone	AFM cantilever deflection	Mechanical deflection of AFM cantilever	LR = 10-1000 ppm DL = 31 ppm	[271]
Nanostructure	PANI NFs	Electrochemical	NH <sub>3</sub>	Resistance	High surface area of NFs	LR = 25 - 100 ppm	[273]

ring		(Gas)					
	PANI NFs	Electro mechanical (Gas)	NH <sub>3</sub>	Resistance	Polar bonds formation and increase in interchain distance	LR = 0.2 – 1.0 ppm	[274]
	PANI NFs	Electro mechanical (Gas)	NH <sub>3</sub>	DC conductivity	Doping-dedoping, porous and 3D nanostructure	DL=10 ppm LR = 10 – 70 ppm	[275]
	Lysine included PANI/PAN NFs composite	Electro mechanical (Gas)	NH <sub>3</sub>	Resistance	Large surface area, core-shell nanostructure, doping with lysine and transformation of PANI chain structure	DL = 2.2 ppm	[276]
	Indium oxide/PANI (In <sub>2</sub> O <sub>3</sub> /PANI) composite NFs (CNFs)	Electro mechanical (Gas)	NH <sub>3</sub>	Resistance	p-n junction formation protonation-deprotonation processes	Detection range = 200 – 1000 ppm	[277]
	Hierarchical G-PANI NF	Electrochemical (Gas)	NH <sub>3</sub>	Resistance	Synergistic effect of PPy and G and high surface area from NF	Detection range = 100 ppb – 100 ppm	[278]
	PANI-PEO CNFs	Electrochemical (Gas)	H <sub>2</sub> S	Resistance	Interaction between PANI and H <sub>2</sub> S-increase in concentration of holes, doping-dedoping process	Detection range = 1 ppb – 10 ppm	[279]
	PANI NFs	Electrochemical (Gas)	CO	Resistance	Introduction of nanocore feature to PANI-increases in contact area-electron transfer process	LD=2.5 ppb	[280]
	PANI-functionalized polyamide 6 (PA 6) (PANI-PA 6) NF-net-binary (NNB) structured membranes	Electrochemical (Gas)	HCl	QCM	Mass changes due to interactions between PANI and HCl	DL = 7 ppb	[281]
	Biofunctionalized dendritic PANI NF	Electrochemical (immunosensor)	Alpha-fetoprotein (AFP)	Portable personal glucometer	Conjugation of glucoamylase	DL = 0.03 ng mL <sup>-1</sup> LR = 0.1 – 50 ng mL <sup>-1</sup>	[282]
	Bishydroxyl-functionalized PANI NF	Optical (Biomolecule)	Vitamin C	UV	Molecular interactions with vitamins depending on the functional groups at the nanosurface	-	[283]
PVdF/PAPBA composite NF	Electrochemical (Biomolecule)	Glu	Amperometry	Boronic acid groups bind the vicinal diol groups in Glu	LR = 1–15 mM	[284]	
PABA NF	Electrochemical (Biomolecule)	Glu	CV	Binding of D-Glu to the boronic acid moiety of PABA	-	[285]	

PANI-manganese dioxide (PANI-MnO <sub>2</sub> ) NFs	Electrochemical (Biomolecule)	H <sub>2</sub> O <sub>2</sub>	CA	Electrocatalytic property of MnO <sub>2</sub> and high surface area of NFs	LR = 5 – 50 μM DL = 0.8 μM	[286]
Laccase-PANI NF	Electrochemical (Biomolecule)	Phenol	Amperometry	Enzyme adsorption and crosslinking processes	-	[287]
Seaweed-PANI NFs	Electrochemical (Biomolecule)	UA	DPV	High catalytic activity in neutral medium	DL = 0.104 μM LR = 0.5 – 500 μM	[288]
Polyamide 6/PANI NFs	Electrochemical (Biomolecule)	Tetracycline (TC) in milk samples	EIS	Random orientation of NFs at the polyamide and PANI interface	DL=1 to 300 ppb LR = 1 – 300 ppb	[289]
1,3,5-Trithiane-Ag-NPs decorated PANI NFs (TAN-AgNP-PANF)	Electrochemical (Biomolecules)	Adenine and Guanine	DPV and CV	Hydrogen bonding interactions between S atom of TAN and hydrogenation of PANI	<u>Adenine</u> LR=0.08 – 25.0 μM DL=24.0 <u>Guanine</u> LR = 0.01 – 150 μM DL = 0.06 μM	[290]
AuNPs functionalized PANI-NF	Electrochemical (immunosensor)	Alpha-fetoproteins	DPV	The enhanced current signal originate from PANI NF and biocompatibility of Au NPs	DL = 0.007 pg mL <sup>-1</sup>	[291]
PANI reinforced NFs	Electrochemical (Ion)	Cl <sup>-</sup>	QCM (Piezo electric)	Mass changes due to doping/dedoping process	DL = 10 ppm	[292]
PANI helical microfibers	Optical (Ion)	Hg <sup>2+</sup>	Trans litmus values based on CIELAB color space	Both “off-on” and “color-change” signals competitive doping reactions of PANI-EB by protonation and Hg <sup>2+</sup> complexation doping	DL = 5 nM	[293]
PANI NW-gold NPs hybrid network	Chemical (Gas)	H <sub>2</sub> S	-	Formation of AuS and improvement in the doping level of PANI leads to increase in conductance	DL = ~0.1 ppb	[295]
Aptamer-functionalized single PANI NW	Electrochemical (Aptamer)	IgE	Conductance	Change in the conductance of the aptamer-functionalized PANI NW due to the specific binding of IgE to the immobilized anti-IgE aptamer	LR = 1.0 pg mL <sup>-1</sup> – 22 ng mL <sup>-1</sup> DL = 0.56 pg mL <sup>-1</sup>	[296]
PANI NWs self-assembled CNT arrays	Electrochemical (Biomolecule)	Nitrate	CA	NF provides large surface area and CNT function as conducting skeleton	DL= 6.1 μM	[297]

	Nanocages-augmented PANI NWs (NCa-PANI NWs)	Electrochemical (Biomolecule)	Glu	Amperometry	Generation of ion-dipole	DL = $\sim 0.657 \mu\text{M}$ LR = 2 – 24 mM	[298]
	C-PANI NW-CDS-NB	Optical (Chiral compound)	Arginine, cysteine	UV	Steric hindrance of bulky groups for competitive doping with CSA results in discrimination of chiral dopants	-	[299]
Multicomponents	GOx-MWNT-PANI	Electrochemical (Biomolecule)	Glu	Amperometry	-	LR = 0.5 - 22 mM	[300]
	{GOx/Au-(SH)PANI-g-MWNT} <sub>n</sub>	Electrochemical (Biomolecule)	Glu	Amperometry	Increase in GOx loading, favorable orientation of GOx, effective electron shuttling between electrode and GOx	LR = 1-9 mM DL = 0.06 $\mu\text{M}$	[301]
	MWNT-g-SPAN-NW/GOx	Electrochemical (Biomolecule)	Glu	Amperometry	Modification of MWNTs using SPAN based on an interconnected network offers direct electron transfer from GOx	LR = 1 - 9 mM DL = 0.11 $\mu\text{M}$	[302]
	Nafion-silica/MWNT-g-PANI/GOx	Electrochemical (Biomolecule)	Glu	Amperometry	Loading of MWNT-g-PANI within the Nafion-silica network augments electron transduction	LR = 1 - 10 mM	[303]
	Prussian blue (PB)/PANI/MWNTs	Electrochemical (Biomolecule)	Glu	Amperometry	MWNT provide good electron transport for PANI-PB combined particle	LR = 0.5 – 4.0mM DL = 0.04 mM	[304]
	Nickel-rGO-PANI	Electrochemical (Biomolecule)	Glu	Amperometry	Inner sphere electron transfer process	LR = 0.1 $\mu\text{M}$ - 1.0 mM, DL = 0.08 $\mu\text{M}$	[305]
	NiO hedgehog-like nanostructures/Au/PANI NFs/rGO NC	Electrochemical (Biomolecule)	Glu	CV and Amperometry	CuO induces formation of NiO(OH) from NiO, which catalysis the Glu oxidation	LR = 0.09-6 mM DL = 0.23 $\mu\text{M}$	[306]
	Nickel oxide (NiO) NP/PANI NW/GO hybrid	Electrochemical (Biomolecule)	Glu	CA	Transformation of NiO to NiOOH and electrocatalysis by Ni <sup>3+</sup> ion	LR = 2 $\mu\text{M}$ to 5.560 mM DL = 0.5 $\mu\text{M}$	[307]
	Cu NPs/PANI/G composite	Electrochemical (Biomolecule)	Glu	Amperometry	Interaction between Cu and PANI via the N atom in PANI	DL = 0.27 $\mu\text{M}$ LR = 0.001 – 3.7 mM	[308]
	G-PANI(COOH)-PEI-Fc/Cu-Multicomponent nanobead (MCNB)	Electrochemical (Biomolecule)	Glu	DPV	Synergistic contribution-electron mediating effect by FC and electrocatalysis by CuNP	LR = 0.50 to 15 mM DL = 0.16 mM	[309]
G/PANI/AuNPs/GOx(FAD)	Electrochemical	Glu	DPV	Direct electrochemistry for GOx	LR = 3.5 – 5.3 mM	[310]	

	(Biomolecule)					(whole blood) LR = 2.5 – 5.3 mM (serum)	
PANI/active carbon-nanometer-sized TiO <sub>2</sub> (n-TiO <sub>2</sub> )	Electrochemical (Biomolecule)	Glu	CA	Direct electron transfer for GOx	LR = 0.02 mM to 6.0 mM DL = 18 μM		[311]
AuNP-PVP-PANI NCs	Electrochemical (Biomolecule)	Glu	CA	Direct electron transfer for GOx	LR = 0.05 mM - 2.25 mM DL = 1.0 × 10 <sup>-5</sup> M		[312]
Au NPs-PANI NW/ GOx	Electrochemical (Biomolecule)	Glu	DPV	Different biomolecules such as ssDNA and Lamin A antibody cored be immobilized with same matrix	LR = 1 - 20 mM DL = 1 μM		[313]
Ternary NiO/CuO/PANI NC	Electrochemical (Biomolecule)	Glu	Amperometry	Cu ions induce transformation of Ni <sup>2+</sup> to Ni <sup>3+</sup> , PANI augments the current signal	LR = 20 to 2500 μM DL = 2.0 μM		[314]
Poly(trimethoxysilyl propyl aniline) (PTMSPA)/HRP-GOx composite	Electrochemical (Biomolecule)	Glu	Amperometry	PTMSPA acts as an electron transducer due to the presence of covalently linked PANI chains in the silica framework and the close proximity between the enzymes and PANI chains	LR = 1 – 20 mM DL = 100 μM		[315]
Boron nitride NTs (BNNTs)-PANI-Pt-GOx	Electrochemical (Biomolecule)	Glu	Amperometry	Electrostatic field and hydrophobicity of the BNNTs	LR = 0.01 – 5.5 mM DL = 0.18 μM		[316]
PANI/ PAA/GOx	Electrochemical (Biomolecule)	Glu	Amperometry	Biocatalysis by GOx and electrocatalysis by PANI/ PAA	LR = up to 1.1 mM DL = 0.06 ± 0.02 mM		[317]
PANI/(pyrene sulfonate/polystyrene sulfonate) functionalized SWNT/GOx	Electrochemical (Biomolecule)	Glu	CV	Charge transport through PANI/SWNT causes enhancement of electrical contact with GOx and results in oxidation of Glu.	-		[318]
HRP/PANI/PEG–MWNT	Electrochemical (Biomolecule)	H <sub>2</sub> O <sub>2</sub>	Amperometry	PANI coating on PEG–MWNT reduces the intercalation distance and facilitates direct electron transfer for HRP	LR = 4.98 – 43.1 μM DL = 0.5 μM		[319]
MWNT-g-PANI(O)/cyt c	Electrochemical	H <sub>2</sub> O <sub>2</sub>	Amperometry	Interconnected units of PANI and	LR = 0.5 μM to		[320]

	(Biomolecule)				MWNT provide synergistic catalytic contribution towards H <sub>2</sub> O <sub>2</sub> oxidation	1.5 mM;	
G-CNT-Nafion/AuPt NPs	Electrochemical (Biomolecule)	H <sub>2</sub> O <sub>2</sub>	SWV		Synergistic effects from the components	LR = 5.0x10 <sup>-7</sup> – 1.0x10 <sup>-4</sup> M DL = 1.7x10 <sup>-7</sup> M	[321]
HRP/PTMSPA@GNR	Electrochemical (Biomolecule)	H <sub>2</sub> O <sub>2</sub>	Amperometry		PANI units in PTMSPA facilitates the electron wiring between HRP and the electrode	LR = 1x10 <sup>-5</sup> – 1x10 <sup>-3</sup> M DL = 0.06 μM	[322]
Prussian blue (PB)/PANI/GO NCs	Electrochemical (Biomolecule)	H <sub>2</sub> O <sub>2</sub>	CV		Large number of functional groups nucleation of PB within PANI/GO improvement in electrocatalysis	LR=5.0 μM to 1.275 mM, DL=1.9 μM	[323]
HRP/PANI/MWNT-COOH/Au	Electrochemical (Biomolecule)	H <sub>2</sub> O <sub>2</sub>	Amperometry		Adsorption between negatively charged PANI/MWNT-COOH and positively charged HRP results in good sensitivity to H <sub>2</sub> O <sub>2</sub>	LR = 86 μM - 10 mM	[324]
Nanodiamond (ND)-NS(HRP)	Electrochemical (Biomolecule)	H <sub>2</sub> O <sub>2</sub>	Amperometry		PANI chains electrically wires the entrapped HRP-nanopores in the sponge structure -provides 3D channels for the passage of analytes and the passage of H <sub>2</sub> O <sub>2</sub> to the electrode surface	LR = 1-45 mM DL = 59 μM	[325]
Pt NP-PANI NCs hosted in mesoporous silica film (PtNPs@PANI/MSF)	Electrochemical (Biomolecule)	H <sub>2</sub> O <sub>2</sub>	DPV and CA		PANI confined in the micropores provides large surface area	LR = 1 – 100 μM	[326]
Ag NPs/PANI/halloysite nanotube NCs	Electrochemical (Biomolecule)	H <sub>2</sub> O <sub>2</sub>	CV and Amperometry		Anchoring of Ag NPs and high surface area of Pt particles are confined within PANI/halosite NT NC	LR = 0.5 μM to 4.7 mM DL = 0.3 μM	[327]
GNS/Pt/PANI NC	Electrochemical (Biomolecule)	DA	DPV		Synergistic effects from GNS, Pt and PANI	DL = 0.6 μM LR = 2 – 10 μM and 40 – 400 μA	[328]
MWNT grafted silica-PANI network (silica NW) and Au NPs (MWNT-g-silica NW/Au NPs)	Electrochemical (Biomolecule)	DA and AA	DPV		Ascorbate anions are preferentially adsorbed by the –NH <sub>2</sub> groups and DA molecules prefer the hydrophobic MWNT surface	DA LR = 0.1 nM–30 nM DL = 0.1 nM	[329]
Cetyltrimethylammonium bromide-PANI/activated charcoal composite	Electrochemical (Biomolecule)	DA and UA	CV		Specific interactions with DA or AA were generated with the changes in	DA DL = 0.06 μM	[331]

					the activated charcoal	LR = 0.3 – 20 mM UA DL = 0.20 $\mu$ M LR = 1 – 20 $\mu$ M	
SiO <sub>2</sub> @Au NP@PANI NC	Electrochemical (Biomolecule)	UA and AA	DPV		Coordination bond formation between Au NP and PANI – electrostatic attraction and hydrophilic nature of NC	DL = 2 $\mu$ M (UA) and 6 $\mu$ M (AA)	[332]
Au/MWNT(CD-IC)/PVdF-NFM	Electrochemical (Biomolecule)	AA	CV		Synergistic influence of conductive MWNT, catalytic Au NPs and large surface area of the fiber		[333]
ChOx/PANI-Au NPs-CS	Electrochemical (Biomolecule)	Cholesterol	Amperometry		The –NH <sub>2</sub> groups in chitosan provide a hydrophilicity and helps in biomolecule recognition	LR = 1-9 mM DL = 0.06 $\mu$ M	[334]
Au–PANI–G/ GOx	Electrochemical (Protein)	Thrombin	CV		Direct electron transfer of GOx Au–PANI–GR and facilitates electron transfer kinetics		[335]
Multi-armed dendritic PANI nanofibers (MPANFs)/ HRP/ anti-CEA	Electrochemical (Protein)	Carcinoembryonic antibody (CEA)	CV		Sandwich type assay MPANFs served as self-contained electron mediator	LR = 1.0 $\mu$ g mL <sup>-1</sup> - 50 $\mu$ g mL <sup>-1</sup> DL = 0.1 $\mu$ g mL <sup>-1</sup>	[336]
PANI/Au NP/ $\beta$ -mercaptoethylamine (MEA)-ssdA	Electrochemical (Oligonucleotide)	ssdT	DPV		Detection of complementary ssdT through dA–dT bond formation	DL = 10 <sup>-18</sup> M	[337]
PANI–Au NP-modified ITO glass with a tris(2,2-bipyridyl)dichloro ruthenium(II) hexahydrate ([Ru(bpy) <sub>3</sub> ] <sup>2+</sup> )–nanoporous gold (Ru–NPG)	Optical (Oligonucleotide)	DNA	ECL		Captures the target DNA through a sandwich-type hybridization reaction	DL = 0.01 fM	[338]
PANI-NW- AuNPs/ss ODN	Electrochemical (Oligonucleotide)	complementary strand ODN	DPV		Interaction of MB with ss DNA and ds DNA	LR = 10 <sup>-8</sup> – 10 <sup>-5</sup> M DL = 10 <sup>-18</sup> M	[339]
PANI NW biofunctionalization with hepatitis B virus genus/DNA	Electrochemical (Virus)	hepatitis B virus	SWV		Covalent linkage of PANI to the peptide based template	LR = 2.0 – 800 fM DL = 1.0 fM	[340]
PANI-NF–Au NPs/ss DNA	Electrochemical (Bacteria)	<i>Staphylococcus aureus</i>	Amperometry		Increase of DNA capture in the presence of Au NPs	LR = 150 $\times$ 10 <sup>-12</sup> to 1 $\times$ 10 <sup>-6</sup> mol·L <sup>-1</sup> DL = 150 $\mu$ M	[341]
Cyt-C and sulfite oxidase / PANI sulfonate	Electrochemical (Aptamer)	IgE	Amperometry		Reversible conformational changes of aptamers and electron wire		[342]

					generation		
Au NP/PANI/CS-G/DNA	Electrochemical (Cancer cell)	BCR/ABL fusion gene of Chronic myelogenous leukemia (CML)	DPV	GS, PANI, Au NP greatly improved the conductivity, electrochemical surface area and enhances immobilization amount of heparin	LR = 10 pM – 1000 pM DL = 21 pM	[343]	
PANI-g-ND/Au/cyt-C	Electrochemical (Ion)	Nitrite	DPV	Attributes to the “electron wiring” between the redox centers of the immobilized cyt-C and those of the “electron shuttling sites” in the PANI-g-ND/Au matrix	LR = 0.5 $\mu$ M to 3 mM DL = 0.16 $\mu$ M	[344]	
PVdF@silica/Au/cyt-C	Electrochemical (Ion)	Nitrite	CV	Silica improves cyt c immobilization and Au NPs provide electrical contact for transfer of electrons to the electrode	-	[345]	
PANI/PS <sub>NP</sub> -NH <sub>2</sub> /PANI nanocauliflower	Electrochemical (Ion)	Nitrite	Amperometry	Electrostatic attractions between positively charged PANI/PS <sub>NP</sub> -NH <sub>2</sub> and negatively charged nitrite ions	-	[346]	
Sulfite oxidase-cyt-C (SO-cyt-C)-PANI sulfonate (PASA) multilayer film	Electrochemical (Ion)	Sulfite	CV	Two protein multilayer approach. PASA acting as a glue for the cyt-C electron transfer process	-	[342]	
Thiol-incorporated PANI/MWCNT	Electrochemical (Ion)	Cd <sup>2+</sup> and Pb <sup>2+</sup>	DPAdSV	Nafion, PANI, HDT, DMcT and MWNT adsorb Cd <sup>2+</sup> and Pb <sup>2+</sup> and coordinate with the ions.	<u>Cd<sup>2+</sup></u> LR = 0.02 – 20 $\mu$ gL <sup>-1</sup> DL = 0.01 $\mu$ gL <sup>-1</sup> <u>Pb<sup>2+</sup></u> LR = 0.1 – 30 $\mu$ gL <sup>-1</sup> DL = 0.04 $\mu$ gL <sup>-1</sup>	[347]	
GNR@silica-CN-poly(2-amino benzonitrile) (P2ABN)	Optical (Ion)	Hg <sup>2+</sup>	UV	Porous silica causes migration of Hg atoms generated through reduction of Hg <sup>2+</sup> to reach the surface of GNR-Hg <sup>2+</sup> detection occurred through –CN chelation and amalgamation	LR = 50 nM - 5 $\mu$ M DL = 5.4 nM	[348]	
PANI-rGO-Au NC	Electrochemical	Pb <sup>2+</sup>	DPV	rGO offers high surface area – good	LR = 0.005 - 2000	[349]	

		(Ion)			electron transfer	nM DL = 0.002 nM	
	Fe <sub>3</sub> O <sub>4</sub> /PANI/Nafion/(multi-HRP-HCS-Ab <sub>2</sub> )	Electrochemical (Chemical)	Benzo[a]pyrene (BaP)	CV	Multi enzyme labeling - multiplex binding of BaP-Ag and multi-HRP-HCS-Ab <sub>2</sub> label - dual signal amplification	LR = 8 pM – 2 nM DL = 4 pM	[350]
	PANI/WO <sub>3</sub> /GF	Electrochemical (Chemical)	Phenanthrene	-	-	LR = 1.0 - 6.0 pM DL = 0.123 pM	[351]
	p-TSA doped V <sub>2</sub> O <sub>5</sub> @PANI composite	Electrochemical (Gas)	NH <sub>3</sub>	Resistance	Generation high charge carriers	-	[352]
	Tanninsulfonic acid doped PANI-TiO <sub>2</sub> composite	Gas	NH <sub>3</sub>	Resistance	Localized polaron formation-coordination effect, doping-dedoping process	-	[353]
	CSA-doped POA-PS-PANI composite fibers	Electrochemical (VOC)	Ethanol and water	Resistance	Hydrogen bonding interactions between ethanol or water molecules and -NH <sub>2</sub> groups in POA	-	[354]
	CSA-doped PANI/SWNT	Electrochemical (Gas)	NH <sub>3</sub>	Resistance	Opposite electrical resistance responses of CSA-doped PANI and SWNTs eliminated humidity interference	LR = 10 – 80 ppb	[355]

\*If available in the reference paper

CA – Chrono amperometry; CV – Cyclic voltammetry; DPV – Differential pulse voltammetry; ECL – Electro chemiluminescence; EIS – Electrochemical impedance spectroscopy; FET – Field effect transistor; ME – Modified electrode QCM – quartz crystal microbalance; SPR – Surface Plasmon resonance; SWV – Square wave voltammetry; SWAdSV – Square wave adsorptive stripping voltammetry; SWSV – Square wave stripping voltammetry; UV – UV visible spectroscopy

Table 4. Cross-sectional details on the signal transduction mode based sensors utilizing the four functionalization categories of polyanilines (F-PANIs)

Sensor signal transduction mode	Mode of Parent structure functionalization/ modification	Name of FCP (abbreviation) or functional structure in the FCP	Specific analyte(s)
Electrochemical	Substituted / derivatized PANI	Poly(diphenyl aminesulfonic acid) (PDSA)	Humidity[195]
		Imidazole substituted PANI	Pb <sup>2+</sup> [196]
		PANI-pseudo-polyrotaxane (PANI- $\beta$ -CDpNH <sub>2</sub> )	Pb <sup>2+</sup> [199,198]
		Poly(diphenylamine-co-2-aminobenzonitrile) (P(DPA-co-2ABN))	Cd <sup>2+</sup> and Pb <sup>2+</sup> [200]
		PNMA, Poly (N-ethyl aniline), Poly (2,3 dimethyl aniline), Poly (2,5 dimethyl aniline) and Poly (diphenyl amine)	pH[201]
	Functional ion-dopant inclusion	PANI doped with hexafluoroisopropanol (HFIP)	Hydrazine[210]
		Dodecylbenzene sulphonic acid (DBSA)/Potassium dichromate PANI	NH <sub>3</sub> [211]
		Doped PANI-poly(vinyl alcohol) composite membrane	Aliphatic alcohols[214]
		Sulfonated PANI (SPAN)	CO <sub>2</sub> [215]
		Polyoxometalate-(POM) doped PANI	H <sub>2</sub> O <sub>2</sub> [217]
		NPs (Ag NPs)-doped PANI (PANI)	Polychlorinated biphenyl (PCB) [218]
		PANI doped with dinonylnaphthalene sulfonic acid (PANI-DNNSA)	K <sup>+</sup> [219]
		Sodium dodecyl sulfate doped PANI	Hg <sup>2+</sup> [220]
		Functional component inclusion	SWNTs-poly(m-aminophenyl sulfonic acid) (PMABS)
	PANI-SWNTs		NH <sub>3</sub> [222]
	PANI-SWNTs		NH <sub>3</sub> , NO <sub>2</sub> , and H <sub>2</sub> S [223]
	SWNT and PANI		Dimethyl-methyl-phosphonate (DMMP) [224]
	Plasma-treated MWNT/PANI (pf MWNT/PANI)		NH <sub>3</sub> [225]
	PANI/ carboxylic acid-functionalized MWNT (c-MWNT) (PANI/ c-MWNT)		Chloroform[226]
	PANI-wrapped MWNT		NO <sub>2</sub> [227]
	PANI/GO composite		Methanol [228]
	S and N co-doped GQD/PANI hybrid		NH <sub>3</sub> [230]
	rGO-PANI hybrid		NH <sub>3</sub> [232]
Gold-PANI Composite	NH <sub>3</sub> [233]		
PANI/ZnO hybrid	NH <sub>3</sub> [234]		
Cu NP-PANI NC	NH <sub>3</sub> [235]		

	[(PANIS) <sub>x</sub> MoO <sub>3</sub> ] organic-inorganic layered composite	Acetaldehyde[236]
	PNMA/MoO <sub>3</sub> organic-inorganic layered composite	Formaldehyde[237]
	PANI-ZnO NC	NO <sub>2</sub> [238]
	PANI/Silicon carbide (Pani/SiC) NC	Cigarette smoke sensor[239]
	Carboxylated MWNT-PANI NC (MWCNTCOOH/PAn)	Glu[240]
	PANI-poly(ethylene oxide) (PEO) NC	Glu[241]
	G-PANI (G-PANI) NC	Glu[242]
	Au NPs/PANI composite	Glu[244]
	PAPBA/Au NC	Glu[245]
	NiCo <sub>2</sub> O <sub>4</sub> @PANI core-shell NC	Glu[246]
	Au-PANI NC	D-glucosamine[247]
	Poly(2,5-dimethoxyaniline) and phosphotungstic acid	AA[248]
	CNT/PANI-CME	AA[249]
	SPAN- MoS <sub>2</sub> NC	Adenine and Guanine[250]
	Poly (4-amino thiophenol) (PAT) with Au NPs	AA and DA[251]
	PANI-GO NC	Prostate cancer cells and DNA[252]
	PANI-G nanosheet composites	DNA[253]
	AgNPs@PANI NC	DNA/Ag <sup>+</sup> [254]
	G-PANI NC	Zn(II), Cd(II), and Pb(II)[255]
	PANI-ES/Clay NC	Cd <sup>2+</sup> , Pb <sup>2+</sup> and Cu <sup>2+</sup> [256]
	PANI/vanadyl phosphate (PANI-VOPO <sub>4</sub> ) composite	Pb <sup>2+</sup> [257]
Grafted PANIs	MWNT-g-PDPA	CO and H <sub>2</sub> O <sub>2</sub> [259,260]
	MWNT-g-PANI	H <sub>2</sub> O <sub>2</sub> [262]
	MWNTs-g-PANI	Celecoxib (CEL)[263]
	Poly(4-aminobenzene sulfonic acid) (PABS) grafted MWNTs (MWNT-g-PABS)	Sildenafil citrate (SC)[264]
Biofunctionalization	Mannosilated PANI (manno-PANI)	Concanavalline (Con A)[265]
	PANI/dinonylnaphthalenesulfonic acid (PANI/DNNSA)	troponin I-T-C (Tn I-T-C)[266]
	SPAN-ssDNA	dsDNA (cauliflower mosaic virus 35S)[267]
	Con A lectin functionalized PANI	Lipopoly saccharide from Escherichia coli and lipoteichoic acid from Staphylococcus aureus[268]
	Polyclonal antibody fragments cleaved by 2-mercaptoethylamine onto a functionalized PANI matrix containing 2-aminobenzylamine	Serotypes of Ad, Ad5, and Ad3, virus particles[269]

ACCEPTED MANUSCRIPT	Nanostructuring	PANI NFs	NH <sub>3</sub> [273]	
		Hierarchical G-PANI NF	NH <sub>3</sub> [278]	
		PANI-PEO CNFs	H <sub>2</sub> S[279]	
		PANI NFs	CO[280]	
		PANI-functionalized polyamide 6 (PA 6) (PANI-PA 6) NF-net-binary (NNB) structured membranes	HCl[281]	
		Biofunctionalized dendritic PANI NF	Alpha-fetoprotein (AFP)[282]	
		PVdF/PAPBA composite NF	Glu[284]	
		PABA NF	Glu[285]	
		PANI-manganese dioxide (PANI-MnO <sub>2</sub> ) NFs	H <sub>2</sub> O <sub>2</sub> [286]	
		Laccase-PANI NF	Phenol[287]	
		Seaweed-PANI NFs	UA[288]	
		Polyamide 6/PANI NFs	Tetracycline (TC) in milk samples[289]	
		1,3,5-Trithiane-Ag-NPs decorated PANI NFs (TAN-AgNP-PANF)	Adenine and Guanine[290]	
		AuNPs functionalized PANI-NF	Alpha-fetoproteins[291]	
		PANI reinforced NFs	Cl <sup>-</sup> [292]	
		Aptamer-functionalized single PANI NW	IgE[296]	
		PANI NWs self-assembled CNT arrays	Nitrate[298]	
		Nanocages-augmented PANI NWs (NCa-PANI NWs)	Glu[298]	
		Multicomponents	GOx-MWNT-PANI	Glu[300]
			{GOx/Au-(SH)PANI-g-MWNT} <sub>n</sub>	Glu[301]
	MWNT-g-SPAN-NW/GOx		Glu[302]	
	Nafion-silica/MWNT-g-PANI/GOx		Glu[303]	
	Prussian blue (PB)/PANI/MWNTs		Glu[304]	
	Nickel-rGO-PANI		Glu[305]	
	NiO hedgehog-like nanostructures/Au /PANI NFs/rGO NC		Glu[306]	
	Nickel oxide (NiO) NP/PANI NW/GO hybrid		Glu[307]	
	Cu NPs/PANI/G composite		Glu[308]	
	G-PANI(COOH)-PEI-Fc/Cu-Multicomponent nanobead (MCNB)		Glu[309]	
	G/PANI/AuNPs/GOx(FAD)		Glu[310]	
	PANI/active carbon-nanometer-sized TiO <sub>2</sub> (n-TiO <sub>2</sub> )		Glu[311]	
	AuNP-PVP-PANI NCs		Glu[312]	
	Au NPs-PANI NW/ GOx		Glu[313]	
	Ternary NiO/CuO/PANI NC		Glu[314]	
Poly(trimethoxysilyl propyl aniline) (PTMSPA)/HRP-GOx composite	Glu[315]			

Boron nitride NTs (BNNTs)-PANI-Pt-GOx	Glu[316]
PANI/ PAA/GOx	Glu[317]
PANI/(pyrene sulfonate/polystyrene sulfonate) functionalized SWNT/GOx	Glu[318]
HRP/PANI/PEG-MWNT	H <sub>2</sub> O <sub>2</sub> [319]
MWNT-g-PANI(O)/cyt c	H <sub>2</sub> O <sub>2</sub> [320]
G-CNT-Nafion/AuPt NPs	H <sub>2</sub> O <sub>2</sub> [321]
HRP/PTMSPA@GNR	H <sub>2</sub> O <sub>2</sub> [322]
Prussian blue (PB)/PANI/GO NCs	H <sub>2</sub> O <sub>2</sub> [323]
HRP/PANI/MWNT-COOH/Au	H <sub>2</sub> O <sub>2</sub> [324]
Nanodiamond (ND)-NS(HRP)	H <sub>2</sub> O <sub>2</sub> [325]
Pt NP-PANI NCs hosted in mesoporous silica film (PtNPs@PANI/MSF)	H <sub>2</sub> O <sub>2</sub> [326]
Ag NPs/PANI/halloysite nanotube NCs	H <sub>2</sub> O <sub>2</sub> [327]
GNS/Pt/PANI NC	DA[328]
MWNT grafted silica-PANI network (silica NW) and Au NPs (MWNT-g-silica NW/Au NPs)	DA and AA[329]
Cetyltrimethylammonium bromide-PANI/activated charcoal composite	DA and UA[331]
SiO <sub>2</sub> @Au NP@PANI NC	UA and AA[332]
Au/MWNT(CD-IC)/PVdF-NFM	AA[333]
ChOx/PANI-Au NPs-CS	Cholesterol[334]
Au-PANI-G/ GOx	Thrombin[335]
Multi-armed dendritic PANI nanofibers (MPANFs)/ HRP/ anti-CEA	Carcinoembryonic antibody (CEA)[336]
PANI/Au NP/ $\beta$ -mercaptoethylamine (MEA)-ssdA	ssdT[337]
PANI-NW- AuNPs/ss ODN	complementary strand ODN[339]
PANI NW biofunctionalization with hepatitis B virus genus/DNA	hepatitis B virus[340]
PANI-NF-Au NPs/ss DNA	<i>Staphylococcus aureus</i> [341]
Cyt-C and sulfite oxidase, / PANI sulfonate	IgE[342]
Au NP/PANI/CS-G/DNA	BCR/ABL fusion gene of Chronic myelogenous leukemia (CML)[343]
PANI-g-ND/Au/cyt-C	Nitrite[344]
PVdF@silica/Au/cyt-C	Nitrite[343]
PANI/PS <sub>NP</sub> -NH <sub>2</sub> /PANI nanocauliflower	Nitrite[346]
Sulfite oxidase-cyt-C (SO-cyt-C)-PANI sulfonate (PASA) multilayer film	Sulfite[342]
Thiol-incorporated PANI/MWCNT	Cd <sup>2+</sup> and Pb <sup>2+</sup> [347]
PANI-rGO-Au NC	Pb <sup>2+</sup> [349]
Fe <sub>3</sub> O <sub>4</sub> /PANI/Nafion/(multi-HRP-HCS-Ab <sub>2</sub> )	Benzo[a]pyrene (BaP)[350]

		PANI/WO <sub>3</sub> /GF	Phenanthrene[351]
		p-TSA doped V <sub>2</sub> O <sub>5</sub> @PANI composite	NH <sub>3</sub> [352]
		Tanninsulfonic acid doped PANI-TiO <sub>2</sub> composite	NH <sub>3</sub> [353]
		CSA-doped POA-PS-PANI composite fibers	Ethanol and water[354]
		CSA-doped PANI/SWNT	NH <sub>3</sub> [355]
Optical	Substituted / derivatized PANI	Poly(2-Bromo aniline), Poly(2-Chloro aniline), Poly(3-Chloro aniline), Poly(4-Chloro aniline), Poly(o-toluidine), Poly(m-toluidine), Poly(p-toluidine), Poly(N-methyl aniline) (PNMA) and Poly (diphenyl amine)	Proton (pH)[193]
		Poly(diphenyl amine) (PDPA)	pH[194]
	Functional ion-dopant inclusion	PANI-HCl with polyethylene terphthalate	NH <sub>3</sub> [212]
		Diocetyl sodium sulfosuccinate doped PANI	Various alcohols[213]
		Cupric ion doped PANI (Cu <sup>+2</sup> /PANI) hybrid	Glu[216]
	Functional component inclusion	PANI with carbon quantum dots (QCDs)	Glu and H <sub>2</sub> O <sub>2</sub> [243]
		Sulfonic acid doped PANI-wrapped MWNTs	pH[258]
	Nanostructuring	Bishydroxyl-functionalized PANI NF	Vitamin C[283]
		PANI helical microfibers	Hg <sup>2+</sup> [293]
		C-PANI NW-CDS-NB	Arginine, cysteine[299]
Multicomponents	PANI-Au NP-modified ITO glass with a tris(2,2-bipyridyl)dichloro ruthenium(II) hexahydrate ([Ru(bpy) <sub>3</sub> ] <sup>2+</sup> )-nanoporous gold (Ru-NPG)	DNA[338]	
	GNR@silica-CN-poly(2-amino benzonitrile) (P2ABN)	Hg <sup>2+</sup> [348]	
Others	Substituted / derivatized PANI	Rhodamine 6G derivative(RS) of PANI	Hg <sup>2+</sup> [197]
	Biofunctionalization	C//PANI+/PSSA-glu-NH <sub>2</sub> -Apt	Tetrodotoxin[270]
		PANI functionalized AFM cantilever	insect pheromone 2-heptanone[271]
	Nanostructuring	PANI NFs	NH <sub>3</sub> [274]
		PANI NFs	NH <sub>3</sub> [275]
		Lysine included PANI/PAN NFs composite	NH <sub>3</sub> [276]
		Indium oxide/PANI (In <sub>2</sub> O <sub>3</sub> /PANI) composite NFs (CNFs)	NH <sub>3</sub> [277]
PANI NW-gold NPs hybrid network		H <sub>2</sub> S[295]	

**Table 5. Functionalized polythiophenes (F-PT) for sensors and related details: Functionalization approach, name of F-PT, type of sensor (based on analyte), analyte(s) name, detection technique, role of F-PT for sensing and sensor performances.**

Mode of Parent structure functionalization/modification	Name of FCP (abbreviation) or functional structure in the FCP	Type of sensor (Analyte)	Specific analyte(s)	Detection method/Technique	Function/Role of FCP for sensing*	Sensor performances* (LR and DL)	Ref
Substituted / derivatized  Neutral (side group)	Poly(3-hexyl thiophene) (P3HT)	Electrochemical (Gas)	n-hexane, toluene, chloroform, dichloromethane, methanol, and THF	Conductance	Physical interactions between analytes and polymers and swelling of the polymer films.	-	[362]
	Poly(3-triazole dihexyl thiophene) (P3TzdHT), poly(3-triazole hexyl thiophene) (P3TzHT), and poly(3-butyne triisopropylsilyl thiophene) (P3BSiT)	Optical (Nitroaromatic vapors)	Trinitrotoluene (TNT) and dinitrotoluene (DNT)	Fluorescence "quenching"	Dipole–dipole, dipole-induced dipole, and hydrogen bonding interactions of the analyte with the polymer chains	-	[363]
	Poly(4-(Ferrocenylmethylidene)-4 <i>H</i> -cyclopenta[2,1- <i>b</i> :3,4- <i>b'</i> ]-dithiophene), PCPBT-FC	Electrochemical (Humidity)	Humidity sensor	Conductance	Fe <sup>3+</sup> ions in PCPBT-FC functions as Lewis acid to generate H <sub>3</sub> O <sup>+</sup> .	-	[364]
	2,6-dithienyl-4-phenylpyridine (TPP) and 2,6-diphenyl-4-phenylpyridine (PPP) derivatives of PT	Optical (Ion)	Pd <sup>2+</sup>	Fluorescence "quenching"	Intrachain TPP-Pd <sup>2+</sup> binding	LR = 1–100 μM DL = 1 ppm	[366]
	Poly{3-[2-(2-dimethylaminoethylamino)ethoxy]-4-methylthiophene} (PTMA)	Optical (Ion)	Cu <sup>2+</sup> , Co <sup>2+</sup> and Cd <sup>2+</sup>	Fluorescence "turn off/turn on" naked eyes	Synergistic function of co-ordination of metal ions with tridentate and paramagnetic properties of metal ions	DL = 2.5 nM (Co <sup>2+</sup> ), 2.0 nM (Cu <sup>2+</sup> ) and 83 nM (Cd <sup>2+</sup> )	[371]
	Poly(3-alkoxy-4-methylthiophenes)	Optical (Ions and biomolecules)	Nucleotides, folic acid, glutathione, inorganic anions, metal ions, and	Colorimetry and fluorescence	Conformational changes or the aggregation of their π-conjugated backbones	-	[373]

			surfactants				
	Poly (3-aminophenyl boronic acid-co-3-alkylthiophene)	Electrochemical (Biomolecule)	Glu	Potentiometry	Complex formation between the boronic acid functionality of the copolymer and Glu	LR = 5 – 50 mM DL = 0.5 mM	[374]
	Poly(terthiophene benzoic acid) (pTTBA)- covalent attachment of APBA	Electrochemical (Biomolecule)	Glycated hemoglobin HbA1C	Amperometry	Catalytic reduction of H <sub>2</sub> O <sub>2</sub> by HbA1C.	LR = 0.1% to 1.5% DL = 0.052 ± 0.02%	[375]
	Quinine-linked PT-	Optical (Biomolecule)	Carbenicillin	Colorimetry	Electrostatic interactions between quinine and carbenicillin	LR = 0 – 18 μM DL = 0.54 μM	[376]
	PEDOT	Electrochemical (Biosensor)	Bisphenol A (BPA)	Amperometry	-	LR = 40 - 410 μM DL = 22 μM	[377]
	PEDOT-COOH	Electrochemical/optical (Chemical/biomolecule)	Catechol, ascorbic acid, acetaminophen, quercetin, epinephrine and tryptophan	DPV/ Fluorescence “quenching”	Electrostatically binding of inorganic NPs and layer by layer assembly formation.	-	[378]
	PEDOT-IL	Electrochemical (Neurotransmitters)	DA, AA, and UA	DPV	Positive charges in the backbone of PEDOT and cationic sites of IL improves attraction for negatively charged AA and UA, hydrophobicity of PEDOT and imidazole ring of IL contribute for π-π interaction to DA	<u>DA</u> LR = 60 - 1000 μM DL = 1.15 μM <u>UA</u> LR = 8 - 200 μM DL = 0.27 μM	[379]
	PEDOT coupled with polydopamine (PDA) (PEDOT/PDA)	Electrochemical (Neurotransmitter)	DA	Amperometry	Hydrophobic interactions for DA and electrostatic interactions for AA and UA	LR = 1.5 × 10 <sup>-6</sup> to 50 × 10 <sup>-6</sup> mol L <sup>-1</sup> DL = 0.65 × 10 <sup>-6</sup> mol L <sup>-1</sup>	[380]
Substituted / derivatized	Poly(3-(4-methyl-30-thienyloxy)propyltrimethylammonium) (PMTPA)	Optical (Biomolecules)	Cysteine (Cys) and Homocysteine (Hcys)	Colorimetry and fluorescence “quenching”	Complexation with Cys and Hcys through non-covalent interaction	<u>(Cys)</u> LR = 0 - 10 μM DL = 10 <sup>-10</sup> M	[381]
Cationic (side group)	PMTPA	Optical (Biomolecules)	Amino acids and peptides	Colorimetry	The inclusion of 2-cyano-6-methoxy benzothiazole-Cys into the PMTPA	-	[382]

					solution induces an intense circular dichromism optical signal		
PMTPA	Optical (Nucleotide phosphates)	15 nucleotide phosphates (XNPs, where X = A, U, T, G, C, and N = mono, di, tri)	Absorption spectroscopy	Planarization and /or aggregation of PT backbones through synergistic effects of electrostatic interactions and $\pi$ - $\pi$ stacking.	-	[383]	
PMTPA	Optical (Vitamin)	Folic acid	Calorimetry fluorescence "quenching"	Planar conformations and intermolecular $\pi$ - $\pi$ stacking interactions between PMTPA and folic acid	DL = $10^{-8}$ M	[384]	
PEMTEI	Optical	Lysosomal ATP	Fluorescence	Random coil conformation through electrostatic interaction with ATP	DL = $10^{-11}$ M LR = 5 – 2000 nM	[385]	
Poly[3-(1,1'-dimethyl-4-piperidinemethylene)thiophene-2,5-diyl chloride] (PTh-D) and NH <sub>2</sub> -G	Electrochemiluminescence (Biomolecules)	DA	ECL	Electron transfer to result PTh-D* (excited state) for relaxation	LR = 0.1-50.0 $\mu$ M DL = 0.04 $\mu$ M	[386]	
Poly(1H-imidazolium-1-methyl-3-{2-[(4-methyl-3-thienyl)-oxy]ethyl} chloride)	Optical (amino acids)	Nucleic acids and human thrombin	Colorimetry and fluorescence "quenching"	Electrostatic complex between negatively charged oligomers and polymers.	DL = $2 \times 10^{-15}$ mol (human thrombin)	[387]	
Poly 3-[[1-(2-hydrazino-2-oxoethyl)piperidin-4-ylidene]methyl]thiophene hydrochloride (PM1·HCl)	Optical (Ion)	Cu <sup>2+</sup> and Hg <sup>2+</sup>	Fluorescence "quenching"	PM1·HCl-Cu <sup>2+</sup> and PM1·HCl-Hg <sup>2+</sup> Complex formation	<u>Cu<sup>2+</sup></u> LR = $2.0 \times 10^{-10}$ - $1.0 \times 10^{-4}$ M DL = $2.0 \times 10^{-10}$ M <u>Hg<sup>2+</sup></u> LR = $2.0 \times 10^{-9}$ - $1.0 \times 10^{-4}$ M DL = $2.0 \times 10^{-9}$ M	[388]	
Poly[N,N,N-trimethyl-4-(thiophen-3-ylmethylene)-cyclohexanaminium chloride] (PTCA-Cl)	Optical (Surfactant)	SDBS, SDS, SLS and SDC	Colorimetry and fluorescence "turn on"	Electrostatic attraction between the negatively charged sulfonate groups of the surfactants and positively charged PTCA-Cl enhance the interaction- hydrophobic interaction between the alkyl chains of the	DL = $10^{-9}$ M (SDBS)	[389]	

					surfactants results in the transformation of PTCA-Cl aggregate into non-aggregats		
Substituted / derivatized  Anionic (side group)	Poly(2-(2-(4-methylthiophen-3-yloxy)ethyl)malonate acid) (PMTEMA)	Optical (Protein)	Protamines	Colorimetry or fluorescence "quenching"	Positively charged protamine forms a complex with PMTEMA through multiple electrostatic interactions - conformational changes of the PMTEMA backbone.	<u>Fluorescence</u> LR = 0.1 - 30 $\mu\text{g mL}^{-1}$ DL = 0.1 $\mu\text{g mL}^{-1}$ <u>Colorimetric</u> LR = 1.0 - 25 $\mu\text{g mL}^{-1}$	[390]
	Poly[2-(3-thienyl)ethoxy-4-butylsulfonate] (PTEBS)	Optical (Biomolecule)	H <sub>2</sub> O <sub>2</sub>	Calorimetry	Electron transfer from H <sub>2</sub> O <sub>2</sub> to electrode by PTEBS	LR = 0.01 – 0.5 mM DL = 0.004 mM	[391]
	APBA-functionalized poly(5,2':5,2"-terthiophene-3'-carboxylic acid (TTCA)) (APBA-pTTCA)	Electrochemical (Biomolecule)	Glu in human saliva	DPV	Diol group of Glu binds to the boronic acid group and forms tetrahedral boronate ester	LR = 0.9 and 9.1 $\mu\text{M}$ DL = 0.49 $\mu\text{M}$	[392]
	Poly(2-(2-(4-methylthiophen-3-yloxy)ethyl)malonate acid) (PMTEMA) with malonic acid group in side chain	Optical (Gas)	CO <sub>2</sub>	UV	Changes in conjugation length of PT and molecular ordering.	-	[393]
Functional ion-dopant inclusion	PEDOT doped with SDS/CTAB	Electrochemical (Drug)	Isoniazid (INH)	CV	With SDS, an electrostatic interaction between SDS and protonated INH. With CTAB, adsorption of cationic surfactant leads to positively charged hydrophilic layers and repuls cationic INH	LR = 0.1 - 8 $\mu\text{mol}\cdot\text{L}^{-1}$ and 10 - 100 $\mu\text{mol}\cdot\text{L}^{-1}$ DL = 32 nM L <sup>-1</sup> and 45 nM L <sup>-1</sup>	[395]
	PEDOT doped with anions	Electrochemical (Drug)	Acetaminophen	DPV	Strong PEDOT induced catalytic effect with a concomitant decrease in over potential for redox reaction	LR = 5 $\mu\text{M dm}^{-3}$ to 65 $\mu\text{M dm}^{-3}$ DL = 0.3 $\mu\text{M dm}^{-3}$	[396]
	PEDOT-SDS	Electrochemical (Biomolecules)	Simultaneous determination of catecholamine (CA) and serotonin (ST)	LSV	Electrostatic interactions between surfactant film and CA/ST	<u>CA</u> LR = 0.05-10 $\mu\text{mol}\cdot\text{L}^{-1}$ DL = 48 n $\text{mol}\cdot\text{L}^{-1}$ <u>ST</u> LR = 20-100 $\mu\text{mol}\cdot\text{L}^{-1}$	[397]

						DL = 71 nmol·L <sup>-1</sup>	
	PEDOT/GO	Electrochemical (Biomolecule)	Acetaminophen	CV	Formation of adduct between AP and PEDOT/GO	LR = 10-60 μM DL = 0.57 μM	[398]
	Ni <sup>2+</sup> / Cu <sup>2+</sup> hexacyanoferrate-doped PEDOT (NiHCF-PEDOT) and (CuHCF-PEDOT)	Electrochemical (Biomolecule)	AA	Amperometry	Network structure of PEDOT allows dispersion of metal particles and accelerate electron transfer	<u>NiHCF-PEDOT</u> LR = 5x10 <sup>-6</sup> – 3 × 10 <sup>-4</sup> M DL = 1x10 <sup>-6</sup> M <u>CuHCF-PEDOT</u> LR = 1.8x10 <sup>-3</sup> – 1.8x10 <sup>-2</sup> M DL = 7.1x10 <sup>-4</sup> M	[399]
	Ferrocene carboxylic acid (Fc <sup>-</sup> ) and Fe(CN) <sub>6</sub> <sup>4-</sup> doped PEDOT	Electrochemical (Vitamins)	Simultaneous determination of Vitamin B <sub>2</sub> , vitamin B <sub>6</sub> , and vitamin C	DPV	Improvements in electrical and catalytic properties of PEDOT due to the presence of Fc <sup>-</sup> and Fe(CN) <sub>6</sub> <sup>4-</sup>	<u>Vitamin B<sub>2</sub></u> LR = 0.1-300 μM DL = 0.05 μM <u>Vitamin B<sub>6</sub></u> LR = 0.5-1500 μM DL = 0.1 μM <u>Vitamin C</u> LR = 1.5-2000 μM DL = 0.7 μM	[400]
	PEDOT/CNT	Electrochemical (Biomolecule)	DA	DPV	-	LR = 0.1 to 20 μM DL = 20 nM	[401]
	GO-doped PEDOT composite	Electrochemical (Chemical)	HQ and catechol (simultaneous detection)	DPV	-	<u>HQ</u> LR = 2.5 to 200 μM DL = 1.6 μM <u>CT</u> LR = 2 to 400 μM DL = 1.6 μM	[402]

	PEDOT–Polyethylene imine (BPEI) composite	Electrochemical (Gas)	CO <sub>2</sub>	Resistance	BPEI dedopes PEDOT and transforms to HCO <sub>3</sub> <sup>-</sup> and dopes PEDOT on interaction with CO <sub>2</sub> .	DL = 1000 ppm	[403]
	PEDOT:PSS and Zinc Stannate (ZnSnO <sub>3</sub> ) NC	Electrochemical (Gas)	Skin humidity	Impedance	Cubic crystalline structure of ZnSnO <sub>3</sub> and porosity of the sensing film	LR = 0% - 90%	[405]
	HFIP-PT/SWCNT	Optical (Gas)	Dimethyl methylphosphonate (DMMP)	Fluorescence “turn on”	HFIP promotes strong interaction between DMMP and HFIP-PT	LR = 0.05 - 25 ppm	[406]
	G-encapsulated PEDOT (PEDOT/GR)	Electrochemical (Ion)	Nitrite	CV	Catalytic capabilities of GR towards nitrite	LR = 0.3 - 600 μM DL = 0.1 μM	[407]
Functional component included F-PTs	PEDOT-MWNT-COOH NC	Electrochemical (Biomolecule)	AA	Amperometry	Large surface area and good conductivity of the NC	LR = 100 μM - 20 mM, DL = 4.2 μM	[408]
	PEDOT-deep eutectic solvents (DES)	Electrochemical (Biomolecule)	AA, DA and UA	QCM	Electrostatic interactions and doping-dedoping process		[409]
	PT-poly (3-thienyl boronic acid)	Electrochemical (Biomolecule)	DA	EIS	Interaction between DA and boronic groups in the polymers	LR = 7.8 - 125 μM DL = 0.3 μM	[410]
	PEDOT-ionic liquid 1-butyl-3-methylimidazolium bromide (BMIMBr)	Electrochemical (Biomolecule)	bisphenol A (BPA)	Amperometry	Surface hydrophilic anions of IL-adsorption controlled electrochemical oxidation of BPA	LR = 0.1-500 μM DL = 0.02 μM	[411]
	PT-G NC	Electrochemical (Gas)	NO <sub>2</sub>	Resistance	Adsorption-desorption processes, good electron transfer process for NO <sub>2</sub> due to π-π interactions	DL = 10 ppm LR = 1 - 10 ppm	[412]
	PEDOT-G NC	Electrochemical (Gas)	NO <sub>2</sub>	EIS	G provides high surface area to improve repeatability	-	[413]
Biofunctionalization	Copolymer of thiophene (Th), thiophene-3-acetic acid (Th–COOH), and dicyclopentadienyl iron-1,4-dienylmethyl-2-(thiophen-3-yl)acetate (Th–Fc)/ GOx	Electrochemical (Biomolecule)	Glu	Amperometry	Fc units in copolymer film influence catalytic current response-Copolymer mediates electron transfer between GOx and electrode	LR = 0.5 - 3 mM DL = 2.5x10 <sup>-6</sup> mM	[414]
	Poly(3-methylthiophene (3MT)/thiophene-3-acetic acid (T3A))/ GOx	Electrochemical (Biomolecule)	Glu	Amperometry	Poly-l-lysine acts as effective linker to GOx. 2,5 dihydroxy (DHP) groups function as electron mediator.	LR = 0-20 mM	[415]
	PT functionalized with MB (PMT-MB)/ssODN	Electrochemical and optical	dsODN	DPV and UV	Electrostatic interactions between PMT-MB and dsODNs	LR = 6.37 nM - 0.204 μM (DPV)	[416]

	(Oligonucleotide)					LR = 0.74 – 14.8 $\mu$ M (UV)	
SELEX-synthesized 76-mer biotinylated aptamer incorporated in a dendritic generation 1-poly(propylene imine)-PT (G1PPT-co-PEDOT)/ssDNA	Electrochemical (Oligonucleotide)	Endocrine disrupting compound (EnDC) 17 $\beta$ -estradiol	SWV		EnDC binds to the ssDNA aptamer	LR = 0.1-100 nM	[417]
Poly(4-hydroxyphenyl thiophene-3-carboxylate) (PHPT)/DNA	Electrochemical (Oligonucleotide)	ODN	CV		Binding of ODN probes with target ODN at the PHPT/ODN electrode	LR = 1.49-7.45 nM DL = 1.49 nM	[418]
PT derivatives based on the protection of –COOH groups in pentafluorophenylthiophene-3-acetate, 4-chlorobenzylthiophene-3-acetate, and N-hydroxyphthalimidothiophene-3-acetate with substituted benzyl groups/ODN	Electrochemical (Oligonucleotide)	DNA	CV		Formation of hydrogen bonds	-	[419]
PEDOT:PSS/ ssDNA	Electrochemical (Oligonucleotide)	DNA	OECT-drain source current		Surface potential Modulation of the gate electrode induced by the immobilization and hybridization of the DNA molecules on the gate surface	LR = upto 1 nM DL = 10 pM	[420]
Ascorbate oxidase (AO)/PEDOT-lauryl sarcocinate (SL)	Electrochemical (Vitamin)	Vitamin c	Amperometry		AO in the PEDOT/SL film catalyzes bioelectrochemical oxidation of Vc and PEDOT/SL mediates electron transfer	LR = 0.002–14 mM DL = 0.464 $\mu$ M	[421]
M13-K07-PEDOT	Electrochemical (Virus)	Antibody (p-Ab)	EIS		PEDOT-virus layer intrinsically limits non-specific binding of antibody	LR = 6 to 66 nM DL = 6 nM	[422]
Quinone-Fused PT	Electrochemical (Bacteria)	E. coli	SWV		Polyvalent linkage to carbohydrates	DL = 25 cell/mL	[423]
Tosylate-doped PEDOT (PEDOT:TsO) covalent functionalized with two aptamer probes	Electrochemical (drug)	Ampicillin and kanamycin A	EIS		TsO of PEDOT:TsO and PEDOT-OH:TsO affinity to the drugs.	(Ampicillin) LR = 100 pM to 1 $\mu$ M DL = 10 pM	[424]

						(Lanamycin A) LR = 10 nM to 1 mM DL = 1 nM	
	PEDOT/alcohol dehydrogenase (ADH)	Electrochemical (Vapour)	Ethanol	Amperometry	-	linear range = 21-1688 ppm	[425]
	PEDOT:PSS/ tyrosinase(Tyr)	Electrochemical (Phenolic compound)	Bisphenol A (BPA), 4-tert octyl phenol (OP), 4-Nonyl phenol (NP)	Amperometry	PEDOT:PSS transports electrons from Tyr to electrode surface	<u>BPA</u> LR = $2 \times 10^{-8}$ - $9 \times 10^{-6}$ M DL = $1.9 \times 10^{-8}$ M <u>OP</u> LR = $5 \times 10^{-8}$ - $7 \times 10^{-6}$ M DL = $3.7 \times 10^{-8}$ M <u>NP</u> LR = $1 \times 10^{-7}$ - $6 \times 10^{-6}$ M DL = $9.5 \times 10^{-8}$ M	[426]
Nanostructured F-PTs	Copolymer of PEDOT and PEDOT-COOH (PEDOT-co-PEDOT-COOH) NW/ ODN	Imaging(Cancer cell)	ODN	Resistance	Electrostatic interaction of ODN on the surface of copolymer	LR = upto 1 nM DL = 10 fM	[427]
	PEDOT-COOH nanodots/ anti-EpCAM	Imaging (Tumor cell)	Tumor cell	Cell capturing microscope	Specific capture of MCF7 cells than that of HeLa cells	-	[428]
	Hydroxylated PEDOT (PEDOT-OH) NTs	Electrochemical (Nerve agent)	Dimethyl methyl phosphonate (DMMP)	Resistance	DMMP forms a hydrogen bonding base to accept electron from PEDOT-OH	LR = 10 ppt - 50 ppb DL = 10 ppt	[429]
	PEDOT NPs/ ssDNA	Optical (Oligonucleotide)	DNA	Fluorescence "turn on"	Electrostatic interaction between PEDOT and negatively charged ssDNA and no binding interaction with DNA base and dsDNA	DL = 30 pM	[430]
	Palladium NPs (Pd NPs)-incorporated PEDOT (Pd/PEDOT) nanospheres	Electrochemical (Biomolecule)	H <sub>2</sub> O <sub>2</sub>	Amperometry	PEDOT serves as platform for anchoring PdNPs	LR = $2.5 \times 10^{-3}$ - 1.0 mM DL = 2.84 $\mu$ M	[370]

PT nanofilm	Electrochemical (Biosensor)	Glu	Potentiometry	Intermolecular hydrogen bonding interactions and electrostatic interactions	LR = 1 – 9 mM	[431]
PEDOT NFs modified pencil graphite electrode (Ox-PEDOT-nf/PGE)	Electrochemical (Biomolecule)	UA	CV	Interaction between ox-PEDOT and hydroxyl groups at the electrode surface	LR = 0.01-20.0 $\mu$ M DL = 1.3 nM	[433]
Nanoporous-PEDOT	Electrochemical (Biomolecule)	NADH	Amperometry	Porous network structure of PEDOT facilitate electron transfer	LR = 5 - 45 $\mu$ M DL = 3.8 $\mu$ M	[434]
Nanostructured biotinylated PT derivative (PTBL)	Photoelectrochemical (Drug)	Streptavidin	Photo-current	Negative applied potentials, promotes hole transfer from PTBL film to Au electrode surface and facilitate the hole-electron separation.	-	[435]
Nanostructured PEDOT/ $\beta$ -cyclodextrin (PEDOT/ $\beta$ -CD)	Electrochemical	Hyperoside and shikonin (simultaneous)	CV and DPV	Electrocatalytic activity due to unique PEDOT: $\beta$ -CD configuration	LR = 0.007 – 5.0 $\mu$ M (shikonin) LR = 0.003 – 10 $\mu$ M (hyperoside)	[436]
ZnO/PT NFs	Electrochemical (Gas)	NH <sub>3</sub>	Resistance	Charge transfer to PEDOT and hole transfer mobility formation of p-n junction	-	[437]
Ag NPs/PEDOT NTs	Electrochemical (Gas)	NH <sub>3</sub>	Resistance	Increase in surface area and conductivity by Ag NPs	LR = 1-100 ppm DT = 1 ppm	[438]
Poly [2-(3-thienyl)ethanol butoxycarbonylmethylurethane] (PURET) NPs	Optical (Nitroaromatic explosive)	DNT and TNT	Fluorescence and photoluminescence “quenching”	Improved polymer-analyte interaction	-	[439]
PEDOT NTs	Electrochemical (Gas)	NO <sub>2</sub>	Resistance	Hole carriers density changes by electron transfer	DL = 80 ppb LR = 0.2 - 20 ppm	[440]
PEDOT NRs-GO	Electrochemical (Ion)	Nitrite	Amperometry	GO acts as stabilizing agent for PEDOT due to the abundance of hydrophilic groups	LR = 4 $\mu$ M - 2.48 mM DL = 1.2 $\mu$ M	[367]
PEDOT hollow microflowers (PEDOT-HMF)	Electrochemical (Ion)	Nitrite	Amperometry	High surface area of flower like structure of PEDOT	LR = 50 - 7500 $\mu$ M DL = 0.59 $\mu$ M	[441]
PEDOT NRs/rGO NC	Electrochemical	Hg <sup>2+</sup>	DPV	rGO assists the enhanced	LR = 10.0 nM - 3.0	[442]

		(Ion)			preconcentration of $\text{Hg}^{2+}$ ion and electro reduction to $\text{Hg}^0$ .	$\mu\text{M}$ DL = 2.78 nM	
Multicomponents	BPEI-Fc/PEDOT:PSS/GOx nanobeads	Electrochemical (Biomolecule)	Glu	Amperometry	Enhanced in diffusion and electron transfer rate by BPEI-Fc/PEDOT:PSS	LR = 0.5 - 4.5 mM	[443]
	GOx/GS-PEDOT:PSS	Electrochemical (Biomolecule)	Glu	Amperometry	Efficient direct electrochemistry of GOx, good electron transfer rate and high electron mobility were collectively achieved	LR = 20–900 $\mu\text{M}$ DL = 3 $\mu\text{M}$	[444]
	PVA incorporated PEDOT:PSS/ GOx	Electrochemical (Biomolecule)	Glu	OECT	Retention of biological activity of enzyme		[445]
	PEDOT NFs–Pd/GOx	Electrochemical (Biomolecule)	Glu	Amperometry	Synergistic augmentation of nanofibrous PEDOT and Pd NPs for enhancement of sensor performances	LR = 0.5 - 30 mM DL = 75 $\mu\text{M}$	[446]
	NPG/PEDOT/GOx	Electrochemical (Biomolecule)	Glu	Amperometry	3D porous structure of Au and inherent stability of PEDOT provide robust matrix for GOx loading	LR = 0.1 – 15 mM DL = 10 $\mu\text{M}$	[447]
	GO doped PEDOT modified with copper NPs	Electrochemical (Biomolecule)	Glu	Amperometry	Synergistic effects from Cu NPs, PEDOT and GO	LR = 0.1 $\mu\text{M}$ to 1.3 mM DL = 47 nM	[448]
	PEDOT PAA/poly(4-lithium styrenesulfonic acid) (PSSLi)	spectrophotometric (Biomolecule)	Glu	Spectrophotometry	Covalent linkage formation between PAA and GOx	-	[449]
	Poly(2-(2,5-di(thiophen-2-yl)-1H-pyrrol-1-yl) acetic acid) functionalized with lysine (lys) and poly(amidoamine) PAMAM derivatives/ GOx	Electrochemical (Biomolecule)	Glu	Amperometry	The hyperbranched structure of PAMAM provides stability.	<u>Lys functionalized</u> LR = 0.01 – 2.4 mM DL = 19.0 $\mu\text{M}$ <u>PAMAM functionalized</u> LR = 0.02 – 1.2 mM DL = 3.47 $\mu\text{M}$	[450]

PEDOT / poly(methylene blue) (PMB)/GOx (PEDOT/PMB/GOx)	Electrochemical (Biomolecule)	Ascorbate anions and Glu	Amperometry	PMB mediates electron transfer between electrode and enzyme catalytic center	<u>ascorbate anion</u> LR = upto 7 mM DL = 12.5±1.3 µM <u>Glu</u> LR = 0.02 - 1.4 mM DL = 7.2 µM	[451]
PEDOT:PSS–Nafion	Electrochemical (Biomolecule)	DA	DPV	The combined components resulted good electrochemical activity, reproducibility and, fast electron transfer, and low swelling	LR = 0.10 - 50 µM DL = 0.03 µM	[452]
Au NP/ PEDOT/SDS	Electrochemical (Biomolecule)	DA	LSV	Adsorption of DA cations on Au NPs and also interaction of hydrophobic DA cation with hydrophobic part of PEDOT- Au acts as a promoter for electrochemical reaction of DA at the electrode	LR = 0.5 - 20 µmol L <sup>-1</sup> and 25 -140 µmol L <sup>-1</sup>	[453]
Pd/PEDOT/rGO	Electrochemical (Biomolecule)	DA	DPV	Pd NPs enhanced electrocatalytic activity	DL = 1-200 µM LR = 0.14 µM	[454]
CS/ uricase/PTBA-Pt <sub>nano</sub>	Electrochemical (Biomolecule)	UA	Amperometry	-	LR = 5 µM - 1.2 mM DL = 1 µM	[455]
Meldola blue-incorporated PEDOT:PSS (PEDOT:PSS-MDB)	Electrochemical (Biomolecule)	H <sub>2</sub> O <sub>2</sub>	Amperometry	Electron mediating effect of MDB	LR = 0.1 - 120 µM, DL = 0.1 µM	[456]
PEDOT nanowhiskers–AuNPs–Hemoglobin	Electrochemical (Biomolecule)	H <sub>2</sub> O <sub>2</sub>	Amperometry	PEDOT transfers electron from the active center of Hb to electrode	LR = 1 µM - 1100 µM DL = 0.6 µM	[457]
Ethyl sulfate-functionalized PEDOT (PEDOT–EtSO <sub>4</sub> )/ascorbate oxidase (AO)/IL/Nf	Electrochemical (Biomolecule)	Vitamin C/H <sub>2</sub> O <sub>2</sub>	Amperometry	-	LR = 8.0×10 <sup>-7</sup> - 1×10 <sup>-3</sup> M DL = 0.147 µM	[458]
Ag NP-incorporated PEDOT:PSS/DNA	Electrochemical (Oligonucleotide)	DNA	DPV	Hybridization via intercalation of the ruthenium complex	LR = 1.0×10 <sup>-15</sup> M - 1.0×10 <sup>-9</sup> M, DL = 5×10 <sup>-16</sup> M	[459]

PEDOT/Au NPs/ Thiolated capture strand DNA	Electrochemical (Oligonucleotide)	ODN	CV	Reduction of hydroquinone and mediate electron transfer to the HRP labeled protein strand	LR = 150 pM - 1 mM	[460]
PEDOT/Au NPs/DNA	Electrochemical (Oligonucleotide)	DNA	CC	Au NPs promoted hybridization of single and double bond mismatched target DNA	LR = $1.0 \times 10^{-13}$ - $1.0 \times 10^{-15}$ M DL = $2.6 \times 10^{-16}$ M	[461]
Poly[3-(3'-N,N,N-triethylamino-1-propyloxy)-4-methyl-2,5-thiophene hydrochloride] (PMNT) DNA/PMNT and DNA/miRNA/PMNT	Optical (Oligonucleotide)	miRNA and RNase H activity	Colorimetry	Conformational and colorimetric changes of PMNT in the DNA/PMNT duplex and DNA/miRNA/PMNT triplex	-	[462]
PEDOT/MnO <sub>2</sub> nanoellipsoid	Electrochemical (Neuronal)	PC12 cells	Amperometry	Neurite outgrowth was facilitated by PEDOT and cell differentiation was facilitated by MnO <sub>2</sub>	-	[463]
AuNPs/PEDOT/G	Electrochemical (immunosensor)	Carcinoembryonic antigen	DPV	Large amount of Au NP loading improve electrochemical property	LR = 0.0004 to 40 ng mL <sup>-1</sup> DL = 0.1 pg mL <sup>-1</sup>	[464]
GS/PEDOT:PSS	Electrochemical (Biomarker)	H <sub>2</sub> O <sub>2</sub> , NAD <sup>+</sup> /NADH, and Fe(CN) <sub>6</sub> <sup>3-/4-</sup>	CV	Enhancement of sensor performance with high reproducibility	H <sub>2</sub> O <sub>2</sub> LR = 1.3-7.6 mM DL = 194.37 μM NADH LR = 50-1500 μM DL = 17.28 μM Fe(CN) <sub>6</sub> <sup>3-/4-</sup> LR = 0.5-320 μM DL = 0.36 μM	[465]
Au/PEDOT:PSS co-immobilization of lipase, glycerol kinase, and glycerol 3-phosphate oxidase	Electrochemical (Biosensor)	Triglyceride	Amperometry	enhanced electrochemical signal for the analyte by Au NPs	LR = 0-531 mg/dL, DL = 7.88 mg/dL	[466]
Poly [N-9'-heptadecanyl-2,7-carbazole-alt-5,5-(4',7'-di-2-thienyl-2',1',3'-benzothiadiazole)] (PCDTBT) and [6,6]-phenyl C71-butyric acid methyl ester (PC70BM) /PEDOT:PSS	Optical (Hormone)	Human thyroid stimulating (TSH)	Microfluidic chemiluminescence	High detection reproducibility and specificity	LR = 0.03 - 10 ng/mL	[467]

	Pd NP-decorated PEDOT:PSS	Electrochemical (Reducing compounds)	Hydrazine and NADH	Conductivity	PdNPs serve as reaction sites for oxidation of hydrazine/NADH and the release of electrons reduces PEDOT	DL = 0.5 $\mu\text{M}$ (hydrazine) DL = 10 $\mu\text{M}$ (NADH)	[468]
	SDS/CTAB-doped PEDOT/MWNT	Electrochemical (Pesticide)	Cypermethrin (CYP), deltamethrin (DEL), fenvalenate (FEN) and dicofol (DCF)	DPV	Good electron transfer and large surface area	<u>CYP</u> LR = 0.015 – $5 \times 10^4 \mu\text{g L}^{-1}$ DL = 0.015 $\mu\text{g L}^{-1}$ <u>DEL</u> LR = 0.063 – $5 \times 10^4 \mu\text{g L}^{-1}$ DL = 0.063 $\mu\text{g L}^{-1}$ <u>FEN</u> LR = 0.061 – $5 \times 10^4 \mu\text{g L}^{-1}$ DL = 0.061 $\mu\text{g L}^{-1}$ <u>DCF</u> LR = 0.01 – $5 \times 10^4 \mu\text{g L}^{-1}$ DL = 0.01 $\mu\text{g L}^{-1}$	[469]
	Iron oxide NPs ( $\text{Fe}_2\text{O}_3$ NPs), PEDOT-rGO NC $\text{Fe}_2\text{O}_3$ NPs/rGO/PEDOT	Electrochemical (Biosensor)	Acetylcholine (ACh)	CV	Synergistic effects of $\text{Fe}_2\text{O}_3$ NPs, rGO and PEDOT	LR = 4.0 nM to 800 $\mu\text{M}$ DL = 4.0 nM	[470]
	3D-PEDOT- $\text{Cu}_x\text{O}$ hybrid	Electrochemical (Gas)	Hydrazine	Amperometry	Efficient electron transfer and mass transfer and interactions between PEDOT and $\text{Cu}_x\text{O}$	LR = 0.5 $\mu\text{M}$ - 53 mM DL = 0.2 $\mu\text{M}$	[471]
	$\text{O}_2$ plasma-treated SWNTs and a PEDOT/PSS composite	Electrochemical (Gas)	Trimethylamine (TMA)	Resistance	Electrons from the methyl groups of TMA molecules combine with the holes of the p-type PEDOT/PSS grains leading to the variations of delocalization degree of conjugated $\pi$ electrons of PEDOT chains-PEDOT:PSS acts as olfactory receptor and functionalized SWNT acts as signal transducing pathway	LR = 6 - 90 ppb	[472]

O <sub>2</sub> plasma-treated SWNTs and a PEDOT/PSS composite	Electrochemical (Gas)	NH <sub>3</sub> , TMA	Resistance	Hole conducting PEDOT:PSS interacts with hole donating analyte to result increase in delocalization of degree of conjugated $\pi$ -electrons	LR = 2 – 300 ppm (NH <sub>3</sub> ) LR = 6 – 1000 ppb (TMA)	[473]
PEDOT:PSS/TiO <sub>2</sub> -IDE	Electrochemical (Gas)	NO	Resistance	Reduction of depletion region results increase in conductivity	DL = 1 ppb	[474]
WO <sub>3</sub> -PEDOT:PSS NCs	Electrochemical (Gas)	NO <sub>2</sub>	Resistance	Hetrojunction formation and creation of space charge region	DL = 30 ppb LR = 50 – 200 ppb	[475]
N-GQDs/PEDOT-PSS NC	Electrochemical (Gas)	VOC	Resistance	Doping – dedoping and swelling upon diffion of VOC	LR = 1 – 1000 ppm	[476]
PEDOT:PSS-PVA NC	Electrochemical (Humidity)	Humidity	Resistance	Change ion capacitance and dielectric constant of the film	-	[477]
Iron oxide-embedded PEDOT:PSS NC	Electrochemical (Humidity)	Humidity	Resistance	Dopole moment of water causes screening effect between conducting sites in PEDOT. Iron oxide contributes to increase in sensitivity	LR = 30 - 70% RH	[478]
magnetic ribbon-coated PEDOT:PSS	Wireless (Humidity)	Humidity	Mechanical resonance frequency	-	-	[479]
RG-O:PIL/PEDOT	Electrochemical (Gas)	Methanol, chloroform, tetrahydrofuran, benzene	Resistance	Synergistic effect of hybrid materia-. PEDOT functions as adsorbant, GR provides surface area and PIL unit enables high sensitivity	LR = 1 - 90 ppm	[480]
SWCNT/p-tert butyl calixarene-substituted PT	Electrochemical (Chemical)	Xylene isomers	Resistance	Calixarene linked PT differentiates the isomers of xylene because of the shape-persistent hydrophilic binding pockets of the cone conformation and host-guest chemistry	-	[481]
Alcohol dehydrogenase /Ru(bpy) <sub>3</sub> <sup>2+</sup> / PEDOT-PSS-G	Optical (Chemical)	Ethanol	Electrochemiluminescence (ECL)	PEDOT-PSS-G provides conducting pathway to connect electroactive material sites- ECL signal was generated by the reaction between ruthenium species and NADH	LR = 2.5x10 <sup>-5</sup> – 2.5x10 <sup>-2</sup> mol/L DL = 2.5x10 <sup>-6</sup> mol/L	[482]

Co NPs/PEDOT/GS	Electrochemical (Ion)	Nitrite	Amperometry	PEDOT functions as effective dispersant for CoNPs. CoNPs provide fast mass transport for improved electroactivity	LR = 0.5 $\mu$ M - 240 $\mu$ M, DL = 0.15 $\mu$ M	[483]
Phosphovanadomolybdates H <sub>6</sub> [PMo <sub>9</sub> V <sub>3</sub> O <sub>40</sub> ]-PEDOT-Au NPs	Electrochemical (Ion)	Nitrite	Amperometry	Synergistic effects from the components	LR = 2.5 $\times 10^{-9}$ M- 1.43 $\times 10^{-3}$ M DL = 1.0 $\times 10^{-9}$ M	[484]
Hemin-PEDOT functionalized boron-doped diamond	Electrochemical (Ion)	Peroxynitrite	Amperometry	Oxidation of PON is mediated by Hemin-PEDOT	DL = 10 $\pm$ 0.5 nM LR = 3 – 10 nM	[485]
PEDOT:PSS-stabilized gold NPs (Au@PEDOT)	Electrochemical (Ion)	Hg(II)	LSV	Au NPs in Au@PEDOT:PSS served as the substrate for Hg deposition-accompanied by amalgamation	LR = upto $\mu$ M DL = 0.05 $\mu$ M	[486]
PEDOT:PSS-coated cotton fiber	Electrochemical (Ion)	NaCl	OECT (source-drain current)	Large number of fibers interconnect along with PEDOT:PSS and contribute to the conduction along the cotton fiber	LR = 30-60 mM	[487]
SiMO-PEDOT/MWCNT hybrid composite	Electrochemical (Ion)	Persulfate (S <sub>2</sub> O <sub>8</sub> <sup>2-</sup> )	Amperometry	SiMO and PEDOT assisted electrocatalysis	LR = 1-3333 $\mu$ M DL = 1 $\times 10^{-6}$ M	[488]
PVP-PEDOT:PSS	Strain	Strain	Current		linear elastic response to strain up to 4% curled structure of microfibers	[489]
ZnO NR/PEDOT:PSS hybrid	light sensor	ultraviolet light	Photocurrent	p-n heterojunction formation – photoinduced hole generation – passivation effect of PEDOT		[490]
PEDOT-IPN	Mechanical	Strain	Pulse width modulation	Voltage generated in response to mechanical deformation	-	[491]

\*If available in the reference paper

CC – Chrono coulometry; CV – Cyclic voltammetry; DPV – Differential pulse voltammetry; ECL – Electro chemiluminescence; EIS – Electrochemical impedance spectroscopy; LSV – Linear sweep voltammetry; OECT – Organic electrochemical transistor; SWV – Square wave voltammetry; UV – UV visible spectroscopy

**Table 6. Cross-sectional details on the signal transduction mode based sensors utilizing the four functionalization categories of polythiophenes (F-PTs)**

Sensor signal transduction mode	Mode of Parent structure functionalization/ modification	Name of FCP (abbreviation) or functional structure in the FCP	Specific analyte(s)	
Electrochemical	Substituted / derivatized	Poly(3-hexyl thiophene) (P3HT)	n-hexane, toluene, chloroform, dichloromethane, methanol, and THF[362]	
		Neutral (side group)	Poly(4-(Ferrocenylmethylidene)-4 <i>H</i> -cyclopenta[2,1-b:3,4-b']-dithiophene), PCPBT-FC	Humidity sensor[364]
			Poly (3-aminophenyl boronic acid-co-3-alkylthiophene)	Glu[374]
			Poly(terthiophene benzoic acid) (pTTBA)- covalent attachment of APBA	Glycated hemoglobin HbA1C[375]
			PEDOT	Bisphenol A (BPA) [377]
			PEDOT-IL	DA, AA, and UA[379]
			PEDOT coupled with polydopamine (PDA) (PEDOT/PDA)	DA[380]
			Poly[3-(1,1'-dimethyl-4-piperidinemethylene)thiophene-2,5-diyl chloride] (PTh-D) and NH <sub>2</sub> -G	DA[386]
	APBA-functionalized poly(5,2': 5,2''-terthiophene-3'-carboxylic acid (TTCA)) (APBA-pTTCA)	Glu in human saliva[392]		
	Functional ion-dopant inclusion	PEDOT doped with SDS/CTAB	Isoniazid (INH) [395]	
		PEDOT doped with anions	Acetaminophen[396]	
		PEDOT-SDS	Simultaneous determination of catecholamine (CA) and serotonin (ST) [397]	
		PEDOT/GO	Acetaminophen[398]	
		Ni <sup>2+</sup> / Cu <sup>2+</sup> hexacyanoferrate-doped PEDOT (NiHCF-PEDOT) and (CuHCF-PEDOT)	AA[399]	
		Ferrocene carboxylic acid (Fc <sup>-</sup> ) and Fe(CN) <sub>6</sub> <sup>4-</sup> doped PEDOT	Simultaneous determination of Vitamin B <sub>2</sub> , vitamin B <sub>6</sub> , and vitamin C[400]	
		PEDOT/CNT	DA[401]	
		GO-doped PEDOT composite	HQ and catechol (simultaneous detection) [402]	
		PEDOT–Polyethylene imine (BPEI) composite	CO <sub>2</sub> [403]	
		PEDOT:PSS and Zinc Stannate (ZnSnO <sub>3</sub> ) NC	Skin humidity[405]	

		G-encapsulated PEDOT (PEDOT/GR)	Nitrite[407]
Functional component included F-PTs		PEDOT-MWNT-COOH NC	AA[408]
		PEDOT-deep eutectic solvents (DES)	AA, DA and UA[409]
		PT-poly (3-thienyl boronic acid)	DA[410]
		PEDOT-ionic liquid 1-butyl-3-methylimidazolium bromide (BMIMBr)	bisphenol A (BPA) [411]
		PT-G NC	NO <sub>2</sub> [412]
		PEDOT-G NC	NO <sub>2</sub> [413]
Biofunctionalization		Copolymer of thiophene (Th), thiophene-3-acetic acid (Th-COOH), and dicyclopentadienyl iron-1,4-dienylmethyl-2-(thiophen-3-yl)acetate (Th-Fc)/ GOx	Glu[414]
		Poly(3-methylthiophene (3MT)/thiophene-3-acetic acid (T3A))/ GOx	Glu[415]
		PT functionalized with MB (PMT-MB)/ssODN	dsODN[416]
		SELEX-synthesized 76-mer biotinylated aptamer incorporated in a dendritic generation 1-poly(propylene imine)-PT (G1PPT-co-PEDOT)/ ssDNA	Endocrine disrupting compound (EnDC) 17 $\beta$ -estradiol[417]
		Poly(4-hydroxyphenyl thiophene-3-carboxylate) (PHPT)/DNA	ODN[418]
		PT derivatives based on the protection of -COOH groups in pentafluorophenylthiophene-3-acetate, 4-chlorobenzylthiophene-3-acetate, and N-hydroxyphthalimidothiophene-3-acetate with substituted benzyl groups/ODN	DNA[419]
		PEDOT:PSS/ ssDNA	DNA[420]
		Ascorbate oxidase (AO)/PEDOT-lauryl sarcocinate (SL)	Vitamin c[421]
		M13-K07-PEDOT	Antibody (p-Ab) [422]
		Quinone-Fused PT	E. coli[423]
		Tosylate-doped PEDOT (PEDOT:TsO) covalent functionalized with two aptamer probes	Ampicillin and kanamycin A[424]
		PEDOT/alcohol dehydrogenase (ADH)	Ethanol[425]
		PEDOT:PSS/ tyrosinase(Tyr)	Bisphenol A (BPA), 4-tert octyl phenol (OP), 4-Nonyl phenol (NP) [426]
	Nanostructured F-PTs		Hydroxylated PEDOT (PEDOT-OH) NTs
		Palladium NPs (Pd NPs)-incorporated PEDOT (Pd/PEDOT) nanospheres	H <sub>2</sub> O <sub>2</sub> [370]
		PT nanofilm	Glu[431]
		PEDOT NRs grown on GO (PEDOT/GO)	Rutin[432]
		PEDOT NFs modified pencil graphite electrode (Ox-PEDOT-nf/PGE)	UA[433]
		Nanoporous-PEDOT	NADH[434]

		Nanostructured PEDOT/ $\beta$ -cyclodextrin (PEDOT/ $\beta$ -CD)	Hyperoside and shikonin (simultaneous) [436]
		ZnO/PT NFs	NH <sub>3</sub> [437]
		Ag NPs/PEDOT NTs	NH <sub>3</sub> [438]
		PEDOT NTs	NO <sub>2</sub> [440]
		PEDOT NRs-GO	Nitrite[367]
		PEDOT hollow microflowers (PEDOT-HMF)	Nitrite[441]
		PEDOT NRs/rGO NC	Hg <sup>2+</sup> [442]
	Multicomponents	BPEI-Fc/PEDOT:PSS/GOx nanobeads	Glu[443]
		GOx/GS-PEDOT:PSS	Glu[444]
		PVA incorporated PEDOT:PSS/ GOx	Glu[445]
		PEDOT NFs–Pd/GOx	Glu[446]
		NPG/PEDOT/GOx	Glu[447]
		GO doped PEDOT modified with copper NPs	Glu[448]
		Poly(2-(2,5-di(thiophen-2-yl)-1H-pyrrol-1-yl) acetic acid) functionalized with lysine (lys) and poly(amidoamine) PAMAM derivatives/ GOx	Glu[450]
		PEDOT / poly(methylene blue) (PMB)/GOx (PEDOT/PMB/GOx)	Ascorbate anions and Glu[451]
		PEDOT:PSS–Nafion	DA[452]
		Au NP/ PEDOT/SDS	DA[453]
		Pd/PEDOT/rGO	DA[454]
		CS/ uricase/PTBA-Pt <sub>nano</sub>	UA[455]
		Meldola blue-incorporated PEDOT:PSS (PEDOT:PSS-MDB)	H <sub>2</sub> O <sub>2</sub> [456]
		PEDOT nanowhiskers–AuNPs–Hemoglobin	H <sub>2</sub> O <sub>2</sub> [457]
		Ethyl sulfate-functionalized PEDOT (PEDOT–EtSO <sub>4</sub> )/ascorbate oxidase (AO)/IL/Nf	Vitamin C/H <sub>2</sub> O <sub>2</sub> [458]
		Ag NP-incorporated PEDOT:PSS/DNA	DNA[459]
		PEDOT/Au NPs/ Thiolated capture strand DNA	ODN[460]
		PEDOT/Au NPs/DNA	DNA[461]
		PEDOT/MnO <sub>2</sub> nanoellipsoid	PC12 cells[463]
		AuNPs/PEDOT/G	Carcinoembryonic antigen [464]
		GS/PEDOT:PSS	H <sub>2</sub> O <sub>2</sub> , NAD <sup>+</sup> /NADH, and Fe(CN) <sub>6</sub> <sup>3-/4-</sup> [465]
		Au/PEDOT:PSS co-immobilization of lipase, glycerol kinase, and glycerol 3-phosphate oxidase	Triglyceride[466]

		Pd NP-decorated PEDOT:PSS	Hydrazine and NADH[468]
		SDS/CTAB-doped PEDOT/MWNT	Cypermethrin (CYP), deltamethrin (DEL), fenvalenate (FEN) and dicofol (DCF) [469]
		Iron oxide NPs (Fe <sub>2</sub> O <sub>3</sub> NPs), PEDOT-rGO NC Fe <sub>2</sub> O <sub>3</sub> NPs/rGO/PEDOT	Acetylcholine (ACh) [470]
		3D-PEDOT-Cu <sub>x</sub> O hybrid	Hydrazine[471]
		O <sub>2</sub> plasma-treated SWNTs and a PEDOT/PSS composite	Trimethylamine (TMA) [472]
		O <sub>2</sub> plasma-treated SWNTs and a PEDOT/PSS composite	NH <sub>3</sub> ,TMA[473]
		PEDOT:PSS/TiO <sub>2</sub> -IDE	NO[474]
		WO <sub>3</sub> -PEDOT:PSS NCs	NO <sub>2</sub> [475]
		N-GQDs/PEDOT-PSS NC	VOC[476]
		PEDOT:PSS-PVA NC	Humidity [477]
		Iron oxide-embedded PEDOT:PSS NC	Humidity [478]
		RG-O:PIL/PEDOT	Methanol, chloroform, tetrahydrofuran, benzene[480]
		SWCNT/p-tert butyl calixarene-substituted PT	Xylene isomers[481]
		Co NPs/PEDOT/GS	Nitrite [483]
		Phosphovanadomolybdates H <sub>6</sub> [PMo <sub>9</sub> V <sub>3</sub> O <sub>40</sub> ]-PEDOT-Au NPs	Nitrite[484]
		Hemin-PEDOT functionalized boron-doped diamond	Peroxyxynitrite[485]
		PEDOT:PSS-stabilized gold NPs (Au@PEDOT)	Hg(II) [486]
		PEDOT:PSS-coated cotton fiber	NaCl[487]
		SiMO-PEDOT/MWCNT hybrid composite	Persulfate (S <sub>2</sub> O <sub>8</sub> <sup>2-</sup> )[488]
Optical	Substituted / derivatized	Poly(3-triazole dihexyl thiophene) (P3TzdHT), poly(3-triazole hexyl thiophene) (P3TzHT), and poly(3-butyne triisopropylsilyl thiophene) (P3BSiT)	Trinitrotoluene (TNT) and dinitrotoluene (DNT) [363]
	Neutral group)	(side PT 2,6-dithienyl-4-phenylpyridine (TPP) and 2,6-diphenyl-4-phenylpyridine (PPP) derivatives of PT Poly{3-[2-(2-dimethylamino-ethylamino)ethoxy]-4-methyl-thiophene} (PTMA)	Pd <sup>2+</sup> [366]
		Poly(3-alkoxy-4-methylthiophenes)	Cu <sup>2+</sup> , Co <sup>2+</sup> and Cd <sup>2+</sup> [371]
		Quinine-linked PT-	Nucleotides, folic acid, glutathione, inorganic anions, metal ions, and surfactants[373]
			Carbenicillin[376]

		PEDOT-COOH	Catechol, ascorbic acid, acetaminophen, quercetin, epinephrine and tryptophan[378]
Substituted / derivatized  Cationic (side group)		Poly(3-(4-methyl-30-thienyloxy)propyltrimethylammonium) (PMTPA)	Cysteine (Cys) and Homocysteine (Hcys) [381]
		PMTPA	Amino acids and peptides[382]
		PMTPA	15 nucleotide phosphates (XNPs, where X = A, U, T, G, C, and N = mono, di, tri) [383]
		PMTPA	Folic acid[384]
		PEMTEI	Lysosomal ATP [385]
		Poly(1H-imidazolium-1-methyl-3-{2-[(4-methyl-3-thienyl)-oxy]ethyl} chloride)	Nucleic acids and human thrombin[387]
		Poly 3-{[1-(2-hydrazino-2-oxoethyl)piperidin-4-ylidene]methyl}thiophene hydrochloride (PM1·HCl)	Cu <sup>2+</sup> and Hg <sup>2+</sup> [388]
		Poly[N,N,N-trimethyl-4-(thiophen-3-ylmethylene)-cyclohexanaminium chloride] (PTCA-Cl)	SDBS, SDS, SLS and SDC[389]
Substituted / derivatized  Anionic (side group)		Poly(2-(2-(4-methylthiophen-3-yloxy)ethyl)malonate acid) (PMTEMA)	Protamines[390]
		Poly[2-(3-thienyl)ethyloxy-4-butylsulfonate] (PTEBS)	H <sub>2</sub> O <sub>2</sub> [391]
		Poly(2-(2-(4-methylthiophen-3-yloxy)ethyl)malonate acid) (PMTEMA) with malonic acid group in side chain	CO <sub>2</sub> [393]
Functional ion-dopant inclusion		HFIP-PT/SWCNT	Dimethyl methylphosphonate (DMMP) [406]
Nanostructured F-PTs		PEDOT NPs/ ssDNA	DNA[430]
Multicomponents		Poly[3-(3'-N,N,N-triethylamino-1-propyloxy)-4-methyl-2,5-thiophene hydrochloride] (PMNT) DNA/PMNT and DNA/miRNA/PMNT	miRNA and RNase H activity[462]
		Poly [N-9'-heptadecanyl-2,7-carbazole-alt-5,5-(4',7'-di-2-thienyl-2',1',3'-benzothiadiazole)] (PCDTBT) and [6,6]-phenyl C71-butyric acid methyl ester (PC70BM) /PEDOT:PSS	Human thyroid stimulating (TSH) [468]
		Alcohol dehydrogenase /Ru(bpy) <sub>3</sub> <sup>2+</sup> / PEDOT-PSS-G	Ethanol[482]
Others	Nanostructured F-PTs	Copolymer of PEDOT and PEDOT-COOH (PEDOT-co-PEDOT-COOH) NW/ ODN	ODN[427]
		PEDOT-COOH nanodots/ anti-EpCAM	Tumor cell[428]
		Nanostructured biotinylated PT derivative (PTBL)	Streptavidin[435]

		Poly [2-(3-thienyl)ethanol n-butoxycarbonylmethylurethane] (PURET) NPs	DNT and TNT[439]
	Multicomponents	PEDOT PAA/poly(4-lithium styrenesulfonic acid) (PSSLi)	Glu[449]
		magnetic ribbon-coated PEDOT:PSS	Humidity [479]
		PVP-PEDOT:PSS	Strain[489]
		ZnO NR/PEDOT:PSS hybrid	ultraviolet light[490]
		PEDOT-IPN	Strain[491]

**Table 7. Functionalized polyfluorenes (P-PF) for sensors and related details: Functionalization approach, name of F-PF, type of sensor (based on analyte), analyte(s) name, detection technique, role of F-PF for sensing and sensor performances.**

Mode of Parent structure functionalization/modification	Name of FCP (abbreviation) or functional structure in the FCP	Type of sensor (Analyte)	Specific analyte(s)	Detection method/Technique	Function/Role of FCP for sensing*	Sensor performances* (LR and DL)	Ref
Substituted / derivatized  Neutral (side group)	Poly(9,9-bis(6'-benzimidazole)hexyl)fluorene- <i>alt</i> -1,4-phenylene (PBP)	Optical (Ion)	inorganic phosphate (Pi) and Fe <sup>3+</sup>	Fluorescence "turn on"	Fluorescence of PBP due to simultaneous electron transfer, competent energy migration, and exciton delocalization	-	[496]
	4-poly[9,9'-(N-carbazole-hexyl)fluorene] (PNCHF)	Optical (ion)	Fe <sup>3+</sup>	Fluorescence "quenching"	Fe <sup>3+</sup> ion with empty 'd' shell electronic structure contributes to the strong metal-ligand interaction to form ligand to metal state complexes which exhibits a higher quenching response to Fe <sup>3+</sup>	LR = 5x10 <sup>-6</sup> M – 2x10 <sup>-4</sup> M	[497]
	Poly[(9,9-bis(propenyl)-9H-fluorene)-co-(9,9-dihexyl-9H-fluorene)] (P1), poly[(9,9-bis(carboxymethylsulfonyl-propyl)-fluorenyl-2,7-diyl)-co-(9,9-dihexyl-9H-fluorene)] (P2), and poly[(9,9-dihexylfluorene)-co- <i>alt</i> -(9,9-bis-(6-azidoethyl)fluorene)] (P3)	Optical (ion)	Fe <sup>3+</sup>	Fluorescence "quenching"	Fe <sup>3+</sup> ion forms ferrocene like complex with P2. Fe <sup>3+</sup> ions form complex with thioglycolic acid groups through electrostatic interactions	-	[498]
	Poly{(4,4'-azobenzene)-2,7-[9,9-bis(6'- <i>N,N,N</i> ,-trimethyl ammonium)hexyl fluorene] dibromide} (PFAB) and reduced to PFAB-L	Optical (ion)	pH, Fe <sup>3+</sup>	Fluorescence "turn-on" (pH) "quenching" (Fe <sup>3+</sup> )	The association between Fe <sup>3+</sup> and -NH-NH- group disturb the face to face π-π stacking interaction and facilitates electron transfer to result fluorescent quenching. Fluorescence of PFAB-L was affected by pH through the protonation of -NH-NH- group.	-	[499]
	Fluorene-based material containing triple azacrown ether (FTC)	Optical (ion)	Fe <sup>3+</sup>	Fluorescence "quenching"	Interaction between Fe <sup>3+</sup> ion and the lone pairs of the nitrogen atom on the	-	[500]

					azocrown ether. quenching is by electron transfer from the fluorine unit to the metal ion		
Benzo[c][1,2,5]selenadiazole (BSe) functionalized fluorene	Optical (ion)	Hg <sup>2+</sup>	Fluorescence "quenching"	Selective to Hg <sup>2+</sup> due to structural rigidity of BSe unit and strong Hg <sup>2+</sup> -BSe binding	DL = 1.9x10 <sup>-7</sup> mol L <sup>-1</sup>	[501]	
Meta- and para-linked poly(arylene ethynylene)s containing l-aspartic acid-functionalized fluorene units	Optical (ion)	Hg <sup>2+</sup>	Fluorescence "quenching"	Meta-linked polymer facilitates coordination between the aspartic acid groups in the polymer and Hg <sup>2+</sup> ions through a conformational transformation	DL = 10 nM	[502]	
(poly[(9,9-dihexylfluorene-2,7-diyl)-alt-co-(9,9-bis[6'-(1-imidazolyl)hexyl]fluorene-2,7-iy)])	Optical (ion)	Cu <sup>2+</sup>	Fluorescence "quenching"	Conjugated $\pi$ stacking luminescence properties of PF and the metal ion coordinating ability of imidazole	-	[503]	
Imidazole-functionalized PF derivatives	Optical (ion)	CN <sup>-</sup> /Cu <sup>2+</sup>	Fluorescence "turn-on/turn-off"	Selective quenching of PF fluorescence by coordination of the imidazole group with Cu <sup>2+</sup> ions.	DL = 1 $\mu$ g/L (Cu <sup>2+</sup> ) DL = 18 $\mu$ g/L (CN <sup>-</sup> )	[504]	
PF derivative linking -NH <sub>2</sub> group in PF with 3-glycidoxypropyl silane	Optical (ion)	Cu <sup>2+</sup>	Fluorescence "quenching"	Cu <sup>2+</sup> ions quench the fluorescence via electron transfer	-	[505]	
Copolyfluorene (PFBI) pendant benzimidazolyl group from poly[(9,9-dihexylfluorene)-alt-(9,9-dibromopentylfluorene)] (PFBr)	Optical (ion)	Cu <sup>2+</sup>	Fluorescence "turn off"	Pendant benzimidazolyl group quenches the fluorescence of PFBI upon binding with Cu <sup>2+</sup> ions	-	[506]	
Organoboron-appended PF (PFBP)	Optical (ion)	CN <sup>-</sup>	fluorescence "turn off"	Covalent bond formation between CN <sup>-</sup> ion and trivalent boron centers of the side chains of PFBP and also due to 'soft-soft interactions' between the boron center and CN <sup>-</sup> ions	DL = 0.5 $\mu$ M	[507]	
Coil-rod-coil ABA tri-block copolymer P(MMA-co-NBDAE)-b-PF-b-P(MMA-co-NBDAE) (where MMA and NBDAE are methyl methacrylate, and 4-(2-acryloyloxyethylamino)-7-nitro-2,1,3-benzoxadiazole, respectively)	Optical (ion)	F <sup>-</sup>	fluorescence "turn-off"	Blue-emitting conjugated PF block and green-emitting NBDAE moieties (with F <sup>-</sup> turn-off characteristics) within the PMMA block served as FRET donors and switchable acceptors	DL = 4.78 $\mu$ M (~0.09 ppm)	[508]	

	Electrospun nanofibrous membrane doped with a PF derivative (P9)	Optical (Protein)	Heme proteins (Haemoglobin (Hb), myoglobin (Mb) and cytochrome c (cyt c))	Fluorescence "quenching"	Fluorescence energy transfer (FRET) between the PF and heme prosthetic groups	LR = $2.0 \times 10^{-8}$ - $3.0 \times 10^{-6}$ M DL = $1.2 \times 10^{-8}$ M	[509]
	(Poly[(9,9-bis(30-((N,N-dimethylamino)N-ethylammonium)propyl)-2,7-fluorene)-alt-2,7-(9,9-p-divinylbenzene)-alt-fluorene)-alt-2,5-dimethyl-p-phenylenediamine] (PF-NH <sub>2</sub> ))	ECL biosensor (cancer biomarker)	Ovarian protein antigen (CA125)	ECL	ECL of PF-NH <sub>2</sub> induced a light emission that decreases regularly with the increase in CA125 concentration.	LR = 0.50 - 500 U mL <sup>-1</sup> DL = 0.087 U mL <sup>-1</sup>	[510]
	Poly(9,9-dioctylfluorene) (PFO) chelated with terbium ions (Tb <sup>3+</sup> )	Optical biosensor (biomarker)	Calcium dipicolinate (CaDPA) biomarker of bacterial spore	Fluorescence "turn on"	Sharp fluorescence peaks of β-phase PFO dots and narrow-band emissions of the Tb <sup>3+</sup> ions enabled CaDPA detection	DL = ~0.2 nM.	[511]
	Poly(9,9-dioctylfluorene) (PFO)	Optical (gas)	Methamphetamine (MAPA)	Fluorescence "turn on"	Hydrogen bonding interaction causes electron density changes at TPP or MTPP. Amine donates electrons and recovers fluorescence through coordination with MTPP	-	[512]
Substituted / derivatized Cationic (side group)	Poly{(1,4-phenylene)-2,7-[9,9-bis(6'-N,N,N-trimethyl ammonium)-hexyl fluorene] dibromide} cationic conjugated polymer (CCP)	Optical biosensor (cancer DNA)	DNA methylation of RASSF1A, OPCML and HOXA9 promoters of ovarian cancer samples	FRET	Methylated DNA was amplified by PCR, and the methylation level was detected through FRET between CCP and fluorescein	-	[513]
	α-mannose-containing PF derivative (sugar bearing PF derivative, PF-S) containing benzothiadiazole (BT)	Optical biosensor	Con A	Fluorescence "turn-on"	Specific interaction between Con A and α-mannose leads to polymer aggregation and increase in BT emission intensity	LR = 1 nM - 250 nM	[514]

	Hyper branched CPEs containing phosphorescent Ir (III) (HP-PE)	Optical biosensor	Heparin	Fluorescence "quenching"	Electrostatic interactions between HP-PE and with sulfonic acid groups present in heparin	LR = 0 - 44 $\mu$ M DL = 50 nM	[515]
	Polyfluorene derivative (PBT) with 20 mol% 2,1,3-benzothiadiazole (BT)	Optical biosensor	Heparin	Naked eye	Electrostatic attraction between polymer and heparin result in FRET	LR = 30 nM - 48 $\mu$ M	[516]
	Phosphorescent Iridium(III) complexes conjugated with cationic polyfluorenes	Optical biosensor	Heparin	Fluorescence	Electrostatic interaction between cationic PF and anionic heparin	LR = 1 – 10.9 $\mu$ M	[517]
	Polyfluorene derivative (PFP-aa) bearing two amino and four carboxylic acid groups in each repeat unit	Optical (pH)	pH range = 3 to 12 D-fructose	Fluorescence "quenching"	Overall negative or positive charges in PFP-aa varied depending on the pH, and the charges caused electrostatic repulsion between the polymer chains, resulting in different aggregation states and energy transfers. PFP-aa acts as pH indicator to detect D-fructose	LR = 0-36x10 <sup>-3</sup> M DL = 2.0x10 <sup>-3</sup> M	[518]
	PFO films doped with palladium tetraphenylporphyrin (PdTPP)	Optical (gas)	Amines	Fluorescence "turn-on"	PdTPP quenched the fluorescence of PFO via electron energy transfer	-	[519]
Substituted / derivatized	Poly(9,9-bis(6'-sulfate)hexyl) fluorene- <i>alt</i> -1,4-phenylene sodium salt (P1)	Optical (ion)	Fe <sup>3+</sup> and Pi	Fluorescence "quenching" (Fe <sup>3+</sup> ) "turn-on" (Pi)	Static fluorescence quenching mechanism	LR = 4.24 – 4.37 mg dL <sup>-1</sup>	[520]
anionic (side group)	Phosphonate-functionalized fluorescent PF	Optical (ion)	Fe <sup>3+</sup>	Fluorescence "quenching"	-	DL = 8.4 ppb (THF) DL = 0.14 ppm (aq. Solutions)	[522]
	Dendronized PF derivatives with carboxyl pendants	Optical (ion)	Hg <sup>2+</sup> and Cu <sup>2+</sup>	Fluorescence "quenching"	Carboxyl groups associate with metal ions through electrostatic interactions	LR = 0.1 $\mu$ M – 8.5 $\mu$ M (Cu <sup>2+</sup> )	[521]
	PF derivative with two L-aspartic acids in the side chain of every repeat fluorine unit	Optical (ion)	Hg <sup>2+</sup>	Fluorescence "quenching"	Polyamide in PFA coordinates effectively with Hg <sup>2+</sup> and the branched side chain reduce the aggregation of PF	LR = 10 nM – 2.65 $\mu$ M DL = 10 nM	[523]
	anionic PF-CPEs (PBPSO <sub>3</sub> Na) and cationic PF-CPEs with three boronic acid functional viologens (BBVs): [N,N'-4,4'-bis(benzyl-2"-boronic acid)-	Optical biosensor	D-fructose	Fluorescence "turn-on"	Electrostatic interactions between BBV and PBPSO <sub>3</sub> Na and positions of boronic groups determine the selectivity to D-fructose	LR = 1.0 mM - 100.0 mM	[524]

	bipyridinium dibromide ( <i>o</i> -BBV), N,N'-4,4'-bis(benzyl-3"-boronic acid)-bipyridinium dibromide ( <i>m</i> -BBV), and N,N"-4,4"-bis(benzyl-4"-boronic acid)-bipyridinium dibromide ( <i>p</i> -BBV)]						
Nanostructuring	Carboxylic acid-functionalized anionic polyfluorene PF-COOH	Optical (Biosensor)	ssDNA	Fluorescence	Specific ssDNA detection amino modified oligo nucleoids are attached to PF-COOH	-	[525]
	Polyfluorene NWs	Optical (Biosensor)	Fluorescent biological azide	Fluorescence	Fluorescence resonance energy transfer	-	[526]
	solution-dispersible hyperbranched conjugated polymer NPs (FT-HBCPNs)	Optical (ion)	Fe <sup>3+</sup>	Fluorescence	$\pi$ -electron transfer complex formation	3.09 $\times$ 10 <sup>-7</sup> mol L <sup>-1</sup>	[527]
	Rod-coil-coil tri-block copolymers, polyfluorene-block-poly(N-isopropylacrylamide)-block-poly(N-methylolacrylamide) (PF-b-PNIPAAm-b-PNMA)	Optical	Temperature	Fluorescence "turn-on/turn-off"	Below LCST incident light absorbed by the PF blocks, resulting in PL luminescence. Above LCST light absorption of PF blocks suppressed resulting in PL quenching.	-	[528]

\*If available in the reference paper

ECL – Electro chemiluminescence; FRET - Fluorescence resonance energy transfer

Table 8. Cross-sectional details on the signal transduction mode based sensors utilizing the four functionalization categories of polyfluorenes (F-PFs)

Sensor signal transduction mode	Mode of Parent structure functionalization/ modification	Name of FCP (abbreviation) or functional structure in the FCP	Specific analyte(s)
Optical	Substituted derivatized	Poly(9,9-bis(6'-benzimidazole)hexyl)fluorene- <i>alt</i> -1,4-phenylene (PBP)	inorganic phosphate (Pi) and Fe <sup>3+</sup> [496]
		4-poly[9,9'-(N-carbazole-hexyl) fluorene] (PNCHF)	Fe <sup>3+</sup> [497]
	Neutral (side group)	Poly[(9,9-bis(propenyl)-9H-fluorene)-co-(9,9-dihexyl-9H-fluorene)] (P1), poly[(9,9-bis(carboxymethylsulfonyl-propyl)-fluorenyl-2,7-diyl)-co-(9,9-dihexyl-9H-fluorene)] (P2), and poly[(9,9-dihexylfluorene)-co- <i>alt</i> -(9,9-bis-(6-azidohexyl)fluorene)] (P3)	Fe <sup>3+</sup> [498]
		Poly{(4,4'-azobenzene)-2,7-[9,9-bis (6'- <i>N,N,N</i> ,-trimethyl ammonium)hexyl fluorene] dibromide} (PFAB) and reduced to PFAB-L	pH, Fe <sup>3+</sup> [499]
		Fluorene-based material containing triple azacrown ether (FTC)	Fe <sup>3+</sup> [500]
		Benzo[ <i>c</i> ][1,2,5]selenadiazole (BSe) functionalized fluorene	Hg <sup>2+</sup> [501]
		Meta- and para-linked poly(arylene ethynylene)s containing l-aspartic acid-functionalized fluorene units	Hg <sup>2+</sup> [502]
		(poly[(9,9-dihexylfluorene-2,7-diyl)- <i>alt</i> -co-(9,9-bis[6'-(1-imidazolyl)hexyl]fluorene-2,7-iy)])	Cu <sup>2+</sup> [503]
		Imidazole-functionalized PF derivatives	CN <sup>-</sup> /Cu <sup>2+</sup> [504]
		PF derivative linking -NH <sub>2</sub> group in PF with 3-glycidoxylpropyl silane	Cu <sup>2+</sup> [505]
		Copolyfluorene (PFBI) pendant benzimidazolyl group from poly[(9,9-dihexylfluorene)- <i>alt</i> -(9,9-dibromopentylfluorene)] (PFBr)	Cu <sup>2+</sup> [506]
		Organoboron-appended PF (PFBP)	CN <sup>-</sup> [507]
		Coil-rod-coil ABA tri-block copolymer P(MMA- <i>co</i> -NBDAE)- <i>b</i> -PF- <i>b</i> -P(MMA- <i>co</i> -NBDAE) (where MMA and NBDAE are methyl methacrylate, and 4-(2-acryloyloxyethylamino)-7-nitro-2,1,3-benzoxadiazole, respectively)	F <sup>-</sup> [508]
		Electrospun nanofibrous membrane doped with a PF derivative (P9)	Heme proteins (Haemoglobin (Hb), myoglobin (Mb) and cytochrome c (cyt c)) [509]
Poly(9,9-dioctylfluorene) (PFO) chelated with terbium ions (Tb <sup>3+</sup> )	Calcium dipicolinate (CaDPA) biomarker of bacterial spore[511]		

		Poly(9,9-dioctylfluorene) (PFO)	Methamphetamine (MAPA) [512]
Substituted derivatized	/	Poly{(1,4-phenylene)-2,7-[9,9-bis(6'-N,N,N-trimethyl ammonium)-hexyl fluorene] dibromide)}	DNA methylation of RASSF1A, OPCML and HOXA9 promoters of ovarian cancer samples[513]
Cationic(side group)		α-mannose-containing PF derivative (sugar bearing PF derivative, PF-S) containing benzothiadiazole (BT)	Con A[514]
		Hyper branched CPEs containing phosphorescent Ir (III) (HP-PE)	Heparin [515]
		Polyfluorene derivative (PBT) with 20 mol% 2,1,3-benzothiadiazole (BT)	Heparin [516]
		Phosphorescent Iridium(III) complexes conjugated with cationic polyfluorenes	Heparin [517]
		Polyfluorene derivative (PFP-aa) bearing two amino and four carboxylic acid groups in each repeat unit	pH range = 3 to 12 D-fructose[518]
		PFO films doped with palladium tetraphenylporphyrin (PdTPP)	Amines[519]
Substituted derivatized	/	Poly(9,9-bis(6'-sulfate)hexyl) fluorene- <i>alt</i> -1,4-phenylene sodium salt (P1)	Fe <sup>3+</sup> and Pi[520]
		Phosphonate-functionalized fluorescent PF	Fe <sup>3+</sup> [522]
		Dendronized PF derivatives with carboxyl pendants	Hg <sup>2+</sup> and Cu <sup>2+</sup> [521]
anionic (side group)		PF derivative with two L-aspartic acids in the side chain of every repeat fluorine unit	Hg <sup>2+</sup> [523]
		anionic PF-CPEs (PBPSO <sub>3</sub> Na) and cationic PF-CPEs with three boronic acid functional viologens (BBVs): [N,N'-4,4'-bis(benzyl-2"-boronic acid)-bipyridinium dibromide ( <i>o</i> -BBV), N,N'-4,4'-bis(benzyl-3"-boronic acid)-bipyridinium dibromide ( <i>m</i> -BBV), and N,N"-4,4"-bis(benzyl-4"-boronic acid)-bipyridinium dibromide ( <i>p</i> -BBV)]	D-fructose[524]
Nanostructuring		Carboxylic acid-functionalized anionic polyfluorene PF-COOH	ssDNA[525]
		Polyfluorene NWs	Fluorescent biological azide[526]
		solution-dispersible hyperbranched conjugated polymer NPs (FT-HBCPNs)	Fe <sup>3+</sup> [527]
		Rod-coil-coil tri-block copolymers, polyfluorene-block-poly (N-isopropylacrylamide)-block-poly(N-methylolacrylamide) (PF-b-PNIPAAm-b-PNMA)	Temperature[528]
Others	Substituted derivatized	(Poly[(9,9-bis(30-((N,N-dimethylamino) N-ethylammonium)propyl)-2,7-fluorene)- <i>alt</i> -2,7-(9,9-p-divinylbenzene)- <i>alt</i> -fluorene)- <i>alt</i> -2,5-dimethyl-p-phenylenediamine] (PF-NH <sub>2</sub> )	Ovarian protein antigen (CA125) [510]
	Neutral (side group)		

ACCEPTED MANUSCRIPT